

SLURRY EROSION

Uses, Applications and Test Methods

MILLER/SCHMIDT, editors

ASTM STP 946

SLURRY EROSION: USES, APPLICATIONS, AND TEST METHODS

A symposium sponsored by
ASTM Committee G-2 on Erosion and Wear,
National Association of Corrosion Engineers,
Slurry Technology Association, and
American Society for Metals
Denver, CO, 26–27 June 1984

ASTM SPECIAL TECHNICAL PUBLICATION 946
John E. Miller, White Rock Engineering,
and Frederick Schmidt, E. I. du Pont
de Nemours & Co., editors

ASTM Publication Code Number (PCN)
04-946000-29



1916 Race Street, Philadelphia, PA 19103

Library of Congress Cataloging-in-Publication Data

Slurry erosion.

(ASTM special technical publication; 946)

“ASTM publication code number (PCN) 04-946000-29.”

Includes bibliographies and index.

1. Hydraulic conveying—Congresses.
2. Slurry Pipe lines-Corrosion—Congresses. I. Miller, John E. (John Evans, 1909– . II. Schmidt, Frederick E. (Frederick Edward), 1945– . III. ASTM Committee G-2 on Erosion and Wear. IV. Series.
TJ898.S548 1987 621.8'672 87-920
ISBN 0-8031-0941-5

Copyright © by AMERICAN SOCIETY FOR TESTING AND MATERIALS 1987
Library of Congress Catalog Card Number: 87-920

NOTE

The Society is not responsible, as a body,
for the statements and opinions
advanced in this publication.

Foreword

This publication, *Slurry Erosion: Uses, Applications, and Test Methods*, contains papers presented at the international symposium of the same name held in Denver, Colorado on 26–27 June 1984. The symposium was sponsored by ASTM Committee G-2 on Erosion and Wear, the National Association of Corrosion Engineers, the Slurry Transportation Association (now the Slurry Technology Association), and the American Society for Metals. John E. Miller, White Rock Engineering, and Frederick Schmidt, E.I. du Pont de Nemours & Co., presided as symposium chairmen and were coeditors of this publication.

Related ASTM Publications

Materials Evaluation under Fretting Conditions, STP 780, 04-780000-29

Selection and Use of Wear Tests for Coatings, STP 769, 04-769000-29

Erosion: Prevention and Useful Application, STP 664, 04-664000-29

A Note of Appreciation to Reviewers

The quality of the papers that appear in this publication reflects not only the obvious efforts of the authors but also the unheralded, though essential, work of the reviewers. On behalf of ASTM we acknowledge with appreciation their dedication to high professional standards and their sacrifice of time and effort.

ASTM Committee on Publications

ASTM Editorial Staff

David D. Jones
Janet R. Schroeder
Kathleen A. Greene
Bill Benzing

Contents

Overview	1
-----------------	---

MATERIALS

Ball Mill and Hub Test Methods for Slurry Erosion Evaluation of Materials—W. J. SCHUMACHER	5
Discussion	17
Slurry Erosion and Abrasion of Metal-Ceramic Coatings—	
A. A. SAGÜÉS, D. K. SPENCER, V. K. SETHI, AND G. A. SARGENT	19
Discussion	44

PROCESS (FUEL) SLURRIES

The Relative Erosivity of Coal-Oil, Coal-Water, and Petroleum Coke-Oil Slurries—Y.-H. LEE AND H. M. CLARK	47
Erosivity of Coal Particles in Coal-Solvent Slurries—A. V. LEVY, N. JEE, AND G. SORELL	62
The Validity of Fuel Recycling During Erosivity Testing Using Coal-Water Liquid Fuels—K. G. SEDMAN, J. C. THORNLEY, R. D. GILDERS, AND G. R. HOEY	78
A Review of Pipeline Slurry Erosion Measurements and Research Recommendations—R. M. SUMMER	91

APPLICATIONS

Comparison Between Laboratory Characterization and Field Performance of Steel Mud Pump Liners Coated with CM 500L, a Tungsten-Carbon Alloy—D. G. BHAT AND Y. R. DEKAY	103
Discussion	116
Corrosion Rate Measurements and Corrosion-Erosion Protection in Limestone Slurry Scrubbers—P. A. BURDA	118
Discussion	139

Jet-in-Slit and Vibratory Methods for Slurry Erosion-Corrosion Tests of Materials—Y. OKA, M. MATSUMURA, M. YAMAWAKI, AND M. SAKAI 141

The SAR Number for Slurry Abrasion Resistance—J. E. MILLER 155
Discussion 164

TEST METHODS

A New Flow-Through Slurry Erosion Wear Test—B. W. MADSEN AND R. BLICKENSBERGER 169
Discussion 184

Test Approach for Dense Slurry Erosion—M. C. ROCO, P. NAIR, AND G. R. ADDIE 185

Experience with the Wet Sand/Rubber Wheel Abrasion Test—G. A. SALTZMAN, T. O. MEREDIZ, D. K. SUBRAMANYAM, AND H. S. AVERY 211
Discussion 241

Hydraulic and Metallurgical Criteria in Slurry Pumping System Design—S. K. SINHA 243

Indexes 261

Overview

Although the transportation of solids in the form of slurries is basically older than history—the blood circulating system in mammals involves the use of a positive displacement pump forcing a slurry of solid corpuscles in liquid serum through a complex pipeline—the slurry transportation of solids through long pipelines has been undertaken only in about the last 25 years.

The first long coal-slurry pipeline was built in 1957 from Cadiz, Ohio to Cleveland, a distance of 110 miles. The success of this project prompted the construction of pipelines in Arizona, Tasmania, Brazil, Mexico, and Russia, to name just a few locations. These systems have proven their worth, and slurry pipelining is now a viable and competitive method of solids transportation.

In the domain of abrasive wear, particularly that wear encountered in handling abrasive solid particles, much work has been done in the past half century with regard to “dry” abrasivity, but only in more recent years has interest grown in “wet” abrasivity, namely slurries.

With the advancement of the slurry pumping industry, a need naturally arose for data on the effects of different slurries on equipment as well as for data on the most abrasion-resistant materials available. It was logical that ASTM Committee G-2 on Wear and Erosion would inherit that task. Subcommittee G2.30 on Abrasive Wear agreed that a symposium on the subject would be of value to the slurry industry. Therefore, the International Symposium on Slurry Erosion: Uses, Applications and Test Methods was organized and sponsored by ASTM, The National Association of Corrosion Engineers, The Slurry Transportation Association (now known as the Slurry Technology Association), and the American Society of Metals. The Symposium was held in Denver, Colorado, on 26–27 June 1984.

The fact that most long slurry pipelines utilize water as the fluidizing medium introduces a pernicious combination of abrasion-corrosion, the effects becoming exponential over the effects of abrasivity alone added to the effects of corrosivity alone. Accordingly, corrosion engineering becomes involved in slurry pumping. Unless the test slurry is purposely inhibited, the effect of both abrasion and corrosion will appear in most test procedures described in this book, whether intended or not. This is as it should be for, after all, if the slurry being considered for a pipeline is corrosive, one would have to accept the combined effects on the “wear” of the pipeline equipment.

Herein one will find details of a wide variety of tests that cover the development of such wear- and corrosion-resistant materials, including metals, organic materials, and coatings. Many of the tests pertain to coal slurry, perhaps the most important phase of the industry.

2 SLURRY EROSION

There could be speculation and perhaps controversy over the slurry erosion tests described in these papers, but each one has merits that could be important to the industry. Anyone involved with slurry pumping should find the information contained in this book of value. The publication is worthwhile as a stimulus to much more needed study, investigation, and experiment aside from its value as a communication tool between the laboratory and the field.

John E. Miller

White Rock Engineering, Dallas, TX;
symposium cochairman and coeditor

Potential Areas For Standards Development

A panel discussion was held at the conclusion of the two-day international symposium. The specific topics reviewed focused on each of the four program areas: Materials, Process (Fuel) Slurries, Applications, and Test Methods.

The following list is a summary of the symposium consensus that future work in each area would benefit and advance the field of slurry technology:

- Develop a “guide” for data logging and test procedures to improve the correlation of laboratory tests with field performance tests.
- Sponsor “round-robin” test comparisons and publication of results.
- Develop slurry erosion terminology and definitions for addition to G-40 [ASTM Terminology Relating to Erosion and Wear (G 40-83)].
- Standardize (nonstandard) uses of the Miller Number G-75 practice, for example, materials, pH, and slurry content [Test Method for Slurry Abrasivity by Miller Number (G 75-82)].
- Develop reference materials, slurries, and blank test methods.
- Promote test methods and develop procedures for polymer and elastomer materials evaluation.
- Sponsor future symposia on the basic mechanics of erosion-corrosion focused on analytical methods, for example, electrochemical analysis.

The G-2 committee on Wear and Erosion actively encourages the participation of academic, industrial, and government laboratory investigators to join in the development of slurry erosion standards.

Frederick Schmidt

E. I. du Pont de Nemours & Co., Inc.
Experimental Station, Wilmington, DE;
symposium cochairman and editor

Materials

Ball Mill and Hub Test Methods for Slurry Erosion Evaluation of Materials

REFERENCE: Schumacher, W. J., “Ball Mill and Hub Test Methods for Slurry Erosion Evaluation of Materials,” *Slurry Erosion: Uses, Applications, and Test Methods, ASTM STP 946*, J. E. Miller and F. E. Schmidt, Jr., Eds., American Society for Testing and Materials, Philadelphia, 1987, pp. 5–18.

ABSTRACT: Abrasive wear under wet sliding conditions can be very severe on alloy steels, not to mention expensive. Armco has developed an austenitic stainless steel called NITRONIC 30 having superior wear resistance compared to abrasion-resistant (AR) steels and most stainless steels. Two different laboratory tests were used to characterize the corrosive wear of these steels, a hub test and a ball mill test. Different corrodents of varying degrees of severity were used such as distilled water, synthetic sea water, synthetic nickel mine water, and a mixture of sodium chloride plus acetic acid. Other variables such as surface roughness and bulk hardness were also studied.

KEY WORDS: alloy and stainless steels, corrosion-erosion, low stress abrasion

Abrasive wear under wet sliding conditions can be extremely severe on alloy steels leading to expensive replacement of critical equipment. The South Africans encounter wet corrosive conditions in their mines and have found that a ferritic stainless steel called 3Cr 12 provides a cost-effective solution to their corrosive wear problems in chutes, liners, and conveyor belt equipment used in ore handling. This alloy is a modified Type 409 stainless steel which has improved corrosion resistance over alloy steels and abrasion-resistant (AR) steels at a relatively low cost compared to other stainless steels.

In the United States, Type 304 stainless steel has found wide use in coal-handling equipment such as chutes, bins, hoppers, and screening because of good corrosion resistance, durability, and maintenance-free performance.

Another reason for the popularity of Type 304 is the great improvement over alloy steels regarding “slideability.” Type 304 polishes smooth, while AR steels rust, which causes buildup of material and lowers flow rates. Type 304–

¹ Senior staff engineer, Armco, Inc., Middletown, Ohio.

lined coal hopper cars can be discharged three times faster than unlined cars because of improved slideability [1]. This feature also results in reduced freeze-up problems during the winter.

Armco has recently developed a new austenitic stainless steel called NITRONIC 30 having outstanding corrosive wear resistance. NITRONIC 30 is more cost-effective than not only Type 409 and Type 304 stainless steels, but also carbon and alloy steels. Much work has been conducted at the Armco Research Laboratories to characterize the corrosive wear of stainless and alloy steels. This paper will review the attractive properties inherent in the NITRONIC 30 alloy.

Test Program

Materials

A variety of stainless steels was selected from the not so corrosion-resistant (Type 409, Type 410) through intermediate grades (Type 304, 17-4 PH, NITRONIC 30) to very corrosion-resistant (Type 316). The effect of surface roughness was studied using NITRONIC 30, and the effect of higher hardness produced by cold-working was studied using Type 316. The alloy steels tested were: AISI 1065, 4340, Hadfield manganese, and the “Cadillac” of AR steels—Astralloy V.² An aluminum alloy, 6061, was also tested since it has been used for coal hopper cars to a limited degree. The compositions, heat treatments, and hardness of these alloys are listed in Table 1.

Test Methods

Hub Test

Industrial laboratory wear tests must be economical to run while producing reliable relative ranking of materials. One such test method is the Armco Hub Test. This test was patterned after typical farming implements used to till the soil such as disks, plowshares, cultivator sweeps, furrow shovels, spikes, and chisels. It is a low-stress abrasion test. An overall view of the apparatus is shown in Figure 1A. The slurry container on the right has three hubs, each capable of holding eight specimens as shown schematically in Fig. 1B. The hub is slotted to restrain the movement of the specimen as it passes through the slurry. After preliminary tests in corrosive slurries, the hubs (carbon steel) and the container (Type 304 stainless steel) interior were coated with a polymer to preclude corrosion. Nylon washers were also inserted between the hub and specimens to prevent galvanic corrosion; there was no evidence in any tests of this condition.

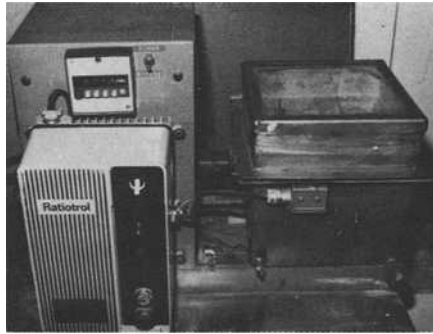
² Trademark of Astralloy-Vulcan Corp.

TABLE 1—Compositions, heat treatments, and hardness of test alloys.

Alloy	Chemical Analysis, Weight %								Heat Treatment ^a	Hardness, (HR)
	C	Mn	Si	Cr	Ni	Others				
T409	0.01	0.25	0.57	10.89	0.16	0.39Ti			1350°F—1 h—WQ	B85
T410	0.11	0.33	0.54	12.34	0.21	...			1800°F—15 min—WQ + 1000°F—2 h—AC	C33
17-4PH	0.04	0.60	0.51	15.72	4.45	3.26Cu, 0.27Cb			1900°F—15 min—WQ + 900°F—1 h—AC	C44
NITRONIC 30	0.04	7.39	0.38	16.73	2.31	0.19N, 0.75Cu			1950°F—15 min—WQ	B90
T304	0.07	1.66	0.48	18.45	8.90	...			1925°F—15 min—WQ	B75
T316	0.06	1.77	0.56	17.46	12.93	2.2Mo, 0.38Cu			1950°F—30 min—WQ	B73
AISI 1065	0.67	0.76	0.30			Cold rolled 50%	C35
AISI 4340	0.34	0.69	0.30	0.63	1.92	0.27Mo			1500°F—15 min—WQ + 400°F—2 h—AC	C47
Hadfield Mn	0.79	13.20	...	0.16	0.07	0.99Mo			1500°F—20 min—OQ + 400°F—2 h—AC	C49
Astralloy V	0.25	1.00	0.30	1.60	3.60	0.35Mo			1850°F—15 min—WQ	B93
AI 6061	0.60	0.25	...	0.25Cu, 1Mg, balance Al			1650°F—15 min—AC	C45
									As-received (T6)	B59

^a WQ = water quenched; AC = air cooled; OQ = oil quenched.

A.



B.

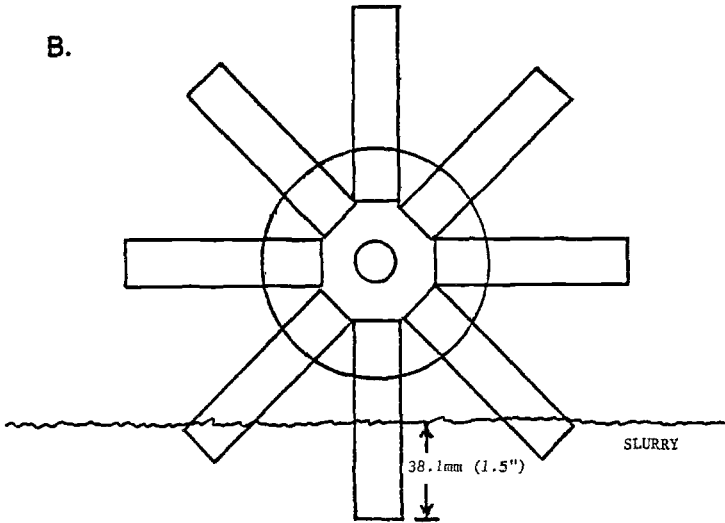


FIG. 1—(a) Hubble wear test machine—slurry container at right is 254-mm (10 in.) on each edge; (b) schematic diagram of specimen arrangement on hub; three identical hubs mounted on horizontal shaft, about 76.2 mm (3 in.) between center and outside hubs.

The next most important parameter to be selected was the abrasive itself. AFS 50/70 sand was too fine and tended to cling to the specimens. However, this sand or quartz or both were excellent fillers to raise the volume of abrasives to the desired level. The sand was filled until it just met the specimen's edge when vertical. A coarser abrasive, pea gravel plus mill slag, was found to be ideal as the top layer that interacted with the specimens to cause the corrosive wear. Pea gravel is a very common abrasive, especially in mining and farming applications.

Specimens were fabricated from sheet stock and measured 2.54 by 12.7 by 88.9 mm (0.1 by 0.5 by 3.5 in.). The specimens were mounted to the hub with wing nuts for easy installation. One specimen of each alloy was mounted on

each hub and all alloys tested at the same time in a particular slurry. Specific details of other parameters such as speed, time, and corrosive conditions are listed in the relevant tables and figures.

Ball Mill Test

This test method was similar to the one the Canadians used in extensive work [2–5] to study the corrosive effects in grinding media for nickel mines. The U.S. Bureau of Mines also uses this type of test to conduct corrosive wear studies. The closed container is a 5.3-L porcelain jar which is rotated by rolls in a horizontal plane. The specimens measured 2.54 by 12.7 by 43.2 mm (0.1 by 0.5 by 1.7 in.) and were free to tumble in the slurry. Duplicates of all alloys were tested at one time in a particular slurry while the slurry was replaced after each 16-h period.

Again it was found that AFS 50/70 sand was inadequate as the abrasive because the light weight specimens tended to lodge in the compacted sand; consequently, only pea gravel was used as the abrasive. This test was also considered a low-stress abrasion test under the operating conditions for these experiments.

Results and Discussion

Hub Test

Three series of tests were run, one dry and two with different corrodents. Since different conditions, as noted in the tables, were used for the corrosive series, only the relative differences among the alloys should be compared between the series. In the first corrosive series, a mixture of 5% sodium chloride + 0.5% acetic acid was used as a very corrosive brine slurry with an abrasive mixture of quartz, pea gravel, and slag. An identical dry series was also conducted to determine the synergistic degradation caused by the corrodent addition. The results are shown in Fig. 2.

In the dry tests the two alloy steels ranked the best, followed by NITRONIC 30, 17-4 PH, and Type 409. Certainly the less costly alloy steels would be more cost-effective than the stainless steels under these conditions. However, this same rank was not true for the corrosive series because of the much greater volume loss of the alloy steels relative to the stainless grades—even Type 409, just as the South Africans had demonstrated [6–8]. Armco NITRONIC 30 ranked first and was three times better than Type 409 and four to five times better than Hadfield manganese and AISI 4340.

In the second corrosive hub test, a much less severe corrodent—distilled water—was used, but the results were the same, as shown in Fig. 3. The stainless alloys as a class outperformed the alloy steels including Astralloy V, which replaced the Hadfield manganese steel. NITRONIC 30 again ranked first

10 SLURRY EROSION

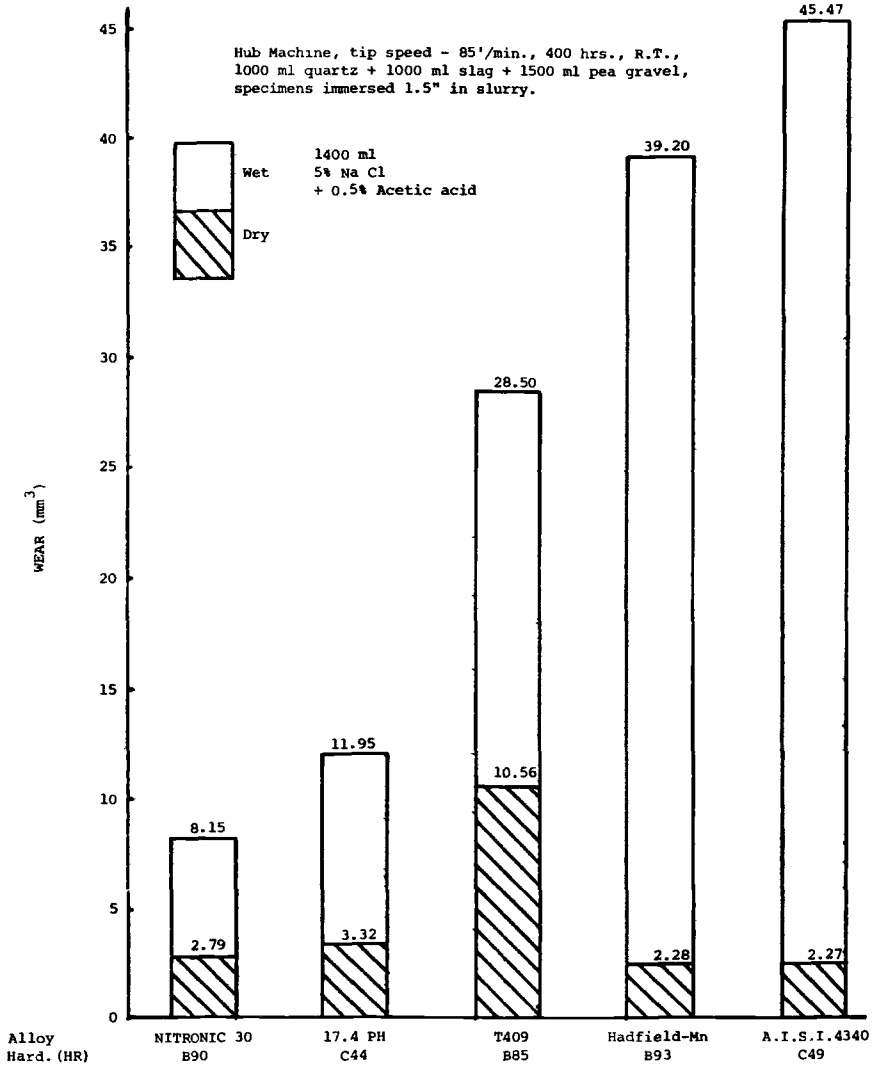


FIG. 2—Abrasive wear of alloy and stainless steels under dry and wet corrosive conditions.

of the stainless alloys and was over four times better than the alloy steels. The aluminum alloy 6061 was by far the poorest alloy tested and wore over 20 times faster than NITRONIC 30 and four times faster than the steels.

The effects of corrosion and wear on the specimens can be seen clearly in Fig. 4. NITRONIC 30, Type 304, and Type 6061 were free of any pitting attack. Type 409 and Type 410 exhibited slight pitting, and the alloy steels

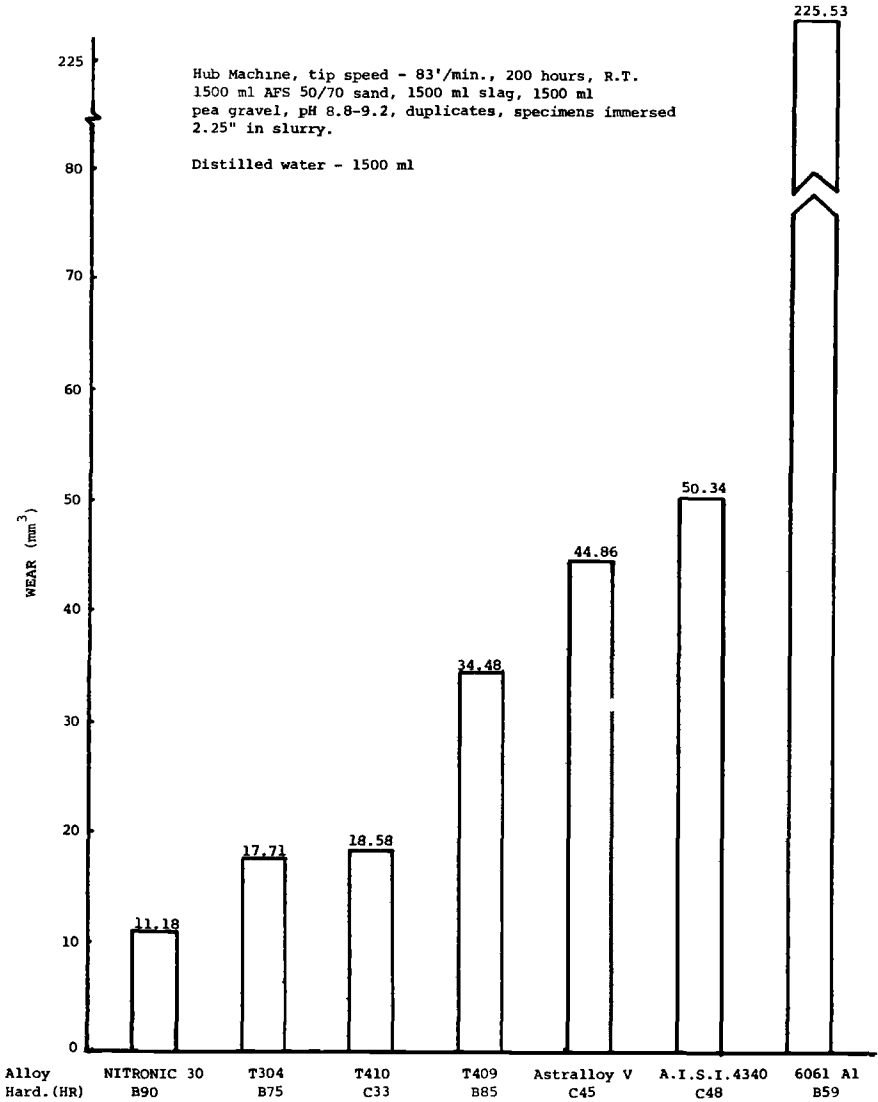


FIG. 3—Corrosive wear of alloy and stainless steels.

were heavily attacked. Alloy 6061 exhibited gross wear as noted by the rounded tip, while the other alloys had much less rounding.

Ball Mill Test

In these tests 5 16-h periods were conducted with a fresh slurry each period. The results in Fig. 5 again showed the stainless steels to be far superior to alloy

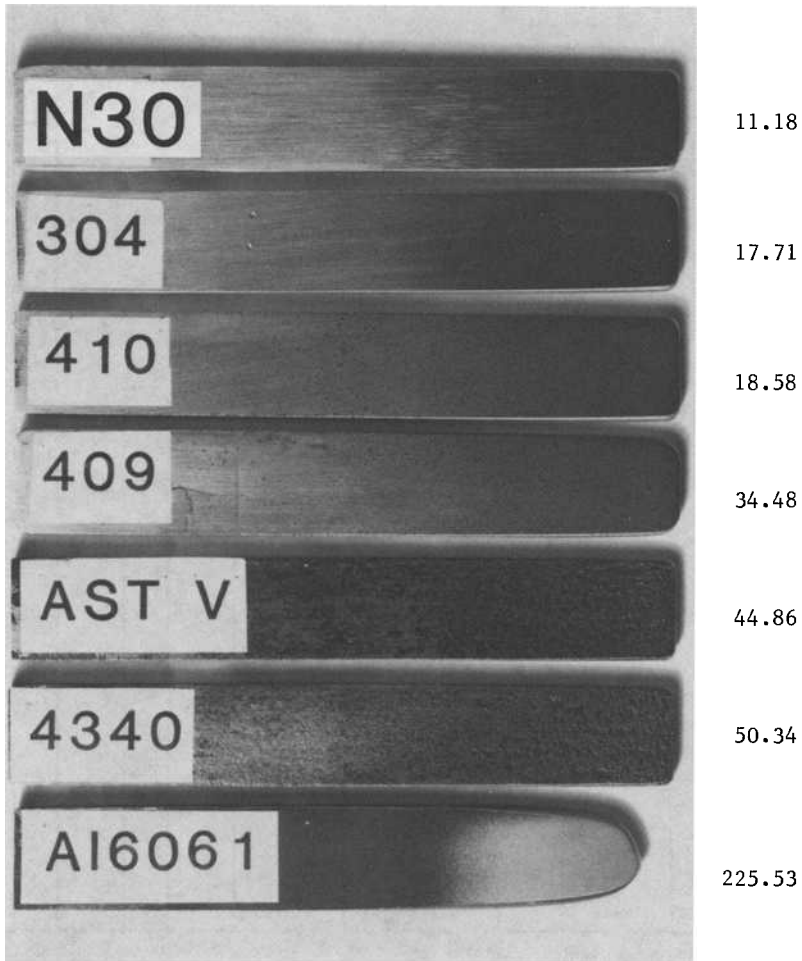
Volume Loss (mm^3)

FIG. 4—Hub test worn specimens taken from Fig. 3 data.

steels under corrosive conditions despite the high hardness of the latter. The improved corrosion resistance of Astralloy V over AISI 1065 also helped it to outperform the high carbon steel.

In the second ball mill series, a synthetic seawater called “Sea Salt” was used {ASTM Specification for Substitute Ocean Water [D 1141-75 (1980)]}. Cumulative volume loss for each 16-h period is recorded in Table 2 and plotted in Fig. 6. All the stainless steels vastly outperformed the two alloy steels by

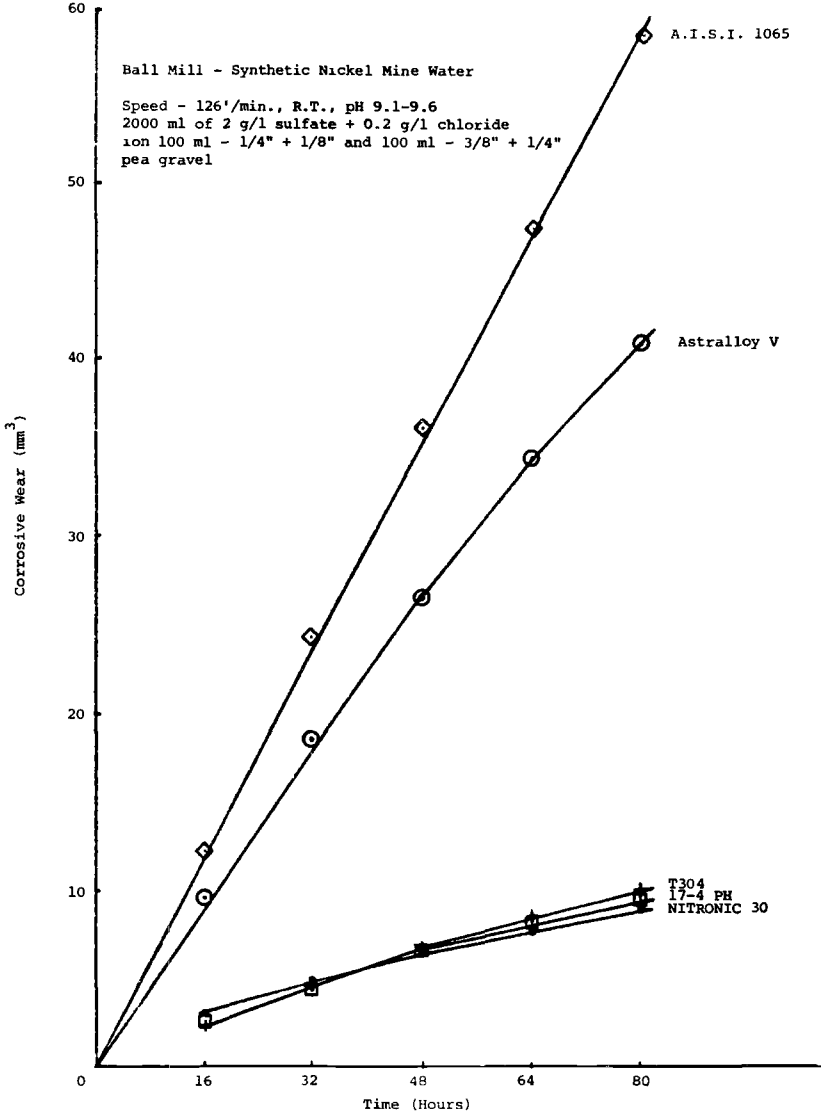


FIG. 5—Corrosive wear of alloy and stainless steels.

four to eight times. NITRONIC 30 ranked first among the stainless alloys despite a rough surface of $2.67 \mu\text{m}$ ($105 \mu\text{in.}$) compared to the typical $0.8 \mu\text{m}$ ($32 \mu\text{in.}$) for all other specimens. A less corrosion-resistant alloy would be expected to have higher wear rates if the specimen surface were rough due to crevice corrosion.

TABLE 2—Corrosive wear of alloy and stainless steels, ball mill, synthetic seawater, speed—0.64 m/s (126 ft/min), 16-h periods.^a

Period No.	NITRONIC 30		CUMULATIVE VOLUME LOSS, MM ³							
	Smooth, Hard (HR)	Rough, B89	17-4PH, C44	T304, B75	T316 Ann., B73	T316 C.R. 50%, C35	T409, B82	AST.-V, C45	ASTI 4340, C48	
1	1.28	1.36	1.51	1.66	1.95	1.98	2.37	7.29	7.60	
2	1.55	1.56	1.79	2.01	2.45	2.51	2.74	12.75	14.04	
3	2.36	2.38	2.76	3.02	3.70	3.79	4.10	18.69	20.31	
4	3.39	3.46	3.98	4.29	5.39	5.55	5.95	24.19	26.60	
5	3.97	4.01	4.70	5.01	6.40	6.61	6.94	29.06	31.78	
			RELATIVE RANK							
NITRONIC 30	1.00	1.00	1.17	1.25	1.60	1.65	1.73	7.25	7.93	

^a ph = 8.3 after tests, 2000 mL of liquid, 200 mL - 6.4 mm + 3.2 mm (- 1/4-in. + 1/8-in.) pea gravel, duplicates, fresh slurry each period.

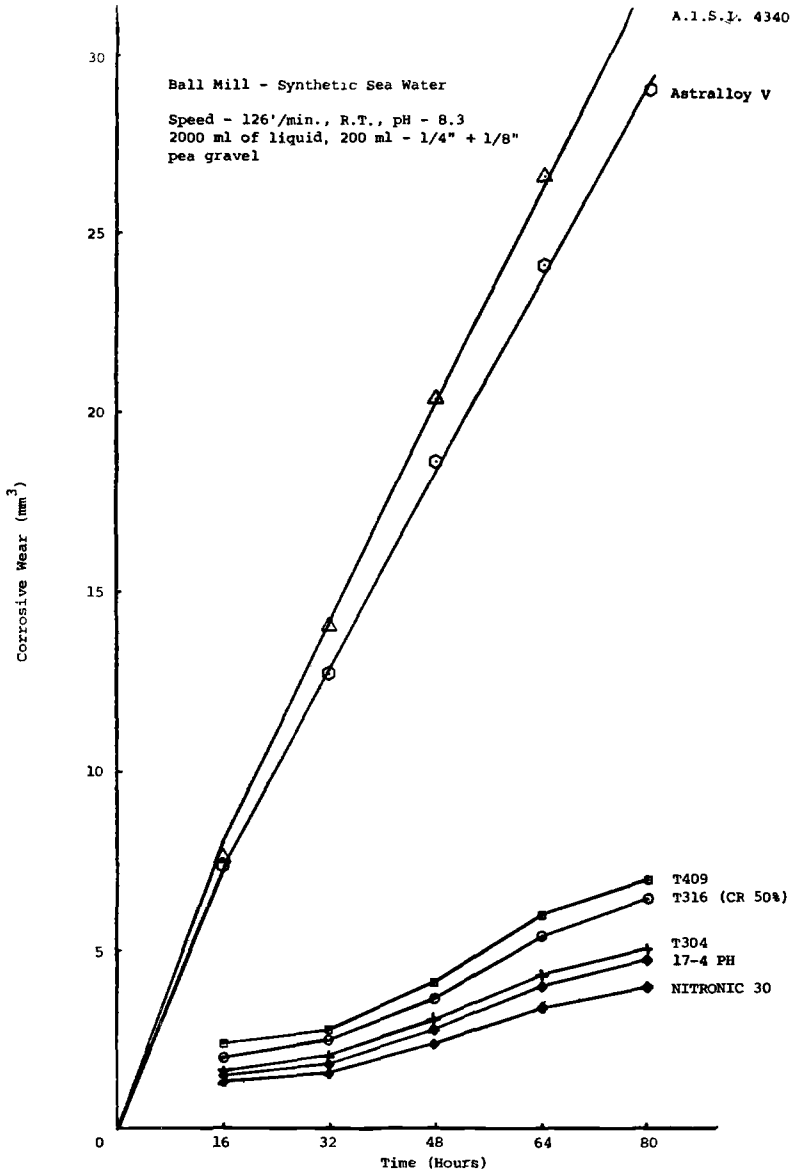


FIG. 6—Corrosive wear of alloy and stainless steels.

It was also interesting to note that Type 304 was better than Type 316 despite the latter's superior corrosion resistance. This shows that the higher work-hardening capacity of Type 304 was more important in reducing the overall corrosive wear. NITRONIC 30 was the best austenitic alloy for the same reason—the worn surfaces have been measured at close to HRC 50 in previous

tests. This is the reason that no difference was noted between the Type 316 annealed and cold-rolled specimens. Even annealed material rapidly work hardens and attains high surface hardnesses; prior cold-working is unnecessary to do this. This has been observed by many investigators [9-11].

Conclusions

Several conclusions about corrosive wear resistance became apparent from tests conducted at Armco Research, namely:

1. Stainless steels are much more abrasion resistant than alloy steels under even just mildly corrosive conditions.
2. Armco NITRONIC 30 is more cost-effective than Type 409 and Type 304 stainless steels, which are typically used in wet abrasive applications.
3. Increased surface roughness did not alter the corrosive wear of NITRONIC 30.
4. Increased initial bulk hardness did not alter the corrosive wear of Type 316.
5. In applications involving corrosive wear, NITRONIC 30 stainless steel appears as an outstanding candidate for providing effective resistance to these severe conditions.

References

- [1] *Nickel Topics*, Vol. 31, No. 1, 1978, pp. 8-9.
- [2] Lui, A. W. and Hoey, G. R., *Canadian Metallurgical Quarterly*, Vol. 14, No. 3, 1975, pp. 281-285.
- [3] Hoey, G. R. et al., *CIM Bulletin*, Feb. 1977, pp. 105-109.
- [4] Hoey, G. R. and Lui, A. W., *Anti-Corrosion*, March 1977, pp. 5-7.
- [5] Brigham, R. J., *Canadian Metallurgical Quarterly*, Vol. 15, No. 4, 1976, pp. 389-393.
- [6] Melville, M. L., Third South African Corrosion Conference, March 1980.
- [7] Thomas, C. R., *Journal of the South African Institute of Mining and Metallurgy*, Vol. 81, No. 10, Oct. 1981, pp. 288-302.
- [8] Allen, C., *Journal of the South African Institute of Mining and Metallurgy*, Vol. 81, No. 10, Oct. 1981, pp. 289-297.
- [9] Richardson, R. C., *Wear*, Vol. 10, 1967, pp. 291-309.
- [10] Khrushchov, M. M., and Babichev, M. D., *Issled Iznashivaniya Metallov*, Izd. Akad. Nauk, Moscow, 1960, Chap. 2, N.E.L. Transl. No. 889.
- [11] Schumacher, W. J., *Metal Progress*, Vol. 114, No. 6, Nov. 1978, pp. 32-36.

DISCUSSION

G. Sorrell¹ (written discussion)—How do you explain the far better comparative erosion resistance between stainless and carbon/alloy steel under dry versus wet condition, even with distilled water? More specifically, is oxygenated distilled water sufficiently aggressive to cause appreciable erosion-corrosion, or is there a change in wear mechanism between wet and dry conditions?

W. Schumacher (author's closure)—Hoey and Bednar³ and Swan⁴ have shown that oxygenated water *is* sufficiently aggressive to cause appreciable erosion-corrosion to steels because the metal loss is controlled by the oxygen reduction reaction. Alloys like Ni-Hard and AISI 440C stainless exhibited sharp increases in wear rates in aerated slurries compared to deaerated slurries; in contrast, austenitic stainless steels were unaffected by aeration and were about equivalent to AISI 440C at Hardness Bracknell C (HRC) 55 to 60 and much better than Ni-Hard at HRC 65.

B. S. Phull² (written discussion)—(1) In the hub test the linear velocity varies with the radial distance from the center of the shaft. Shouldn't some attempt to document wear with linear velocity be made in this type of test? (2) Did the specimens have any scale on the surface on test completion? If so, how was the scale removed? Could the presence of the scale have contributed to improved wear resistance indication? (3) Was any attempt made to characterize the "degradation" or smoothing of slurry particles with time? (4) Was there any evidence to suggest that the slurry particles could have produced a "shot-peening effect" in the ball mill test? Metallographic examination would be the obvious way to look for this effect.

W. J. Schumacher (author's closure)—(1) No attempt was made to study the effect of linear velocity on wear in the hub test. The tip velocity was kept reasonably constant for all tests, and the data were compared within each group wear-tested at the same time. (2) The alloy steels always had some scale present after a test period, while the stainless steels had very little. A stiff, bristle brush was used to remove the scale. The retention of scale on the alloy steel specimens would result in lower weight loss readings; this would make the stainless alloys even more erosion-resistant relative to the alloy steels. (3) The quartz abrasive was used as filler and did not interact much with the specimens. The mill slag

¹ Exxon Research & Engineering Co., Florham Park, NJ 07932.

² Lague Center for Corrosion Technology, Wrightsville Beach, NC 28480.

³ Hoey, G. R. and Bednar, J. S., "Erosion-Corrosion of Selected Metals in Coal Washing Plant Environments," *Materials Performance*, April 1983, pp. 9–14.

⁴ Swan, J. D., "Controlling Corrosion and Abrasion in Preparation Plants," *Coal Age*, July, 1968, pp. 66–71.

did tend to round off, but the pea gravel was smooth to start with. If the slag caused cutting, it was only in the very beginning of the test because the wear scar quickly became polished. In the ball mill tests, the gravel was changed every 16-h period, and no significant degradation was observed. (4) Impact between the abrasives and specimen was quite low under these test conditions. However, in other sliding tests, it was definitely shown that highly deformed surface layers were present with hardness values approaching HRC 50.

Alberto A. Sagüés,¹ Diane K. Spencer,² Vijay K. Sethi,² and Gordon A. Sargent³

Slurry Erosion and Abrasion of Metal-Ceramic Coatings

REFERENCE: Sagüés, A. A., Spencer, D. K., Sethi, V. K., and Sargent, G. A., "Slurry Erosion and Abrasion of Metal-Ceramic Coatings," *Slurry Erosion: Uses, Applications, and Test Methods, ASTM 946*, J. E. Miller and F. E. Schmidt, Jr., Eds., American Society for Testing and Materials, Philadelphia, 1987, pp. 19–44.

ABSTRACT: Four coatings, including tungsten carbide wear-resistant and cobalt-base corrosion-resistant materials, were tested for abrasion and erosion performance in silica sand and in Alundum slurries. A 1018 carbon steel sample was also tested for comparison. The abrasion tests were conducted with a wet sand rubber wheel device, whereas a slurry jet impingement apparatus was used in the erosion tests. The results revealed that the abrasive wear performance improves dramatically as the coating hardness increases. By contrast, the erosion performance was not clearly related to the hardness of the materials tested. The wear mechanisms and the suitability of the test methods to evaluate coatings are discussed.

KEY WORDS: erosion, abrasion, slurry, coatings, test methods, hardness, tungsten carbide, alumina, silica, Alundum, cobalt

Introduction

Advanced fossil fuel technologies, such as coal liquefaction, tar sand processing, and state-of-the-art coal beneficiation, require the handling of slurries in conditions conducive to erosion as well as to abrasion. For example, modern direct coal liquefaction processes involve pressure letdown by several thousand psi (1 psi = 6.9×10^3 Pa) in oil streams containing typically 10% solids [1]. The operation is accomplished by means of a pressure letdown valve with an

¹ Formerly, Kentucky Center for Energy Research Laboratory, Lexington, KY 40512; presently, Department of Civil Engineering and Mechanics, University of South Florida, Tampa, FL 33620.

² Kentucky Center for Energy Research Laboratory, Lexington, KY 40512.

³ Formerly, Department of Metallurgical Engineering and Materials Science, University of Notre Dame, Notre Dame, IN 46556; presently, College of Engineering, University of Dayton, Dayton, OH 45469.

orifice or narrow channel configuration where velocities can be in the order of 100 m/s. Extensive erosive wear of these valves has been observed, leading at times to costly plant shutdowns and the rebuilding or the complete redesigning of the units affected [2]. Block valves, usually of the ball type, flank the letdown valves to isolate them for repair or maintenance purposes. The block valves must remain leak-free at the high-pressure differentials encountered, which means that their sealing surfaces are to be free of scratches or gouges. The sealing surfaces must move against each other with large normal forces while in contact with the process stream containing abrasive solids. Abrasion resistance of the sealing trim elements is thus another important materials requirement. The mechanical configuration of these critical pressure letdown and block valves is such that both erosion and abrasion may affect the same element of the component, and thus the resistance of the material to both modes of deterioration must be known and optimized.

Because the development of these new energy technologies is still in its early stages, relatively few data are available on how materials will perform under the conditions exemplified above. During the last few years, government and private industry have supported research aimed to improve the understanding of phenomena responsible for erosion and abrasion by slurries in the area of coal conversion, and to facilitate the selection of materials for those applications. Erosion studies have concentrated on: (1) the behavior of materials in slurries of actual coal-derived liquids and particulates, aimed to rank the response of valve trim materials using a jet impingement technique [3]; (2) parametric studies using well-characterized model slurries and target materials, both in rotating slurry test pots [4] and jet impingement testers [5,6]; and (3) detailed analyses of component performance and failures in actual pilot plant service [7,8]. Abrasion research directed toward the same technologies has included parametric studies and fundamental mechanistic investigations as well as hardware test plans [9,10]. Little information is available in the open literature on the comparative performance of a given material when exposed to erosive versus abrasive slurry wear conditions.

Coatings consisting of metallic binders with ceramic second phase inclusions are used in critical process components to improve their corrosion or their mechanical wear resistance. For example, the outer surface of valve balls are frequently coated with tungsten or chromium carbide-cobalt binder coatings for flow control applications in the petroleum industry. The use of similar coatings has spread to direct coal liquefaction pressure letdown train components [2]. For high-temperature applications, cobalt-based thermal barrier coatings provide corrosion resistance but at a reduced mechanical wear performance.

Because of the importance of coatings in the energy technologies, a study was initiated to establish the comparative performance of a set of these materials under erosive and abrasive conditions. A secondary objective was to determine the suitability of slurry wear test methods for thin coatings.

The materials selected included two wear-resistant coatings, which rely on

tungsten carbide for their performance. Two softer high-temperature coatings and a carbon steel sample were also included to provide a range of materials hardness and thus evaluate the effect of this parameter on abrasive versus erosive wear performance. All the coatings were applied on a carbon steel substrate. The apparatuses used in this study were a jet impingement slurry erosion tester and a wet sand rubber wheel abrasion testing (WSAT) machine.

In a preliminary phase of the study, the materials were tested using 400-grit alumina particles in the slurry jet impingement erosion tester, and using 50 to 70 grit silica sand in the WSAT device. The results revealed that while the abrasion resistance of the coatings and the steel generally improved as the hardness of the materials increased, there was no such correlation in the case of erosion. All the materials eroded at relatively comparable rates [11]. The hardness of silica was higher than that of steel and of the softer coatings, but lower than that of the harder coatings tested. Alumina, on the other hand, was harder than all of the materials tested. Erosion experiments using gas-driven particulate and slurry jets have demonstrated that the hardness of the impinging particulates can be important in determining the rate of erosion of the target material [6,12]. In the case of abrasion, it is well-established that the hardness of the abrasive relative to that of the material being worn determines the severity of the wear [13]. This led to the question of whether the difference in results obtained with the erosion versus the abrasion tests was due to a difference in the mechanism of wear or to an effect derived from the different hardness of the particulates used. To elucidate this question, the experiments were extended to include both kinds of particles in each type of test while using comparable particle sizes and an improved slurry jet erosion measuring technique. The results are reported in this paper.

Experimental

Materials

The compositions, properties, minimum-applied thicknesses, and typical service applications of the coatings are listed in Table 1. The substrate for the coatings was in all cases 1018 carbon steel. The same steel was also used as a reference standard material for comparison purposes. The hardness of the coatings was measured in Diamond Pyramid Hardness (DPH) units, using a microindenter force of 300 g. The hardness of the 1018 steel reference blocks was measured to be ~64 HRB and was converted to equivalent DPH units (~110 DPH) for comparison with other materials. The coated surfaces were ~56 mm × 25 mm (2.2 in. × 1 in.), and the substrate was 12.5 mm (½ in.) thick. Some of the erosion specimens were cut to smaller sizes to improve weighing accuracy. The coatings and substrate were supplied by Union Carbide Coatings Service, Indianapolis, Indiana. One of the coatings, LW 26, is proprietary, and its composition cannot be disclosed at this time. Additional

TABLE 1—Materials tested.

Material	Method of Application	Composition	Uses	Approximate DPH	Minimum Coating Thickness, μm
LCO-17	D-Gun, heat treated	Co-25Cr-7Al-10Ta-0.75Y-2C-0.7Si + 10% Al_2O_3	High temperature wear resistance, corrosion resistance	740	200
LCO-22	Plasma, heat treated	Co-32Ni-21Cr-8Al-0.5Y	High temperature corrosion resistance	490	200
LW-5	D-Gun, not heat treated	WC-20Cr-7Ni	Wear resistance, slurries, petroleum	1080	250
LW-26	Fused coating, heat treated	WC + binder (proprietary)	...	1150	250
1018 CS standard	110 (HRB 64)	...

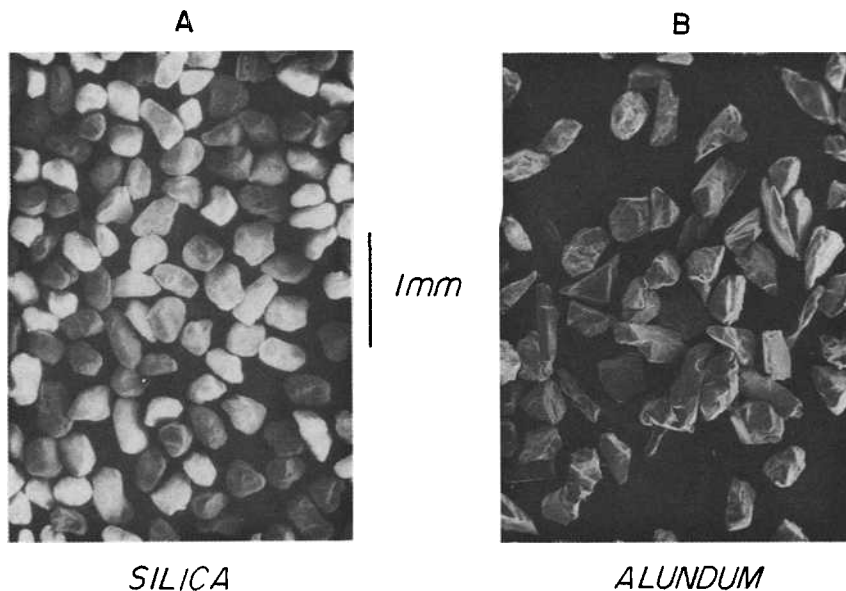


FIG. 1—(a) 50- to 70-grit silica sand particles; (b) 60-grit Alundum particles.

information on the properties and applications of some of the other coatings can be found in Refs 14 and 15.

Particulates

The silica used was 50- to 70-grit Ottawa sand, a test sand used by the American Foundrymen's Society, consisting of rounded grains (Fig. 1A). This abrasive is the one used in the standard wet abrasion test currently being developed by ASTM Committee G-2 and also in the recently developed ASTM standard, Practice for Conducting Dry Sand/Rubber Wheel Abrasion Test (G 65-84).

The alumina used was in the form of 60-grit angular Alundum particles (Fig. 1B). The Alundum was Type E-17, Alundum 1200, supplied by the Norton Co. The main impurity in the Alundum detectable by energy dispersive X-ray spectroscopy was titanium.

Abrasion Test Procedures

The wet sand abrasion tests were conducted generally following the Recommended Practice previously being developed by Division 18, Abrasive Wear of Ferrous Materials of the Society of Automotive Engineers (SAE) Iron and Steel Technical Committee, and now being established by ASTM Committee G-2.

The procedure is briefly described in following paragraphs, with some deviations used to adapt it to the nature of the materials and particles used. The test characteristics have been discussed in detail in previous literature [16–18].

The WSAT test machine has a 17.5-cm (7-in.)-diameter wheel, whose outer 1-cm (0.4-in.) rim is neoprene rubber. The wheel rotates while submerged in a slurry of 1500-g silica sand in 940 g of water. The specimen to be tested for abrasion resistance is pressed with known force [222 N (50 lb)] against the rubber wheel in a “brake shoe” arrangement. Sand particles become trapped between the rubber wheel and the specimen, with resulting wear of the specimen. The weight of the specimen before and after performing the test for a predetermined number of wheel revolutions is measured, and the weight loss determined. The specimens tested in this manner were dried in an oven at 50°C for 30 min before weighing. This was done to ensure that any water that may have been trapped in pores of some of the coatings is removed. Under the recommended procedure, a run-in of 1000 revolutions, using a wheel whose rim has a hardness of 50 Shore A Durometer, is conducted at the beginning of the test. Three tests, also consisting of 1000 revolutions each, are then performed with wheels of increasing nominal hardness (50, 60, and 70 Shore A durometer). The resulting weight losses are converted into volumes and then plotted in the form of log volume loss versus actual wheel hardness. A straight line is fitted to the data using a least squares approximation, and the ordinate intercept of that line at 60 durometer is used to define the result of the test. The test parameters used in this study are listed in Table 2.

The main deviations from the proposed Recommended Practice (SAE) involved the type of abrasive used, the number of revolutions, and for the alumina tests, the slurry density. For the silica tests, the number of revolutions used for the LCO 22 coating was 100 instead of 1000. The deviation was dictated by the high wear rate of the coating; wastage of the full thickness of the coating would have taken place during a longer test. Because of the expected highly abrasive nature of the angular Alundum particles, it was feared that excessive machine

TABLE 2—Abrasion test parameters.

Apparatus	Fargo abrasion testing machine SAE Model (wet abrasion)
Wheel diameter	175 mm (7 in.) typical
Load	220 N (50 lb) nominal
Slurry	Silica tests: distilled water, 940 g; AFS testing, sand 50 to 70, 1500 g Alundum tests: distilled water, 1500 g; Alundum 60, 225 g
Number of revolutions and run-in	1000 except as indicated in text

wear and premature coating wastage would take place if 1500-g solids/940-g water were used in the alumina tests. Therefore, a much more dilute Alundum slurry was used instead (225-g solids/1500-g water, or 13 weight %). The number of revolutions with the Alundum slurry was typically 1000 for the softer materials, except for the LCO 22 where 200 revolutions were used for the 70-durometer wheel and 2000 to 6000 for the two hardest coatings. The number of revolutions for the latter was large to obtain measurable weight losses. Measurements in the LW 5 indicated that virtually the same wear rate values were obtained with 2000 and 6000 revolution tests. The highest weight losses per 1000 revolutions in the dilute Alundum slurry tests were roughly an order of magnitude lower than those measured in the silica tests. The potentially obscuring effects of running the Alundum tests at a lower slurry density were investigated by performing a series of tests at different slurry densities.

Erosion Test Procedures

The erosion tests were conducted using the apparatus shown in Fig. 2. A stirred autoclave with a capacity of 3780 mL (1 gal) is filled with a slurry of 4 weight % solids in water and then pressurized to a regulated, predetermined value. A valved slurry transfer line ends in a 4.8-mm ($\frac{3}{16}$ -in.) nozzle that faces the material specimen to be tested at a distance of 9.5 mm ($\frac{3}{8}$ in.). The specimen can be tilted using an angle vise so that different angles of jet impingement are possible. In this investigation the measurements have been limited to only 90° impingement tests; 30° impingement tests using the same particulates are currently being planned. The test is conducted by opening the valve in the transfer line and letting a predetermined amount of slurry impinge on the specimen. The slurry velocity is computed from the length or period of time the valve was open, the amount of liquid recovered, and the dimensions of the nozzle. All tests were conducted at a nominal velocity of 17.4 m/s (57 ft/s). The test parameters used in this study are shown in Table 3. The samples were exposed to four consecutive shots of ~2000 mL of slurry, ultrasonically cleaned in methanol, dried in an oven at 85°C for 20 min, and weighed. The procedure was repeated a minimum of three times, always impinging upon the same spot. The depth of the erosion crater was measured after the last specimen exposure by means of a dial micrometer gage on a comparator table. To reduce weighing inaccuracies, the erosion test samples were smaller in size than those used in the abrasion tests. A careful weighing procedure involving the use of two analytical balances and repeat weighings was instituted. Blank runs using only water as the eroding medium, and the limitations inherent to the length of the erosion exposures, established a minimum observable rate of $\sim 10^{-6}$ g/g (typically $\sim 10^{-4}$ mm³/g) for the sample sizes and materials tested. The measured values, with one exception, were 5 to 10 times higher than the detectable limit.

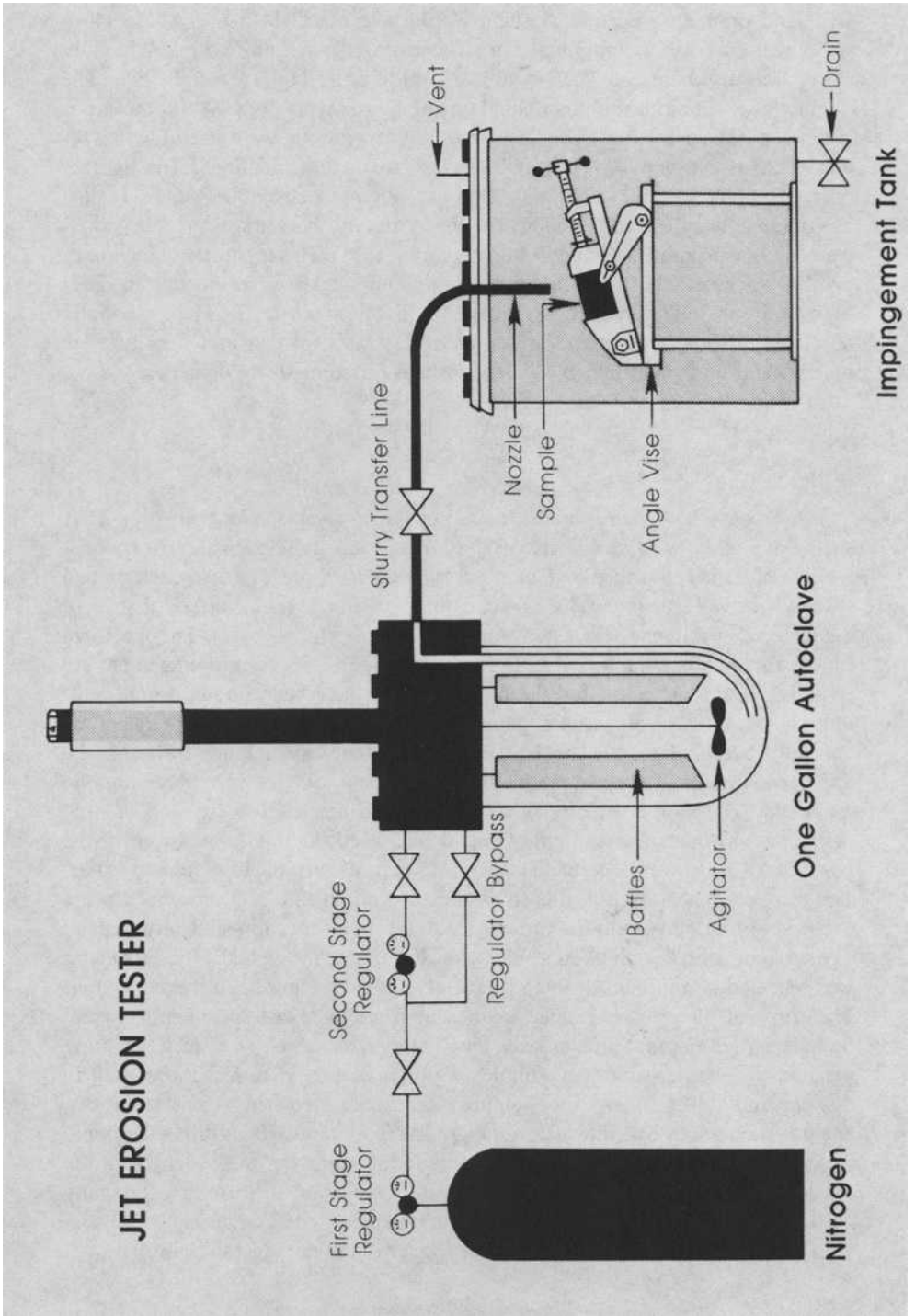


FIG. 2—Schematic of the erosion test apparatus.

TABLE 3—Erosion test parameters.

Nozzle diameter	4.8 mm ($\frac{3}{16}$ in.)
Nozzle to sample distance	9.5 mm ($\frac{3}{8}$ in.)
Jet velocity	17.4 m/s (57 ft/s) nominal
Eroding particulates	50 to 70 AFS testing sand and 60 Alundum
Slurry composition	4 wt% solids in water
Solids loading	Four times 80 g, repeated
Impingement angle	90°

Results

Abrasion Tests, Materials Loss

Silica—The materials loss results for the silica runs are presented in Fig. 3 as mm³ lost per 1000 revolutions, as a function of the measured wheel durometer. It should be noted that the results for the LCO 22 have been extrapolated from 100-revolution exposures. The materials ranking remains the same for all three wheel durometers. There is relatively little experimental scatter within each three-wheel sequence, especially for the materials showing the highest wear. Repeat tests conducted with the 60-durometer wheel confirmed the same materials ranking.

The 60-durometer intercepts are plotted in Fig. 4 as a function of the hardness of the material tested. For the coatings, the wear rates follow a decreasing trend with increasing hardness of the material tested. The carbon steel is out of the sequence but still presents a high wear rate commensurate with its low hardness. There is a very large difference, two to three orders of magnitude, between the abrasive wear resistance of the LW 26 and that of the LCO 22 or the carbon steel.

Alundum—Figure 5 shows the material losses as a function of wheel durometer for the Alundum runs. The materials performance ranking is, as in the case of the silica sand tests, virtually the same for all three durometer wheels. The materials ranking is also the same as in the silica sand tests, with the difference between the LCO 22 and the 1018 carbon steel not as pronounced.

The 60-durometer intercepts are plotted in Fig. 6 as a function of the material hardness. Again, a trend of increasing wear resistance with material hardness is observed. The ratio between the abrasive wear resistance of the best performer (LW 26) and the worst ones (LCO 22, 1018 carbon steel) is still large, approximately a factor of 50, but not as high as it was in the case of the silica sand.

The Alundum tests were performed at a much lower slurry density than that of the silica tests. To establish whether that may prevent a valid comparison between the relative behavior of the materials under both abrasives, some slurry density variation tests were performed. Materials at the extremes of observed

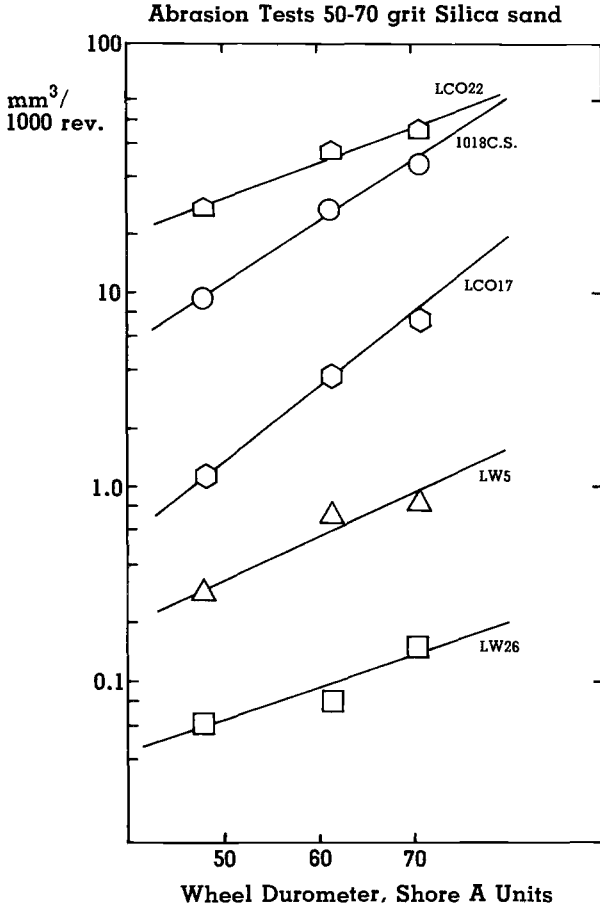


FIG. 3—Volume loss per 1000 revolutions in wet rubber wheel silica abrasion tests of the five materials examined. The LCO 22 values are extrapolated from 100 revolution tests.

wear performance, namely 1018 carbon steel and LW 26, were tested with the 70-durometer wheel (for easily measurable weight loss) at three slurry densities: 7, 13, and 23 weight %. The results are shown in Fig. 7. The logarithm of the volume loss per 1000 revolutions approximates a linear function of the slurry density within the variable interval tested. More importantly, the ratio of wear of one material to that of the other remains quite constant in the slurry concentration range tested. Also shown in Fig. 7 are data for carbon steel obtained with silica slurries of various densities, this time extending to the value used in the standard test. Over this larger concentration interval, the data suggest a deviation from a simple linear graphic relationship. Notice that at 13% slurry concentration the wear rate of carbon steel with silica is several times smaller than with Alundum.

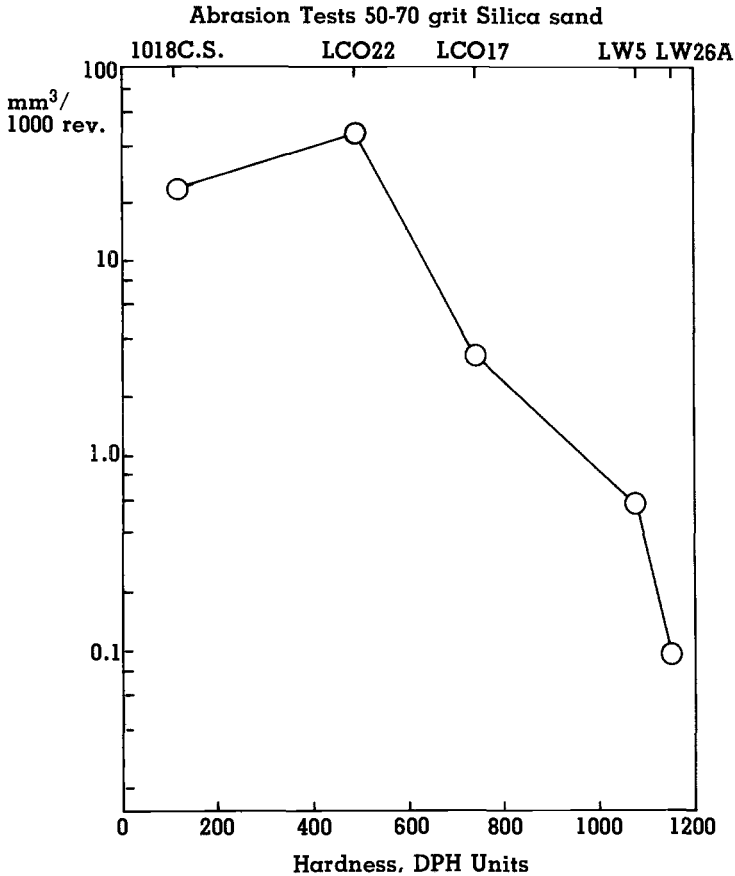


FIG. 4—60-durometer intercepts of volume loss per 1000 revolutions in wet rubber wheel silica abrasion tests, as a function of the hardness of the materials examined. The LCO 22 values are extrapolated from 100 revolution tests.

Erosion Tests, Materials Loss

The weight losses experienced after every set of four consecutive shots were converted into erosion rates and evaluated statistically. For each material and erodent, the average erosion rate of all sets and the average erosion rate of all sets minus the first were evaluated. The two averages were found to be very similar in every case, suggesting that steady-state erosion rates are reached early during the exposure sequence. Nevertheless, the first set in each case was considered as a run-in and not used to compute the reported erosion rate value.

Figure 8A shows the erosion rates so evaluated, expressed in mm³/g of erodent for all materials and erodents tested. Dial gage measurements of the erosion

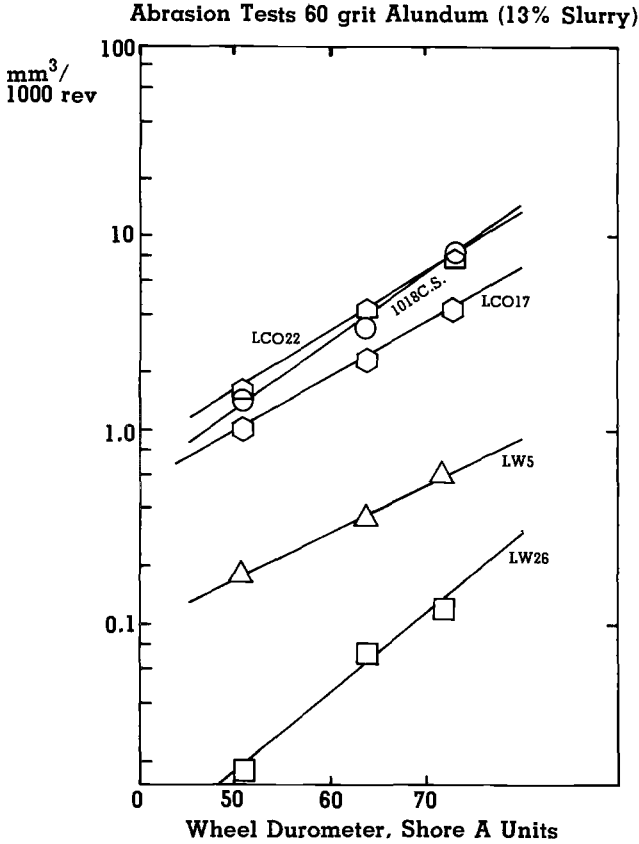


FIG. 5—Volume loss per 1000 revolutions in wet rubber wheel Alundum abrasion tests of the five materials examined. The slurry density and numbers of revolutions used are nonstandard.

crater depth were also made for all the specimens tested and are reported in Figure 8B as $\mu\text{m/g}$ of erodent. All craters had a visible diameter of roughly 8 mm. Within the experimental scatter characteristic of the measuring techniques used, the dimensional change and weight loss data are in reasonable agreement.

A striking feature of the erosion results is that, with the possible exception of the LW 26 eroded with silica, the erosion rates of all coatings deviate typically by a factor of two or less from that of carbon steel. The silica-eroded LW 26 cannot be ranked adequately because its average erosion rate, evaluated with the most accurate method (weight loss), is only about twice as high as the minimum detectable value.

The erosion data are plotted with the same vertical logarithmic scale factor used in the presentation of the abrasion results. A comparison of Figs 4 and 6

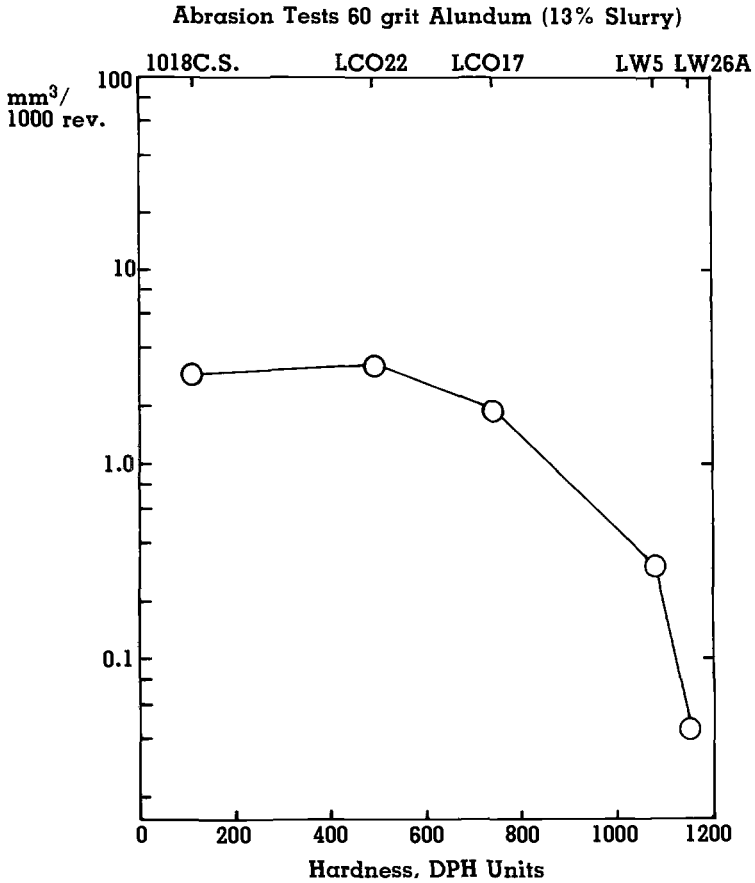


FIG. 6—60-durometer intercepts of volume loss per 1000 revolutions in wet rubber wheel Alundum abrasion tests, as a function of the hardness of the materials examined. The slurry density and numbers of revolutions used are nonstandard.

with Fig. 8 reveals the large difference of dependence on materials hardness for both modes of wear. While the abrasive wear shows a strong decreasing trend with increasing material hardness, the erosion data show little correlation with hardness; the materials erode at comparable rates in most cases.

Wear Morphology

Abrasion Tests—The surfaces of the abraded samples were examined with a scanning electron microscope (SEM). Near the center of the abrasion scar, on the softer materials (carbon steel, LCO 22) mainly straight, long scratches were

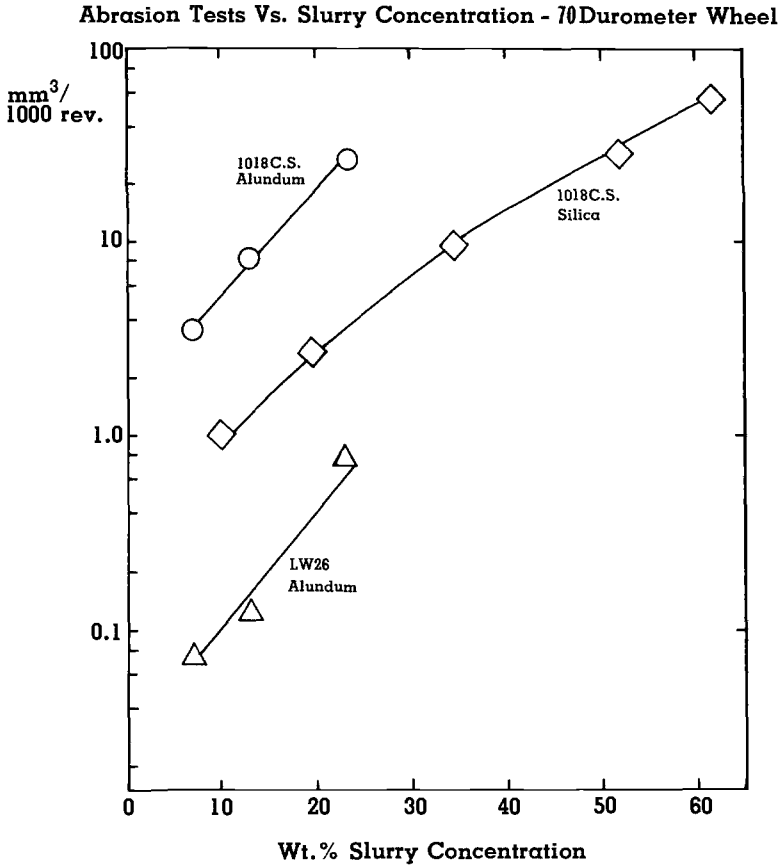


FIG. 7—Volume loss per 1000 revolutions in wet rubber wheel abrasion tests using various silica and Alundum slurry concentrations, and the 70-durometer wheel.

observed. The appearance was similar for the Alundum-and-silica-tested samples, as illustrated in Fig. 9 for the LCO 22 coating. The width of the scratches was much smaller than the particle size of either abrasive, but the scratches tended to be more pronounced for the Alundum-abraded samples. The surface appearance is characteristic of that expected from soft and ductile materials [18]. The harder coatings (LCO 17, LW 5, and LW 26) also showed long scratches. However, these were generally narrower than those observed from the LCO 22 and the carbon steel. In some cases the scratches were almost invisible. The surface appearance tended to be less uniform for the harder materials, with some evidence of localized damage. Figure 10 shows the Alundum-and-silica-abraded surfaces of the LCO 17. Surface singularities are probably the result of precipitates intersecting the specimen surface. The LW 5,

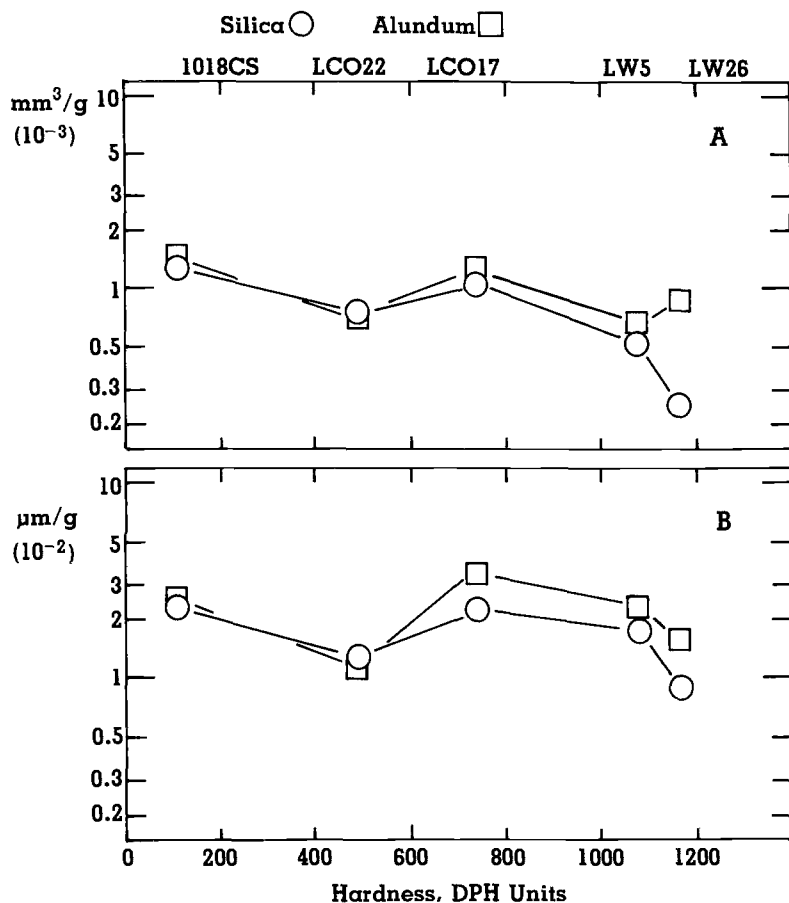


FIG. 8—(a) Erosion rates, evaluated for both erodents from weight loss measurements, as a function of the hardness of the materials examined; (b) Erosion crater depth divided by total weight of solids impinging on the crater, as a function of the hardness of the materials tested. The crater diameter was ~ 8 mm. Both graphs are plotted using the same logarithmic scale as in Figs. 4 and 6. All erosion tests are at a 90° particle impingement angle.

which had not undergone a postdeposition heat treatment, has a high degree of initial porosity. These pores are revealed in the abraded surface, as in Fig. 11, which shows the Alundum-and-silica-abraded surfaces. Part of the irregularities on the surface are due to the tungsten carbide (WC) precipitates in the alloy. The Alundum-abraded sample shows linear scratches finer than those observed on the softer coatings. The linear scratches on the silica-abraded LW 5 are still present, but they are barely detectable. The LW 26-abraded surface reveals the microstructure of the coating, which contains large carbides. Examination at high magnification suggests that some of these precipitates may have cracked

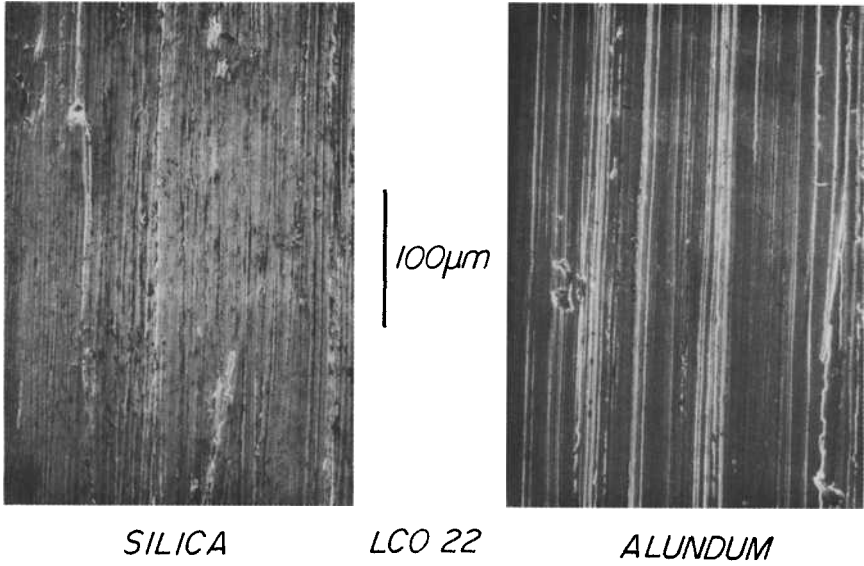


FIG. 9—Appearance of the surface near the center of the abrasion scar for the LCO 22 tested with Alundum and silica.

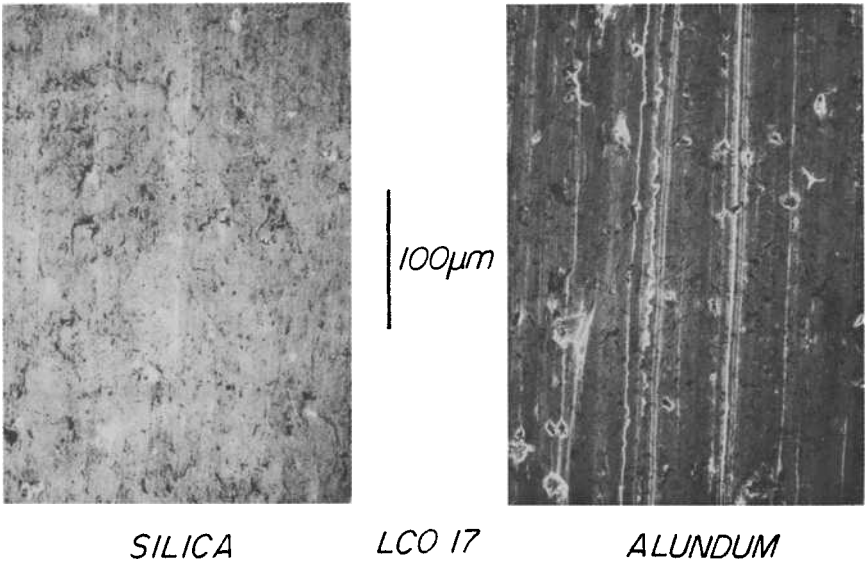


FIG. 10—Appearance of the surface near the center of the abrasion scar for the LCO 17 tested with Alundum and silica.

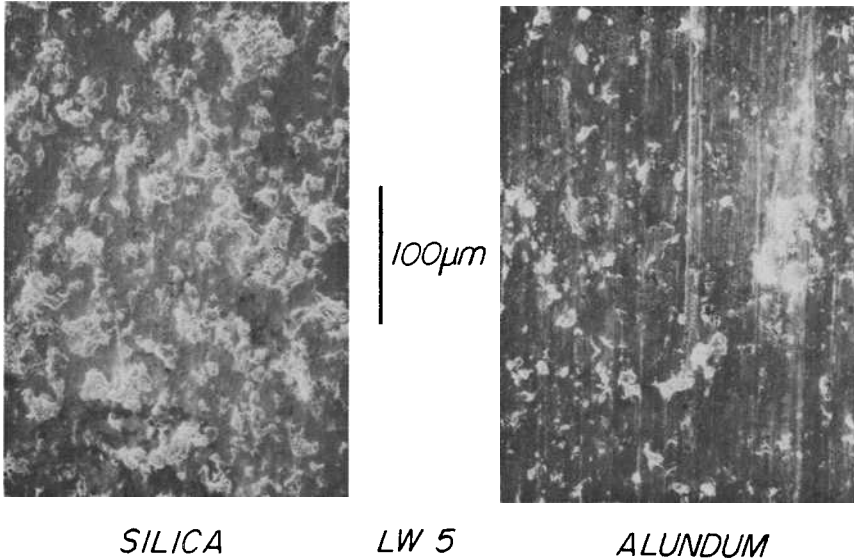


FIG. 11—Appearance of the surface near the center of the center of the abrasion scar for the LW 5 tested with Alundum and silica.

during the abrasion test and that some portions may even have dislodged from the binder.

Erosion Tests—The surface morphology of the carbon steel, LCO 22 and LCO 17 samples eroded with Alundum, did not show dramatic qualitative differences from material to material. In all cases, at the center of the erosion crater the topography consisted of apparently overlapping impacts, with plastic shear lips. This is exemplified in Fig. 12A for the case of the LCO 17. The typical distance between the lips was in the order of micrometers, much smaller than the average size of the eroding particles themselves. Toward the edge of the erosion crater the damage was quite directional and, as in the center of the crater, suggestive of significant plastic deformation. The LW 5 (Fig. 12B) and the LW 26 tended to show less of a ductile appearance at the center of the crater, although shear lips were conspicuous near the edges.

The samples of carbon steel, LCO 22 and LCO 17 eroded with silica, showed the same general features as their Alundum-eroded counterparts (Fig. 13A). Although the silica particles are much less angular than the Alundum particles, the typical size of the microfeatures on the surface of these three materials was about the same for either erodent. The LW 5 and LW 26 showed even less evidence of plastic deformation (Fig. 13B) than in the Alundum case at the center of the crater and at the edges.

Unlike the case of the abraded surfaces, little evidence of the heterogeneous microstructure of the coatings could be derived from the appearance of the

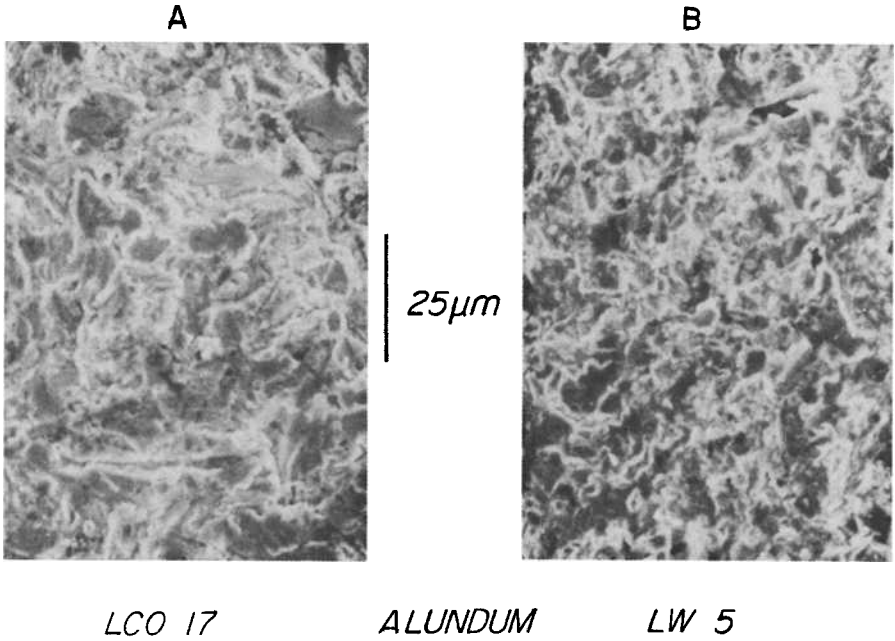


FIG. 12—Appearance of the 90° Alundum-eroded surfaces for (a) LCO 17 and (b) LW 5, near the center of the erosion crater.

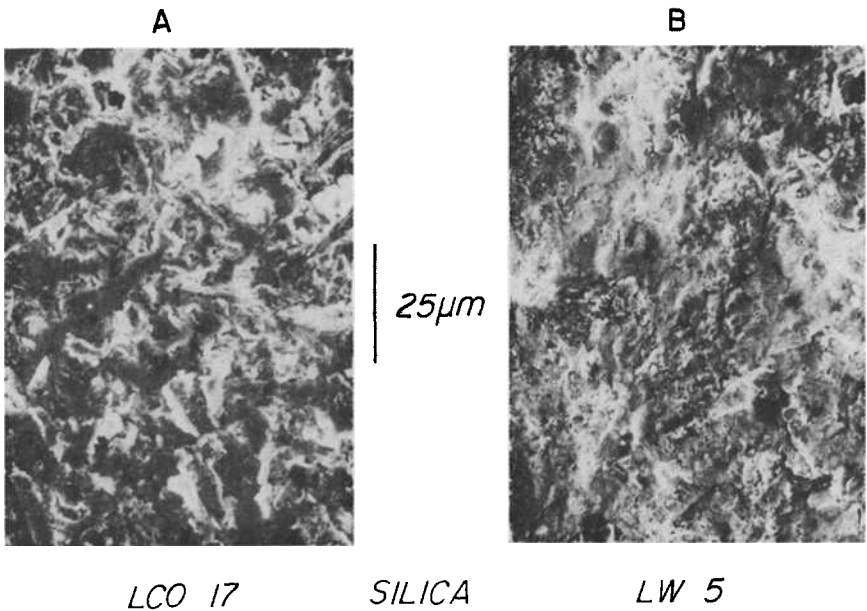


FIG. 13—Appearance of the 90° silica-eroded surfaces for (a) LCO 17 and (b) LW 5, near the center of the erosion crater.

eroded surfaces. Only the LW 26 eroded with silica tended to show occasional precipitates among the erosion features. The porosity of the LW 5 was not readily apparent in the SEM micrographs of the samples tested with either erodent.

Discussion

Abrasion Performance

The abrasion behavior of the coatings and the base metal follows general trends of decreasing wear with increasing material hardness. This is observed for the two abrasives tested. The ratio of wear of the softest to wear of the hardest materials is less when using Alundum than when using silica particles. This is in keeping with the idealized behavior outlined by Farmer [13]. An abrasive of intermediate hardness (silica, ~750 DPH) would indent and wear the softer materials but cause little or no wear in the harder coatings. The Alundum (~2100 DPH), harder than all the materials tested, would cause finite wear on all of them and thus compress the range of response. Although this is generally observed, the situation is complicated because of the heterogeneous nature of the coatings, some of which consist of a mixture of hard and soft phases. The indentation measurements used to determine hardness represent intermediate values and do not predict how individual components in the microstructure will wear. The microstructural observations of the abraded surfaces revealed well-defined abrasion scratches when using silica for portions of the surface of even the hardest coatings. Those portions, scratched either by the silica or by dislodged carbides, presumably correspond to the softer phases. Conversely, the carbides and other precipitates in the coatings have hardness values of the same order as Alundum and will increase the resistance to abrasion by Alundum above that expected from the measured values of indentation hardness. Thus, the transition in relative response observed here as a result of using Alundum instead of silica is probably less abrupt than that which would be observed with homogeneous materials of equivalent hardness.

The use of different slurry concentrations for the Alundum and silica tests permits only comparisons of the relative behavior between materials, but not of absolute values. The work by Swanson and Klann [18] indicates that angular particles, as the Alundum used here, result in much greater volume loss in steel relative to that observed when using the rounded silica sand. On that basis, the softer materials used in this study could be expected to show greater volume loss in Alundum tests than on silica tests of equal slurry concentration. This is verified for the case of carbon steel, by the data in Fig. 7. For the harder materials, not only the angularity of the particles but also the heterogeneous nature of the test material itself, as just mentioned, become important. The interaction of all these factors is complex, and additional experiments (for

example, tests with angular silica particles) would be required to better separate the variables involved.

Abrasion Test Method

The WSAT has been the subject of continuing improvement and increasing reliability [17]. For bulk materials it offers with reasonable reproducibility a relative measurement of wide-stress-range abrasion resistance [17]. The use of a reduced number of revolutions for the LCO 22 in some of the runs is a necessary compromise to avoid wearing through the coating. This reduction, which may introduce significant extrapolation errors when used for some thin, hard coatings [19], does not appear to be a problem for softer materials. The hard coatings evaluated with silica as the abradant suffered very small weight losses. The relative error of these measurements is expected to be large, and the use of a higher number of revolutions may be a way of improving the accuracy in future measurements.

Possible undesirable deterioration of the test machine precluded the use of a standard slurry concentration during the alumina abrasion tests. The evidence presented in Fig. 7 indicates that the ratio of wear between two extreme materials does not appear to be a significant function of the slurry concentration, at least within the concentration range studied. Changing the slurry density in the wet sand test is somewhat analogous to changing the sand feed rate in the Dry Sand Rubber Wheel Abrasion Test (DSAT), which is described by ASTM G 65-84. Avery [17] has developed a quantitative description for varying the sand feed rate in the DSAT and showed how reducing the feed rate reduces the opportunity factor for abrasion but increases the severity factor because the applied load per particle becomes higher. That analysis assumed that there was no direct contact between the rubber wheel and the specimen surface. In the WSAT it is not possible to make a similar straightforward analysis because the equivalent sand feed rate is unknown. It can only be qualitatively expected that the opportunity factor will be less at lower slurry densities. The results in Fig. 7 would indicate that the effects of changing the opportunity factor are greater than those resulting from any corresponding changes of the severity factor in the opposite direction. The changes in the severity factor cannot be evaluated because, even though the hardest wheel (70 durometer) was used in the slurry density tests, it is not known whether enough particles were present to prevent direct wheel contact with the specimen. Nevertheless, the observation that the ratio of wear of carbon steel to wear of LW 26 does not change over the Alundum concentration range studied suggests that the abrasion mechanisms of each material follow similar dependences on the applied load per particle and (if any) on the area density of particles in the rubber-specimen contact zone. At least for this investigation, where large relative differences of wear response from material to material exist, the just-stated observations appear to indicate that the materials ranking should not deviate significantly if higher slurry concentrations are used.

A final comment involves the depth of the material affected by the abrasion tests. For carbon steel and the softer coatings, a significant percentage of the coating thickness is penetrated during the test. For the more wear-resistant coatings, the depth of penetration even after several thousand revolutions is only a few micrometers. Caution should be exercised in interpreting these results since the outer surface of the coating may have significantly different properties from those deeper in. Longer run-in exposures may be an improvement to be considered in the development of future procedures for surface-modified materials.

Erosion Performance

The magnitude of the observed erosion rates (~ 0.3 to 1×10^{-3} mm³/g, or ~ 3 to 10×10^{-6} g/g) is of the same order as reported for comparable hard material-particle combinations by other investigators. For example, Elkholy [6] reports wear rates of $\sim 1.5 \times 10^{-3}$ mm³/g ($\sim 12 \times 10^{-6}$ g/g) for cast iron eroded at 90° by water slurry of 0.4- to 0.5-mm-diameter sand at an interpolated velocity of 17.3 m/s (57 ft/s). He also found that the erosion rate at 60° impingement was only slightly lower than that at 90°. Levy and Yan [20] report erosion rates of $\sim 4 \times 10^{-4}$ mm³/g ($\sim 3 \times 10^{-6}$ g/g) for carburized AISI 8620 steel eroded at 30° by a 20- to 40-mesh sand-water slurry at the same velocity. Data for 90° impingement were not given, but investigations using the same apparatus [5] with other slurries and a variety of other target materials indicated that erosion rates at 90° were typically 1½ to 2 times higher than those at 30°. It is interesting to notice that the erosion rate obtained in the present investigation for the carbon steel is of the same order of magnitude as values extrapolated from data reported by Levy and Chik [12] for 1020 carbon steel eroded at 90° by 180 to 250 μm alumina in an air jet at 80 m/s. Assuming a velocity exponent $n = 2.25$ [21], one obtains $\sim 6 \times 10^{-4}$ mm³/g ($\sim 5 \times 10^{-6}$ g/g) as the expected erosion rate at 17.3 m/s, which compares well with the present values.

Because the measured erosion rates for coatings were generally close to that of the carbon steel used as a substrate, special attention was given during the tests to ensure that the coating had not been unknowingly penetrated, thus erroneously ascribing the erosion behavior of the carbon steel to the coatings. The measurements of the depth of the erosion crater revealed that typically 10 to 20% of the thickness of the coating had been penetrated during the tests used in computing the erosion rates. It can be concluded therefore that the observed erosion behavior is indeed representative of the coatings as applied on their substrate.

The erosion response of the materials tested, with the possible exception of the LW 26 eroded by silica, is not clearly related to the hardness of the target and bears little relationship to the observed abrasion behavior. As indicated in the Introduction, the earlier results, where erosion by alumina was of the same order for all the materials, could have been interpreted as a result of alumina

being harder than all those materials. That does not appear to be the case. The complementary silica tests reported here show that even with an erodent softer than some of the coatings, all the materials (with one possible exception) erode at comparable rates. The possible exception involves the hardest coating (LW 26). However, the LW 5, which is very close in hardness to the LW 26, shows wear rates comparable to those of the softer materials. Elkholy [6] examined the effect of varying the ratio of hardness of the erodents to that of the target material in sand slurry erosion. He found that erosion increased as the ratio increased until a critical ratio (typically ~ 2) was reached. Above that the hardness ratio had a lesser effect on the erosion rate. Levy and Chik [12] observed a similar behavior in air-driven tests. The absence of that type of a clear transition in the present results may be related to the heterogeneous nature of the coatings (as was pointed out in the discussion of the abrasion results). Softer portions of the structure may be undergoing deformation under particle impact, even though the average hardness of the material is high. In the case of the LW 5, the porosity of the coating may have also contributed to make its erosion performance with silica not as good as what one would have expected from simple hardness ratio considerations. This is discussed in more detail in the section entitled Erosion Test Method.

The microstructural evidence supports the idea that plastic deformation plays an important role in most of the cases, with the possible exceptions of the LW 5 and LW 26 eroded with silica. The observed microstructure is compatible with an erosion mechanism involving extrusion lip formation, and detachment either simultaneously or after subsequent impacts. These mechanisms can be operational under 90° impact and have been described in detail in the literature [22–24]. The LW 5 and LW 26 silica-eroded microstructures suggest that brittle fracture may be the predominant element in material removal, at least in these 90° tests.

Erosion Test Method

The experimental complications of testing erosion by slurries exceed those encountered in conventional gas-driven solid particle erosion tests. The slurry velocity chosen for these tests represents a compromise between using a velocity slow enough to be easily determined, and yet high enough to result in measurable erosion rates.

An unconstrained slurry jet originating from a pressurized container is likely to develop a complex three-phase flow, without a well-defined angle of particle impingement and particle impact velocity. In pneumatically pressurized systems as the present one is, velocity transients can occur due to the entry of driving gas into the transfer line, particularly near the end of a run. This can result in higher effective average test velocities and a corresponding increased target wear. This complication, present in our preliminary work [11,25], was minimized in this investigation by means of an improved slurry agitation configuration and

control method, and by leaving about one fourth of the slurry still in the autoclave at the end of the run.

Gas intrusion in transfer lines cannot be totally prevented and may be an important factor affecting reproducibility of test results from different laboratories. Conversely, for ranking studies such as the present one, the test conditions are similar for all materials and comparative behavior can still be established. Difficulties may arise when the test conditions are near a material's threshold response parameters. For example, during preliminary tests conducted while significant gas intrusion was suspected in the transfer line, the LW 5 showed an erosion rate at 90° impingement several times higher than those of the other materials. Cracks were observed initiating at the pores of this eroded material. After the measures to minimize gas intrusion were implemented, the LW 5 showed no distinctive erosion performance. Presumably, the kinetic energy per particle during velocity transients was high enough to initiate and propagate cracks that could not have developed during tests conducted at the nominal test velocity. It is expected that tests conducted with the present equipment configuration, but at higher velocities, would again show higher relative wear of the LW 5 once a velocity threshold is exceeded. Levy et al. [25] have shown evidence of the sensitivity of coatings to test conditions in air-driven solid particle erosion experiments.

The angle of particle impingement, as evidenced by the eroded surface morphology reported earlier, represents a range of values instead of the nominal 90° ascribed to the tests. This is likely to account for the absence of a strong dependence of erosion on the nominal angle of impingement reported in other investigations using unconstrained jets [5,26]. Based on that, and on preliminary tests conducted with these coatings at 30° nominal impingement with silica, the relative material performance reported here is expected to be roughly representative of that measured at lower nominal angles of impingement. Important deviations may occur at very small angles of impingement because of the different brittle-ductile response of the materials tested, or in cases where a threshold phenomenon exists, such as that just mentioned for the LW 5. A more accurate evaluation of the angular dependence of erosion can only be conducted with elaborate test geometries, such as the constrained, two-dimensional stream arrangement reported elsewhere in these proceedings [27].

Another factor affecting angle of impingement dependence measurements is the evolution of crater geometry during the time a test is conducted. In these experiments the crater aspect ratio (depth/width) was always very low (typically, $<5 \times 10^{-3}$), and its effect should be negligible.

Corrosion in the impingement zone cannot be separated from erosion in this test arrangement. For the carbon steel, the erosion crater surface was visibly discolored between tests. A series of short consecutive tests, with some corrosion as observed between tests, may produce a measured wear rate per gram of erodent higher than that observed in a continuous test. The carbon steel erosion rates reported here may be affected that way. The coatings showed no observable

corrosion products on their eroded surfaces. However, some corrosion of the carbon steel substrate took place during the normal exposure procedure. Blank runs, conducted with water only and no solids, revealed that the resulting weight change was of the same magnitude as the resolution limit of the weighing techniques. Virtually no erosion damage was observed during the blank runs.

Summary

The most striking result of this investigation is the different response of the materials when tested under erosive versus abrasive conditions using exactly the same kind of particles. Whereas the abrasion response appears to follow a generally predictable relative ranking strongly affected by the hardness of the materials, no such general conclusion can be made for the erosion behavior at 90° impingement. The effects of using particles of different hardness and geometries are, in the case of heterogeneous coating structures, less defined than those expected in the wear of more homogeneous materials. The results underscore the need for a better understanding of the mechanisms leading to erosive wear if reliable predictive laboratory tests are to be used to select materials and coatings. Under these circumstances, actual field tests and applications experience appear to be a mandatory complement to investigations under controlled conditions.

The wet rubber wheel abrasion test appears to differentiate well the materials tested. The slurry jet erosion test technique, although conceptually simple, is sensitive to many experimental parameters. Additional research is needed to establish its potential as a standard technique.

Acknowledgment

The authors are indebted to Tim Abner and Don Parrish for assisting with the erosion measurements, and to Godwin Oghide, Karla Thompson, and V. Carol Hill for performing the abrasion tests. Drs. M. Keshavan and Robert Tucker of Union Carbide Coatings Service provided the sample materials and helpful discussions of the test results. Funding was provided by the Kentucky Department of Energy Research and Development, Kentucky Energy Cabinet.

References

- [1] Jones, J. P., Buchheim, G. M., Lendvai-Lintner, E., and Sorell, G., "Materials Performance in the EDS Coal Liquefaction Pilot Plant," Paper No. 80, Corrosion/84, National Association of Corrosion Engineers, Houston, TX, 1984.
- [2] Bond, N. D., "H-Coal Pilot Plant High Pressure and Temperature Let-Down Valve Experience," *Proceedings 1981 Symposium on Instrumentation and Control for Fossil Energy Processes*, ANL-81-62, CONF-810607, Argonne National Laboratory, Argonne, IL, Jan. 1982, p. 654.
- [3] Clauer, A. H., Wright, I. G., and Shetty, D. K., "Slurry Erosion of Let-Down Valve

- Materials," International Symposium on Slurry Erosion: Uses, Applications, and Test Methods, Denver, CO, June 1984, ASTM, 1916 Race St., Philadelphia, PA.
- [4] Levy, A. and Hickey, G., "Liquid-Solid Particle Slurry Erosion of Steels," LBL-17239, Lawrence Berkeley Laboratory, Berkeley, CA, April 1984.
- [5] Levy, A. and Yau, P., "Erosion of Steels in Liquid Slurries," LBL-15658, Lawrence Berkeley Laboratory, Berkeley, CA, Dec. 1983.
- [6] Elkholy, A., *Wear*, Vol. 84, 1983, pp. 39-49.
- [7] Sagüés, A., Sethi, V., Ganesan, P., Ragle, H., and Searles, R., *Journal of Materials for Energy Systems*, Vol. 6, 1984, pp. 87-99.
- [8] *Materials and Components in Fossil Energy Applications*, a DOE newsletter, DOE/FE-0053/51, Department of Energy, Washington, DC, 1 Aug. 1984 and previous issues.
- [9] Shetty, H. R., Kosel, T. H., and Fiore, N. F., *Wear*, Vol. 84, 1983, pp. 327-343.
- [10] Gardner, J. F. and Holtz, T. R., "Prototype Lockhopper Valve Testing and Development Project Test Plan," DOE/MC-143, Department of Energy, Washington, DC, April 1981.
- [11] Sagüés, A., Sargent, G., and Spencer, D., "Slurry Abrasion/Erosion Behavior of Metal-Ceramic Coatings," Proceedings of the 37th MFPG Meeting, *Mechanical Properties, Performance and Failure Modes of Coatings*, National Bureau of Standards, Washington, DC, 10-12 May, 1983.
- [12] Levy, A. and Chik, P., *Wear*, Vol. 89, 1983, p. 151.
- [13] Farmer, H. N., "Factors Affecting Selection and Performance of Hard Facing Alloys," in *Proceedings, Symposium on Materials for the Mining Industry*, Vail, CO, July 1974, R. Q. Barr, Editor, Climax Molybdenum Co., Greenwich, CT, 1975, p. 85.
- [14] Quets, J. M. and Tucker, R. C., *Thin Solid Films*, Vol. 84, 1981, p. 107.
- [15] Taylor, T. A., *Journal Vacuum Science and Technology*, Vol. 12, 1975, p. 790.
- [16] Borik, F., "Rubber Wheel Abrasion Test," Paper 700687, Society of Automotive Engineers, New York, NY, 1970.
- [17] Avery, H. S., "An Analysis of the Rubber Wheel Abrasion Test," in *Wear of Materials 1981*, Proceedings of the International Conference on Wear of Materials, March 30-April 1981, American Society of Mechanical Engineers, New York, 1981, p. 367.
- [18] Swanson, P. A. and Klann, R. W., "Abrasive Wear Studies Using the Wet-Sand and Dry Sand Rubber Wheel Tests," in *Wear of Materials 1981*, Proceedings of the International Conference on Wear of Materials, March 30-April 1981, American Society of Mechanical Engineers, New York, 1981, p. 379.
- [19] Saltzman, G. A., "Wet Sand Rubber-Wheel Abrasion Test for Thin Coatings," Selection and Use of Wear Tests for Coatings, ASTM STP 769, R. G. Bayer, Ed., American Society for Testing Materials, Philadelphia, 1982, pp. 71-91.
- [20] Levy, A. and Yan, J., "Sand-Water Slurry Erosion of Carburized AISI 8620 Steel," LBL-17241, Lawrence Berkeley Laboratory, Berkeley, CA, May 1984.
- [21] Foley, T. and Levy, A., *Wear*, Vol. 91, No. 1, 1983, pp. 45-64.
- [22] Shewmon, P. and Sundararajan, G., *Annual Review of Material Science*, Vol. 13, 1983, pp. 301-318.
- [23] Sundararajan, G., *Wear*, Vol. 84, 1983, pp. 217-235.
- [24] Levy, A., "The Platelet Mechanism of Erosion of Ductile Metals," LBL-15240, Lawrence Berkeley Laboratory, Berkeley, CA, May 1984.
- [25] Levy, A., Bakker, T., Scholz, E., and Azadabeh, M., "Erosion of Hard Metal Coatings," in *High Temperature Protective Coatings*, S. C. Singhal, Ed., The Metallurgical Society of AIME, New York, NY, 1983, p. 339.
- [26] Sargent, G. A., Spencer, D. K., and Sagüés, A., "Slurry Erosion of Materials," in *Corrosion-Erosion-Wear of Materials in Emerging Fossil Energy Systems*, Proceedings of the January 27-29, 1982 Conference in Berkeley, CA., Al Levy, Ed., National Association of Corrosion Engineers, Houston, TX, 1982, p. 196.
- [27] Roco, M. C., "Test Approach for Dense Slurry Erosion," this publication.

DISCUSSION

*K. Metz*¹ (*written discussion*)—(1) Have you tried any “Hipped” coatings, which are supposed to decrease the porosity of cemented carbides? (2) Have you tried any of the amorphous or RSP microcrystalline alloy powders that are supposed to have “good” wear and corrosion properties? (3) How about some of the ionboronizing processes—they may have fewer cracks or porosity. (4) How did you determine the actual velocity of the slurry hitting the test pieces? (5) What do you think is the maximum velocity achievable with your apparatus? (6) Did you see any wear on the nozzle itself?

A. Sagiés, D. Spencer, V. Sethi, and G. Sargent (authors' closure)—(1–3) Up to now, we have test results only for the materials presented in the paper. Depending on the availability of personnel and funding, we may continue testing using some cobalt-base hard facings. (4) The jet velocity was indirectly determined by measuring the volume of liquid transferred during the amount of time the valve was open. The resulting volumetric rate was converted into a linear speed by dividing by the area at the tip of the nozzle. (5) We have achieved velocities of ~40 m/s with the present nozzle configuration. A smaller nozzle may permit reaching perhaps 100 m/s. (6) The nozzle did show some minor wear in the form of a uniform broadening of its bore. The nozzle dimensions were measured frequently to ensure consistent velocity calibration. Nozzle replacement was rarely needed.

¹ Dresser Industries—Security Division, P.O. Box 24647, Dallas, TX 75224.

Process (Fuel) Slurries

The Relative Erosivity of Coal-Oil, Coal-Water, and Petroleum Coke-Oil Slurries

REFERENCE: Lee, Y.-H. and Clark, H. McI., “**The Relative Erosivity of Coal-Oil, Coal-Water, and Petroleum Coke-Oil Slurries,**” *Slurry Erosion: Uses, Applications, and Test Methods, ASTM STP 946*, J. E. Miller and F. E. Schmidt, Eds., American Society for Testing and Materials, Philadelphia, 1987, pp. 47–61.

ABSTRACT: The relative erosivity (defined as the ratio of the rate of mass loss from a target specimen tested in one slurry and the rate of mass loss in another slurry) for coal-water, coal-oil, and petroleum coke-oil slurries has been determined using pot testers with a rotating flat-plate specimen of either mild steel or 304 stainless steel with a tip speed of 18.3 m/s. Pittsburgh No. 8 seam coal and Whiting medium sulfur coke, both ground to passing 200 mesh, were used together with high flash distillate fuel oil. Slurry viscosity was measured before and after testing, and surface damage was examined using the scanning electron microscope. The effects of slurry concentration (solids loading), velocity, and target material were noted. Evidence of erosion-corrosion was observed for slurries with added stabilizers and for water-based slurries. The erosivity increased in the order coke-oil, coal-oil, coal-water and with increasing solids loading up to about 50% after which a decrease was observed. Comments on problems of erosivity measurement using pot testers are included.

KEY WORDS: erosion, coke, petroleum coke, coal, slurry, erosivity, pot tester, erosion-corrosion, mild steel, stainless steel, velocity, concentration, slurry stability

In recent years, increasing attention has been paid to the need for the adaptation of industrial boiler facilities for the utilization of different fuels. The situation has been brought about in part by sharp changes in the price and availability of suitable fuels and by environmental regulation. As the price of fuel oil has risen in the last decade, the advantages and problems associated with the combustion of slurry fuels in fuel oil-fired boilers have received greater consideration, although work with such fuels has a long history [1,2]. Problem areas include

¹ Graduate student and associate professor, respectively, Mechanical Engineering Department, University of Kansas, Lawrence, KS 66045.

slurry instability (the tendency of suspended solid particles to settle out of the slurry during storage), combustion characteristics, ash and pollution control, the need to minimize changes in the boiler combustion system, and wear and erosion of combustion nozzles, valves, and pipework in the fuel-handling system. At the same time, work on materials for severe temperature or corrosion conditions has expanded greatly, leading to an improved understanding of the important factors governing erosive wear [3].

The present work is concerned with assessment of the erosivity of petroleum coke powder as a solid component in oil slurries. No standardized test exists for the determination of slurry erosivity under all conditions. In order to obtain flow velocities similar to those prevailing in industrial oil combustion nozzles, a test apparatus was designed incorporating a metal specimen rotating in a bath of slurry. The system allows rapid assessment of relative erosivity and is economical in time and materials.

Materials

Coke

Whiting medium sulfur petroleum coke was received in the ground condition (<200 mesh, 50% greater than 13 μm , maximum particle size 74 μm). The ash content was 0.15% and the sulfur 3.2%. This material was used for the preparation of all coke slurries. The as-received powder was examined in the scanning electron microscope (SEM) (Fig. 1a). Particles can be seen to be angular, often with sharp corners or edges. The apparent density of particles (that is, including any closed pores but excluding open pores) was measured as $1370 \pm 10 \text{ kg/m}^3$ using a standard weighing bottle with either acetone or methyl alcohol as a suspension medium. No coke-water slurries were prepared since coke is hydrophobic, and, in a mass of coke particles and water, the coke is floated by entrapped air, making the preparation of a uniform slurry impossible.

Coal

Pittsburgh Seam No. 8 coal was received as powder (<200 mesh, 50% greater than 19 μm). The ash content was 5.4% and the sulfur 1.5%. As-received coal powder was viewed in the SEM (Fig. 1b). Particles seemed very similar in angularity to coke. It was not possible to identify or distinguish mineral particles while examining the as-received coal in the SEM. Because of the significantly greater ash content, mineral particles from the coal were extracted using a 40% aqueous solution of sodium bromide, specific gravity 1.4. This method was not quantitative and tended to favor the collection of larger particles. The residue was viewed in the SEM (Fig. 1c). Particles were observed to be angular, often with rough surfaces and thus likely to contribute to metal removal by erosion. The apparent density of the coal particles was

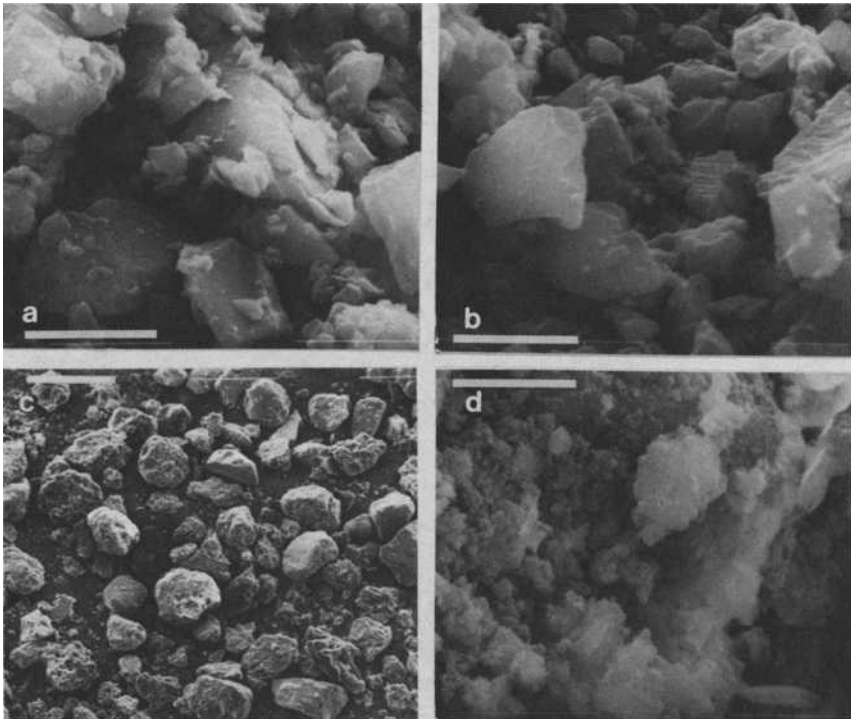


FIG. 1—Coke and coal solids used in slurry erosivity testing: (a) as received petroleum coke, bar is 10 μm ; (b) as-received coal, bar is 10 μm ; (c) extracted coal mineral particles, bar is 100 μm ; and (d) petroleum coke following 200 h of erosion testing, bar is 10 μm .

1480 \pm 40 kg/m^3 . The hydrogen ion concentration (pH) of water left 24 h in contact with the coal was moderately acidic, pH 4, as compared with pH 7 for the coke.

All oil-based slurries except one stabilized slurry (detailed in following paragraphs) were made up using high flash distillate fuel oil, flash point 67°C, sulfur 0.3%, specific gravity 0.87.

All water-based slurries were made up using Lawrence city water, pH 7.7.

Most erosion tests were conducted on AISI 304 stainless steel in the annealed state, hardness 86 R_B . Some tests used hot finished mild steel, hardness 59 R_B .

Experimental

The matrix of erosion tests conducted in this study is given in Table 1. In addition, two premixed stabilized slurries were examined, that is, slurries to which proprietary additions had been made with a view to retarding particle aggregation or settling. The first consisted of 50% <10- μm coal in water,

TABLE 1—Erosion test program.

Solid Component, <200 Mesh	Coke				Coal		
	Solid Content, Mass %	30	40	50	60	30	50
Liquid component							
High flash fuel oil	ss ^a /ms ^b	ms	ss/ms	ms	ss	ss/ms	
Water	ss	ss	

^a ss = AISI 304 stainless steel.

^b ms = mild steel.

stabilized with the surfactant Lomar-D, the second, 50% <4- μ m coke in light furnace oil, stabilized with three Nopcosperse surfactants—RG1, VBR7, and 17.

Testing was carried out using three identical machines of the form shown in Fig. 2. These machines were constructed of stainless steel, and each pot had a capacity of about 3.8 L. The coupon specimen (Fig. 3), 19.05 mm wide, 3.18 mm thick, and 101.6 mm in diameter with radiused ends, was attached by a cap screw to the lower end of the shaft using a nylon separator washer (to prevent the establishment of a corrosion couple between specimen and shaft) and was rotated at 3450 rpm via a belt drive, representing a tip speed of 18.3 m/s.

The pot was fitted with four vertical baffles to break up the rotational flow pattern. Because of the high rotational speed, strong turbulence was generated in the slurry, together with a tendency for a rise in slurry temperature. To control temperature, four water-cooled copper coils were located through the lid of the pot, one coil in each quadrant, and one coil at the bottom of the pot. Tests were conducted nominally at room temperature.

All slurries were prepared on a mass percent basis using as-received coal or coke. Powders were dried at 88°C prior to blending with the carrier liquid and mixing for 20 min using a mechanical stirrer. Coke-oil slurries mixed most easily, followed by coal-oil, with coal-water slurries the most difficult to mix. The most easily mixed slurries were also those most resistant to settling.

The flat coupon erosion specimens were ground to size and finished using 600-mesh silicon carbide paper. A material was sought with well-established wear properties that would allow the comparison of erosivity of different slurries. Mild steel was satisfactory in oil-based slurries, but suffered general corrosion in water-based slurries. AISI 304 stainless steel was then selected. Specimens were weighed within 0.5 mg, rotated in the slurry for 24-h periods, reweighed, and replaced on the shaft in the same orientation throughout the test. Tests continued for about 200 h or until the trend of the weight loss curve was well established.

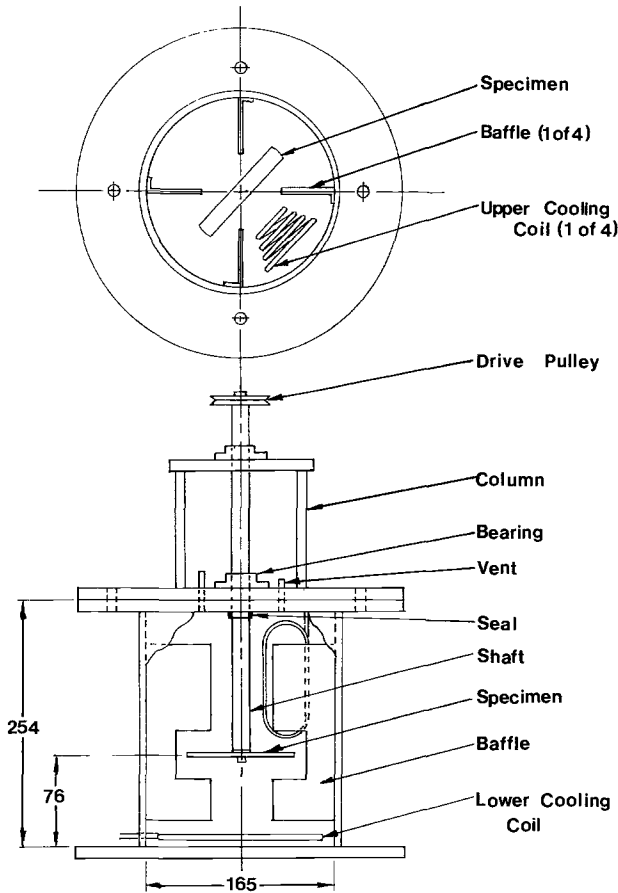


FIG. 2—Slurry pot tester, dimensions in mm.

Results and Discussion

In general, 30% slurries, whether coke- or coal-based, did not show any tendency to temperature rise as the test progressed. By contrast, 50% slurries composed of any components did tend to heat up during testing. This was found to be due in part to changes in the oil-based slurries as revealed by viscosity measurements conducted before and after erosion testing using a Brookfield RVT viscometer (Fig. 4). Viscosity values for the base oil are included for comparison purposes. Since the 30% slurries maintained constant temperature in the test, mechanical agitation is thought to be the principal contributor to the viscosity increase and not change in temperature. It is to be noted that the increase in viscosity was significantly greater for the coke-oil slurries than for

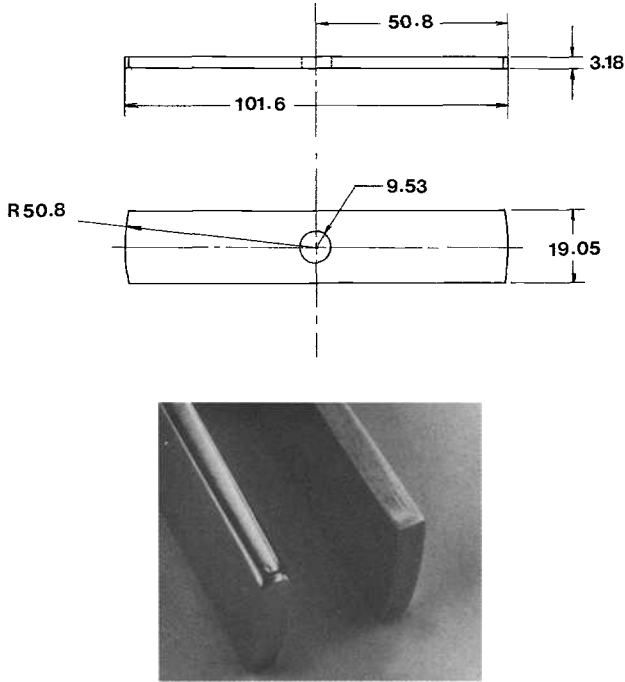


FIG. 3—(Top) Specimen geometry, dimensions in mm. (Bottom) Tip of two stainless steel samples. Right, untested, left, tested 183 h in 50% coal-water slurry. Material has been removed principally from the edge of the leading face.

coal-oil, indicating that this phenomenon is a function of the nature of the solid/liquid interface, allowing the coke to act to some extent as a thickening agent similar to those used in grease formation.

Erosion Test Results

Mass loss data for stainless steel specimens comparing 30% and 50% coke-oil, coal-oil, or coal-water slurries are given in Fig. 5. These curves are the average of either two or three tests for each slurry. The results show that increasing loading from 30 to 50% increases the erosivity of the slurry, that coal is more erosive than petroleum coke, and that water-based slurries yield a greater rate of material loss than oil-based slurries. Using the value of mass loss at 50 h as a measure of erosivity, relative values of erosivity are given in Table 2. Essentially similar values are derived by a comparison of the initial slope of the mass loss curves as has been proposed [4].

Mass loss curves are given in Fig. 6 for mild steel specimens tested in coke-oil slurries with loadings between 30 and 60% coke. These results show that

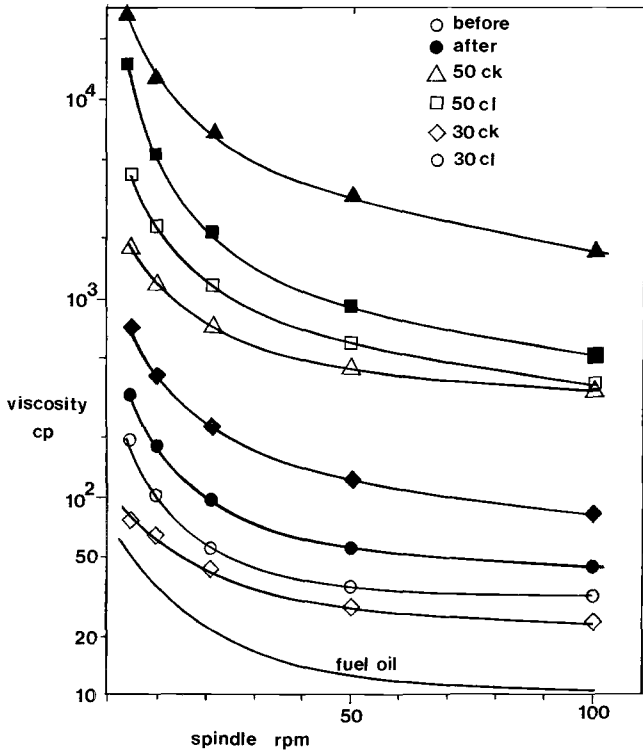


FIG. 4—Viscosity versus spindle speed for various oil-based slurries before and after erosion testing (200 h). (Ck = coke, cl = coal). The viscosity of the fuel oil is also shown. Brookfield RVT viscometer, Spindle No. 4, room temperature.

erosive mass loss increases with loading up to some maximum value and then starts to decrease again. Presumably at very high loadings—over 50%—solid particles start to shield the eroding surface to an increasing extent so that, even though the number of particles/unit volume is high, there is a decreasing number of particles able to produce mass loss by impact through penetration to the free surface of the specimen. Material removal will continue to be rapid where slurry particles are moving rapidly across the metal surface.

Erosive mass loss curves for 50% loading of coke and coal in oil for stainless steel and mild steel specimens are shown in Fig. 7. For both target materials, coke is about half as erosive as coal. This may be contributed to by a number of factors:

1. Coke has a lower apparent density than coal, so that the energy dissipated/impact is less for coke, on the average.

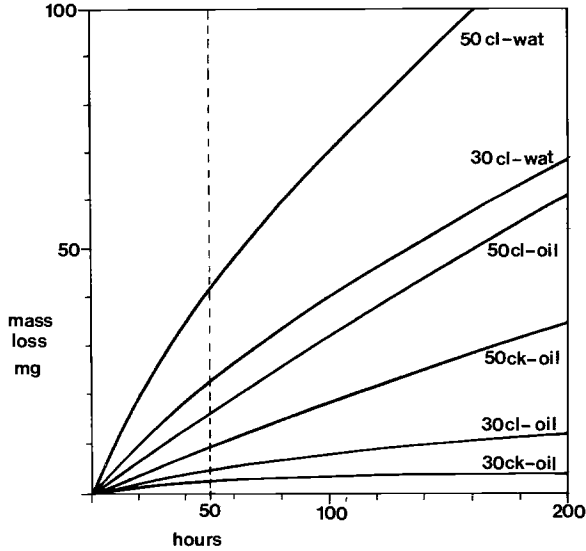


FIG. 5—Mass loss versus time curves for erosion testing of stainless steel specimens in various slurries (oil = fuel oil, wat = water).

2. Coke slurries tend to become more viscous than coal slurries at longer testing times, reducing the erosivity.
3. Degradation of coke particles may occur at longer testing time, further reducing average energy/impact.
4. Coke contains significantly less ash or mineral content than coal, so there are no high-density particles to cause enhanced damage rates.
5. Coke is softer than coal so that the impact of a given size of particle will produce less damage.

The first three of these points are not felt to be significant since the initial rate of mass loss for coke slurries is always lower than that for the equivalent

TABLE 2—Relative erosivity of coal and coke slurries (as assessed for AISI 304 stainless steel specimens).

50 Hours	30 Coke-Oil	30 Coal-Oil	50 Coke-Oil	50 Coal-Oil	30 Coal-Water	50 Coal-Water
30 coke-oil	1.0
30 coal-oil	1.8	1.0
50 coke-oil	3.7	2.1	1.0
50 coal-oil	4.7	2.6	1.5	1.0
30 coal-water	8.3	4.7	2.3	1.5	1.0	...
50 coal-water	13.3	8.3	4.0	2.7	1.8	1.0

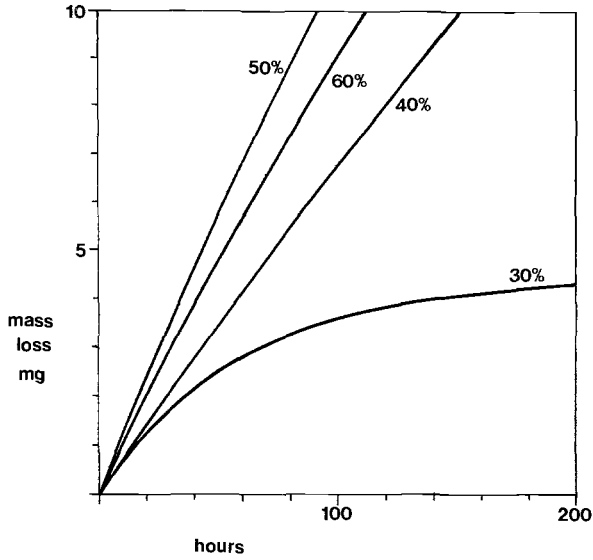


FIG. 6—Mass loss versus time curves for erosion testing of mild steel specimens in various coke-oil slurries, solids loading as indicated.

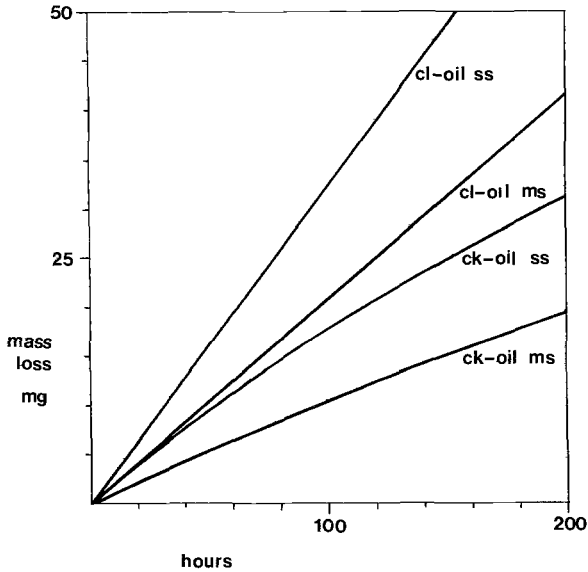


FIG. 7—Comparison of erosive mass loss versus time for stainless steel (ss) and mild steel (ms) in 50% coke- or coal-oil slurries.

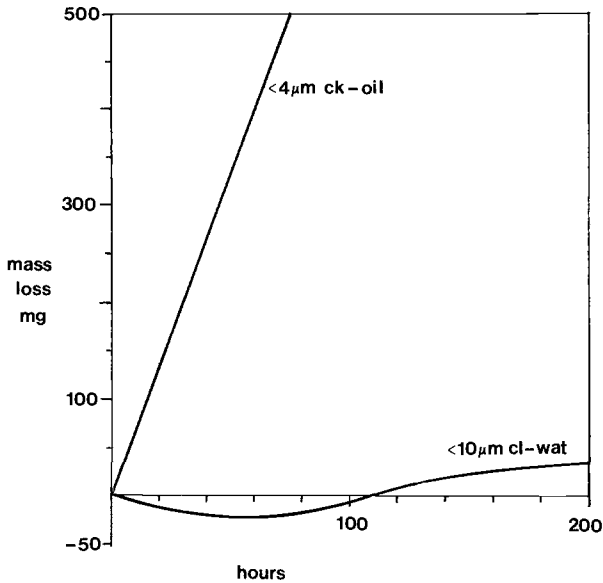


FIG. 8—Mass loss versus time curves for the erosion testing of two 50% fine-grind stabilized slurries. Stainless steel specimens.

coal slurry and the difference in apparent density is not large. The mineral content of coal is probably important since particles were often angular and probably rather hard. Evidence of comminution of coke during testing was observed in the SEM (Fig. 1*d*), and such processes no doubt lead to a reduction in the rate of removal of material as shown in Fig. 5 for coke slurries after longer testing times.

Mass loss graphs for the two 50% fine-grind slurries with surfactant additions are shown in Fig. 8. The coal/water slurry using a stainless steel specimen showed an initial mass gain, followed by a slow decrease in mass. However, the specimen rapidly became coated with a rather uniform layer of partially hydrated iron oxide—rust—containing trace amounts of manganese and chromium, which undoubtedly caused the increase in mass. The anomalous change of mass undoubtedly reflects an erosion-corrosion interaction during which corrosion products adhered to the sample in areas not subject to direct erosive impact. Removing the coal by centrifuging allowed the pH of the liquid to be determined as 8.5. This contrasts with other coal-water slurries that were found to be significantly acidic (pH 4).

Figure 8 also shows mass loss data for the 50% fine-grind coke slurry in light furnace oil with surfactant additions and a stainless steel target. This slurry produced by far the greatest rate of weight loss, some 50 times greater than the 50% 200 mesh coke-oil slurry. There were corrosion deposits on this specimen, particularly near the attachment point to the shaft.

Both of these slurries were extremely resistant to settling, but the rapid formation of adherent corrosion product for the coal-water-surfactant slurry and the very high material loss combined with corrosion for the coke-oil-surfactant slurry point to significant erosion-corrosion interaction. We regard the very high rate of material loss upon testing in the latter slurry as quite anomalous. In principle the small particle size and high slurry viscosity should lead to a very low erosion rate were corrosion absent. This highlights one of the problems of successful use of slurry fuels, namely, that a solution to one problem (in this case slurry stability) may accentuate a problem in some other area. The use of stabilizing additions must be carefully assessed in terms of their effect on erosion-corrosion phenomena.

Further evidence of erosion-corrosion interaction was revealed by examination of surface damage using the SEM. Figure 9a shows the center of the leading face of a stainless steel specimen tested for 200 h in 50% <200-mesh coke in oil. A typical pattern of erosion is shown. Heavy surface distortion is apparent, and either cracking or the hammering out of erosion platelets [5] can be clearly seen. However, Fig. 9b shows the center of the leading face of a stainless steel specimen tested for 200 h in 50% <200 mesh coal-water slurry. This specimen showed a rate of mass loss more than twice that of the specimen in Fig. 9a, Fig. 5, but the surface is virtually free of gross erosion damage, with only some small ill-defined craters visible. This difference is believed to be caused by erosion-corrosion interaction in the coal-water slurry for stainless steel, erosion damage being dissolved away by corrosive action, which may be enhanced by the observed acidity of coal-water slurries.

Stainless steel derives its corrosion-resistant properties under normal circumstances from a layer of chromium oxide. Under the influence of particle impact, this layer will be rapidly removed and will be unable to reform. If the slurry is noncorrosive or if corrosion processes cannot be initiated (oil slurries without surfactant additions), the rate of material loss will reflect the mechanical properties of the steel. Under conditions where corrosion can exist (water slurries or slurries with surfactant additions), a potential can be set up between different parts of the specimen, for example, the rapidly moving nonprotected outer region and the more slowly moving inner region.

Evidence of the effect of specimen rotation speed on surface damage was obtained for mild steel tested 170 h in 50% (200-mesh) coke-oil (Fig. 10). This shows the center of the leading face at an increasing distance from the rotating shaft such that the speed of rotation was 5.5, 8.0, and 14.5 m/s. Both the number of impacts/unit area and the size of the craters increase with increasing speed.

If particle impact energy is proportional to $(\text{velocity})^2$ and the impact crater diameter is proportional to $(\text{energy})^{1/3}$, the maximum crater diameter should increase according to $(\text{velocity})^{2/3}$, in this case in the ratios 1:1.33:2. Within the limitation of the photographic sample, there is some evidence for this kind of relationship. As is common in erosion damage, the maximum crater size is

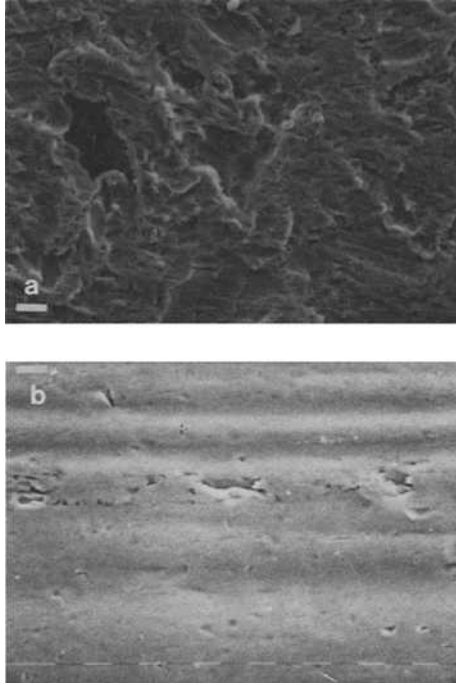


FIG. 9—Center of tip of leading face of stainless steel specimens tested as indicated. Location of area on sample is shown schematically at right: (a) 200 h in 50% coke-oil slurry, bar is 10 μm ; (b) 200 h in 50% coal-water slurry, bar is 10 μm .

considerably smaller than the maximum particle diameter (in this case 74 μm) [6].

The changing aspect of the damage pattern on the specimen's leading face can be seen from Fig. 11. The top micrograph is taken very close to the top of the leading face where slurry is moving rapidly across the surface. The bottom micrograph shows the center of the leading face in which essentially normal particle impact occurs. The center micrograph shows the intermediate position where oblique impact dominates.

Material removal proceeded most rapidly, as expected, where the solid particles impacted the metal surface at a low angle (Fig. 11, top). Surface disturbance appears to be severe in the normal impact region (Fig. 11, bottom), but the rate of metal removal was low, as evidenced by the shape of the eroded tip of the sample.

Industrial scale combustion tests of petroleum coke-oil slurries are either currently planned or have been carried out [7,8]. Advantages seen for this type of fuel, apart from a cost saving compared with 100% liquid fuel, include low

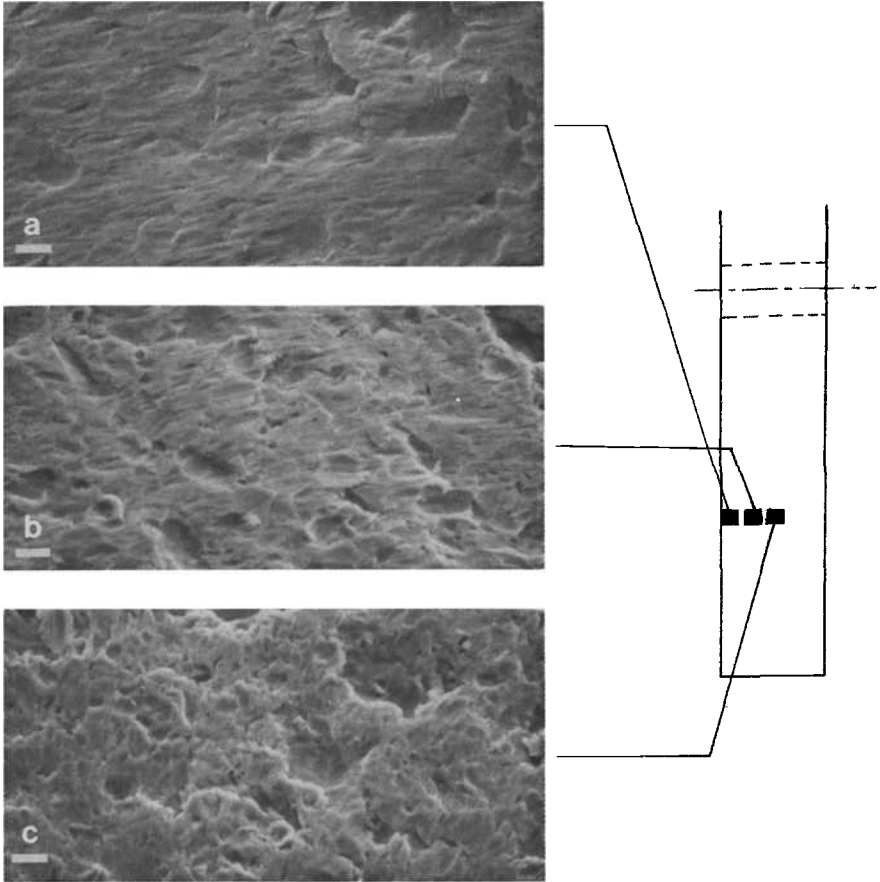


FIG. 10—Center of the leading face of a mild steel erosion specimen tested in 50% coke-oil slurry. Areas situated at increasing distance from the specimen rotation axis, as shown schematically on right. Bar is $10\ \mu\text{m}$ in all cases: (a) rotational speed 5.5 m/s; (b) rotational speed 8.0 m/s; and (c) rotational speed 14.5 m/s.

ash content and low erosivity. The present investigation confirms the low erosivity of coke slurries compared with equivalent coal slurries. However, the present work also shows that the material loss rate can be greatly increased by the addition of additives designed to stabilize the slurry, even though the solid particle size is very small. The effect of the additives (of unknown nature) in the present investigation was much more dramatic than any other variable examined, including change of solid, viscosity, and concentration, all of which had a rather minor effect. Further work on the effect of stabilizing additives would be warranted on the basis of this evidence.

Experimental investigation of slurry erosion is made particularly difficult

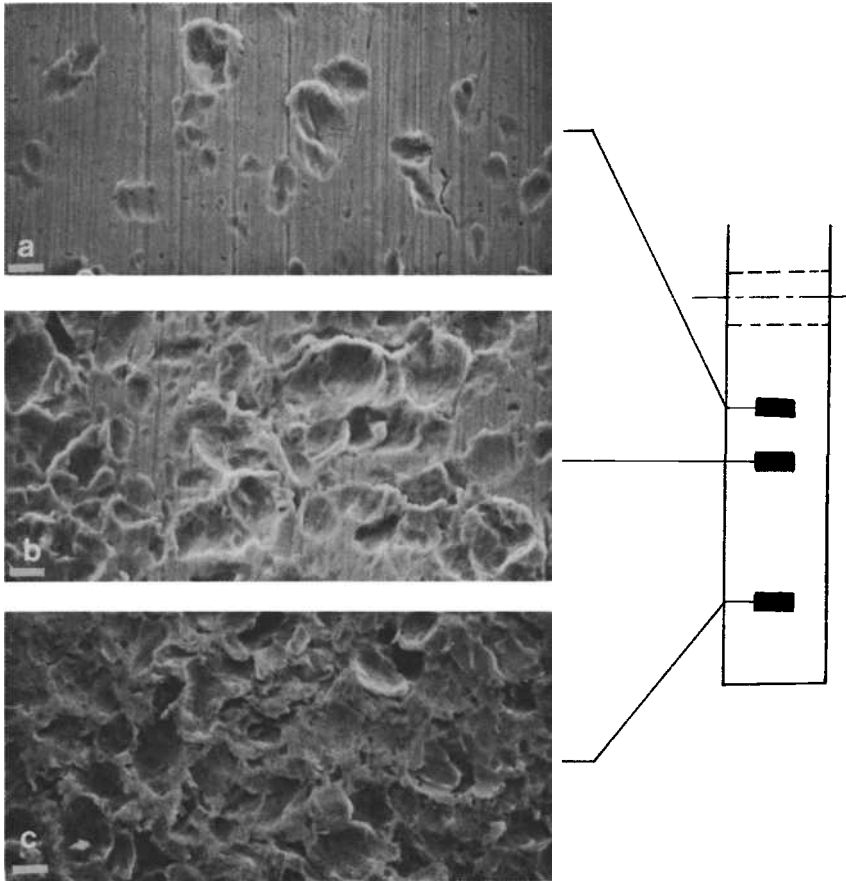


FIG. 11—Variation of erosion damage pattern of a mild steel specimen tested 170 h in 50% coke-oil slurry. Location of areas is shown schematically on right. The upper and lower specimen surfaces lie to the left and right of the figure. Bar is 10 μm in all cases: (a) upper edge of leading face; (b) $3/4$ position of leading face; (c) center of leading face.

because of the conflicting demands of producing accurately measurable rates of material loss within an acceptable time period, simulating industrial conditions using industrial materials and controlling the many variables, some of which are not independent. Typically, the high-speed slurry pot testers in common use [4,9] cause the specimen to sweep out a volume some thousands of times greater than the total pot volume in each hour of testing. It is not surprising that some slurry particle comminution takes place during the test. Similarly, vigorous stirring can lead to grease formation in certain oil-based slurries, causing a rapid rise in viscosity and problems in temperature control. Further, unless the slurry is quite benign, any erosion-corrosion interaction can greatly enhance the rate of material loss as fresh metal is continuously exposed by the removal of

corrosion products through particle impact. With erosive mass losses measured in milligrams per day over substantial areas, the average amount of metal removed is measured only in thousands of atomic layers/hour.

These problems have been faced by the use of recirculating slurry supplies and careful temperature and corrosion control [9], but the problem of controlled measurement of erosion at very low rates remains formidable.

Conclusions

Comparison of the erosivity of coke-oil and coal-oil slurries shows that petroleum coke is about one half as erosive as coal in an oil-based slurry. Coal-water slurries produced a higher rate of mass loss than the equivalent coal-oil slurry, but this may be due in part to erosion-corrosion interaction. In oil-based slurries, 304 stainless steel eroded at about twice the rate of mild steel, while the rate of mass loss for mild steel specimens in coke-oil slurries was shown to be a maximum at about 50% for varying solids loading. Two fine-grind additive stabilized slurries tested showed either general corrosion or a sharply enhanced rate of material loss. This finding underscores the need for careful assessment of the effect of additives on slurry properties other than stability.

Acknowledgment

The authors would like to acknowledge the assistance of the Amoco Oil Company in providing the petroleum coke, coal, fuel oil, and premixed slurries used in this investigation, together with appropriate analyses.

References

- [1] Morrison, G. F., "Conversion to Coal and Coal/Oil Firing," Report No. ICTIS/TR07, International Energy Agency Coal Research, London, Dec. 1979.
- [2] Fifth International Symposium on Coal Slurry Combustion, Tampa, FL, Department of Energy, Pittsburgh Energy Technology Center, Apr. 1983.
- [3] Levy, A. V., "Corrosion/Erosion of Materials in Coal Liquefaction Environments," *Proceedings*, Conference on Corrosion/Erosion of Coal Conversion System Materials, National Association of Corrosion Engineers, Berkeley, CA, 1979.
- [4] Tsai, W., Humphrey, J. A. C., Cornet, I. and Levy, A. V., *Wear*, Vol. 68, No. 3, May 1981, pp. 289-303.
- [5] Levy, A. V., "The Platelet Mechanism of Erosion of Ductile Metals," *Wear*, Vol. 108, No. 1, March 1986, pp. 1-21.
- [6] Cousens, A. K. and Hutchings, I. M., *Proceedings*, International Conference on the Wear of Materials, American Society of Mechanical Engineers, New York, Apr. 1983, pp. 382-389.
- [7] Beshore, D. G. and Yagiela, A. S., *Proceedings*, Fifth International Symposium on Coal Slurry Combustion, Tampa, FL, Department of Energy, Pittsburgh Energy Technology Center, Apr. 1983, pp. 283-303.
- [8] Nunn, R. C., Richardson, W. L. and Bollen, W. M., Fourth International Symposium on Coal Slurry Combustion, Orlando, FL, Department of Energy, Pittsburgh Energy Technology Center, May 1982.
- [9] Hoey, G. R. and Bednar, J. S., *Materials Performance*, Vol. 22, No. 4, Apr. 1983.

Erosivity of Coal Particles in Coal-Solvent Slurries

REFERENCE: Levy, A. V., Jee, N., and Sorell, G., “Erosivity of Coal Particles in Coal-Solvent Slurries,” *Slurry Erosion: Uses, Applications, and Test Methods*, ASTM STP 946, J. E. Miller and F. E. Schmidt, Jr., Eds., American Society for Testing and Materials, Philadelphia, 1987, pp. 62–77.

ABSTRACT: An investigation of the erosivity of particles of several different coals and respective vacuum bottoms from the Exxon Donor Solvent (EDS) coal liquefaction pilot plant of the Exxon Coal Liquefaction Process (ECLP) was carried out. Kerosene and tetrahydrofuran (THF) were used as the liquids in slurries containing 30 weight % particles. The particles were of several sizes, shapes, integrities (fracture strength), and ash contents. It was determined that the primary factors having a direct effect on erosivity were particle size and ash content/composition. Particle shape and resistance to fracturing upon impact had important secondary effects. All of these factors are interrelated and can counter each other under certain conditions. Slurry pot testing proved valuable as a reproducible method for comparative erosion studies, but should not be relied upon to produce quantitative erosion data for equipment design purposes.

KEY WORDS: erosion, coal slurry, coal liquefaction, wear

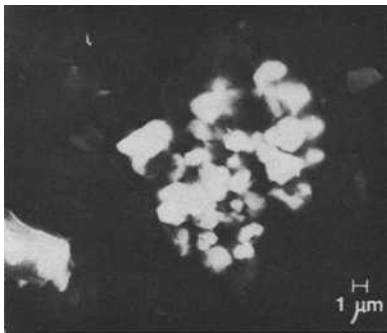
Many different coals will be used in coal liquefaction plants, each containing different compositions and quantities of erosive mineral matter. It is the ash or mineral matter in coal that is primarily responsible for the erosion of the metal containment surfaces of the equipment through which the coal slurries flow [1,2]. The carbonaceous matter in coal is soft and friable and, therefore, has very little erosivity. The composition, quantity, morphology, size, shape, and location of the ash particles in the coal particles and the same aspects of separate mineral particles that accompany the coal are the variables that determine the erosivity of coal-solvent slurries. The purpose of this investigation was to determine the erosivity of hydrocarbon-based slurries containing ground coal or ash-rich vacuum bottoms obtained from the Exxon Coal Liquefaction Process

¹ Lawrence Berkeley Laboratory, University of California, Berkeley, CA 94720.

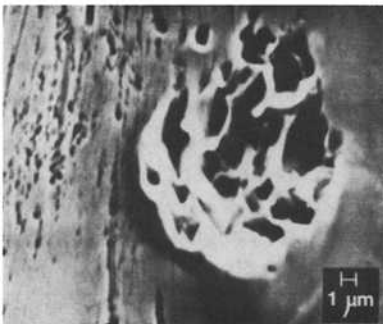
² Exxon Research & Engineering Co., Florham Park, NJ 07932.

(ECLP), the 250-ton/day Exxon Donor Solvent (EDS) coal liquefaction pilot plant in Baytown, Texas. A schematic of the ECLP plant is contained in Ref 1.

The erosivity of several oxides, some of which are contained in coal, has been studied in gas-solid particle erosion [3]. It was determined in these tests that the weaker oxides, as assessed by their hardness, fractured upon impact and, as a result, were much less erosive than the stronger oxides which did not. It was also determined that the shape of the erosive particles had a significant effect on their erosivity, with angular particles being considerably more erosive than spherical particles. In Ref 4 the size, shape, and location of the oxides in the ground coal particles were related to the effect that they had on the metal being eroded. Figure 1 [4] shows that the carbonaceous constituents of the coal (dark) hold the mineral constituents (white) much as a tool holder maintains the position of a tool. The resultant imprints of the oxide particles in the target metal surface have the same shape as the mineral constituents in the coal. It is



**PYRITE ON
COAL SURFACE**



**IMPRINT ON
1050 C.S. SURFACE**

**30° IMPACT
18 m/s**



FIG. 1—Pyrite crystallites in coal and impression in eroded steel [4].

by this means that the finely divided, hard oxides in the relatively soft coal cause the coal particles to be erosive.

The size of the coal particles is another factor that has been shown to be directly related to their erosivity [5]. The mass of each coal particle directly relates to its kinetic energy as it impacts an eroding surface. The larger coal particles, therefore, have a greater capacity to drive the mineral particles in their surfaces into the target. Thus, even with very fine mineral particles embedded in much larger coal particle “tool holders,” the erosivity of a slurry can be related to the overall size of the coal particles.

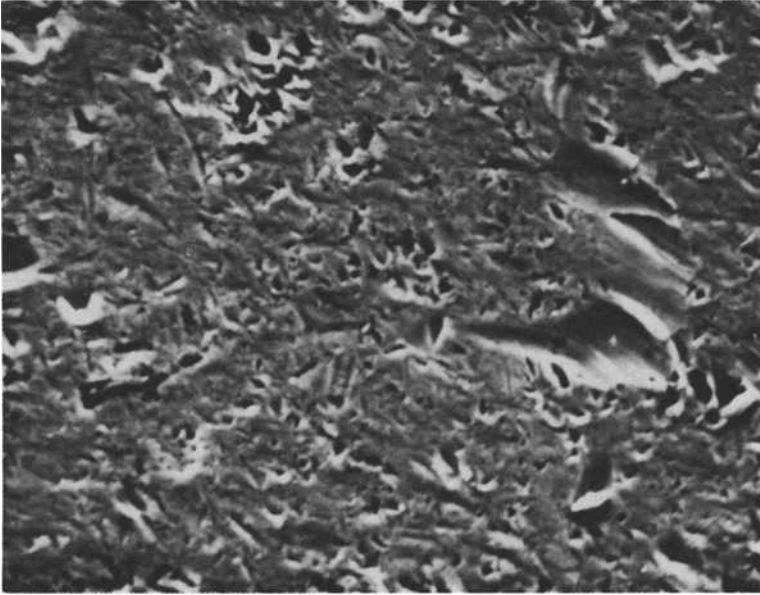
Another size factor that affects the overall erosivity of a coal mixture is the presence of oxide contaminant particles such as silica (SiO_2) that are separate from the coal but that have the same size as the coal particles. Coal cleaning operations remove a high percentage of these particles, but not all. The remaining mineral particles have a considerably greater erosivity than the ash-containing coal particles of the same size and probably account for the principal amount of erosion that occurs. Figure 2 shows a typical eroded surface of 304SS when -200 mesh ($74 \mu\text{m}$) coal was used in a kerosene-coal slurry [6]. The large crater that can be seen on the right side of the photo was caused by a single oxide particle, probably SiO_2 or aluminum oxide (Al_2O_3), which was the same size as the coal particles. The much greater erosive effect of the larger mineral particle compared to the “paw prints” of ash contained in the coal particles can be seen. Figure 2 is of an area near the periphery of the eroded zone when a jet impingement slurry tester was used.

Another possible aspect of the effect of particle size is the ability of the large particles to offset the particle defeating function that the viscosity and boundary lubrication of the carrier liquid plays in slurry erosion. Their greater mass will result in their ability to drive through the carrier liquid to the eroding surface more effectively.

With this understanding of the nature of coal-solvent slurry erosion, the different ECLP coals and vacuum bottoms to be utilized in the laboratory slurry pot tests were selected to provide a range of different sizes and mineral contents. Their erosivity was studied in coal-kerosene and vacuum bottoms-tetrahydrofuran (THF) slurries. THF has about the same viscosity as kerosene.

Test Conditions

The coal and ground agglomerated vacuum bottoms were shipped from ECLP in metal cans without dehumidifiers. The compositions of the coals and derived vacuum bottoms are listed in Tables 1 and 2, respectively. The particles that did not readily pour from the cans or that showed evidence of clumping due to their moisture content were dried prior to being mixed into a slurry by passing air over shallow trays of the particles for 2 h at 105°C . Particle size distributions listed in Tables 3 and 4 were determined by sieve analyses using a Rotap machine and a set of Tyler sieves. Efforts to determine particle size distribution



5 μ m

FIG. 2—Eroded surface showing effects of sand particles and coal particles.

using a laser detector were not successful because the particles tended to float on top of the liquid carrier used in the laser apparatus.

The coal particles were prepared into 30 weight % particle-kerosene slurries by mixing the two constituents in the slurry pot prior to testing. The vacuum bottoms were prepared in slurries synthesized with THF instead of kerosene. The rationale for using this more effective solvent for carbonaceous coal residues was to dissolve the ash agglomerates to attain smaller particle sizes, approaching the microscopic ash-rich particles existing in hot, liquid vacuum bottoms streams during plant operation.

The erosion tests were carried out in a slurry pot tester, which is described in detail and pictured in Ref 3. It consists of a baffled, stirred, 3-L cylindrical container. Attached to the $\frac{3}{4}$ -HP, motor-driven central shaft are two specimen-holding arms rotating the specimens in a 10.5-cm-diameter circular path at effective velocities from 6 to 15 m/s. The specimens were cold-rolled 1018 steel rods 0.3 cm in diameter by 5 cm long and 1018 steel rods of the same size annealed at 850°C for 45 min and slow cooled. The effective velocity of the slurry was 12 m/s. Test temperature was maintained at 28°C, and the test duration was held to 2 h. The decision to limit conditions to a single velocity,

TABLE 1—*Coal compositions.*

Coal Rank	Illinois No. 6 Bituminous	Wyoming Subbituminous	Martin Lake Low Ash Lignite	Martin Lake High Ash Lignite
Ash, dry wt%	10.9	9.3	9	23
Carbonaceous materials, element analysis, dry wt%				
Carbon	69.1	68.3	67.4	57.0
Hydrogen	5.0	4.8	4.8	4.1
Oxygen	9.4	16.0	16.6	13.9
Nitrogen	1.3	1.0	1.4	1.1
Sulfur	4.3	0.6	0.8	0.9
Total wt% of coal	100.0%	100.0%	100.0%	100.0%
SO ₃ wt% of ash	3.1%	18.0%	14.8%	6.2%

TABLE 2—*Vacuum bottoms compositions.*

	Illinois No. 6	Wyoming	Martin Lake Low Ash	Martin Lake High Ash
Ash, dry wt%	20.8	22.3	22.1	38.3
Sulfur, dry wt%	2.7	0.8	0.9	1.0

NOTE: Elemental analyses: assumed to be in same proportion as for coal.

TABLE 3—*Coal particle size distribution.*

Particle Size	ECLP Illinois No. 6	LBL Illinois No. 6	Wyoming	Martin Lake Low Ash	Martin Lake High Ash
>701 μm	26.7
701 to 425 μm	23.3
425 to 250 μm	17.8
>300 μm	...	0	0	0.16	0.08
300 to 150 μm	...	0.1	0.08	2.69	0.72
250 to 180 μm	9.2
<180 μm	23.0
150 to 90 μm	...	3.2	13.08	13.95	10.06
90 to 38 μm	...	67.5	61.97	68.27	62.25
<38 μm	...	29.2	24.87	14.93	26.89
	100.0%	100.0%	100.0%	100.0%	100.0%
Average particle size	443 μm	65 μm	65 μm	73 μm	64 μm

TABLE 4—*Vacuum bottoms particle size distribution (agglomerated condition).*

Particle Size	ECLP Illinois No. 6	Wyoming	Texas Low Ash
>701 μm	10.6	15.6	10.2
701 to 425 μm	18.4	23.2	18.3
425 to 250 μm	21.6	22.2	21.4
250 to 80 μm	11.3	10.2	11.2
<180 μm	38.11	28.8	38.9
	100.0%	100.0%	100.0%
Average particle size	344 μm	389 μm	341 μm

temperature, and test material was based on earlier work with the slurry pot, which showed that changing these parameters affected erosion to a predictable or minor extent [5].

Results and Discussion

Particle Analysis

Analyses of the ECLP coals and vacuum bottoms listed in Tables 1 and 2 were determined by Exxon Research and Engineering Co. The batch of Lawrence Berkeley Laboratory (LBL) Illinois No. 6 coal, also used in this study, was obtained at an earlier time from another source. The chemical composition of the LBL sample was not determined. However, it can be reasonably assumed that the analysis of the ECLP coal is generally representative for the LBL Illinois No. 6 coal as well.

All of the coals have fairly similar carbonaceous content but differ appreciably in ash (mineral) content. As shown in Table 5, there are also pronounced differences in the relative amounts of constituent oxides in the ash. The high ash Martin Lake lignite contains by far the greatest proportion of mineral matter. Vacuum bottoms are about twice as rich in ash as the raw feed coal being liquefied. However, the composition of the minerals in the bottoms ash stays essentially the same as in the coal since the process conditions in hydroliquefaction are too mild to decompose stable oxides.

Differences in ash content can be directly related to the erosion data obtained in the slurry pot tests. The much weaker carbonaceous materials in the coal account for little of their erosivity directly, even though they account for 90 weight % of the coal. The principal function of the carbonaceous material in the coal particles is to provide the mass necessary to drive the mineral constituents in them into the surface being eroded.

It is shown in Table 1 that the highest ash content coal was the Martin Lake Texas lignite. The other three coals tested had approximately half that amount of ash. Also important to the erosivity of the coal are the amounts of the various

TABLE 5—Ash analysis.

Ash Element Analyses SO ₃ , Free Dry Wt%						
Oxide	Hardness, Kg		Illinois No. 6	Wyoming	Martin Lake Low Ash	Martin Lake High Ash
	Moh	VH, mm				
SiO ₂	7	700	51.6	41.2	41.2	59.7
Al ₂ O ₃	9	1900	16.8	18.7	16.8	13.3
Fe ₂ O ₃	6.75	755	19.2	6.3	11.5	6.8
CaO	4.0 to 4.5	163 to 370	4.4	23.9	20.8	13.2
MgO	5.0 to 6.5	430 to 690	1.1	5.9	6.8	3.3
TiO ₂	5 to 6.5	430 to 690	0.9	1.2	1.3	1.6
Na ₂ O	1.3	1.1	1.2	0.9
K ₂ O	2.4	0.6	0.2	0.5
P ₂ O ₅	0.3	1.1	0.2	0
Total wt% of ash elements			100.0%	100.0%	100.0%	100.0%

oxides that constitute the ash. The stronger oxides, as represented by their listed hardnesses in Table 5, do not fracture into small pieces when they impact the surface and, therefore, can affect a larger area on the eroding surface as the result of their larger size [3]. Thus, the greater the content of such oxides as SiO₂ and Al₂O₃ in the coal, the more erosive it is likely to be. It can be seen that the high ash content lignite has the largest amount of combined silica and alumina (73%). The Illinois No. 6 coal has the second highest content of these two minerals (70.4%), while the other coals have considerably lower amounts.

The shape and distribution of the oxides in the coal also have a strong influence on the erosivity of the coal particles. Petrographic analysis of the coals as shown in Fig. 1 is used to determine this distribution. Unfortunately, this type of analysis was not available for the specific coals tested in this project. Therefore, the nature and effectiveness as erodents of the ash distribution in the coals tested had to be assessed by the resultant erosion rates of the 1018 steel.

The particle size distribution of the coals and vacuum bottoms is shown in Tables 3 and 4. There is a significant amount of small particles, <50 μm, in three of the coals tested. The small particles in these fine grinds probably have a minimum effect on the erosivity of the coals. It is the relatively small percentage of coarser particles, >100 μm, that presumably causes the major amount of the erosion. As will be shown later, it was the coarse coal and vacuum bottoms slurries that proved to be the most erosive.

Coal Erosion

The erosion rates of the 1018 steel were plotted in two ways, showing either cumulative or incremental metal loss. Curves showing cumulative erosion were prepared by measuring the total amount of weight loss that had occurred over

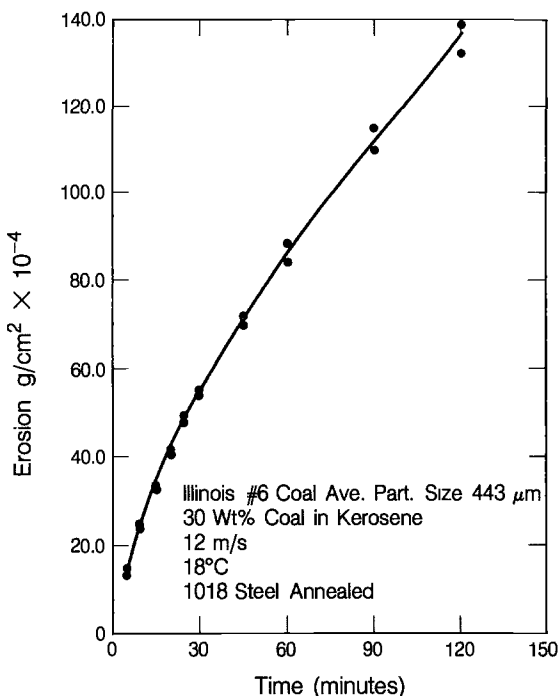


FIG. 3—Cumulative erosion of 1018 steel by 443- μm average diameter Illinois No. 6 coal particles in kerosene.

the front half surface area of the rod specimens up to the selected test time and plotting it against the test time. An analytical balance was used which measured to 0.1 ± 0.3 mg. Figure 3 shows a cumulative type of curve for two specimens tested simultaneously in the slurry pot. In incremental erosion rate plots, the weight loss incurred for each increment of test time is plotted. Thus, each data point represents the amount of loss that had occurred since the last weighing time divided by the elapsed time to obtain the rate of erosion. Figure 4 shows an incremental erosion rate plot for the same two specimens plotted in Fig. 3.

In Fig. 3, the erosion caused by the large particle Illinois No. 6 coal is plotted. A relatively large amount of weight loss occurred after 2 h of exposure. The small curvature in the plot for the first 45 min of testing is attributed to some comminution of the particles as they struck the metal surface, breaking off some angular protrusions, and, generally, decreasing in size by 25 to 50%. The surface texture of the coal particles before and after testing was the same, indicating no polishing of the particles.

The incremental erosion rate curve shown in Fig. 4 provides greater insight into the erosion process that is occurring than the cumulative plot in Fig. 3 because it more clearly shows how the erosion rate decreases from an initial

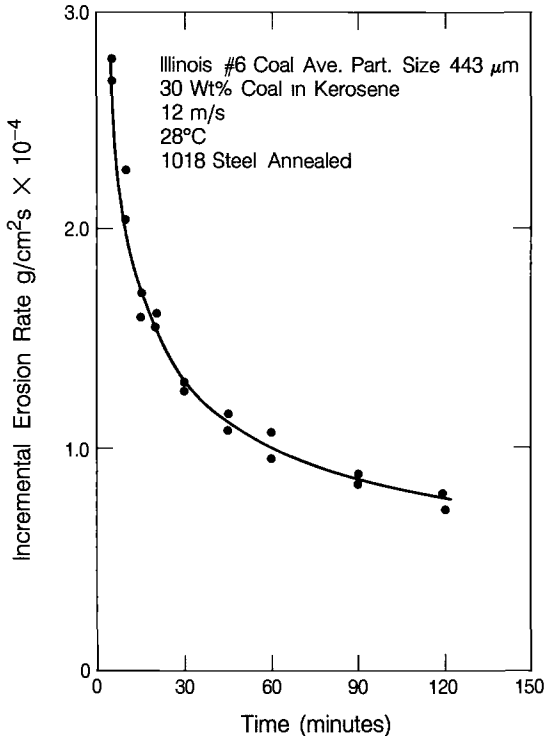
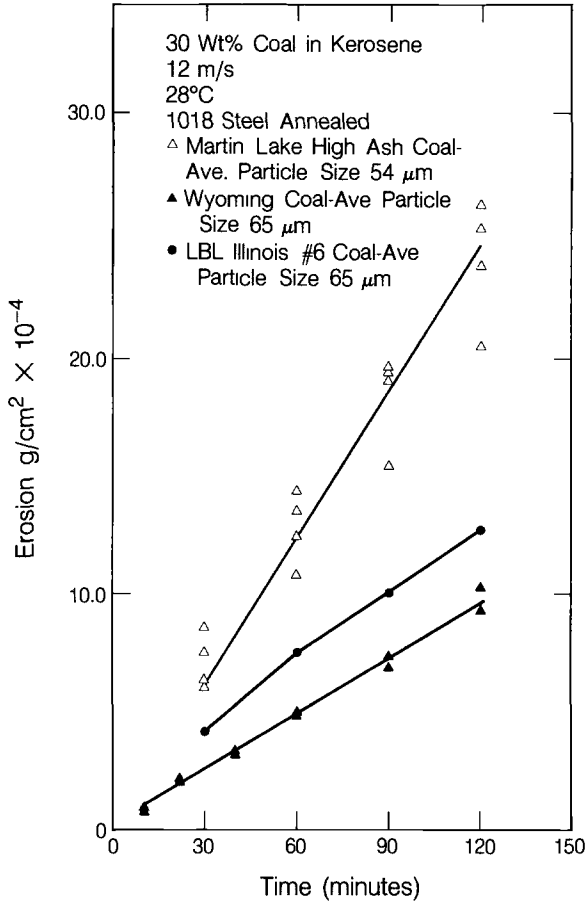


FIG. 4—Incremental erosion rate of 1018 steel by 443- μm average diameter Illinois No. 6 coal particles in kerosene.

high rate toward a lower steady state rate sometime after 120 min. It is harder to discern this behavior in a cumulative weight loss curve. The initial high rate of erosion early in the test followed by a marked rate decrease is the result of three complimentary effects. They are: (1) the progressive cold working of the surface as the result of the plastic deformation of the steel by the impacting particles [7]; (2) the comminution of the coal particles [8]; and (3) the polishing effect that occurs early in the test when the higher, more vulnerable protrusions of metal are knocked off the surface. As the surface work hardens, the erosion rate decreases. After about 2 h of exposure, the eroding surface is reaching a steady state condition where the cold work surface reaches its maximum hardness, the erodent particles reach a constant size and shape, and the initial metal protrusions have been removed. Subsequent increments of particle impacts of the same quantity will cause equivalent amounts of erosion to occur.

Smaller erodent particles cause considerably less erosion to occur. Figure 5 shows the erosion curves from the LBL Illinois No. 6 coal and the ECLP Wyoming coal tests, both of which had the same average particle size, 65 μm . The Illinois No. 6 coal was somewhat more erosive than the Wyoming coal but



XBL 846-8973

FIG. 5—Cumulative erosion of 1018 steel by 65-μm average diameter Illinois No. 6 and Wyoming coal particles in kerosene.

caused only one-tenth the erosion that resulted from the same Illinois No. 6 coal that had a 443-μm average particle size.

The incremental erosion rate curves for the two small coals are shown in Fig. 6. The typical shape of the curve shown in Fig. 4 also occurs when smaller erodent is used. The small weight loss experienced by the 1018 steel when it was eroded by the Wyoming coal made it difficult to obtain consistent weight loss measurements, thereby accounting for the greater spread in the data points for this coal in Fig. 6. It appears that the lower erosivity Wyoming coal causes the 1018 steel to reach steady state conditions sooner than does the more erosive Illinois No. 6 coal. The Wyoming coal causes considerably less erosion than the Illinois No. 6 coal early in the test. Their rates will become closer together

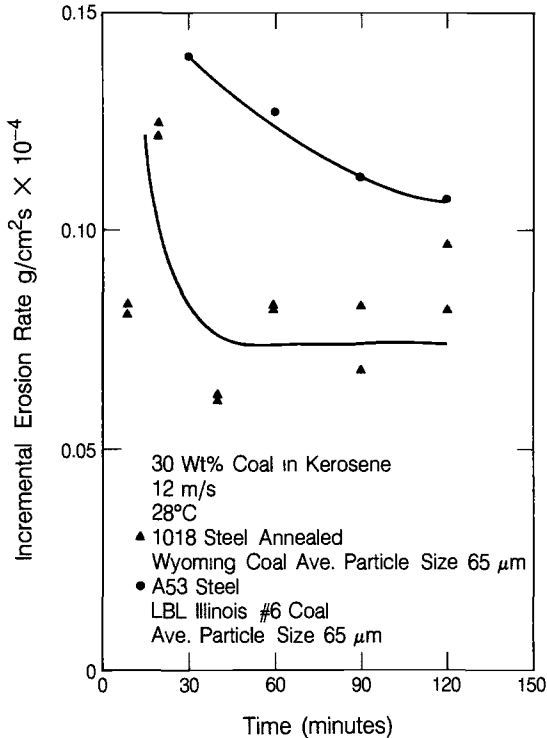


FIG. 6—Incremental erosion rates of 1018 steel by 65- μm average diameter Illinois No. 6 and Wyoming coal particles in kerosene.

after the Illinois No. 6 coal causes the 1018 to reach steady state conditions, primarily because of the same particle size of both coals.

The slope of the incremental erosion rate curve for the 65- μm Illinois No. 6 coal from 30 to 120 min shown in Fig. 6 is considerably less than that of the curve for the 443- μm Illinois No. 6 coal plotted in Fig. 4. This difference is due to the considerably less comminution [8] that occurred for the smaller particles and the decreased amount of work hardening of the steel surface that the lower mass, smaller particles caused.

The marked effect on erosion of the ash content of the coal is illustrated in Fig. 5, showing erosion losses for three different coals having comparable particle sizes. The direct relationship between ash composition and erosion is shown in Fig. 7, which is a cross plot of the cumulative 120-min. erosion losses of these three coals versus their silica plus alumina ash content. The same effect is observed when the incremental, steady state erosion rates for the three coals are plotted. However, the curve is more asymptotic as the SiO_2 and Al_2O_3 content increases. ECLP experience confirms this relationship to the extent that

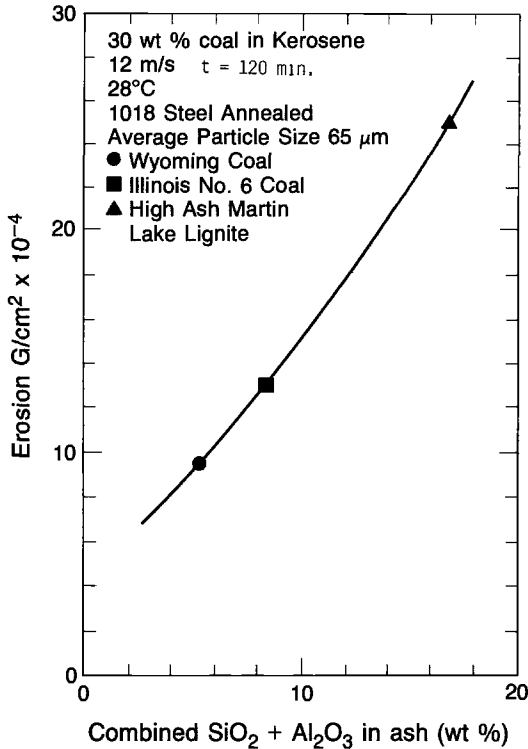


FIG. 7.—Cumulative erosion of 1018 steel by Illinois No. 6, Wyoming, and High Ash Martin Lake Lignite coals versus the combined $\text{SiO}_2 + \text{Al}_2\text{O}_3$ content in ash.

erosion was observed to be considerably more severe during high ash, lignite operation than when lower ash coals were run.

Vacuum Bottoms Erosion

The vacuum bottoms of the three test coals from the ECLP pilot plant were investigated in both their agglomerated and separated particle conditions. A schematic drawing of the process, indicating the location of the vacuum bottoms, is contained in Ref 1. The vacuum bottoms are the heavy-bodied slurry remains of the liquid coal slurry after vacuum distillation has drawn off the useable cuts. It contains primarily the noncarbonaceous, mineral solids that can not be reacted to form liquid product. It has a high ash content (see Table 2).

Kerosene was used as the slurry liquid in the agglomerated particle test. The agglomerates, which consisted of ground solidified bottoms, were separated in other tests by using THF solvent as the slurry liquid which dissolved the carbonaceous material and released the individual particles. Since the ash that has been released from the coal in the liquefaction process is concentrated in the

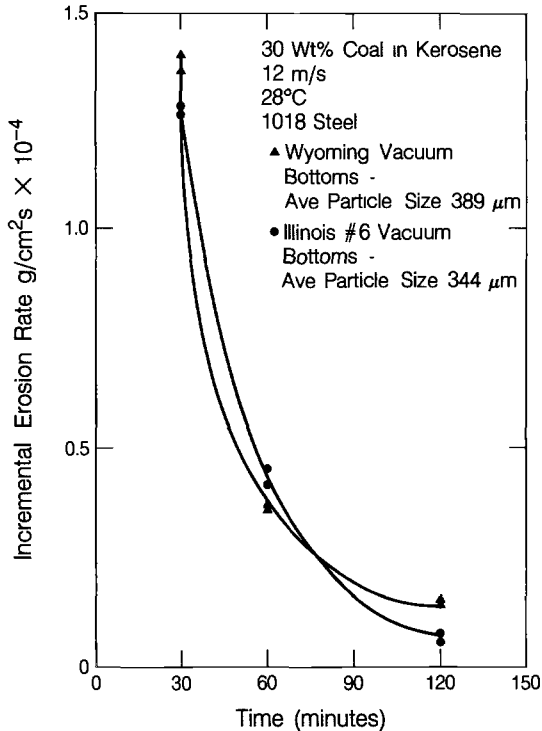


FIG. 8—Incremental erosion rates of 1018 steel by 344- μm average diameter Illinois No. 6 and 389- μm average diameter Wyoming vacuum bottoms particles in kerosene.

vacuum bottoms, (see Table 2), they can be expected to be more erosive than the coals themselves. However, particle size, integrity, and shape also affected the erosivity of these particles.

Figure 8 plots the incremental erosion rates of the 1018 steel by the agglomerated vacuum bottoms from the Illinois No. 6 and Wyoming coals. The large particles (see Table 5) and their high ash contents (see Table 2) resulted in nearly the same erosion rates throughout the test period. The steady state incremental erosion rate for the small Illinois No. 6 coal (Fig. 6) and its larger vacuum bottoms (Fig. 8) are nearly the same, considerably lower than the steady state rate for the large Illinois No. 6 coal (Fig. 4). This is probably due to comminution of the vacuum bottoms during the 2-h test as the particles are really agglomerates of much smaller particles. As these agglomerates are broken down as the result of their repeated impacts on the 1018 steel in the slurry pot, they become both smaller [5] and rounder in shape as their sharper corners are broken off. Both changes reduce their erosivity [3,5].

The two changes in the particles combine to offset the increased erosivity from the high ash content and higher starting particle size of the vacuum

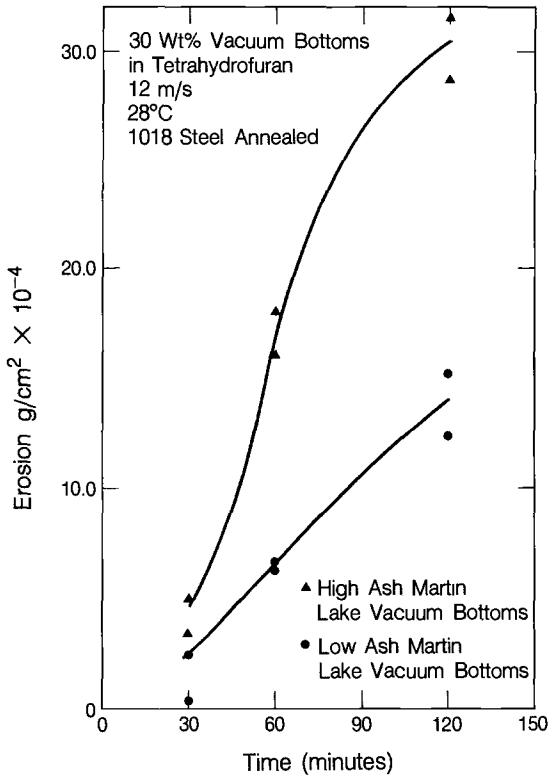


FIG. 9.—Cumulative erosion of high and low ash Martin Lake vacuum bottoms in tetrahydrofuran.

bottoms. The result is the steady state vacuum bottoms erosivity of the coals themselves. While these compensating factors may explain the comparable erosion rates obtained with coals and vacuum bottoms in slurry pot testing, the behavior may not necessarily hold for real plant conditions where the particles pass through the components only once.

The difference in the erosivity of the 38 weight % high ash and 22 weight % low ash content Martin Lake Texas lignites vacuum bottoms at their minimum particle size, unagglomerated, is best seen in the cumulative erosion curve in Fig. 9. In a THF solvent slurry, which dissolved the binder in the agglomerates, resulting in a much smaller erodent particle, the high ash lignite vacuum bottoms have caused considerably more erosion in the 1018 steel than in the low ash lignite vacuum bottoms. The amount of erosion caused by the small, individual particles of low ash lignite vacuum bottoms plotted in Fig. 9 after 2 h of rotation of the specimens in the slurry pot tester is $14 \text{ g/cm}^2 \times 10^{-4}$. The agglomerated form of the same vacuum bottoms tested in kerosene had caused $115 \text{ g/cm}^2 \times 10^{-4}$ to occur after 2 h of testing. Thus, the effect of particle size can readily be seen.

The comminution of the vacuum bottoms can also be assessed by comparing the amount of erosion after 2 h of testing of the large agglomerated lignite vacuum bottoms, $115 \text{ to } 140 \text{ g/cm}^2 \times 10^{-4}$ amount of erosion which was caused by the Illinois No. 6 coal (Fig. 3). The lignite has twice the concentration of ash, 22% compared to 10.9% for the Illinois No. 6 coal, and, therefore, a greater potential erosivity. However, the greater integrity or fracture strength of the Illinois No. 6 coal particles result in their maintaining their size and shape better after 2 h of testing than do the weaker, agglomerates of lignite vacuum bottoms, resulting in a greater total amount of erosion of the 1018 steel by the coal. As just discussed, it appears that in the case of these two kinds of particles, the particle size and shape effects have more influence on the erosivity of the slurry than does the ash content of the particles. While this may hold true for kerosene-base slurries, the situation could change with prolonged testing in THF slurries and real plant streams because of more effective exposure of the abrasive ash particles due to "chemical comminution."

Conclusions

1. The erosivity of coals and vacuum bottoms are affected by the particle size, shape, integrity, and ash content/composition of the particles.
2. Particle size is a dominant factor in coal slurry erosion. In the range investigated, a seven-fold increase in particle size resulted in a ten-fold increase in erosion.
3. Ash content/composition is another important factor influencing coal slurry erosion. Indications are that erosion is roughly proportional to combined SiO_2 and Al_2O_3 content.
4. Particle shape and integrity or fracture strength also play a role, with angular, strong particles being more erosive than rounded, frangible ones.
5. Vacuum bottoms slurry erosion appears to be governed by the same factors as raw coal slurries. For more realistic simulation of plant slurries, THF solvent is preferable to kerosene although it is more difficult to use in the laboratory.
6. Incremental erosion rate curves clearly indicate the onset of steady state erosion and its rate.
7. The factors affecting the erosivity of the particles can be traded off with the resulting erosivity being higher or lower, depending upon which of the factors predominate.
8. The slurry pot is a useful device for conducting comparative erosion studies which can also give some indication of erosion mechanisms but cannot be relied upon for producing quantitative, design erosion rate data.

References

- [1] Lendvai-Lintner, E., Jones, J. P., and Sorell, G., "Erosion Experience at the EDS Coal Liquefaction Pilot Plant," *Proceedings*, NACE Conference on Corrosion-Erosion-Wear of

- Materials in Emerging Fossil Energy Systems, Berkeley, CA, Jan. 1982, National Association of Corrosion Engineers, Houston, TX, pp. 155–178.
- [2] Jones, J. P., Buchheim, G. M., Lendvai-Lintner, E., and Sorell, G., "Materials Performance in the EDS Coal Liquefaction Pilot Plant," *Materials Performance*, National Association of Corrosion Engineers, Houston, TX, May 1985, p. 18.
- [3] Levy, A. V. and Chik, P., "The Effects of Erodent Composition and Shape on the Erosion of Steel," *Wear*, Vol. 89, No. 2, Aug. 1983, pp. 151–162.
- [4] Sargent, G. A., Spencer, D. K., and Saguez, A. A., "Slurry Erosion of Materials," *Proceedings*, NACE Conference on Corrosion-Erosion-Wear of Materials in Emerging Fossil Energy Systems, Berkeley, CA, Jan. 1982, National Association of Corrosion Engineers, Houston, TX, pp. 196–231.
- [5] Levy, A. V. and Hickey, G., "Surface Degradation of Metals in Simulated Synthetic Fuels Plant Environments," Paper No. 154, *Corrosion/82*, National Association of Corrosion Engineers, Houston, TX, Mar. 1982.
- [6] Levy, A. and Yau, P., "Erosion of Steels in Liquid Slurries," *Wear*, Vol. 98, No. 1–3, pp. 163–182, Nov. 1984.
- [7] Levy, A., Yau, P., and Jee, N., "Erosion of Steels in Coal-Solvent Slurries," Paper No. 83, *Corrosion/84*, New Orleans, LA, April, 1984, National Association of Corrosion Engineers, Houston, TX.
- [8] Levy, A., Lochmann, W., and Cornet, I., "Coal Liquefaction Alloy Test Program—Annual Report FY 1978," Report No. LBL 8754, Lawrence Berkeley Laboratory, University of California, Berkeley, CA, Nov. 1978.

K. G. Sedman,¹ J. C. Thornley,¹ R. D. Gilders,¹ and G. R. Hoey²

The Validity of Fuel Recycling During Erosivity Testing Using Coal-Water Liquid Fuels

REFERENCE: Sedman, K. G., Thornley, J. C., Gilders, R. D., and Hoey, G.R., "The Validity of Fuel Recycling During Erosivity Testing Using Coal-Water Liquid Fuels," *Slurry Erosion: Uses, Applications, and Test Methods, ASTM STP 946*, J. E. Miller and F. E. Schmidt, Jr., Eds., American Society for Testing and Materials, Philadelphia, 1987, pp. 78–90.

ABSTRACT: A coal and water fuel was recycled repeatedly through an erosion test loop. The effects of this on the fuel's erosiveness were studied. This was done to determine the feasibility of erosion testing using continuously recycled coal-water fuel. The erosiveness of the coal-water slurry was observed not to be a monotonic function of the number of cycles but was observed to rise to a peak and then decrease. The initial increase in the erosiveness of the slurry was correlated with an increasing liberation of large angular pyrite grains, whereas the subsequent decrease in erosiveness was correlated with the comminution and rounding of the grains of solid matter and with increasing viscosity.

KEY WORDS: coal, slurry, erosion, testing, viscosity, pyrite, aluminum, Type 416 stainless steel, tungsten carbide, alumina

The erosiveness of liquid fuels containing powdered coal has led to erosion problems in burner nozzles, pumps, piping, and valves [1–3], but particularly in nozzles. There is a clear need to perform erosion tests on candidate components or candidate materials which are to see service in plants burning or manufacturing coal/liquid fuel mixtures (CLM). In order to be valid, this testing must be for a substantial period. There are two alternative test methods. One is to take a large quantity of fuel and pass it through the component being tested, once

¹ Metallurgist, metallurgist, and superintendent of pyrometallurgy, respectively, New Brunswick Research and Productivity Council, P.O. Box 6000, Fredericton, New Brunswick, Canada E3B 5H1.

² Research scientist, Canada Centre for Mineral and Energy Technology, 568 Booth Street, Ottawa, Ontario, Canada K1A 0G1.

only. The other alternative is to take a lesser quantity of fuel and recirculate that fuel through the component many times to provide the necessary operating time. This second procedure is generally the more economic regarding fuel usage, but there is a problem in that, if the fuel itself is changed by the recycling, one might expect the fuel's erosiveness to change.

In the work performed here, the passage of coal-water slurry through a small orifice and against a target plate has been used to simulate the component, or material, being tested.

Materials and Equipment

Washed thermal coal was crushed in a ball mill to 75% less than 200 mesh (75 μm), and a top size of 64 mesh (231 μm) was achieved by screening. The coal was a high volatile bituminous coal containing 3 to 3.6% sulfur and 9.3 to 10.8% ash. This crushed coal was mixed with tap water to make a 50% coal 50% water slurry. A wetting agent (A-23, from Diamond Shamrock Chemicals Canada, Inc.) was added to a concentration of 0.2% of the coal's weight to make it easier to mix the coal with the water. Three separate lots of 1140 L of slurry were made at different times.

The slurry was pumped through a 3.2-mm-diameter nozzle at a constant rate of 0.32 L/s using a Moyno progressive cavity pump (Model 3L6). This corresponds to a jet velocity of 40 m/s at the nozzle. The nozzle was a standard polished tungsten carbide wire drawing die.

The jet from the nozzle impinged on the centre of a target material situated 20 mm from the nozzle tip and mounted at 45° to the jet axis. The targets were 25 mm square, and less than 25% of the area of the target facing the nozzle was eroded by the jet. Six targets were mounted on a carousel (Fig. 1), and by rotating the carousel new targets could be presented to be impinged on by the jet.

Three sorts of target materials were employed for the majority of the work.

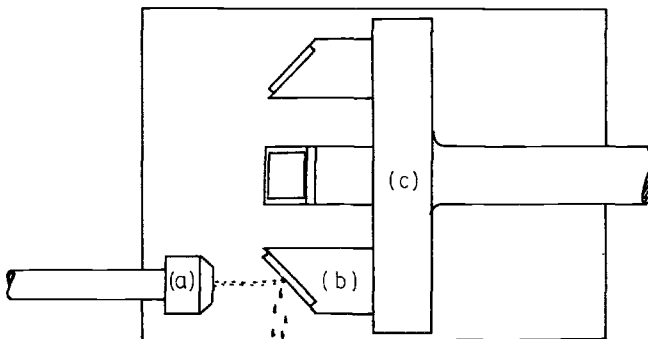


FIG. 1—The spray chamber displaying (a) the nozzle, (b) the sample stands, and (c) the carousel.

These were: pure aluminum of 25.1 Vickers Hardness Number (VHN); hardened Type 416 stainless steel of 525 VHN; and a cemented tungsten carbide of about 1800 VHN. Two tests were performed on an alumina target specimen of 99.7% theoretical density and of a hardness of 2000 VHN.

Erosion Test Procedure

Slurry was pumped out of the storage tank, passed through the nozzle, and, after striking a target, was returned to the storage tank. Each time that a volume of slurry equal to the volume of slurry then in the tank passed through the nozzle, the slurry was considered to have been exposed to one cycle.

Erosivity measurements were performed during selected cycles to determine the erosiveness of the slurry towards hard and soft materials. Then, three weight loss erosivity measurements were performed on new, flat specimens during those cycles, and for the remainder of those cycles the jet was directed against a hard consumable target. The erosivity weight loss measurements during a cycle involved the exposure of a soft target specimen to the jet for 10 min, rotating the carousel so that a hard target specimen was exposed for 20 or 30 min, and exposing a second soft target specimen to the jet for another 10 min. For those cycles when the slurry's erosiveness was not measured, the jet was directed against the hard material throughout the whole cycle. The "hard" target was either hardened Type 416 steel or cemented tungsten carbide. The erosion exposure time for the hardened Type 416 steel target specimens was 20 min and for the tungsten carbide target specimens, 30 min. The erosivity measurement target coupons were ground to a 600 grit finish prior to the measurements and were weighed before and after exposure, and the "soft" targets were always pure aluminum.

Slurry erosivity measurements were performed during a selected cycle following a given number of previous cycles of the slurry. These numbers of prior cycles generally were 0, 1, 3, 5, 10, 20, 35, 70, 100, 150, 200, 250, 300, and 400. The execution of all these cycles for one lot of slurry was called a campaign, and a new lot of slurry was mixed for each of three campaigns. In the first and second campaigns the hard material was Type 416 steel, and in the third campaign it was tungsten carbide. Also in the third campaign, a sample of alumina was exposed to the slurry for one cycle once and for twenty cycles on another occasion. This exposure was early during the third campaign.

Prior to each erosivity determination, a 10-L sample of slurry was removed. No additional slurry was added but water losses from evaporation were corrected. The mixture's pH, solids concentration, and viscosity were measured, the latter by using both a Brookfield viscometer and a Ferranti concentric cylinder viscometer. These measurements were made at the same cycles at which the erosivity determinations were made.

The solid fraction of each sample of slurry was filtered off and dried and then examined to determine the particle size distribution, mineral abundances,

and the particle shape. The particle size distribution was measured both by wet screening and by image analysis. Density separations were conducted using a liquid of specific gravity of 2.4 which concentrated the heavy mineral fraction for examination using X-ray diffraction techniques. The concentrated mineral fraction was also examined by image analysis in order to determine the mineral size, shape, and degree of rounding, as well as the amounts of free quartz and free pyrite.

Results

Slurry Erosivity

The erosiveness of a slurry towards a material is defined here as the loss in weight of a new sample of that material exposed to the slurry jet for a specific period. The change in erosiveness of the three slurries with respect to recycling is displayed in Figs. 2, 3, and 4. It is immediately apparent that the slurry's erosiveness is not a monotonic function of its cycling history. These curves indicate that each slurry initially became more erosive with recycling, reached a maximum value following 100 cycles (Fig. 2) or 20 cycles (Figs. 3 and 4), whereafter the slurry became progressively less erosive with further recycling.

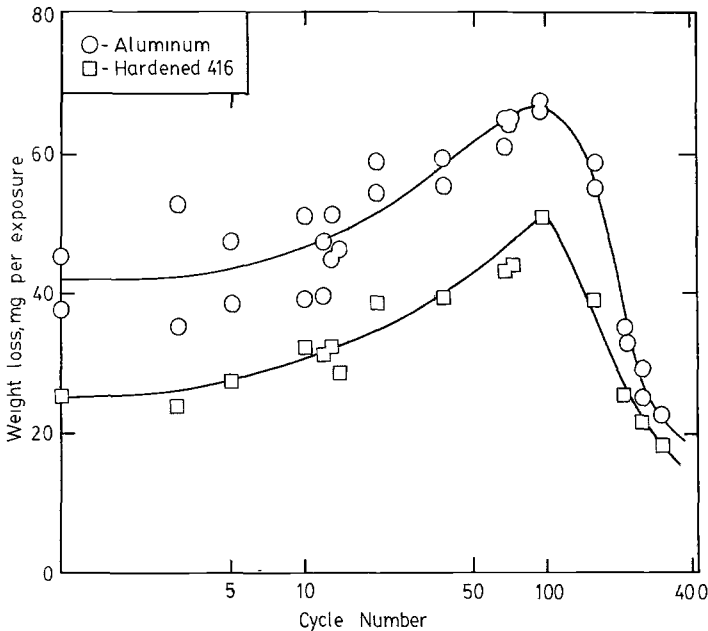


FIG. 2—Erosion results from the first campaign. Note here, and in Figs. 3 and 4, that the weight losses rise to a maximum and then fall.

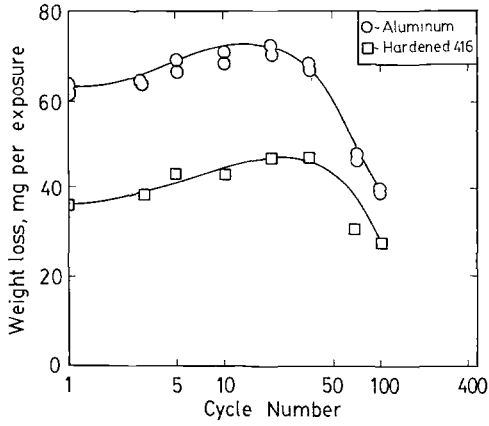


FIG. 3—The pattern of rising and falling weight losses in the second campaign. The pattern is similar to the first campaign.

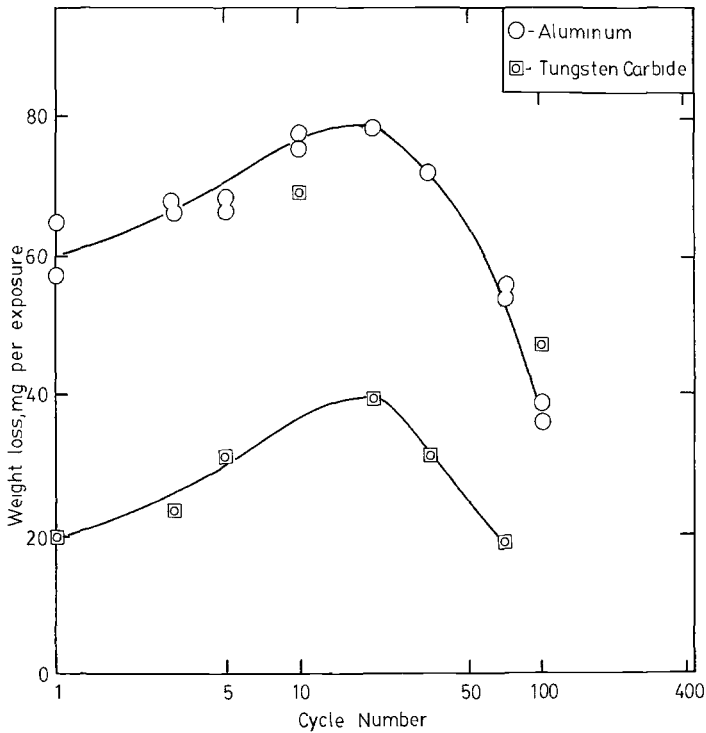


FIG. 4—The pattern of weight loss as the slurry ages in the third campaign. The pattern is similar to Campaigns 1 and 2. Here, however, we have aluminum and tungsten carbide targets.

The location and magnitude of the peak erosivity of the slurry, for the three campaigns, was different. (The three batches of slurry were also somewhat different. The batch made for the first campaign was somewhat coarser grained than that used in the second and third campaigns.)

When the positive slope (initial part of the curve) of the erosiveness against recycling curve was first seen, it was not known whether this was a real slurry property or whether it was an artifact of the testing procedure. A particular concern was that nozzle wear, which others have found to be of major significance [4], might be causing this effect. To examine this hypothesis, erosion tests were conducted using four different nozzles in quick succession on a fairly old slurry (110 cycles). One of these nozzles was brand new, a second had had 42 000 L pumped through it, and the third and fourth were more seasoned still: they had had 182 000 and 430 000 L (400 cycles) pumped through them, respectively. The weight loss results in these erosion trials did not depend in any way upon the history of the nozzle (Fig. 5).

Secondly, one nozzle was left in place following one campaign and used for the succeeding one. The rise, peak, and fall in erosion was obtained in exactly the same way for the two campaigns but with the same nozzle.

It was concluded at this stage that the peaking of the erosiveness was a real slurry property rather than an experimental artifact. Other parameters such as velocity, impingement angle, and solids loading, which would also affect the erosion weight loss, remained as near constant as could reasonably be achieved during each campaign.

The peaking behavior observed in the results from the aluminum erosion target samples was also observed for both hardened martensitic stainless steel and cemented tungsten carbide erosion test targets (Figs. 2, 3, and 4).

It was noted earlier that in the third campaign, alumina was employed as a hard target. The use of the alumina did not change the pattern of the erosion

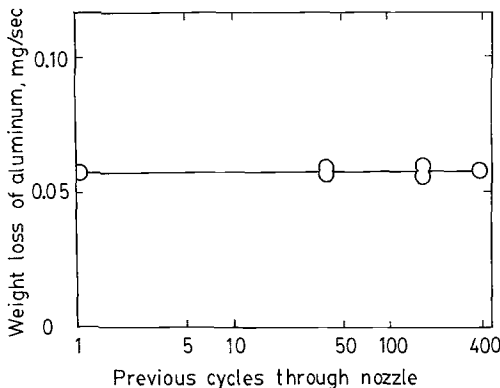


FIG. 5—The effect of prior nozzle history upon weight loss was measured; no effect whatever of nozzle history was found upon weight loss for up to 400 cycles of operation.

results. However, if more campaigns had been employed, then some effects of using an alumina target might have been discernible. It might also be noted that the alumina was, by far, the most erosion-resistant of all of the target materials that were used.

Viscosity, pH, and Particle Size Changes During Recycling

The curves in Fig. 6 indicate that the viscosity of the recycled slurry is constant for at least five cycles, after which the viscosity increases.

The pH of the recycled coal liquid mixtures also exhibited an initial period in which there was no change in pH, after which the pH dropped. Figure 7 displays this behavior for the three campaigns. The change in pH is probably due to the chemical reaction of the coal minerals, largely iron sulfide, with the dissolved oxygen and water to form sulfate ions while removing hydroxyl ions as a result of the hydrolysis of ferric ions. These reactions, the end products of

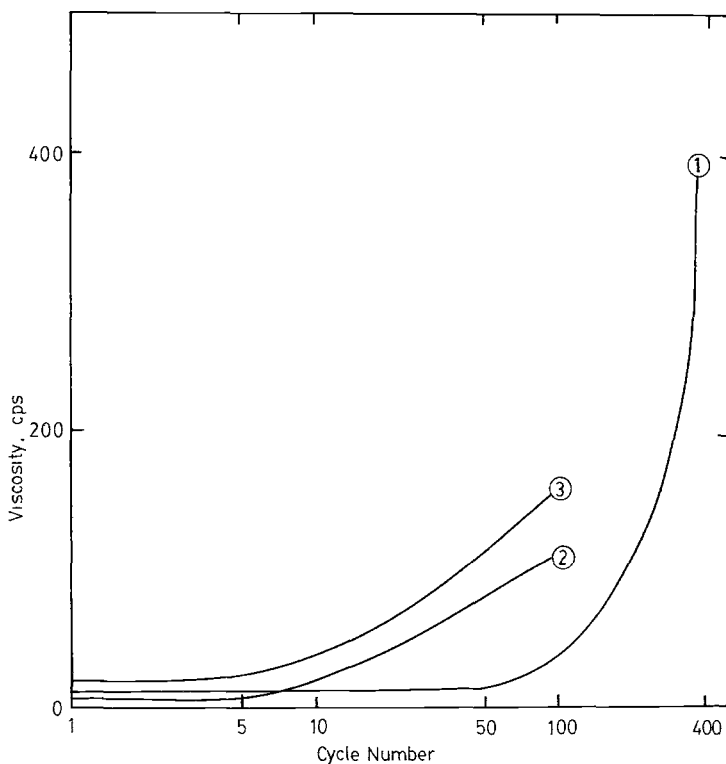


FIG. 6—Following repeated recycling in each campaign, the viscosity increased quite rapidly and the abrasiveness of the slurry fell at the same time. Numbers 1, 2, and 3 on the curves indicate results from Campaigns 1, 2, and 3.

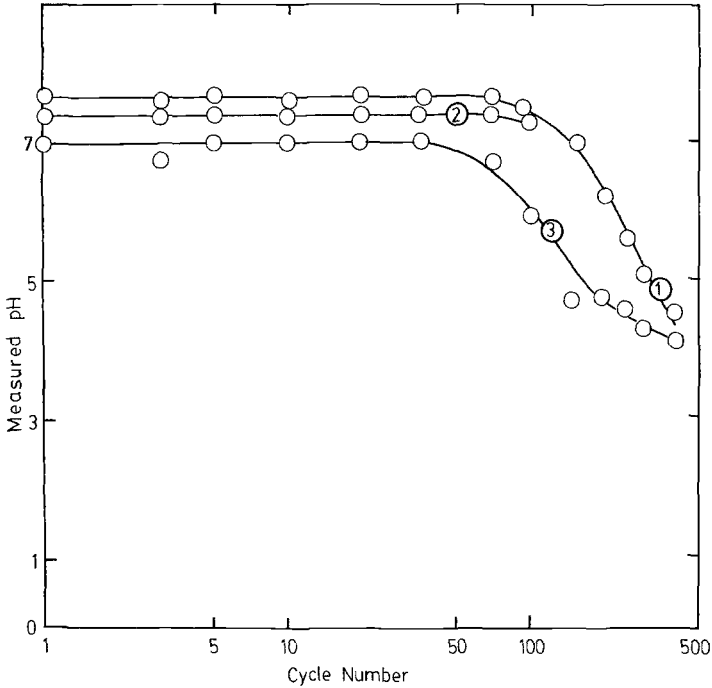


FIG. 7—The slurry reached a pH of 4 to 4.5 after 400 cycles. The increasing acidity did not correspond with the rise in the viscosity. Numbers 1, 2, and 3 on the curves refer to Campaigns 1, 2, and 3.

which are hydrated iron oxides and mineral acids, may be catalyzed by bacteria to a substantial extent and lead to corrosive conditions.

Measurements of the solid's particle size indicated that the average grain size of the solid particles decreased monotonically with recycling. The solid grains are eroded progressively from one slurry cycle to the next. Figure 8 illustrates this point. The three batches of slurry did not have identical initial particle size distributions. However, at the peaks in the erosion curves the three batches of slurry did have very similar particle size distributors (70.4, 69.4, and 68.7% less than 44 μm): The slurry's abrasiveness started to fall as the viscosity reached 50 cP, and this, in turn, occurred when the particle size fell to approximately 69% less than 44 μm .

Mineralogy

Mineralogical examinations were performed both on bulk as recycled coal samples and on those (heavy) fractions which sank in the liquid with a specific gravity of 2.4. (The carbonaceous coal matter itself will float upon a liquid of

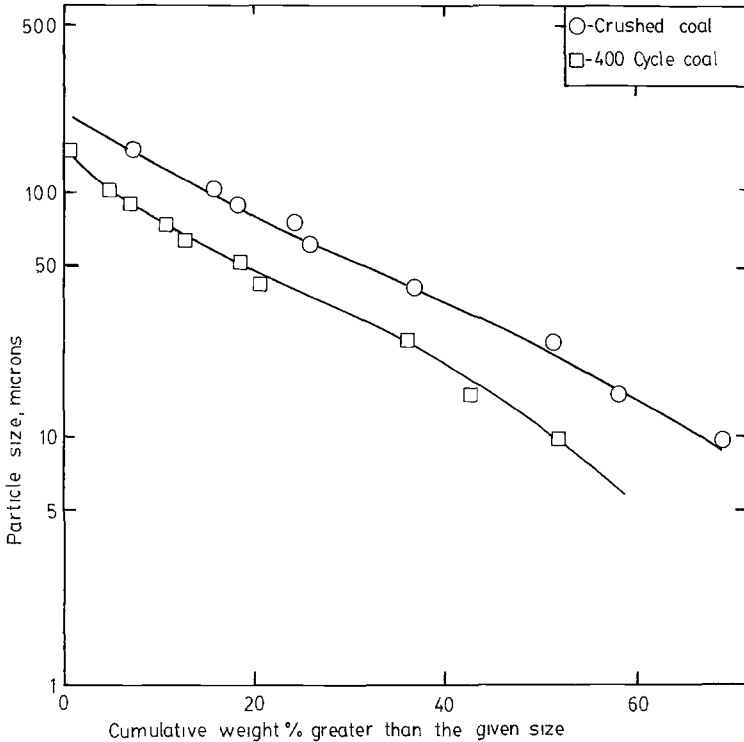


FIG. 8—The solid particles became progressively finer as the slurry was recycled. The reduction in size by about a factor of 2 follows 400 cycles of impingement, 98% of which was on a hardened 416 stainless steel target specimen (Campaign 1).

specific gravity 2.4, but the mineral impurities, provided that they have been freed from encircling light coal, will sink in such a liquid.)

X-ray diffraction of the sink sample indicated that the relative abundance of the softer minerals chlorite, magnetite, and siderite decreased, whereas the harder minerals (pyrite and quartz) increased in relative abundance. However, pyrite was always the most abundant mineral in the sink fraction.

Optical microscopy showed that the mineral matter in all the test samples was mainly in very fine grains of $<20 \mu\text{m}$ with the exception of massive irregular pyrite grains, which exceeded $100 \mu\text{m}$.

Those pyrite grains which were separated in the sink fraction became larger in the early cycles of exposure (Fig. 9). These particular pyrite grains also became more angular after the first few recyclings of the slurry. The shape was characterized as each particle's area in section divided by the square of its perimeter. Initial recycling gave a general decrease in this parameter, indicating more angular particles were predominating in the pyrite sink fraction, but by

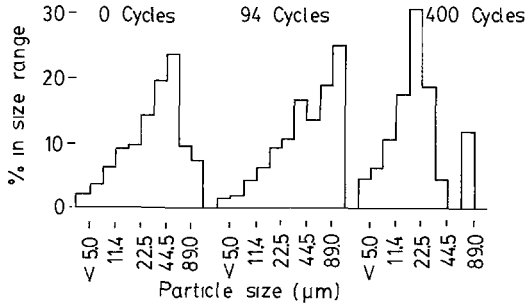


FIG. 9—Particle size distributions for the pyrite in the sink fraction following 0, 94, and 400 cycles in the first campaign. The mean particle size initially increases but subsequently decreases. The decrease in particle size of this “sink pyrite” was first noted following about 100 cycles of recirculation.

the end of each recycling campaign there was a clear increase in the parameter, indicating rounding (Fig. 10).

Discussion

The Cause of Peaking

Corrosion was not considered to be a major factor in the weight loss, since the major pH reduction coincided with a negative, not a positive, slope of the weight loss versus slurry recycling (slurry aging) curve. The corrosion rate of

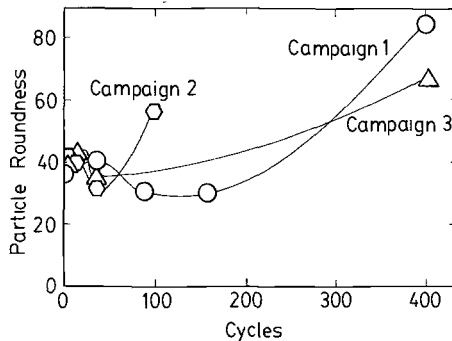


FIG. 10—“Particle roundness” means the proportion (%) of particles having a shape factor greater than 0.03. The shape factor is the particle’s area divided by the square of its perimeter. For a sectioned sphere this would be $(4 \pi)^{-1}$, or about 0.08. A prism of square section and of length six times its width viewed on a side would have a shape factor of 0.031. The particles are the pyrite sink fraction. Note that initially they tend to become more angular but subsequently become quite rounded.

aluminum was measured during this period and was found to be increasing as the pH dropped.

The overall particle grain size constantly decreased as the slurry aged. This can be expected to result in a continuous decrease in erosion rate. The reduction in slurry erosiveness following the peak in the erosion rate does coincide quite well with an increase in the viscosity of the mixture. This corresponds with the prediction [4,5] that erosion by a slurry is inversely related to the viscosity of the slurry. The viscosity of the slurry does not appear to depend sensitively upon solids loading at a loading of 50% [6], which is the loading used in this test. The increase in the viscosity was, therefore, concluded to be a result of reduction in coal particle size, and the decrease in erosiveness following the erosion peak is considered to be a result of increasing slurry viscosity and a result of reducing the overall particle size.

During the time in which the erosion was increasing, the heavy minerals became increasingly liberated and semiliberated, resulting in larger and more angular pyrite and probably also quartz grains being able to strike the target surfaces. It seems reasonable that the erosion will increase as the number of hard large particles in the slurry increases [7], and it is suggested that the initial freeing of these pyrite (and quartz) grains causes the slurry to become more erosive.

Significance of Peaking with Respect to Erosion Testing

Since the location and height of the erosion peak depends on both CLM properties and operational conditions, the exact peak position in any one trial cannot presently be predicted.

From the limited work performed here, the peak position would appear to move towards shorter times as the target plate's hardness is increased. If the peaking behavior is a function of the pyrite particle's liberation by particle fracturing, then the more efficiently the particles are fractured by impacting on a hard target, the sooner we will reach the peak.

If the trend of erosion peaking and the influence of viscosity upon this peaking is a general coal slurry characteristic at high slurry flow rates, then erosion testing involving recycling could be conducted until an increase in viscosity is observed, at which time the erosion test is concluded with that particular batch of slurry. The erosion rate over this period should have remained higher than the original slurry erosivity. This would result in weight losses that would be greater than those obtained when continuously using new slurry.

Aluminum, hardened Type 416 stainless steel, and tungsten carbide all showed the same dependence of erosion rate upon slurry age. The erosion of both of the harder materials rose and fell in phase with the erosion of the soft aluminum. Hence at this 45° impact angle the erosion of one can be predicted from the erosion of another. It is not known whether this pattern can also be extended to alumina, or to other materials of greater erosion resistance than tungsten

carbide, or whether the pattern is valid at angles other than 45°. These investigations will be the subject of future work.

Conclusions

1. The erosivity of a 50% coal 50% water slurry [75% less than 200 mesh (75 μm)] is not a monotonic function of recycling but initially increases, peaks, and then falls.
2. The peaking behavior in the erosion versus recycling curves was observed for aluminum, Type 416 steel, and cemented tungsten carbide. The peaks were all in phase during any particular campaign.
3. Erosion testing using recycled slurry is complicated by the erosion peaking behavior observed, but recycled slurry can be used to yield conservative results.
4. The initial increase in the observed erosiveness of the slurry is thought to be caused by the liberation of pyrite and other hard mineral constituents from encircling softer materials.
5. The decrease in the slurry's erosiveness after the erosion peak coincided with a large increase in slurry viscosity, which in turn coincided with 69% of the particles passing through a 44- μm screen. This viscosity increase in conjunction with the comminution of the harder particles is believed to be responsible for the erosivity decline.

Acknowledgments

This work was supported by the Canadian Centre for Mineral and Energy Technology (CANMET). The authors would like to thank CANMET for this support and for permission to publish the results. We should also like to thank S. G. Whiteway of National Research Council, Halifax for provision of the alumina samples and H. L. J. Drummond and D. Abbott of New Brunswick Research and Productivity Council for their comments on the manuscript.

References

- [1] Thornley, J. C., "Nozzle Erosion During Slurry Firing, Chatham GS, 1978-1979," Report No. E/79/64, New Brunswick Research and Productivity Council, Fredericton, Canada, May 1979.
- [2] Whalen, P. J., Davies, F. W., Lee, L. K., and Mitchell, K. A., "A Study of Coal Agglomeration and Coal-in-Oil Mixture Combustion in a Utility Boiler Period: June 1978 to July 1979," prepared for the Federal Department of Energy, Mines, and Resources Canada, D.S.S. Contract No. 18SQ23440-7-4055-IV, 6 Sept. 1979.
- [3] Whaley, H. and Whalen, P. J., "Burner Nozzle Wear During Coal-Oil-Mixture (COM) Combustion Trials in a Small Utility Boiler," prepared for the Federal Department of Energy, Mines, and Resources Canada, Division Report ERP/ERL 80-85 (op), Nov. 1980.
- [4] Al Taweel, A. M., Murphy, G., and Covill, I. D., "Erosion in Coal Liquid Mixtures Handling Systems," Fourth International Symposium on Coal Slurry Combustion, May 1982, Orlando, FL, Pittsburgh Energy Technology Centre, Pittsburgh, PA.
- [5] Batra, S. K. and Kenney, R. B., "Rheology and Pumping Characteristics of Coal-water Slurry

Fuels Prepared in a Columbia Chase Integrator," Fifth International Symposium on Coal Slurry Combustion and Technology, Tampa, Pittsburgh Energy and Technology Center, Pittsburgh, PA, 1983, p. 1119.

- [6] Al Taweel, A. M., Fadaly, O., Kwak, J., MacKay, G. D. M., McKee, W., "Rheological Properties of Coal/Water and Coal/Oil/Water Mixtures," Fourth International Symposium on Coal Slurry Combustion, Orlando, FL, 1982, Pittsburgh Energy and Technology Center, Pittsburgh, PA.
- [7] Raask, E., "Input Erosion Wear Caused by Pulverized Coal and Ash," *Proceedings, 5th International Conference on Erosion by Solid and Liquid Impact*, published by University of Cambridge, Cambridge, UK, 1979, pp. 41(1-7).

Rebecca M. Summer¹

A Review of Pipeline Slurry Erosion Measurements and Research Recommendations

REFERENCE: Summer, R. M., "A Review of Pipeline Slurry Erosion Measurements and Research Recommendations," *Slurry Erosion: Uses, Applications, and Test Methods*, ASTM STP 946, J. E. Miller and F. E. Schmidt, Jr., Eds., American Society for Testing and Materials, Philadelphia, 1987, pp. 91–100.

ABSTRACT: The basic factors which determine the ability of a slurry to abrade or erode its conduit are the properties of the slurry itself, the properties of the pipe material, and the nature of the flow. The Miller number currently used to predict sliding wear in pumps may be useful to predict relative wear resistance of pipelines until standardized pipeline tests are developed. Values of the hardness parameter of slurry and pipe material show a strong correlation with erosion capability of a slurry, although the derived empirical relationships are only valid for the specific system under study. Future abrasion studies should include: (1) standardization of slurry and pipe material properties and flow characteristics for laboratory and field investigations; (2) determination of the relationship between commonly used abrasion indices and pipeline service life; and (3) continued development of methods for measuring absolute abrasion rates.

KEY WORDS: pipeline abrasion, hardness, Miller number, standardization

The hydraulic transport of solids in pipes is a classical means of transporting natural resources such as sand, gravel, coal, copper, limestone, iron, nickel, phosphorus, and kaolin. Slurry pipelines have a wide application and have been employed in Europe since the early 1800s and in the United States since the 1850s, when gold-bearing sand was transported in California. The longest operating pipeline today in the United States is the Black Mesa line, which is 440 km long.

During this time of industrial development, pipeline erosion, that is, physical wear, was found to be a significant limiting factor in the service life, and therefore in the economic and competitive possibilities of this mode of

¹ Geologist, 1175 Niagara #11, Fort Collins, CO 80522.

transportation. The basic factors which determine pipeline erosion are the properties of the slurry itself, the properties of the pipe material, and the nature of the fluid flow. It is only in the last 20 years that studies have been conducted to measure and predict erosion in pipelines and associated pumping equipment.

A review of these studies indicates that different properties and flow characteristics have been isolated and studied, but in many cases basic controlling parameters or properties have not been reported or are disregarded when evaluating research data. This makes comparisons of laboratory experimental methods and abrasion indices with actual service life, as well as the prediction of service life, very difficult.

The term *erosion* has been used interchangeably with *abrasion* in the literature [1,2]. *Erosion* is defined here as the physical removal of material by (a) cutting or sliding (abrading) wear by impact of a sharp particle at a grazing angle which mechanically removes materials, and (b) deformation or impact wear by impact resulting in surficial fracture and subsequent removal. Particle motion in a slurry includes sliding, rolling, and saltation; hence, both types of eroding processes are inherent in slurry erosion to varying degrees.

The type of erosive wear addressed in this paper includes both mechanisms: cutting, sliding, and abrading erosion and deformation and impact erosion. The term *abrasion* is used only when authors have so defined their respective testing conditions.

The objectives of this paper are to evaluate and compare material parameters and indices used to predict erosion rates and to recommend a standardized approach to erosion studies and methods of prediction. This information is needed by designers to improve pipeline systems design and extend their probable maximum life.

It is recognized that pipeline corrosion is also a significant process active simultaneously with erosion. The factors controlling the wear effects of corrosivity are different and therefore are not considered here.

Review of Technological Advances in Abrasion Testing

Pipeline erosion by slurries is described in the literature by an absolute measure or by relative values. Relative values are either (a) an index of erosion as defined by a standard set of procedures and characteristics of a test or (b) a parameter such as hardness which correlates with measured erosion rates. The erosion index is commonly referred to as an abrasion index and requires an understanding of how a particular value or index of erosion is measured, so that the reliability and applicability of these values to a pipeline design can be assessed.

Absolute Measurement Methods

Absolute measurement of erosion is used to evaluate erosion occurring within operating pipeline systems, as well as on laboratory pipeline models or test

loops. These measurements are also needed to calibrate and assess relative erosion values and simulation models.

The most recent review of absolute measurement techniques was done by Baker et al. [1], who evaluated seven absolute measurement methods used in slurry pipeline research: metrology, weighing, neutron irradiation, surface activation, nucleonic gaging, electrical capacitance, ultrasonic gaging, and permanent magnet gaging. These methods were compared experimentally and evaluated in terms of detecting the removal of 0.025 m of material over a 10-h period, which is equivalent to 1 mm per year within an accuracy of 2.5%. Only weighing and surface activation were considered to be readily applicable to meaningful measurements of pipeline erosion. (Surface activation involves making a test pipe section or test apparatus radioactive and monitoring the increase in radiation of the slurry as the wall is worn away.) Weighing, although simple, requires submersion, so rusting of steel pipes and water absorption by plastic pipes are problematic to precise measurement. Likewise, surface activation or irradiation is not universally accepted because it is not yet applicable to plastic pipes.

Barker et al. [3] suggested that measuring the change in electrical capacitance with change in wall thickness was worthy of further research evaluation. However, studies by Baker et al. [1] indicated that this method requires considerable development due to problems with sensitivity of the measurement to wall thickness and water absorption. Because of these problems, the method does not appear to be as reliable for use in field or laboratory tests as weighing or surface activation.

Relative Erosion Values

Various types of relative erosion values are reported from simulation and model studies to describe and predict the amount of erosion that can be expected in a field pipeline system. Relative or indirect measures are commonly used because they are simple and easy to generate compared to absolute measurements, and they provide guidelines for designers. The advantages, disadvantages, and applicability of erosion indices and indices of hardness are evaluated below to better understand their relationship to the erosion process.

The Miller number, a standard index of sliding wear in pumps, is a measure of the instantaneous rate of mass loss of a standard chrome-iron wear block [ASTM Test for Slurry Abrasivity by Miller Number (G-75-82)]. The test duplicates the back and forth rubbing action of a reciprocating pump. Values are measured by developing a time curve which accounts for loss by both corrosion and abrasion. The Miller number has proven to be a useful parameter for pump design and should only be used to compare life-of-parts in equipments of similar design to the reciprocating pump, according to Miller [4]. The first number of the Miller index is the abrasivity number, or rate of mass loss. Miller [4] states that slurries with values less than 50 are not considered abrasive to a double-acting, piston-type unit. The second number is the attrition number, described as the effect of slurry particle breakdown measured by a loss in

abrasivity as the test proceeds. A positive attrition number indicates that abrasivity increases with time, while a negative number indicates a decrease. Although this number is not currently used to assess pump design and performance, Miller suggested that future studies may use the attrition number in predicting rheological changes.

Schumacher [5] has also studied erosion rates in pumps using a Taber-Met abrader wear testing machine. His results of metal-against-metal wear indicated that steels heat-treated to higher hardness and prior cold working of austenite alloys do not always improve their wear resistance. He also noted that the relative difference in hardness of two test metals is an important factor in the amount of erosion that occurs. More information is needed to adequately compare and evaluate these test results with results using the Miller abrasion apparatus.

Indices of hardness have been widely used to characterize erosion resistance of pipelines. Hardness of both the slurry particle and the pipe surface has been described by the Brinell scale of hardness [ASTM Test for Brinell Hardness of Metallic Materials (E 10-84)]. Brinell Hardness (HB) is a number in kgf/mm^2 relating applied spherical load to the surface area of indentation on the material under test. BH numbers have been translated into a scale correlated with the Mohs hardness scale of minerals by Wilson [6]. It should be emphasized that the scales represent ranges of values. For example, quartz, with a unique value of 7 on the Mohs scale, ranges from roughly 6 to 8 in nature. Likewise, silica sand, which is composed of quartz, exhibits a range of 550 to 800 on the Brinell scale.

Values of common ores and metal pipe materials are listed in order of hardness in Table 1. These values provide a guideline for designers in choosing materials and in evaluating their probable resistance to a particular slurry. For example, of the pipe material tested only iron nickel and chromium alloys have hardness values that are roughly equal to that of silica sand. This suggests that slurries containing silica, for example, coal, can be expected to erode steel pipelines to some extent.

Material hardness can also be described by the Knoop Hardness Number (KHN). The method for determining this index [ASTM Test for Microhardness of Materials (E 384-84)] involves an indentation hardness test using a calibrated machine which forces a rhombic-based indenter into the material under test.

Young and Ruff [7] demonstrated that the hardness of slurry particles as defined by KHN is one factor in determining erosion capability of a pneumatic slurry. A modified jet-type nozzle erosion tester was used to eject particle-gas mixtures at temperatures from 25 to 500°C onto metal surfaces. A wide range of particle sizes and types, velocities, and concentrations was tested against iron- and steel-base alloys. Because other factors, such as sintering of particles to metal surfaces and temperature, interact with the hardness parameter, the relationship between hardness and abrasion was not quantified.

Vickers Hardness Number (VHN) is also cited in the literature [8,9] as a significant index for correlating hardness with erosion rates. As defined in

TABLE 1—Comparison of brinell hardness values of pipe material and slurry particles [6].

Pipe Material	Slurry Material	Brinell Hardness, kgf/mm ²	
General plastics	Graphite	2	
	Bentonite	4	
	Potash	12	
		15 to 45	
	Kaolin	25	
	Anthracite	35	
	Bauxite	90	
	Dolomite	135	
	316 SS and AL bronze		150
	Grey cast iron	Siderite	180
Austenitic MN steel		215	
CA 40 SS		300	
	Asbestos	310	
	Glass	350	
	Taconite	400	
	Silica sand	550 to 800	
Martensitic white Fe, Ni hard IS/3 alloy		550 to 800	
28% Cr iron		600	

ASTM Test for Vickers Hardness of Metallic Materials (E 92-82), the method is similar to the KHN test, except that a pyramidal diamond indenter is used.

Sheldon [8] tested copper-nickel alloys and pure materials using a sand-blasting method to produce erosion. His study indicated that the VHN is the best material parameter to use in predicting wear rates and in modeling erosional processes. The best correlation of hardness with erosion was observed for hardness measured on a fully work-hardened (eroded) surface. He noted that other investigators have shown a similar relationship using abrasive grinding methods, and it is possible that this relationship also typifies abrasion from a liquid slurry media.

A model study of slurried river sand in steel pipes by Hisamitsu et al. [9] showed that erosion rates are inversely proportional to the VHN. Empirical formulas were used to estimate maximum erosion rates within a limit of error of 30%. For example,

$$W_{\text{smax}} = 0.0371V^{2.85}$$

$$\frac{W_{\text{max}}}{W_{\text{smax}}} = 79.6H_v^{-0.95}$$

where

W_{smax} = Maximum erosion rate of nonheated steel,

W_{max} = Average maximum erosion rate of carbon, refined, low alloy steel,

V = Slurry velocity, and

H_v = Vicker hardness of nonheated steel (Ref 8, p. 326).

The study also indicated that for pipe materials of the same hardness, erosion resistance increased from heated steel to nonheated steel and low-alloy steel. As with the Miller number, these experimental formulas should only be applied to systems of similar test equipment and operating conditions defined in the study.

Comparative Results

Matrices comparing published values of hardness measured by the Brinell, Knoop, and VHNS for pipe materials and typical Miller numbers and hardness values for slurry materials are given in Tables 2 and 3, respectively. Table 2 suggests that pipe materials exhibit a range of values, and many steels have hardness values less than silica and alumina (Al_2O_3), although higher than other types of slurry materials as identified in Table 3. Table 3 indicates that Miller numbers for slurries generally increases with increasing slurry particle hardness, although as suggested by Schumacher, improving the hardness of a metal does not always improve its resistance to abrasion (or sliding wear).

There is no generally accepted method for accurately relating or converting the published values of hardness given in Table 2. Approximate conversion values have been developed by ASTM for certain materials for use in cases where comparative tests have been obtained. Overall, values of HV, HB, and KH given in ASTM Hardness Conversion Tables for Materials (E 140-84)² are roughly the same. For example, for nickel and high-nickel alloys, values of HB and HV are similar and values of KH are consistently about 14% higher. For nonaustenitic steel, HV and HB are equivalent, while KH values are 4 to 12% higher. For copper-zinc alloys, low values of HB are nearly equal to values of HV, and high values are about 14% lower than HV. No values are given for KH of copper-zinc alloys.

Various factors such as operator techniques can be very influential in determining correlation coefficients appropriate for a certain set of hardness data and should be taken into consideration when comparing data sets.

Conclusions and Recommended Research

Erosion technology has not advanced to the point that wear rates for a given condition can be tabulated in a handbook. Laboratory tests and indices indicate trends and should not be used to design large-scale pipeline systems without carefully comparing the processes and properties present within the test situation with those in the field.

Studies reviewed herein indicate that abrasion of pumps is better understood

² The full title of this standard is: Hardness Conversion Tables for Metals (Relationship Between Brinell Hardness, Vickers Hardness, Rockwell Hardness, Rockwell Superficial Hardness, and Knoop Hardness).

TABLE 2—Comparison of hardness values for selected pipe materials.

Pipe Materials ^a	Brinell Hardness (Material Parameter), Ref 6 unless indicated, kgf/mm ²	Vickers Hardness (Material Parameter), Ref 8 unless indicated, kgf/mm ²	Knoops Hardness (Material Parameter), Ref 10, kgf/mm ²
General plastics	15 to 45
A53 (mild) steel	120 [10]
Low alloy steel	...	100 to 150 [9]	...
316 low alloy steel	150
Grey cast iron	180
Austenitic Mn steel	215
Carbon steel	...	95 to 240 [9]	...
CA 40 SS	300
Refined steel	...	130 to 630 [9]	...
Martensitic white Fe, Ni	550 to 800 [10]
Hard IS/3 alloy
28% Cr iron	600 [10]
I TEK 500 carbon steel
Inside surface	500 to 650 [10]
Outside surface	250 to 320 [10]
Titanium/vanadium carbide	2500
Iron carbide	1000
Pb: Eroded surface (work hardened)	...	100	...
Annealed surface	...	10 (0.05 N indenter)	...
Sn: Eroded surface (work hardened)
Annealed surface	...	60	...
Cd: Eroded surface (work hardened)	...	200	...
Annealed surface	...	170 (0.05 N indenter)	...
Al: Eroded surface (work hardened)	...	1300	...
Annealed surface	...	250 (0.15 N indenter)	...
Cu: Eroded surface (work hardened)	...	1900	...
Annealed surface	...	500 (0.25 N indenter)	...
Ni: Eroded surface (work hardened)	...	3500	...
Annealed surface	...	250 (0.50 N indenter)	...
40% Cu 60% Ni eroded surface (work hardened)	...	4300	...
Annealed surface	...	2300 (5 N indenter)	...

^a Pipe material is identified according to the authors' description, although it is probable that various alloys are very similar in composition.

TABLE 3—Summary of comparative values of abrasivity and hardness of slurries and slurry materials.

Slurry Material	Miller Number ^a of Slurry [4,11], ASTM G 75-82	Brinell Hardness (Material Parameter) [6], kgf/mm ²	Knoop's Hardness (Material Parameter) [7], kgf/mm ²
Graphite	. . .	2	. . .
Potash	0-0, 11+2	12	. . .
Clay	34
Kaolin	7,30	25	. . .
Coal	6-26, 57-3, 28-14
Anthracite	. . .	35	. . .
Limestone	30+11, 22-2, 46+11, 46-1
Gypsum	41	35	. . .
Bauxite	9,134	90	. . .
Dolomite	4-38	135	. . .
Copper	128-0, 19-8, 128-5	180	. . .
Tar sand	70
Fe ore	28-7, 157-11, 64+1, 234
Phosphate	68, 134-12, 74-7
Pyrite	194-4
Asbestos	. . .	310	. . .
Taconite	. . .	400	. . .
Pumice	500
Silica sand	51-10, 246-9	550 to 800	820
Alumina (Al ₂ O ₃)	2100

^a Miller Number: first number = abrasivity (rate of mass loss). Second number = increasing (+) or decreasing (-) attrition number.

and therefore more predictable than erosion of pipelines. The advancement of technological designs for pipeline erosion is complicated by highly variable fluid hydraulics. More definitive test methods are needed to evaluate new pipe materials and linings for which erosion resistances are unknown. The method for determining the Miller number, which characterizes pump wear, is relatively simple, uses small samples, and tests actual slurry properties. A similar standardized method to simulate and measure erosion in pipelines would improve the predictability of pipeline erosive wear. In the meantime, the Miller number may provide a relative indicator of the abrasive capabilities of slurries in pipes.

Standardization is one of the most critical requirements for the design and study of pipeline system erosion. Material properties and slurry flow characteristics have been isolated and studied by workers in the field, and in particular, the hardness parameter has exhibited the strongest correlation with pipeline erosion. However, many of the basic controlling factors of erosion have not been reported or are disregarded, making correlation of experimental results and erosion indices with pipeline service life very difficult.

Parameters which should be defined and quantitatively described in future work include:

1. Properties of the slurry: particle hardness, hardness as a function of temperature, specific gravity, particle size (and change of size with time), form (geometry), fracture tendency, relative density, sintering tendency.

2. Properties of the pipe: size, composition, structure, hardness, wall surface roughness, pipe orientation.

3. Nature of fluid flow: concentration, velocity, angle of impact, degree of turbulence, particle path, flow perturbations, slurry specific gravity, slurry rheology, slurry coefficient of rigidity, slurry yield stress.

The following recommendations for future study are strongly suggested to promote understanding of processes active during different types of laboratory test experimentation to determine how test results relate to field wear. Implementation of these recommendations are essential to progress in pipeline design and field performance.

1. Standardize a list of properties and flow characteristics known or suspected to affect erosion rates and define this list for each laboratory study and field investigation.

2. Relate commonly used indices to each other, to results of laboratory simulations, and ultimately to service life of pipeline systems.

3. Begin stringent documentation of pipeline service life so that technical design criteria and prediction of erosion in long-distance pipelines can be improved.

4. Evaluate effects of differences between parameters of the slurry and the pipeline material, for example, hardness, and ultimately relate this to erosion design.

5. Require manufacturers to determine a standardized set of erosion-related parameters for all new pipeline materials.

6. Continue to develop equipment and methods for measuring absolute erosion rates.

Acknowledgments

Simons, Li and Associates provided support and the opportunity to evaluate slurry pipeline erosion. Portions of this paper were developed under contract with Brown, Roedy, Bonvillian & Gold. Dr. Robert Faddick, Colorado School of Mines, gave helpful discussion and evaluations.

References

- [1] Baker, P. J., Jacobs, B. E. A., and Bonnington, S. T., "A Guide to Slurry Pipe-Line Systems," BHRA Fluid Engineering, 1979, p. 58.
- [2] Wasp, E. J., Kenny, J. P., and Gandhi, R. L., "Solid-Liquid Flow, Slurry Pipeline Transportation," Gulf Publishing Co., Houston, TX.
- [3] Barker, M. L., Truscott, G. F., and Mech, M. I., *Proceedings of Hydrotransport 3*, BHRA, 1974, pp. J3-33-50.

- [4] Miller, J. E., *Chemical Engineering*, 1974, pp. 103–106.
- [5] Schumacher, W. J., *Metal Progress*, Vol. 114, No. 6, American Society for Metals, Metals Park, Ohio, 1978.
- [6] Wilson, G., *Proceedings of Second International Conference on Hydraulic Transport of Solids in Pipes*, BHRA Fluid Engineering, Cranfield, UK, H2-25-52, 1972.
- [7] Young, J. P., Ruff, A. W., *Journal of Engineering Materials and Technology*, transactions of the American Society of Mechanical Engineers, New York, 1976.
- [8] Sheldon, G. L., *Journal of Engineering Materials and Technology*, transactions of the American Society of Mechanical Engineers, New York, 1976.
- [9] Hisamitsu, N. T., Iseh, Y., Honda, and Takeishi, Y., *Sixth International Technical Conference on Slurry Transportation*, Las Vegas, NV, March 24–27, Slurry Transport Association, Washington, DC, 1981, pp. 319–332.
- [10] Bhargava, R. K. and Parrott, E. R., *Sixth International Technical Conference on Slurry Transportation*, Las Vegas, NV, March 21–27, Slurry Transport Association, Washington, DC, 1981, pp. 351–356.
- [11] Sambells, O. F., *Proceedings of Hydrotransport 3*, BHRA, 1974, pp. J1-1-15.

Applications

Comparison Between Laboratory Characterization and Field Performance of Steel Mud Pump Liners Coated with CM 500L, a Tungsten-Carbon Alloy

REFERENCE: Bhat, D. G. and DeKay, Y. R., "Comparison Between Laboratory Characterization and Field Performance of Steel Mud Pump Liners Coated with CM 500L, a Tungsten-Carbon Alloy," *Slurry Erosion: Uses, Applications, and Test Methods, ASTM STP 946*, J. E. Miller and F. E. Schmidt, Jr., Eds., American Society for Testing and Materials, Philadelphia, 1987, pp. 103–117.

ABSTRACT: A coating of CM 500L (a tungsten-carbon alloy), deposited by a proprietary chemical vapor deposition (CVD) process on a steel mud pump liner, has been developed to give excellent wear resistance against slurry abrasion. The Miller Slurry Abrasivity Test was modified to simulate, as closely as possible, the conditions encountered in the field application. The modified Miller test was used successfully to compare the wear resistance of the coating with the microstructure. This comparison was found to be useful in the development of the coating process, permitting an optimization of the properties of the coating/substrate system for a predictable and acceptable field performance. The modified test procedure is shown to give results which can be used to predict the service life of CM 500L-coated steel mud pump liners with a much greater accuracy than with the conventional procedure.

KEY WORDS: chemical vapor deposition (CVD), controlled nucleation thermochemical deposition (CNTD), tungsten-carbon alloy, slurry abrasion, Miller Slurry Abrasivity Test, property/performance optimization

Transportation of solids through the medium of slurries has received considerable attention in recent years. The main driving force has been the economics of slurry transportation through pipelines as compared to other modes of transportation. As pointed out by Elkholy [1], the cost factor becomes very important when the annual throughput is increased.

¹ Senior research scientist and manager, New Coatings Development, GTE Valeron Corp., Troy, MI 48084.

² Manager, Quality Assurance Laboratory, San Fernando Laboratories, a division of Air Products and Chemicals, Pacoima, CA 91331.

It is clear that, to realize the predicted cost benefits of slurry transportation, one must put together a materials handling system that will be able to withstand the abrasive wear due to the entrained solid particles in the slurry, in addition to the chemical wear caused by the additives in the slurry medium that are designed to stabilize the slurry characteristics. Researchers have addressed the problem of slurry erosion encountered in various applications and have attempted to identify the parameters involved [1-4].

Experts in the field of research on wear agree that laboratory simulation of wear environment in real life is one of the trickiest aspects of wear testing. Wear is an extrinsic property of two surfaces in contact, and therefore, it is generally very difficult to precisely predict the field behavior of materials on the basis of laboratory data. Thus, the development of a well-defined laboratory test for wear in a given application is crucial. In addition, such a test usually has a direct application only in a situation which it closely simulates.

In this paper, we describe the modifications made to the Miller Slurry Abrasivity Test for the development of a wear-resistant coating for mud pump liners. We show the interrelationships between the coating properties, its performance in the laboratory tests and in the field, and the role of a well-defined laboratory simulation in accurately predicting the field performance.

Experimental Procedure

The experimental approach in this program may be divided into three broad categories: development of the CVD process, development of the laboratory test method, and the simulation experiments. These three aspects were, by necessity, interdependent in the sense that the results of the initial tests indicated changes necessary in the coating process, and the results of the early field tests suggested the changes necessary in the laboratory test methods. Therefore, only a brief outline of the basic procedure will be given in this section, and the details will be presented in the following section.

Development of the CVD Process

The coating of CM 500L is deposited by a proprietary chemical vapor deposition (CVD) technique called controlled nucleation thermochemical deposition (CNTD). The basic arrangement of a typical CVD apparatus is shown in Fig. 1. Precursor gases which include the reactant gases and the inert carrier gases are introduced in a heated reaction chamber where the substrate to be coated is maintained at the desired temperature. Chemical reactions take place in the gas phase and a coating is deposited on the substrate. The reaction products are removed from the chamber by suitable means. In this program, several modifications were made in the various CVD process parameters to obtain the desired microstructure and properties of the coating.

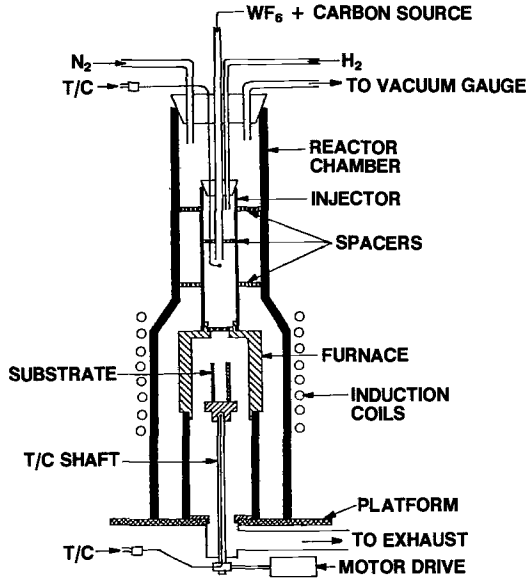


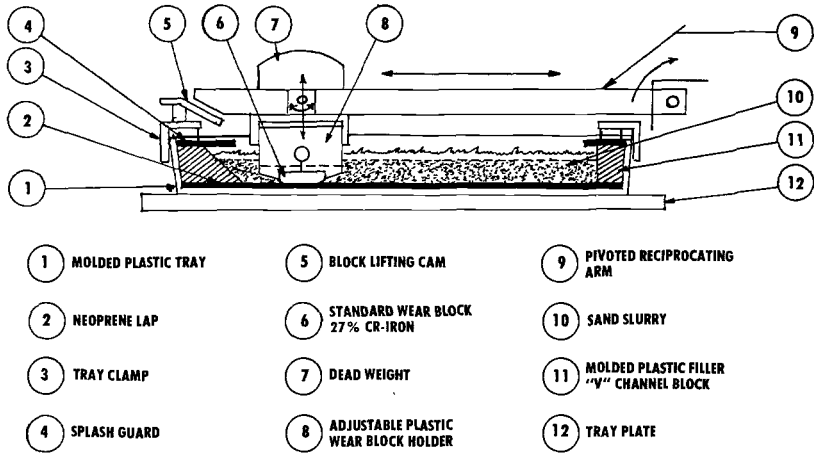
FIG. 1—Schematic of a typical CVD reactor.

Development of the Laboratory Test Method

The basic test used in this study was the Miller Slurry Abrasivity Test. The principles of this test have been described elsewhere [5,6]. The test essentially involves abrading a given reference material—26Cr iron in this case—against slurries made of various types of sands and evaluating the relative wear of the material. This is expressed as the Miller Number, defined as the rate of weight loss at 2 h into the test, and reflects the relative abrasion resistance of the material, or conversely, the relative abrasivity of a given slurry. The schematic diagram of the tester is shown in Fig. 2.

It is clear that this test can be easily adapted to evaluate the abrasion resistance of different materials against a slurry of a given composition. This was the first modification made in the test procedure in evaluating the wear properties of CM 500L and other materials.

The standard Miller test sample geometry requires a 15° bevel at the leading and trailing edges of the reciprocating sample. While this is adequate for avoiding edge chipping during testing of a relatively ductile, uncoated sample, it proves detrimental to a coated sample. As a natural consequence of a deposition process in which a laminar gas flow is maintained, one always gets a slight buildup at the sharp edges and corners of a substrate. Therefore, a slight hone, or radius, is usually applied to the substrate prior to coating. When the coating is extremely hard, brittle, and has a high internal stress due to a significantly different coefficient of thermal expansion as compared to that of the substrate,



SCHEMATIC OF MILLER SLURRY ABRASIVITY TESTER

FIG. 2—Schematic of Miller Slurry Abrasivity tester.

the problem of chipping and fracturing at a sharp edge is accentuated. These conditions exist in the case of CM 500L on steel. Therefore, we changed the sample geometry by replacing the 15° bevel by a generous radius of 3.1 mm at the leading and trailing edges. This allowed us to evaluate the true wear of the coating without introducing errors due to loss of coating by chipping at sharp edges and corners.

A typical test procedure involved abrading a coated test sample for a period of time until the coating showed severe wear. The change of weight of the sample was monitored at regular intervals. Knowing the thickness of the coating, it was possible to predict the wear life of a given type of coating. The various changes made in the procedure of the original Miller test are summarized in Table 1.

This test procedure was used extensively in the development of the deposition process and in correlating hardness, microstructure, and sand erosion behavior of the coating with the slurry abrasion resistance. Further changes were made in the test procedure when it was found that the slurry used in the field was slightly alkaline, while all the laboratory tests were made in the neutral slurry. This prompted a major change, not only in the test procedure but also in the deposition process. A study of the effect of pH of the slurry on the wear of the coating was undertaken. Tungsten and its alloys are quite susceptible to alkaline solutions, and, therefore, we initiated experiments with the deposition conditions with the idea of controlling the microstructural and compositional characteristics of the coating for better corrosion resistance.

These changes in the test procedure and deposition conditions allowed better

TABLE 1—*Modification of the Miller Slurry Abrasivity Test procedure.*

Standard Test	Modification
Different slurry compositions are used to evaluate their abrasivity against a standard reference material.	A fixed slurry composition is used to evaluate the abrasion resistance of various materials/coatings.
Test sample has a 15° bevel at the leading and trailing edges.	Test sample has a blended 3-mm radius on the leading and trailing edges to prevent edge buildup of coatings during deposition.
Miller number, defined as the rate of weight loss at 2 h into the test, is calculated from the data.	Wear rate, defined as volumetric loss per unit time, is determined in the steady-state wear regime.

correlation between properties and performance of the coating in the laboratory tests. In the next step, we modified the test procedure even further to provide a close simulation of the field conditions.

Simulation Experiments

In the field application, the liner remains stationary while a rubber piston reciprocates in the liner to pump the sand slurry. During this operation, a certain amount of radial pressure is exerted on the liner walls. Also, particles of sand may get embedded in the piston and be dragged across the coated surface. Some initial field failures of coated liners had demonstrated this effect.

We, therefore, reversed the test setup completely. The rubber-lined tray was replaced by a tray in which strips of coated steel, taken from an actual liner, were placed at the bottom, coated surface facing up. The test block was made of the same rubber as that used in the piston. The load on the reciprocating area was increased as much as practically feasible, and the tests were resumed. These changes are summarized in Table 2. The test procedure now simulated the relative positions of the stationary and mobile components of the system. It also allowed us to test a coated surface over the actual length of the product. This facilitated the evaluation of the performance of the coating in a wider area, thereby greatly eliminating the possibility of performance variations caused by differences in the properties of the coating on a small, individual wear block, and of a full-size liner coated on the inner surface.

Results and Discussion

Development of the CVD Process

The details of the CNTD process and the properties of the various coatings deposited by this technique are described in earlier papers and reports [7-11].

TABLE 2—*Modifications in the Miller Slurry Abrasivity Test apparatus.*

Test Feature	Standard Miller Test	“Inverted” Miller Test
Wear components	(a) Neoprene rubber strip held stationary in the bottom of the tray (b) Test sample placed in holder attached to reciprocating arm	(a) Buna-N rubber block placed in holder attached to reciprocating arm (b) Coated steel sample strip (cut from liner) held stationary in the bottom of the tray
Wear test sample geometry	(a) Steel block 25.4 by 12.7 by 6.35 mm (b) Wear face area 25.4 by 12.7 mm	(a) Coated steel strip 177.8 by 25.4 by 6.35 mm (b) Wear face area 177.8 by 12.7 mm
Applied load (pressure)	22 N (5 lbf) 105 KPa (15.2 psi)	38 N (8.5 lbf) 178 KPa (25.8 psi)
Strokes per minute	48	56
Test intervals	4 h each—sand slurry unchanged	4 h, 8 h, 16 h, (variable, not exceeding 24 h), sand changed at each interval
pH of slurry	7.0	7.0 and 10.5

The CM 500L coating was evaluated extensively [11], and its properties are summarized in Table 3.

The CNTD process results in an extremely fine-grained deposit, as shown in Fig. 3. This structure exhibits a high hardness and wear resistance. This microstructure is designated as Type A microstructure in the text.

In the course of development of the coating for mud pump liners, we found that, while the Type A microstructure had excellent wear resistance [9–11], this material was relatively susceptible to mild corrosive attack in a slightly alkaline medium, which was encountered in some of the field test sites.

TABLE 3—*Properties of CM 500L coating deposited by the CNTD process.*

Tungsten/carbon alloy coating	
Carbon content	Range: 0.5 to 1.5 weight percent (typical)
Process temperature	350 to 550°C (typical)
Microstructure	Extremely fine (100 to 500 Å) grain size of tungsten with a dispersed carbide phase
Hardness	HV 1800 to 2800 (typical)
Wear resistance	
Erosion	40 to 50 times better than C-2 carbide (against silica)
Abrasion	30 to 40 times better than 27Cr white cast iron
Applications	Sand blast nozzles Sand delivery systems Abrasive slurry transport systems Low load, low impact abrasive environments

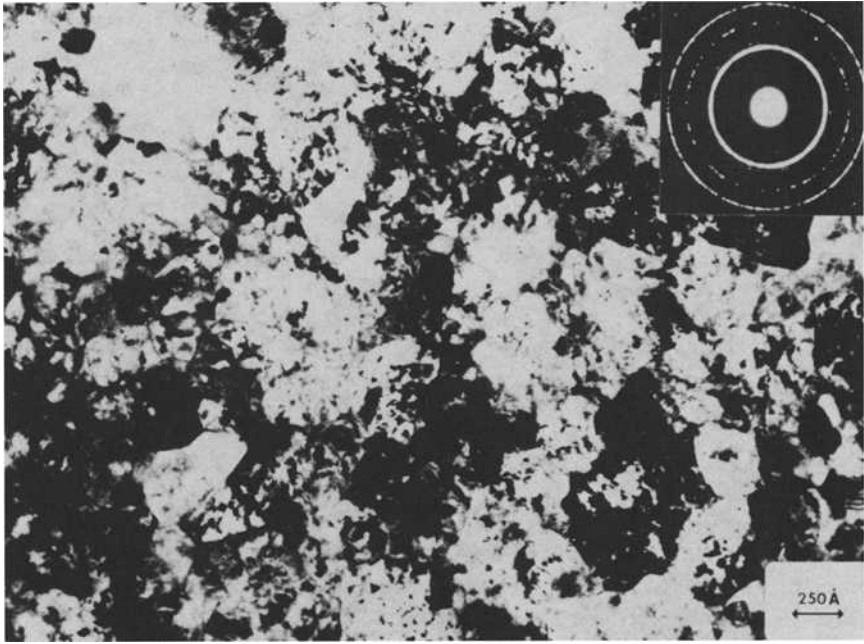


FIG. 3—Transmission electron micrograph of CM 500L, showing the extremely fine-grained microstructure (from Ref 11).

Therefore, the deposition parameters were modified to improve the corrosion resistance by allowing a more uniform dispersion of the W_3C phase in the tungsten matrix. The details of these modifications and the microstructural features cannot be discussed due to their proprietary nature. However, the new microstructure exhibited a high hardness and wear resistance while greatly improving the corrosion resistance and toughness. This microstructure is designated as Type B in the text. The effects of these microstructural modifications on the slurry abrasion resistance of the coating are discussed in the following paragraphs.

Development of the Laboratory Test Method

The procedure for the conventional Miller Slurry Abrasivity Test was described earlier. In the present study, we plotted the cumulative volumetric loss of material due to slurry abrasion as a function of time. Measurement of the loss of material as volume, instead of weight, allows normalization of data for different materials having a wide range of densities. This procedure is also useful in predicting the life of a coating over a surface of known area. A typical plot of cumulative volumetric wear rate as a function of time is shown in Fig. 4

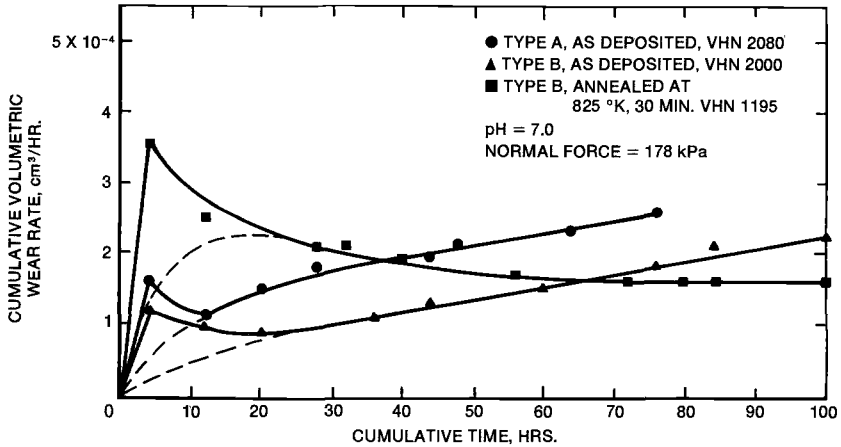


FIG. 4—Slurry abrasion behavior of CM 500L, Type A and Type B, in a neutral slurry.

for the CM 500L coating on AISI 1018 steel in a neutral slurry. Data are presented for the two types of microstructure discussed earlier, Types A and B. We also show data for the Type B microstructure in the as-deposited as well as annealed condition.

All three materials show a high wear rate in the first 4 h, followed by a lower rate of wear. This initial wear rate is related primarily to the removal of surface irregularities of the as-deposited surface. As these irregularities are removed by the rubbing action of the wear block, the surface becomes smoother and the subsequent wear rate becomes more representative of the behavior of the coating. This result is very important. In applications involving wear-resistant coatings, wear tests of short duration are often rendered meaningless due to factors such as the initial surface roughness which give a high initial wear rate. As shown in the case of CM 500L, as well as chrome plating in Fig. 6, the surface reaches a “quasi-steady-state” condition after several hours, typically 20 to 40 h. Therefore, such tests must be carried out until the wear rate is stabilized.

It may be noted that the as-deposited Type A and Type B structures show very similar behavior. The initial wear rate of both materials is similar— 1.6×10^{-4} cm³/h for Type A and 1.2×10^{-4} cm³/h for Type B—after 4 h. The subsequent wear rate for Type A material is approximately 1.5 times higher than that for Type B material. This difference is related to the microstructural differences between the two types of materials. A great improvement in the wear rate is achieved when the Type B material is annealed to a lower hardness, as shown in Fig. 4. The wear rate continues to decrease with time until, after about 65 h, it reaches a steady, constant value independent of time. As mentioned earlier, the Type B microstructure exhibits better toughness than the Type A material. The annealing treatment further improves the toughness, reducing the tendency for sudden, brittle failure of the coating. Figure 5 shows a comparison

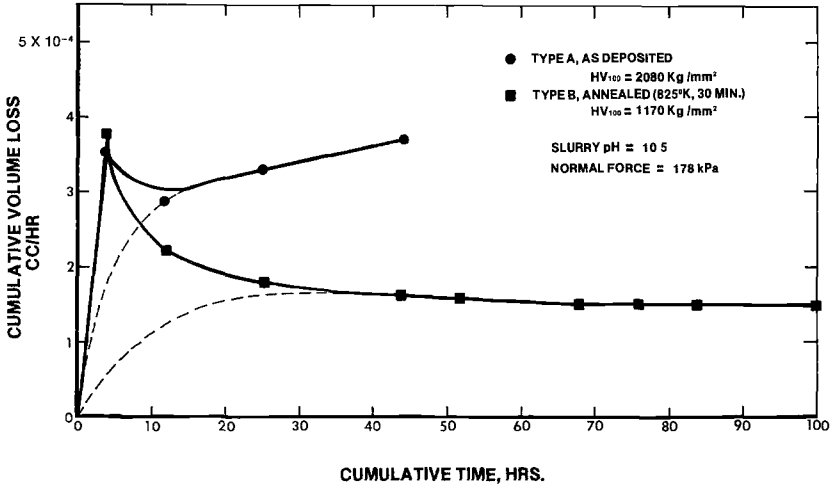


FIG. 5—Slurry abrasion behavior of CM 500L, Type A and Type B, in an alkaline slurry.

of the behavior in an alkaline slurry for the two microstructures. Again, we note that while the Type A material shows a marked degradation of performance as compared to that in the neutral slurry (Fig. 4), the Type B material shows no degradation in a similar comparison.

Simulation Experiments

As pointed out in the previous section, the simulation experiments were made in a test setup in which the conventional Miller test arrangement was completely inverted. Typical results of a test in this "inverted" Miller test apparatus are shown in Fig. 6. Two types of coatings were tested: chromium-plated steel and CM 500L, Type B (annealed). Both coatings had approximately the same hardness. The initial thicknesses of the coatings were 750 to 1000 μm (0.030 to 0.040 in.) and 75 to 125 μm (0.003 to 0.005 in.), respectively, for the chromium plating and CM 500L. CM 500L showed nearly three times better wear resistance than the chromium plating at a slurry pH of 10.5. The chromium plating shows a higher wear rate in the neutral slurry (about $7.2 \times 10^{-4} \text{ cm}^3/\text{h}$) than in the alkaline slurry (about $4.3 \times 10^{-4} \text{ cm}^3/\text{h}$). The reason for this difference was not investigated.

The various tests just described clearly showed that the annealed Type B microstructure had the lowest overall wear rate of all materials tested. We, therefore, extended the test period to simulate the service conditions where the liner is typically expected to last approximately 800 to 1000 h. The results of a 1000-h test on a CM 500L coated steel liner specimen are shown in Fig. 7 for two different pH values of the slurry. At a pH of 7.0, the steady-state wear

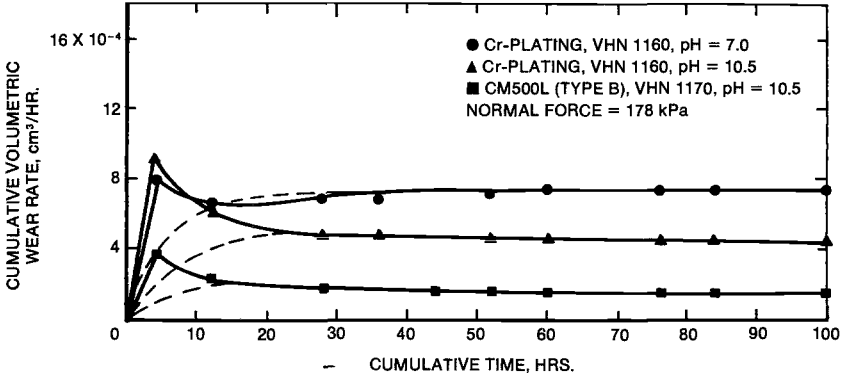


FIG. 6—Comparison of slurry abrasion behavior of chromium plating and CM 500L in the “inverted” Miller test.

rate is approximately 1.6 to 1.7×10^{-4} cm³/h, while at a pH of 10.5, the steady-state wear rate gradually increases from about 1.5×10^{-4} cm³/h to about 1.9×10^{-4} cm³/h. On the basis of these results, a simple calculation showed that a steel liner coated with CM 500L (Type B, annealed) should last approximately 1100 to 1200 h, as shown in Table 4. The criterion for failure, as chosen in this case, was the wear of the coating down to the interlayer. As shown in the table, the liner placed in the field had accumulated more than 1000 h of service as of this writing and was reported to have suffered very little serious damage.

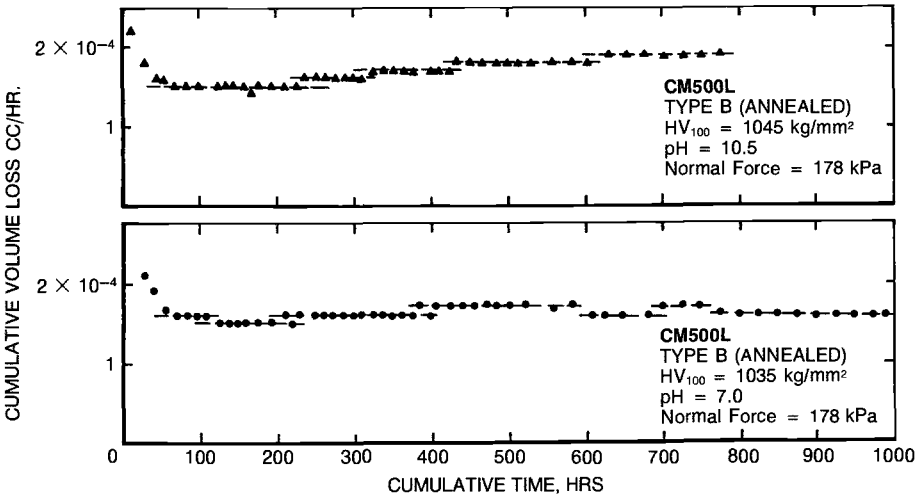


FIG. 7—Results of long-time simulation tests for slurry abrasion resistance of CM 500L coating on steel (Type B material).

TABLE 4—Wear life prediction for CM 500L-coated steel mud pump liner, laboratory test versus field test.

CM 500L Microstructure	pH of Slurry	Maximum Wear Rate, $\mu\text{m}/\text{h}$	Total Coating Thickness, μm		Failure Criterion	Predi- cated Service Life, h	Actual Service Life (h)	Reason For Failure
			Inter- layer	CM 500L				
Type A	7.0	0.19	6	100	Wear to interlayer	526	25	Poor cohesion within CM 500L; loss of adhesion at interface
	10.5	0.20	6	100		500		
Type B (annealed)	7.0	0.09	9	115		2800	1000+	Still in Service
	10.5	0.10	9	115		1150		

A similar calculation for Type A material showed that it should last about 500 h. However, as shown in the table, this liner lasted only 25 h. The cause of failure was found to be loss of adhesion of the coating in a few areas, which caused a catastrophic failure of the liner. Thus, it may be said that when the integrity of the coating is maintained, the wear rate determined in a well-simulated laboratory test can be used to successfully predict the service life of a coating.

Summary and Conclusions

Predictions of wear performance in the field, based on the laboratory testing, are marginally successful at best. The problem usually lies in being able to closely simulate the field conditions in the laboratory environment. The result is usually either an overly simplified test or an unduly harsh one. Often, the test is extremely specific and precludes any generalization. Since the wear resistance of a material is influenced by many external factors, no universally standardized test can be evolved for determining performance under specific conditions.

Several factors came into play in the development of CM 500L coating on steel liners for the mud pump application. The results described in the foregoing clearly demonstrated the close relationship between the test conditions and performance. At the same time, these results showed how easily one may be misled by conclusions based on incomplete information.

The various conclusions resulting from this work can be enumerated as follows:

1. There is a distinct relationship between the hardness of the coating and its performance under a given set of conditions. In the present work, we found that there is an optimum combination of hardness and toughness which gives a high wear resistance. The typical optimum value of hardness for CM 500L was about HV 1200 to 1400. Coatings having a greater hardness showed a tendency for spalling and chipping due to increased brittleness, giving rise to a high wear rate.
2. A combination of fine, uniform microstructure with a minimum of internal stress allowed the coating to have a relatively high toughness and, therefore, a high wear resistance. This type of coating, exemplified by the Type B material, also showed better consistency in composition and performance.
3. In the absence of factors leading to a catastrophic failure of the coating, it is possible to use a simple relationship to predict the wear life of a coating having a consistent microstructure and properties, if a properly designed laboratory simulation test is used as demonstrated in the case of CM 500L-coated steel mud pump liners.

Acknowledgments

We wish to thank Robert A. Holzl, technical director, San Fernando Laboratories, for continued support, encouragement, and valuable discussions, and for critically reviewing the manuscript. The work was initiated while both authors were at San Fernando Laboratories and was completed subsequent to Deepak G. Bhat leaving the company. We wish to thank Art Mouser, Field Engineer of Weatherford U.S., Inc. for his interest and cooperation in providing the field performance data. The many technical discussions with the technical staff at San Fernando Laboratories during the course of this work are also gratefully acknowledged. We wish to thank Colleen Brown and Scarlet Erdosy for their expert assistance in the preparation of the manuscript. Finally, Deepak Bhat would like to thank Paul Woerner, vice-president, Materials Research and Development, GTE-Valeron Corp. for permission to write and present the paper at the International Symposium on Slurry Erosion: Uses, Applications, and Test Methods, held in Denver, Colorado, in June 1984.

References

- [1] Elkholly, A., *Wear*, Vol. 84, 1983, pp. 39-49.
- [2] De Gee, A. W. J., *Wear*, Vol. 92, 1983, pp. 155-159.
- [3] De Bree, S. E. M. et al., *Proceedings*, Third International Symposium on Dredging Technology, Bordeaux, France, March 1980, British Hydromechanical Research Association Fluid Engineering, Cranfield, England, 1980, pp. 299-314.
- [4] De Bree, S. E. M. et al., *Proceedings*, Eighth International Conference on Hydraulic Transport of Solids in Pipes, Johannesburg, Aug. 1980, British Hydromechanical Research Association Fluid Engineering, Cranfield, England, 1982.
- [5] Miller, J., Society of Manufacturing Engineers fall meeting, Pittsburgh, PA, Sept. 1973, AIME Paper Number 73-B-300, American Institute of Mining, Metallurgical, and Petroleum Engineers, New York, 1973.
- [6] *1985 Annual Book of Standards*, Vol. 3.02, ASTM G 75-82, Method for Slurry Abrasivity by Miller Number.
- [7] Holzl, R. A., U.S. Patent No. 4,162,345, 1979.
- [8] Holzl, R. A., *Proceedings*, Sixth International Conference on Chemical Vapor Deposition, Atlanta, GA, 1977, The Electrochemical Society, Princeton, NJ, 1977, p. 107.
- [9] Stiglich, Jr., J. J. and Bhat, D. G., *Ceramic Engineering and Science Proceedings*, July-Aug. 1980, American Ceramic Society, Columbus, OH, 1980, p. 508.
- [10] Stiglich, Jr., J. J. and Bhat, D. G., *Thin Solid Films*, Vol. 72, 1980, p. 503.
- [11] Bhat, D. G. and Holzl, R. A., *Thin Solid Films*, Vol. 95, 1982, p. 105.

DISCUSSION

B. S. Phull¹ (written discussion)—In your early field tests, a coated liner was reported to have failed in 25 h. How was the point of failure established? For example, was the liner examined periodically?

D. G. Bhat and Y. R. DeKay (authors' closure)—The liner, as installed in the pump, is open to the atmosphere at one end. One can look down inside the liner and also reach in to feel the surface of the liner when the pump is not running. This is one way in which the liner can be examined periodically to evaluate the condition of the coating. Another way to establish a possible failure is when a “blowout” occurs during operation. Blowout is a condition wherein the clearance between the liner and piston increases to a point where the slurry being pumped begins to leak out behind the piston as it travels downwards. This may be caused by a uniform wear of the coating, or of the piston, or more catastrophically, by gouging of the liner material due to a breach in the coating at some localized spot. In the case of the liner that failed in 25 h, we found that the coating had lost adhesion and also showed extensive cracking. This resulted in heavy wear in a few spots, causing ploughing of the liner material. We attributed the failure of the coating to insufficient hardness of the substrate material to support the coating.

Ken Metz² (written discussion)—Your modified Miller Test [6] had a better correlation with field performance than the standard test. Do you think this was due to your change in design configuration (“inversion” of test), your change of elastomer used (from neoprene to Buna-N), or to the load change? It would be expected that the change of load and elastomer used would have a significant effect on the absolute wear values obtained, although not necessarily on the ranking of materials. Does your data show this? Do you have data for the dry sand/rubber wheel test on the same materials—do they rank differently?

D. G. Bhat and Y. R. DeKay (authors' closure)—We found that the wear rate of the coating was lower with neoprene than with Buna-N. Our reason for switching to Buna-N, as stated in the paper, was to duplicate the piston material used in the field test. Increasing the effective load and the reciprocating speed of the loading arm also increased the wear rate. We believe that all these factors, including the inversion of the test setup, resulted in a better correlation of wear

¹ Laque Center for Corrosion Technology, Inc., Wrightsville Beach, NC.

² Dresser Industries, Dallas, TX.

rates observed in the laboratory and in the field. It would be difficult to separate the individual contribution of each parameter, although we found that the changes in the load and speed had a greater effect on the laboratory wear rate than the change in the elastomer.

We did not do any testing to check the ranking of materials with the new setup. However, we did not find any change in the ranking between chromium plating and the CM 500L coating as a result of the changes. We did not carry out any dry sand/rubber wheel tests on these materials.

Corrosion Rate Measurements and Corrosion-Erosion Protection in Limestone Slurry Scrubbers

REFERENCE: Burda, P. A., "Corrosion Rate Measurements and Corrosion-Erosion Protection in Limestone Slurry Scrubbers," *Slurry Erosion: Uses, Applications, and Test Methods, ASTM STP 946*, J. E. Miller and F. E. Schmidt, Jr., Eds., American Society for Testing and Materials, Philadelphia, 1987, pp. 118–140.

ABSTRACT: Corrosion and erosion in the limestone slurry scrubber module is described. An electrochemical technique of the two-electrode system was used to determine the corrosion rates. The results were compared with the weight-loss method. The tendency of carbon and stainless steels to pit was also determined. Pitting was expressed as the "pitting factor."

Materials and coating problems were found to vary considerably inside the module depending on location, amount of deposits on surfaces, type of protective coating, and care in surface preparation. Because of deposits formation, the application of the two-electrode polarization instrument method has to be carefully considered for continuous corrosion measurements in erosive-scaling liquids such as the scrubber spray slurry. Application of the "pitting factor" was useful to assess the penetration increase when erosion-corrosion took place. Monolithic linings, reinforced with glass mat, cloth, or flake showed the best erosion resistance. The quality of surface preparation was essential to lining life. It was found, however, that after ten years of scrubber, 25% of the original area of the scrubber coatings was replaced by clad Type 304 stainless steel.

KEY WORDS: scrubber, limestone slurry, corrosivity, erosion, polarization, two-electrode system, corrosion rate, pitting factor, kinetics, corrosion-erosion protection, thermosetting resins, polyester, failure

A wet limestone slurry system has been developed for removal of sulfur dioxide (SO₂) and fly ash from the flue gas of boilers at the Sherburne County coal-fired power generating plant near Minneapolis, which burns Colstrip Montana coal (Table 1).

¹ Corrosion engineer, Pacific Gas and Electric Co., Department of Engineering Research, San Ramon, CA 94583.

TABLE 1—*Typical properties of Colstrip Montana coal (Northern States Power Co. Coal Testing Laboratory).*

Chemical Content	Property	
	Btu/lb	Percent
Btu, as received	8 590	...
Btu, dry	11 600	...
Btu, MAF (moisture, ash free)	13 000	...
Moisture, as received	...	25.7
Ash, dry	...	11.2
Sulfur, dry	...	0.8
Sodium, dry	...	0.035
Coal ash, total	...	98.5
SiO ₂ in ash	...	37.7
Al ₂ O ₃ in ash	...	9.9
TiO ₂ in ash	...	1.0
Fe ₂ O ₃ in ash	...	5.5
CaO in ash	...	19.0
MgO in ash	...	4.1
K ₂ O in ash	...	1.1
Na ₂ O in ash	...	0.42
SO ₃	...	19.6

NOTE: Btu = British thermal unit.

To avoid erosion-corrosion problems during power plant scrubber operations, the company carried out test operations on a scrubber testing module. A test scrubber module [350 m³/min (12 000 ft³/min)] was installed in the existing plant to determine SO₂ removal capacity under various operating conditions. The unit was designed to remove 50% of existing level SO₂ and 99% fly ash (Table 2) from the flue gas treated.

The results of the corrosion tests were evaluated quantitatively to determine the most economic way to achieve adequate protection of the exposed surfaces of Sheburne County power plant scrubber units.

This paper describes the use of weight-loss and linear polarization methods for corrosion measurements in various sections of the pilot plant scrubber. Based on corrosion results analysis, the selection of the materials protection for the scrubber environment is also described.

Linear Polarization Determination of Corrosion Rates

The factors involved in the erosion-corrosion process on the materials surfaces inside the scrubber testing model are:

1. Relatively high level of SO₂ with fly ash at the gas inlet area.
2. Spray slurry in and around the marble bed area.
3. Flow of moisture-saturated gas with slurry particles.

TABLE 2—Chemical composition (%) of fly ash inside scrubber.^a

Analysis	Inlet Scrubber	Outlet Scrubber	Outlet Fan
Phosphorus pentoxide (P ₂ O ₅)	0.25	0.32	0.68
Silica (SiO ₂)	37.89	35.80	29.25
Ferric Oxide (Fe ₂ O ₃)	7.54	3.68	4.12
Alumina (Al ₂ O ₃)	21.87	28.59	25.02
Titanium dioxide (TiO ₂)	0.71	0.69	1.08
Lime (CaO)	19.70	18.30	20.42
Magnesium oxide (MgO)	6.40	6.08	6.95
Sulfur trioxide (SO ₃)	1.65	1.99	3.51
Potassium oxide (K ₂ O)	0.58	0.53	0.34
Sodium oxide (Na ₂ O)	0.59	0.58	1.73
Loss of ignition (carbon = 0.38%)	2.52	3.06	6.67
Phenolphthalein alkalinity	31 mg CaCO ₃ /g	19.4 mg CaCO ₃ /g	...
Total alkalinity	45 mg CaCO ₃ /g	29.2 mg CaCO ₃ /g	...
pH (1% solution)	11.80	11.50	...

^a General Testing Lab., Inc., Kansas City, MO.

The presence of bisulfite, sulfite, and sulfate ions, as the result of the complicated scrubber chemistry process, proposed different environments for polarization characteristics.

The application of electrochemical techniques for the determination of the instantaneous corrosion rate of a metal in aqueous solutions is well established [1,2], and electrochemical techniques have been used to determine the corrosion components of the erosion-corrosion of steel pipes carrying sand, iron ore, potash, and coal slurries at commercial concentrations and velocities [3].

Polarization measurements and observation in common conductive liquids showed that corrosion occurs at the microscopic sites on a metal surface in contact with a conductive liquid. Dissolution of the metal surface tends to proceed rapidly at the anodic sites, but both cathodic and anodic reactions are present. The rate of metal loss is a function of both types of reaction. The resistance of the flow of an electrical current from the conductive liquid into the corroding metal surface is a measurable parameter directly related to the rate of reaction. In the two-electrode system described by Marsh [4], two electrodes of the same material are polarized to a potential difference of ± 20 mV, the current is reversed, and the average current necessary to effect such polarization is used to calculate the corrosion current using the Stern-Geary equation valid only for small polarization: $\Delta\Phi = \Phi_{\text{corr}}$

$$R'p = \frac{\Delta(\Phi - \Phi_{\text{corr}})}{\Delta I} \text{ linear polarization} \quad (1)$$

where

Φ = electrode potential,

Φ_{corr} = corrosion potential, and

I = applied current.

The objective of this study was the application of the two-electrode linear polarization system for direct determination of the corrosion rate in the limestone spray slurry of the test scrubber module. The results were compared with the weight-loss method. The tendency of carbon and stainless steels to pit was also determined. Pitting was expressed as a "pitting factor" [5].

Experimental

Corrosivity in the scrubber depends on the various scrubber locations, for example, SO₂ inlet area, marble bed, duct area, piping system, etc. Changes of parameters in these areas influence corrosion. A summary of chemical conditions in the scrubber are specified in Table 3. It is shown that operating conditions varied in the different tests, and hence a continuous method for the determination of the corrosion rate was necessary.

The two-electrode configuration of the 1120 Magna Corrotor portable instrument [6] was used for corrosion study. The electrical circuit of the portable instrument configuration is shown in Fig. 1. The equipment installation, reading, operating, and measurement data evaluation followed the recommendations prescribed in the Operating Manual [7]. The two-electrode system was applied under different polarization conditions. The corrosion probes with replaceable electrodes for simultaneous determination of electrochemical and weigh-loss data were hung in several scrubber areas as corrosion indicators (Fig. 2).

About 5% of the flue gas and fly ash generated by the 80-MW unit was directed into the scrubber pilot plant with and without a precollector before it entered a precipitator.

The limestone slurry was pumped from a reaction tank by means of a rubber-lined pump. After absorbing the SO₂ from the gas in the marble bed, the slurry returned to the reaction tank. A certain amount of slurry was bled to the thickener.

The weight-loss method was used to check the corrosion results from the polarization measurements. The test materials were (1020) carbon steel (coated and uncoated) [ASTM Specification for Structural Steel (A 36/A 36 M-84a)] and commercial quality Type 316 and Type 304L stainless steels. The metal coupons, 2.54 by 5 by 0.3 cm (1 by 2 by 1/8 in.), and test electrodes (Fig. 3) were prepared according to ASTM Recommended Practice for Preparing, Cleaning, and Evaluating Corrosion Test Specimens (G 1-81) [8].

A dip solution of hydrochloric acid (HCl) (1:1) with 3% hexamethylenetetramine at laboratory temperature 22°C (70°F) was used for removal of mill scale and corrosion products from the carbon steel specimens after scraping off heavy mud and scale deposits. Forty percent nitric acid (HNO₃) at 38 to 40°C (100 to 200°F) was used for cleaning and preparing 316 and T304L stainless steel specimens for evaluation of corrosion rates. The corrosion rates were calculated from the weight results for weight-loss determination in mils per year.

TABLE 3—Summary of scrubber test conditions.

Data	Test 2				
	Test 1	Test 2 ₁	Test 2 ₂	Test 3	Test 4
Time, day/hours	6/144	7/168	24/576	16/384	12/288
% solids in slurry	7	10	10	10	10
Limestone feed rate					
(a) lb/h	67	133	...	7	16
(b) Stoichiometry on 600 ppm SO ₂	50	100	...	5	12
Fly ash feed, lb/h	300	300	300	300	300
Inlet SO ₂ , ppm	862	658	617	594	585
Outlet SO ₂ , ppm	385	125	118	290	265
Inlet temperature, °C (°F)	180 (355.8)	177 (350)	178 (352)	179 (355)	169 (337)
Outlet temperature, °C (°F)	83.7 (182.6)	80.6 (177)	80.6 (177)	78.9 (174)	76.1 (169)
Spray water temperature, °C (°F)	55 (131)	53.9 (129)	54.4 (130)	53.3 (128)	55 (131)
Inlet dew point, °C (°F)	44.7 (112.4)	45.2 (113.4)	46.9 (116.4)
Outlet dew point, °C (°F)	53.3 (128)	53.9 (129.0)	53.4 (128.2)
Spray water, pH	5.7	5.7 to 6.0	6.1
Dissolved Ca, ppm	560	550	500	530	520
Dissolved Mg, ppm	885	1500 to 2500	1900 to 2900	1700 to 4400	2500 to 3500
Dissolved SO ₄ , ppm	6000	6000 to 10 000	9000 to 12 000	10 000 to 17 000	10 000 to 16 000
Dissolved SO ₃ , ppm	1000	900	700	3000 to 4000	2000 to 3000
CaSO ₄ ·2H ₂ O in spray slurry, ppm	...	1.62	1.45	2.20	1.95
CaSO ₄ scaling on the overflow pots	Yes	Yes	Yes	No	Yes
Demister and wall deposits	Heavy	Heavy	Heavy	Light	Light
Barometric pressure, in. Hg	29.26	29.32	29.38	29.30	29.25

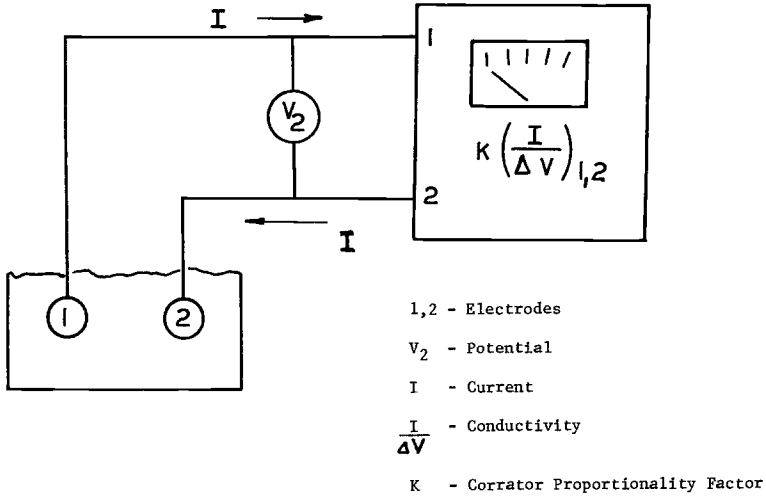


FIG. 1—Two-probe linear polarization system circuit [7].

Discussion of Results

Materials and coating problems were found to vary considerably inside the module depending on such things as location, amount of deposits on surfaces, type of protective coating, and care in surface preparation. Tables 3 and 4 show the test operating conditions and the corrosion aggressivity values determined. There are several criteria for quantitative corrosion weight-loss data evaluation [5,9-10] of which Uhlig's system [5] was used. Uhlig's approach is useful for systems handling chemical media where the attack is uniform, and it was adopted for those scrubber tests showing low corrosion rates for A 36 carbon steel (Table 4). All fall into Uhlig's Class 1 material losses where rate of corrosion is less than $127 \mu\text{m}/\text{year}$ (5 mils/year) [5]. Metals in this category have good corrosion resistance.

Probe Multiplier

The comparison of weight loss corrosion results and polarization instrument corrosion rates determined in different scrubber locations are summarized in Tables 5 and 6.

The meter calibration was chosen to make the standard probe multiplier (k) equal to 1.0 [6]. Under these conditions the probe multiplier for the specific system (K_{sp}) is equal to the factor which relates the electrical polarization properties of the metal probes to their weight-loss corrosion rates in the scrubber environment.

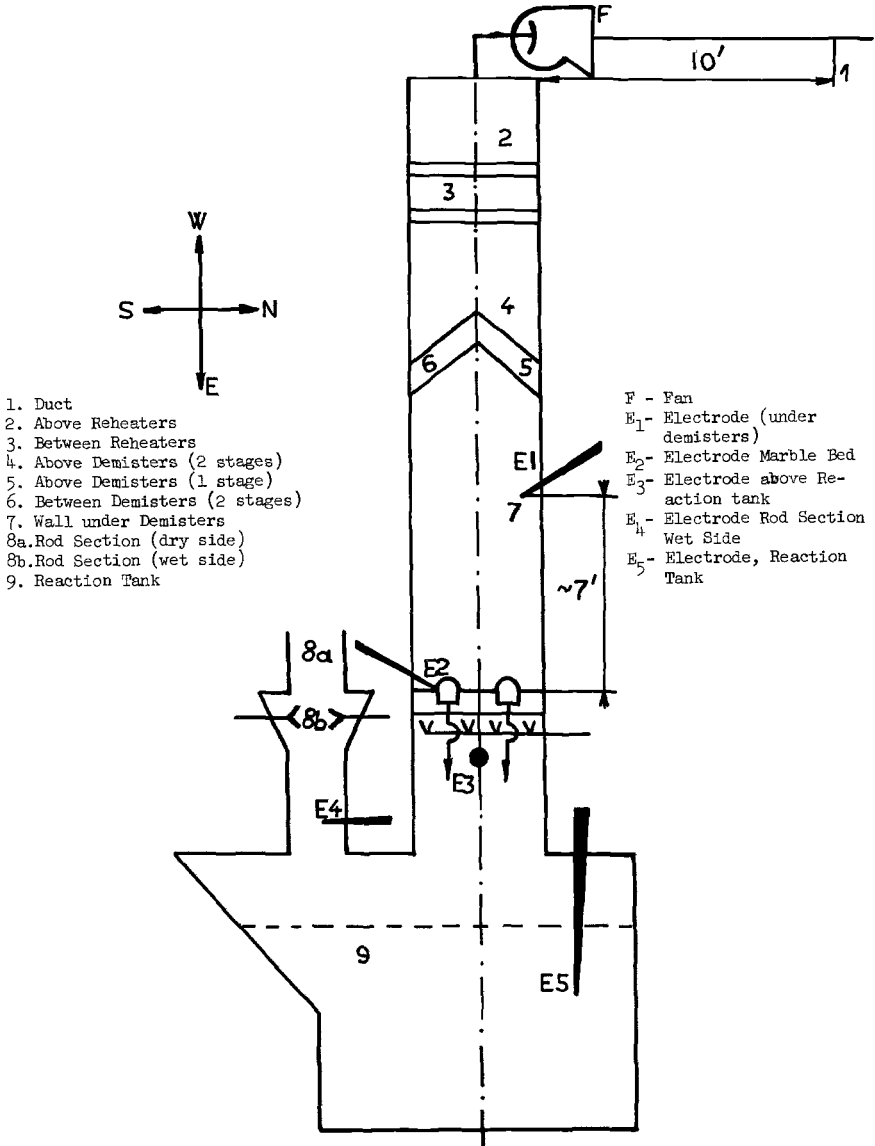


FIG. 2—Test locations in scubber with primary precollector.

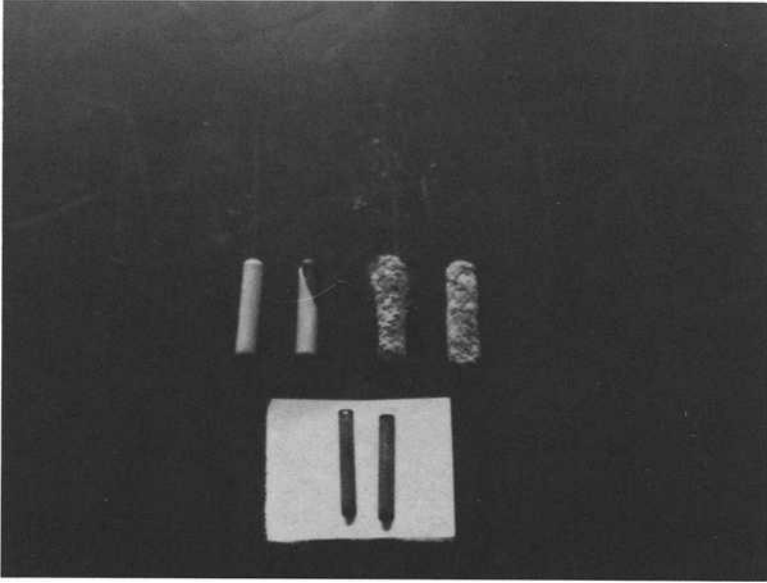


FIG. 3—Replaceable electrodes of the 1120 Magna Corrotor instrument.

$$K_{sp} = \frac{\overline{MPY}}{\overline{mpy}} \cdot k \quad (2)$$

where

\overline{MPY} = average weight loss corrosion rate during test period (mils/year),
and
 \overline{mpy} = average instrument corrosion rate (mils/year).

The probe multiplier for the specific system (K_{sp}) may be different for different alloys and must be determined experimentally for each alloy in a given scrubber environment.

The polarization meter was applied under different polarization conditions when the scrubber operated with and without a primary collector (Tables 5 and 6, Fig. 2). The instrument corrosion rates were generally much higher than weight loss corrosion rates determined in corresponding scrubber areas. Therefore, the majority of probe multipliers for the scrubber slurry environment were not in agreement with the instrument manufacturer [7]. Our results verified the prediction that scrubber slurry multipliers would not be of the same magnitude as those determined for mild steel in ordinary cooling waters which fall in the range of 0.5 to 3.0 [7]. It was found that the instrument reading multipliers are dependent on the properties of the final rusty layer on the metal surfaces. Different kind of rust or deposits on the metal surface (Figs. 4 and 5) result in

TABLE 4—Influence of scrubber locations on corrosion loss of A 36 carbon steel.

Locations	Test 2														
	Test 1			Test 2 ₁			Test 2 ₂			Test 3			Test 4		
	Weight Loss, mg	Mils/Year	Weight Loss, mg	Mils/Year	Weight Loss, mg	Mils/Year	Weight Loss, mg	Mils/Year	Weight Loss, mg	Mils/Year	Weight Loss, mg	Mils/Year	Weight Loss, mg	Mils/Year	
1. Duct	0.038	0.001	0.032	0.001	0.011	0.001	0.023	0.001	0.011	0.001	
2. Above reheaters	0.029	0.001	0.089	0.003	0.089	0.003	0.023	0.001	0.023	0.001	
3. Between reheaters	0.115	0.01	0.307	0.001	0.323	0.01	0.288	0.01	0.288	0.02	0.288	0.02	
4. Under reheaters	0.776	0.02	0.424	0.02	0.281	0.02	0.281	0.02	0.281	0.02	
5. Above demisters	0.684	0.08	0.938	0.10	1.24	0.04	0.865	0.004	0.785	0.05	0.785	0.05	0.785	0.05	
6. Between demisters	0.427	0.05	0.542	0.06	1.607	0.05	1.793	0.08	0.772	0.08	0.772	0.05	0.772	0.05	
7. Under demisters	0.335	0.04	0.184	0.02	0.641	0.02	0.793	0.04	1.052	0.04	1.052	0.06	1.052	0.06	
8. Wall under demisters (83 in. above marble bed north)	0.274	0.01	0.332	0.02	
9. Marble bed north	0.438	0.01	1.653	0.07	
10. Marble bed center	0.455	0.05	0.467	0.05	1.219	0.04	1.304	0.06	2.138	0.06	2.138	0.13	2.138	0.13	
11. Marble bed south	0.426	0.04	0.476	0.01	
12. Marble bed west	0.232	0.07	
13. Wet side SO ₂ inlet	3.112	0.37	3.524	0.4	0.411	0.01	18.774	1.10	18.774	1.10	
14. Reaction tank	0.384	0.05	3.326	0.15	7.856	0.15	7.856	0.47	7.856	0.47	
15. Slurry tank	0.283	0.03	

NOTE: Mils/year = 0.001 in./year = 0.0254 mm/year, 1, 2, 3, 4 = test conditions (Table 3). Test locations (Fig. 2). Coupons: 1 by 2 by 1/2 in.; 1 in. = 2.54 cm.

TABLE 5—The influences of the scrubber locations with precollector on corrosion loss of A 36 carbon steel, 316, and T304L stainless steels.

Locations	Weight Loss Method, 51 Days		Polarization Instrument Readings						Metal Surface Description
	Weight Loss, mg ^e	Mils/Year	Weight Loss, mg ^b	Mils/Year	Time, Days	Reading, Mils/Year	Multiplier		
1. Duct	0.075	0.001	
2. Above reheaters	0.130	0.000 2	
3. Between reheaters	0.323	0.005	
4. Above demisters (2 stages)	1.713	0.02	
5. Above demisters (1 stage)	0.961	0.01	
6. Between demisters	2.386	0.03	
7. Wall under demisters (83 in. above marble bed)	0.814	0.01	
8. Rod section	0.252	0.004	
(a) Gas dry side	4.060	0.06	3.182	5.82	1	5.50	1.06	Rust	
(b) Wet side	0.05 ^c	0.02	5	1.20	0.02	Black deposit	
	0.009 ^d	0.2	8	0.70	0.03	Black deposit	
9. Reaction tank wall	0.545	0.25	4	0.60	0.42	Rust	
10. Marble bed	0.183	0.08	4	0.90	0.09	Scale	
11. Reaction tank	0.593	0.008	0.028	0.01	8	10.20	0.000 6	Scale	

^a Coupons: 1 by 2 by 1/8 in. Test Locations (Fig. 2).

^b Corrosion Probes: 10 cm² × 1 in. = 2.54 cm; 1 Mil/year = 0.001 in./year = 0.025 mm/year.

^c 316 SS.

^d T 304L.

TABLE 6—Linear polarization meter and weight loss corrosion rates of A 36 carbon steel and 316 stainless steel in different scrubber locations without precollector.

Test Locations	Test 1						Descriptor Multiplier, K_{sp}	Reading, Mils/Year	Descriptor Multiplier, K_{sp}
	1 Day			6 Days					
	Weight Loss, mg	Mils/Year ^a	Reading Mils/Year	Weight Loss, g	Mils/Year ^a	Reading, Mils/Year			
Under demisters (83 in. above M.B.)	0.044	0.08	0.40	0.081	0.03	0.49	0.5		
Marble bed	0.046	0.08	0.34	0.037	0.01	0.28	0.04		
SO ₂ inlet	0.177	0.32	0.31	0.542	0.20	0.23	0.9		
	Test 2 ₁ (4 Days)						Test 4 (7 Days)		
Test Locations	Weight Loss, mg	Mils/Year ^a	Reading, Mils/Year	Weight Loss, g	Mils/Year ^a	Reading, Mils/Year	Descriptor Multiplier, K_{sp}		
Under demisters (83 in. above M.B.)	0.033	0.02	0.44	0.082	0.02	0.72	0.3		
Marble bed	0.02	0.01	0.28	0.200	0.05	0.64	0.8		
SO ₂ inlet	1.930	0.9 ^b	0.27	0.008 ^c	0.002 ^c	0.18 ^c	0.01 ^c		
Reaction tank (spray water)	0.296	0.08	24.7	0.017		

NOTE: 1, 2, 4 = conditions of tests (Table 3). Mils/Year = 0.001 in./year = 0.0254 mm/year. Test Locations (Fig. 2) M.B. = marble bed.

^a Corroder probes, 10 cm². Weight loss corrosion rates.

^b Erosion.

^c 316 SS, 20 days test.



FIG. 4—Rusts and deposits of the scrubber demisters area.

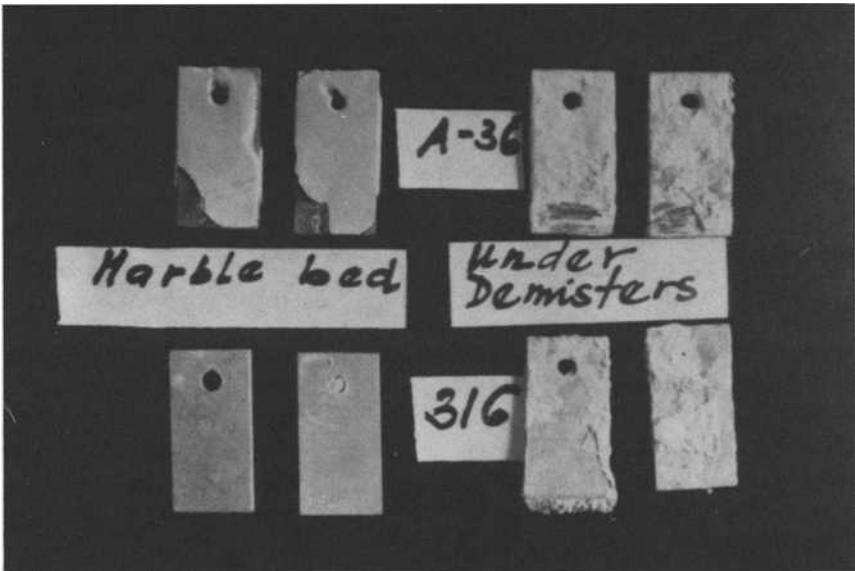


FIG. 5—Deposits and scales from the scrubber marble bed and under demisters areas.

TABLE 7—Distribution and chemical composition (%) of deposits inside scrubber.

Locations	Test 1 (7% Solids Slurry, 6 Days)				Test 2 ₁ (10% Solids Slurry, 7 Days)			
	Ca	Mg	SO ₃	SO ₄	Ca	Mg	SO ₃	SO ₄
Between reheaters	10.90	0.19	0	23.3
Above demisters	3.5	0.29	0	3.2
Between demisters	6.24	0.87	4.37	7.98	8.02	2.22	0	5.3
Under demisters	14.2	1.91	9.59	4.09
North wall, 83 in. above M.B.	15.5	1.42	2.78	18.96	21.5	0.34	1.79	51.45
Marble bed north side
Marble bed center
Marble bed south side	21.6	0.78	1.36	68.87
Marble bed corrosion probes	25.0	0.41	1.36	64.67	21.8	0.57	1.75	51.30
Wet Side of SO ₂	16.1	1.52	6.74	6.65	15.2	1.52	6.10	3.98
Inlet	11.2	2.9	4.65	0.92
Reaction tank	18.7	1.05	5.56	30.13

NOTE: 1, 2₁, 2₂, 3, 4 = tests conditions (Table 3). Test Locations (Fig. 2). M.B. = marble bed.

different polarization characteristics of the scrubber environment, and these vary in different scrubber areas. The descriptor slurry multiplier constants found were in the 0.5 to 3.0 range prescribed by the instrument manufacturer only when an adhesive film of red brown rust was formed on the metal surface. Relatively higher constant (Table 6) was indicated under erosion conditions when the surface was not protected by rust. When slurry and scale deposits were present, the multiplier constants were in the range 10^{-3} to 10^{-2} under the absolute low corrosion rate of 0.25 to 2.54 $\mu\text{m}/\text{year}$ (10^{-2} to 10^{-1} mils/year) (Table 5). Absolute low corrosion rate and corrosivity depend mainly on various scrubber conditions in different locations for the example SO₂ inlet, marble bed, duct area, piping system, etc. It is obvious that the low absolute corrosion rates and the polarization characteristics will be more sensitive to slurry and calcium sulfate scale deposits (Fig. 5). These deposits form a barrier for complete polarization, and, therefore, the application of the two-electrode polarization instrument method has to be carefully considered for continuous corrosion measurement in erosive-scaling liquids such as the scrubber spray slurry (Table 7).

Pitting Factor [5]

This factor represents the ratio of deepest metal penetration to the average metal penetration as determined by the weight-loss method. Because the two-electrode instrument also permits the determination of pitting depth by direct readings, it allows fast determination of the pitting factor if average metal penetration is available from weight-loss results. Deepest metal penetrations

TABLE 7—(Continued)

Test 2 (10% Solids Slurry, 24 Days)				Test 3 (10% Solids Slurry, 17 Days)				Test 4 (10% Solids Slurry, 12 Days)			
Ca	Mg	SO ₃	SO ₄	Ca	Mg	SO ₃	Ca	Ca	Mg	SO ₃	Ca
10.4	3.1	0	2.1	9.42	2.4	0	14.1	11.6	2.29	0	2.70
...	2.5	0.50	0	2.0	3.3	0.73	0	1.8
...	7.52	0.48	0	2.5	6.3	0.01	1.96	0
16.3	0.89	6.34	10.9	16.7	0.30	0.34	2.89	10.2	0.4	0	0
19.4	0.54	3.18	36.89	14.40	0.80	0.80	22.44
...	22.0	0.44	1.77	47.28
22.6	0.94	1.22	56.4
...
...
...
...	13.1	0.69	0.04	4.05

caused by the scrubber environment areas are summarized in Table 8. In spite of some authorities who question the validity of the direct measurement of metal penetration on the basis of theory, it was found that this method was useful to assess the penetration increase when erosion-corrosion took place on the surfaces that did not have protective films, particularly in the scrubber inlet and/or rod section of the precollector. Besides determining the relative pitting characteristics of metals, it was shown that the method is useful for determining the durability of coatings. The method was applied for basic steel redesigns and for the relative comparison of coating durability in areas where high rates of corrosion showed up.

In these areas, the presence or absence of deposits on the metal appeared to have a dominant influence. For example, a one hundred times higher corrosion rate was found in the gas inlet area when only light deposits occurred. The area around the demisters showed relatively low corrosion as long as the surface stayed clean. But when there were deposits and scale formation on the supporting brackets, they suffered heavy deterioration due to steel-to-steel contact corrosion. This is shown in Figs. 6 and 7. Scale formation also brought on severe contact corrosion where stainless and carbon steels were joined. Figure 8 shows such an area with carbon steel loss of 50 to 60%.

Just how much the kinetics of corrosion are influenced by the contact between dissimilar metals and by the presence of scaling deposits is indicated in Fig. 9. The plot covers 59 days of scrubber operation and shows for three areas how the gradual formation of scale changed the kinetics of corrosion dramatically. Since present experience shows that it would be difficult to eliminate scale and deposits entirely from metal surfaces, it is essential, therefore, that contact

TABLE 8—Influence of spray slurry on pitting of A 36 carbon steel, 316 SS, and T 304L stainless steels.

Location	Scrubber Without Precollector													
	Test 1				6 Days				Test 2, (4 Days)				Test 4 (7 Days)	
	Max PF	<i>d</i> , Mils/Year	<i>P</i> , Mils	Max PF	<i>d</i> , Mils/Year	<i>P</i> , Mils	Max PF	<i>d</i> , Mils/Year	Max PF	<i>d</i> , Mils/Year	<i>P</i> , Mils	Max PF	<i>d</i> , Mils/Year	<i>P</i> , Mils
Under demisters (83 in. above M.B.)	4.0	0.08	0.32	4.6	0.03	0.14	3.8	0.02	0.076	2.50	0.02	0.050		
Marble bed	0.50	0.08	0.04	0.39	0.01	0.004	0.1	0.1	0.001	2.0	0.05	0.10		
SO ₂ inlet	3.0	0.32	0.97	5.30	0.2	0.90	2.50	0.88	1.4	4.0 ^a	0.002	0.0028		
Location	Scrubber With Precollector													
	Max PF	<i>d</i> , Mils/Year	<i>P</i> , Mils	Max PF	<i>d</i> , Mils/Year	<i>P</i> , Mils	Max PF	<i>d</i> , Mils/Year	<i>P</i> , Mils	Max PF	<i>d</i> , Mils/Year	<i>P</i> , Mils	Max PF	<i>d</i> , Mils/Year
	Max PF	<i>d</i> , Mils/Year	<i>P</i> , Mils	Max PF	<i>d</i> , Mils/Year	<i>P</i> , Mils	Max PF	<i>d</i> , Mils/Year	<i>P</i> , Mils	Max PF	<i>d</i> , Mils/Year	<i>P</i> , Mils	Max PF	<i>d</i> , Mils/Year
Rod section wet side	5.40	5.8	31.4	1										
Marble bed	6.50 ^b	0.02	0.13	5										
Reaction tank gas side	2.30	0.08	0.19	4										
Reaction tank slurry	4.0	0.03	0.10	4										
	12.0	0.01	0.076	8										

NOTE: PF = pitting factor = P/d = average of metal penetration (mils/year) by weight loss of Corrotor probes. *P* = deepest metal penetration at the end of the year (mils), Mils/year = 0.001 in./year = 0.0254 mm/year. 1, 2, 4 = conditions of tests (Table 3). Test locations (Fig. 2).

^a 316 SS stainless steel.

^b T 304L.

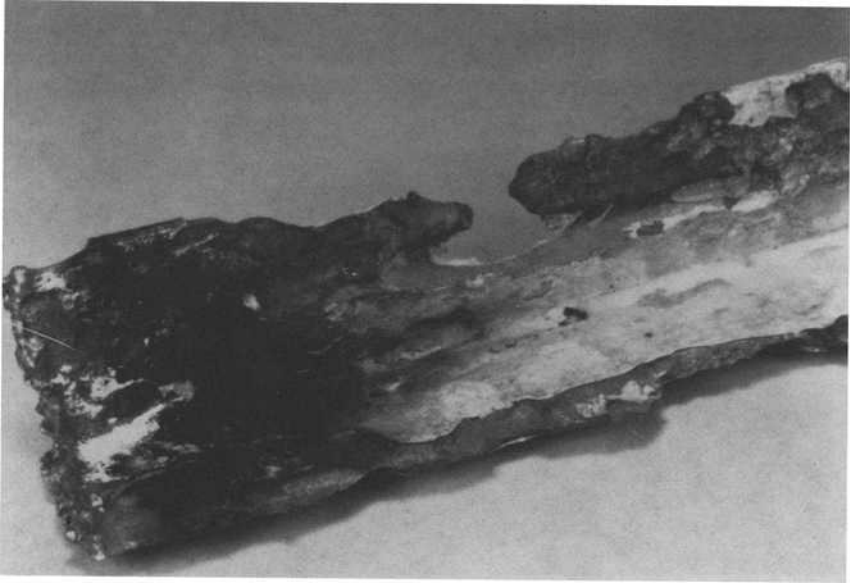


FIG. 6—Corrosion failure of demister supporting brackets during scrubber tests. (Deterioration was due to steel to steel contact corrosion brought on by deposits and scale formation during operation).

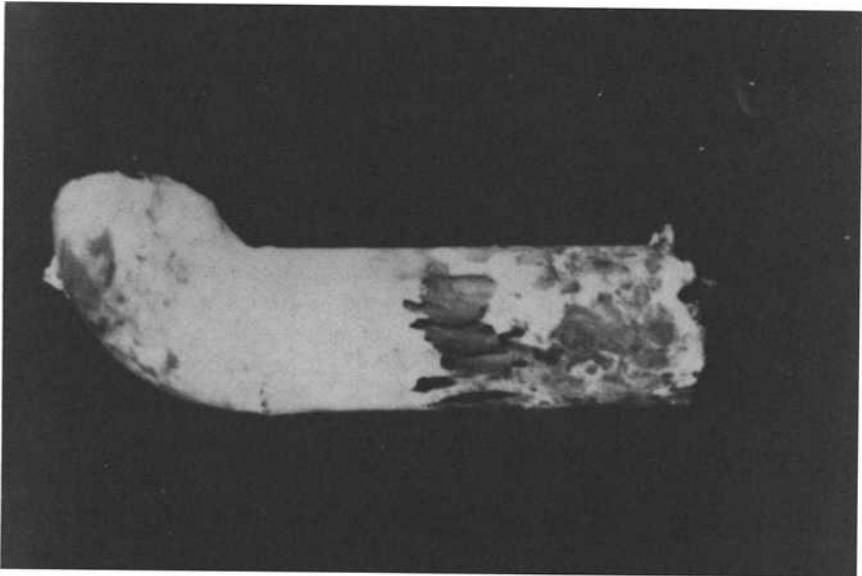


FIG. 7—Erosion-Corrosion failure of pipe [10 cm (4 in.)] after 1100 h of scrubber operation.

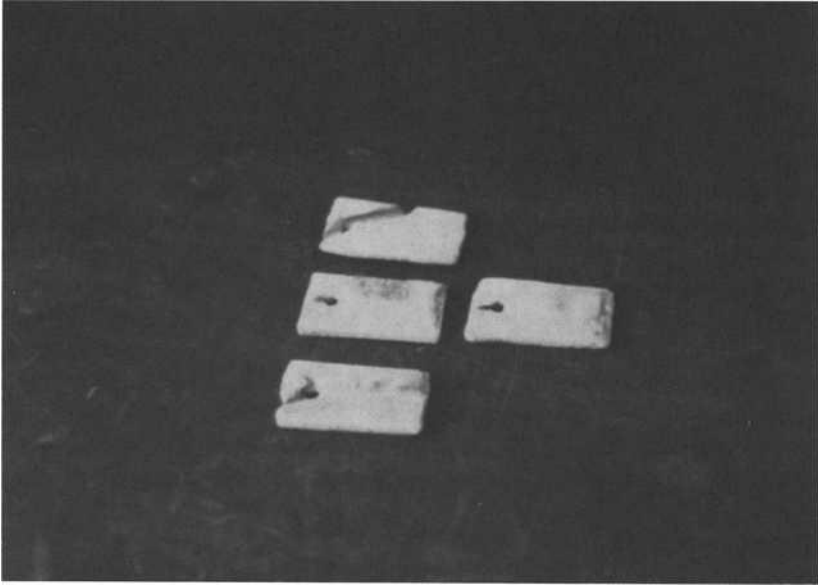


FIG. 8—Severe contact corrosion where stainless and carbon steels were in contact under scale which formed during scrubber operation.

between metals of different corrosion potentials be avoided where they are exposed to scrubber environment.

Materials Selection

These findings leave the materials designer a choice between two solutions for corrosion protection: (1) the use of protective coatings [11]; and/or (2) a change of basic steel material [12,13]. Usually the use of more corrosion-resistant alloys is an expensive step, and coatings can be utilized instead.

The two most important properties of coatings in wet scrubbers are resistance to erosive hydrodynamic conditions and good heat transfer. Since there is not much actual experience with coatings in scrubbers, a testing program was set up at Northern States' scrubber module (Fig. 2). Several coatings were tested for 5000 h.

For these tests in a wet limestone system, the Ceilcote corrosion-resistant monolithic lining showed the best erosion resistance. These linings are formulations of thermosetting resins, usually epoxy or polyester. They can be reinforced with glass mat, cloth, or flake. This contributes to tensile and flexural strengths and helps lower the coefficient of thermal expansion of the lining to that of the substrate. To gain maximum chemical resistance, the reinforcing material is sealed with a finish coat.

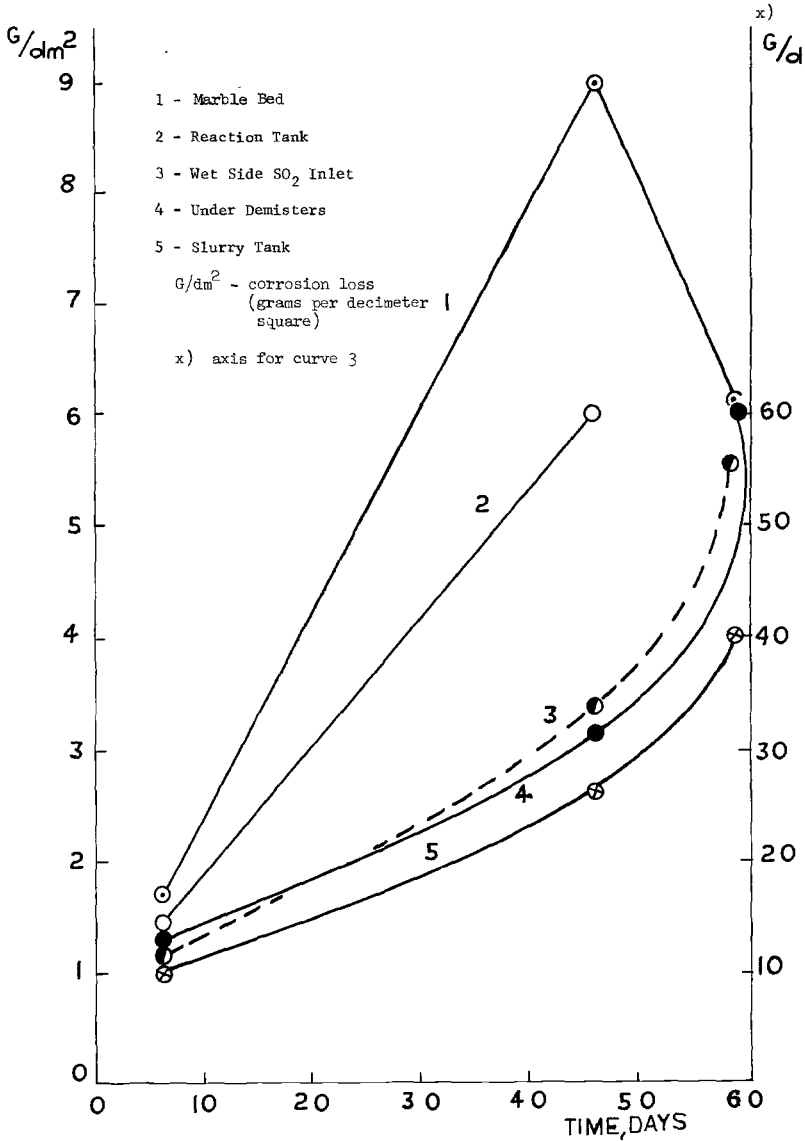


FIG. 9—Kinetics of corrosion are influenced by the formation of scale and deposits during 59-day scrubber run. (The three lower curves show rapid increase in corrosion as deposits are formed).

These linings range in thickness from 1016 to 3175 μm (40 to 125 mils). This compares with thicknesses from 127 to 508 μm (5 to 20 mils) for many coatings. In the tests at Northern States Power Co., the linings turned in a superior performance for severe operating conditions such as high temperature, severe chemical immersion service, thermal shock, impact, and abrasion (Table

3). Properties of the linings, rates of application, and theoretical costs are shown in Table 9.

The utility installed these linings in 24 scrubbers at the Sherburne County Generating Plant. Linings extended from 0.61 m (2 ft) below the normal waterline to the expansion joint at the scrubber outlet. Protection was also applied at the scrubber inlet just beneath the rod section.

The areas around the marble beds were lined with nominal 3.2-mm ($\frac{1}{8}$ -in.)-thick polyester reinforced with glass mat No. 505AR. The main shell and scrubber inlet were lined with nominal 1000 to 1500- μm (40 to 60-mil)-thick flake glass reinforced polyester No. 151. The mist eliminator washer blower support beams and the reheater support beams were protected by a nominal 760 to 1000 μm (30 to 40 mils) of flake-filled polyester No. 252. The distribution vanes beneath the marble bed were lined with a nominal 1500 to 2000 μm (60 to 80 mils) of flake glass reinforced polyester No. 103.

It was estimated that these linings will give satisfactory corrosion protection for at least ten years with minimum maintenance.

Coating Failures

The protective coating was successfully used in the scrubber operation for more than ten years. It was found, however, that after ten years of operation 25% of the original area of the scrubber coatings was replaced by clad 304SS. The coating did not survive long-time excessive heat and high hydroerosion

TABLE 9—Characteristics of Ceilcote systems, rates of application, and estimated costs.

Specification	Polyester Series		
	100	200	500
Thermal conductivity, kcal/h m °C (Btu in./h ft ² °F)	0.15 (1.22)	0.12 to 0.25 (1 to 2)	0.53 (4.26)
Coefficient of thermal expansion, in./in. °F	12 to 16 $\times 10^{-6}$	9 to 12 $\times 10^{-6}$	12.4 $\times 10$
Heat resistance on steel, °C (°F)	82.2 (180)	60 (140)	82.2 (180)
Surface preparation	White metal	White metal	White metal
Method of application	Roller trowel	Brush spray	Brush trowel
Number of applications	Two	Two	Two
Nominal film thickness, mils	70	35	125
Coverage, ft ² /gal	30 (35 mils)	35 (35 mils)	20 (125 mils)
Curing time/h at 21.1°C (70°F)	24	12	24.28
Spark testing, volts	5000	2500	20 000
Daily work rate of normal work area (per application per finisher per day)	600 ft ²	2000 ft ²	250 ft ²
Theoretical material cost, \$/ft ²	103 (70 to 80 mils) \$1.69	252 (35 mils) \$0.57	505 (125 mils) \$1.60

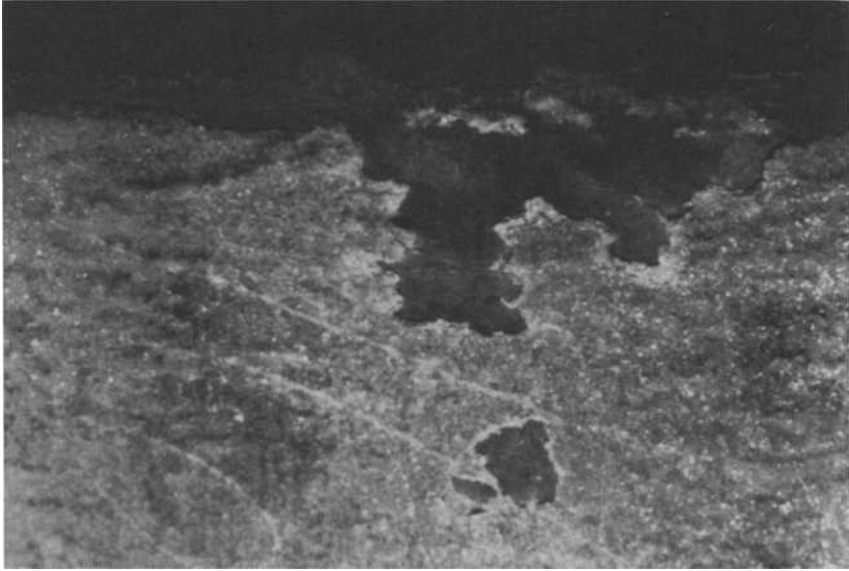


FIG. 10—*Failure of protective lining in scrubber where surfaces preparation failed to remove weld splatters.*

around reheaters and demisters areas.² Industry experience shows that most coating failures result from high corrosion aggressivity in the environment, unsatisfactory coating application, and poor surface preparation. These influences also were evident during the tests on the module. For example, in an area where the corrosion aggressivity on carbon steel is 800 $\mu\text{m}/\text{year}$ (31.4 mils/year), Ceilcote linings failed after as little as five days of test. In these areas, lined carbon steel had to be replaced with 316L stainless steel which had a maximum penetration of 3.4 $\mu\text{m}/\text{year}$ (0.133 mils/year).

Air content in coatings can result in poor adhesion and eventual failure of the coating. Generally, good quality of coating is accompanied by minimum air contents.

Surface preparation is vital to coating life. Unlike a mechanical defect in the scrubber system which is found during startup and repaired, poor surface preparation can result in adhesion loss or rust-through after a few months of operation with a system that should have lasted ten years.

Mill scale and weld splatters will, in time, pop off the steel and carry the lining or coating with them. Oil, moisture, dust, and other foreign material on the metal surface will prevent proper adhesion.

In the scrubber tests, surface preparation was found to be the most important

² Private communication, G. Kaas, Northern States Power Co., Feb. 1984.

single factor in lining life. Where weld splatter had not been removed, chipping off of the linings was found after 1100 h of operation (Fig. 10). Where sandblasting was improperly done, lining failure was found after 1500 to 1800 h. In comparison, linings on properly prepared surfaces were in excellent condition after ten years of operation.

For new construction, blast cleaning gives the best surface preparation. For equipment as complicated as a scrubber, meticulous mechanical cleaning is essential after welding. This may require the use of needle guns, chippers, or grinders which are not high-volume production tools, but which may be the best means available for the finished weldments. Whatever the means, quality surface preparation is essential to lining life.

References

- [1] Fontana, M. G. and Greene, N. D., *Corrosion Engineering*, McGraw-Hill, New York, 1967, p. 344.
- [2] "Electrical and Electrochemical Methods for Determining Corrosion Rates," NACE Unit Committee T-3L, National Association of Corrosion Engineers, Houston, TX, April 1983.
- [3] Postlethwaite, J., Tinker, E. B., and Hawrylak, M. W., *Corrosion*, Vol. 8, 1974, p. 285.
- [4] Marsh, G. A., *Proceedings*, 2nd International Congress on Metallic Corrosion, New York, 1963, National Association of Corrosion Engineers, Houston, TX, p. 936.
- [5] Uhlig, H. H., *Corrosion and Corrosion Control*, John Wiley & Sons, New York, 1971, p. 14.
- [6] Finley, H. F., "Descriptive Information on Rohrback Instruments Corrosometer and Corrotor Corrosion Monitoring Systems," Rohrback Co., Santa Fe Springs, CA, 1979.
- [7] "Operating Manual 1120 Corrotor," Rohrback Co., Santa Fe Springs, CA, 1979.
- [8] *1985 Annual Book of ASTM Standards*, Vol. 03.02, ASTM G-81, Recommended Practice for Preparing, Cleaning, and Evaluating Corrosion Test Specimens, ASTM, Philadelphia, PA, p. 88.
- [9] Nelson, G., "Corrosion Data Survey, Shell Development Co.," National Association of Corrosion Engineers, Houston, TX, 1961.
- [10] Robald, E., *Corrosion Guide*, Elsevier Publishing Co., New York, 1975.
- [11] Burda, P. A., *Power Engineering*, Vol. 79, No. 8, 1975, pp. 48-51.
- [12] Paul, G. T., *Materials Performance*, Vol. 20, No. 2, 1981, pp. 44-48.
- [13] Crow, G. L. and Horsman, H. R., *Materials Performance*, Vol. 20, No. 7, 1981, pp. 35-45.

DISCUSSION

B. S. Phull¹ (written discussion)—Your statement that carbon steel can be used economically in flue gas desulfuration (FGD) system scrubber environments, particularly in conjunction with coatings, is not necessarily true for all situations. The first generation of scrubbers were fabricated from carbon steel because the severity of corrosion problems was not fully appreciated. This led to extensive in-situ applications of coatings with attendant problems. Coatings in general failed rapidly by delamination. (There are areas in scrubbers where coatings cannot be considered because of the high process temperature.) The present generation of scrubbers routinely utilizes the more corrosion-resistant materials of construction, for example, Type 316 stainless steels, Inconel 625, Hastelloy G3, and Hastelloy C-276. Titanium is a prime candidate but is limited by fabrication problems. These corrosion-resistant materials offer a cost-effective advantage over, say, a 20-year design life compared to carbon steel. Therefore, it is erroneous to suggest that the more corrosion-resistant materials have an intrinsic cost penalty just because the initial capital cost of materials and fabrication is high. Less downtime through failure and maintenance will overcompensate for the high initial cost when considered over a long design life. (2) You showed relatively poor correlation between weight loss and linear polarization corrosion rates obtained with a commercial corrosion rate meter. Did you try to compare actual weight loss on the coupons with the calculated weight loss for your linear polarization electrodes (the latter is easily obtained from integrated corrosion rate versus time data)? Instantaneous corrosion rates should be used with caution and really used to indicate trends rather than absolute values.

P. A. Burda (author's closure)—B. S. Phull's statements are not in disagreement with the conclusions stated in the Materials Selection and Coating Failures sections of this paper.

The point of the paper, however, is to provide designers of "present generation" FGD systems with corrosion data of not only stainless steel but also of coated carbon steel surfaces exposed in limestone slurry scrubbers.

Coated carbon steel has been used successfully for more than ten years in scrubbers. This field experience proved that up to 75% of the exposed carbon steel surfaces can still be used with properly applied coatings and that their application would reduce the construction cost of new FGD systems.

B. S. Phull's materials suggestions, on the other hand, will not eliminate serious corrosion problems such as intergranular and galvanic corrosion and

¹ Laque Center for Corrosion Technology, Inc., Wrightsville Beach, NC 28480.

corrosion around the welds. These problems are common in present FGD generation scrubbers regardless of the use of expensive, corrosion-resistant metals and alloys. Figure 8 shows the serious galvanic corrosion problem when stainless steel was applied. Tables 4 through 6, on the other hand, compare relatively low corrosion rates of carbon steel.

Yoshinori Oka,¹ Masanobu Matsumura,¹ Masaaki Yamawaki,²
and Matsushige Sakai³

Jet-in-Slit and Vibratory Methods for Slurry Erosion-Corrosion Tests of Materials

REFERENCE: Oka, Y., Matsumura, M., Yamawaki, M., and Sakai, M., “**Jet-in-Slit and Vibratory Methods for Slurry Erosion-Corrosion Tests of Materials,**” *Slurry Erosion: Uses, Applications, and Test Methods, ASTM STP 946*, J. E. Miller and F. E. Schmidt, Jr., Eds., American Society for Testing and Materials, Philadelphia, 1987, pp. 141–154.

ABSTRACT: Slurry erosion-corrosion tests were conducted on metallic materials of practical use by two kinds of testing apparatuses. One is a vibratory apparatus which uses a magnetostriction vibratory unit commonly used for the accelerated cavitation testing of materials. The other is a jet-in-slit apparatus by which a jet of slurry impinges on the test surface. The test results obtained by each apparatus showed a good agreement in the order of merit of the materials. The test results of the jet-in-slit apparatus agreed with the actual service performance of the material in relative magnitude of damage rates.

By making a comparison of the erosion-corrosion parameters between the testing apparatuses and the actual service conditions in the field, the testing conditions required for quantitative assessment of erosion-corrosion damage were discussed.

KEY WORDS: slurry, erosion, erosion-corrosion, testing method, pump

Erosion-corrosion of metallic materials has become a major problem as various skillful approaches are being made to obtain energy from a wide variety of sources other than oil. For example, cavitation erosion-corrosion attacked the pit tube of a geothermal power plant, through which underground water containing sulfur compounds boiled out. Dispersed water droplets in the steam caused the

¹ Assistant and professor, respectively, Department of Chemical Engineering, Hiroshima University, Saijo, Higashi-Hiroshima 724, Japan.

² Senior research metallurgist, Mazda Pump Manufacturing Co., Nogami, Takarazuka 665, Japan.

³ Senior staff scientist, Chubu Electric Power, Inc., Central Technical Research Laboratory, Nagoya 461, Japan.

degradation of the turbine blades, which were used to recover energy from the relatively low pressure process steam. The slurry erosion-corrosion occurring on the materials containing coal slurry in its liquefaction process is a well-known example.

The slurry erosion-corrosion problem we encountered was concerned with the conservation of environments rather than of energy. Serious damage occurred to the pump components, which circulated cleaning liquid to remove the sulfur compounds from the stack gas of a steam power plant. The cleaning liquid was of high acidity containing solid particles of gypsum. Our first attempt to evaluate the erosion-corrosion resistance of metals by using Stauffer's Grinding Pot Device [1] failed. The test results were scattered badly because the amounts of weight loss were small when compared with the weight of the finger-shaped specimen. Furthermore, an unexpected result happened. An increase in the weight of the specimen occurred. This might be attributed to a thick corrosion layer and deposits on the rear-side surface of the specimen where solid particles of the slurry scarcely impinged [2].

For these reasons, a new testing apparatus was developed which made use of a magnetostriction vibratory unit commonly used for the accelerated cavitation erosion testing of materials [3]. The apparatus successfully determined the weight loss of the specimen caused by the combined attack of particles impingement erosion and corrosion. This was due to the fact that the whole of the test surface was subjected to uniform erosion-corrosion conditions. A weak point of the apparatus, however, was that cavitation damage to the specimen could not be avoided when particles of a diameter smaller than 50 μm were used. Another type of testing apparatus was developed in which a jet of slurry impinged on the test surface, and particles of any size could be used [4].

By using the apparatuses, slurry erosion-corrosion tests were conducted on metallic materials of practical use. The results determined in each apparatus showed a good agreement in the order of merit of the materials. Two of the materials were used for the slurry pump components, and fortunately we had the opportunity to compare the actual service performance of the materials with their test results. They agreed fairly well, and so it has been proved that the testing apparatuses are suitable for the assessment of slurry erosion-corrosion resistance of materials.

However, the test parameters of the apparatuses, especially the particle impingement parameters, were apparently different from those of pumps in the field. It is certainly desired that materials should be tested under conditions as close as possible to those of the actual machines in the field. But, an apparatus operated under the same conditions as the field would make no sense without simplicity, economy in operation, and applicability for wide use, which are indispensable conditions for testing apparatuses. In the setting up of test conditions, therefore, we must make critical choices for the parameters, which should coincide with those of the actual machines. Discussion on this aspect is included in following paragraphs.

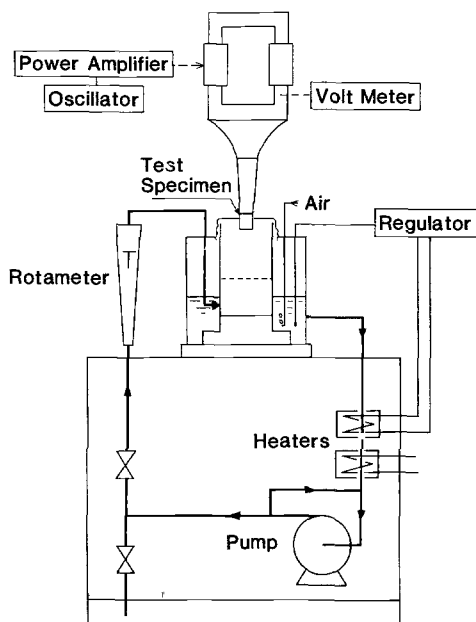


FIG. 1—Schematic diagram of vibratory testing apparatus.

Testing Apparatus and Procedure

Two kinds of testing apparatus were used in this investigation. One is the vibratory apparatus, which uses a magnetostriction vibratory unit. Figure 1 shows the schematic diagram of the apparatus. A uniform slurry is set up in a fluidized-bed bath, that is, solid particles are suspended uniformly in an upward flow of liquid. The specimen is a column 16 mm in diameter by 22 mm high with the side wall entirely covered by a vinyl tape except for the circular bottom of the test surface. It is vibrated axially at a high frequency of 19.9 kHz in the slurry. The peak-to-peak amplitude is 20 μm . The particle impact parameters were determined by inspecting the size and shape of the craters on the surface and are given in Table 1 [5]. It was also confirmed that no cavitation damage

TABLE 1—Test conditions.

	Impact Velocity, m/s	Impact Angle	Impact Parameter	Slurry Particles
Vibratory apparatus	2.2	90°	Frequency of 19.9 kHz	Silica sand 60 wt%
Jet-in-slit apparatus	1.7	90°	Flow rate of 2 L/min	Silica sand 6 wt% Gypsum 12 wt%

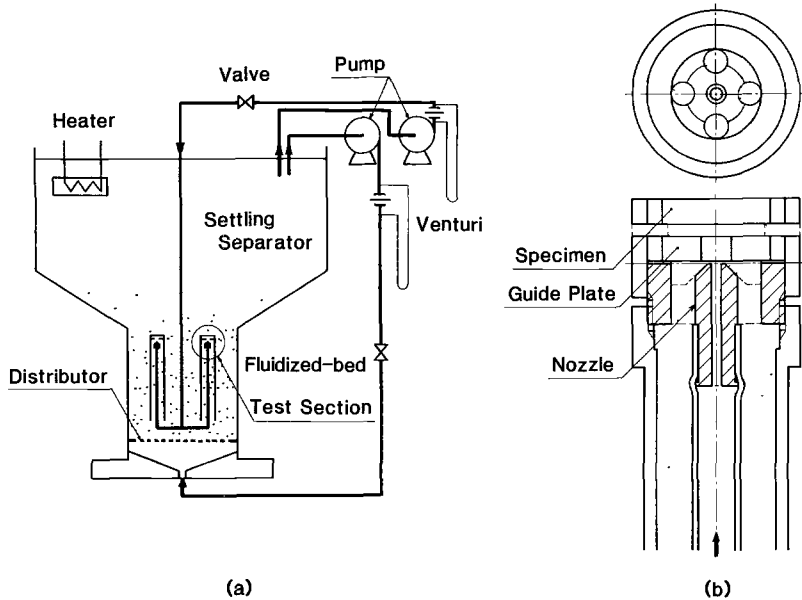


FIG. 2—Schematic diagram of (a) jet-in-slit testing apparatus and (b) test section.

occurred on the test surface, provided that particles over $50\ \mu\text{m}$ in diameter were used for the slurry [3].

The other is a jet-in-slit apparatus (Fig. 2). The main tank of transparent polyvinyl chloride resin consists of two sections placed one over the other. In the lower section of smaller diameter, a fluidized bed is set up. In the upper section of the tank, the slurry exhausted from the test section is separated into solid particles and clear liquid. Solid particles precipitate to fall down into the fluidized bed below. The bulk of the clear liquid is circulated by the pump into the test section and the rest into the underside of the distributor to set up the fluidized bed. The liquid jet from the nozzle ($1.6\ \text{mm}$ diameter) located in the center of the test section sucks up the slurry, which is mixed with the jet liquid to impinge upon the surface of the test specimen ($18\ \text{mm}$ in diameter by $4\ \text{mm}$ high) and thereafter exhausted radially through the slit between the specimen and guide plate. The damage occurs at the area of jet impingement on the specimen as well as on the surface outside this area, which is due to the radial flow. Four pieces of these test sections are installed in the tank.

Both apparatuses have common features: (1) the damage develops only on the testing surface of the specimen—no other part of the apparatus is damaged; (2) the amount of particles, the specimen size, and the power consumption are all small; and (3) the reproducibility of the test results is excellent. The most important feature is that the entire test surface is subjected to erosion and

TABLE 2—*Chemical compositions and physical properties.*

Specimen	Chemical Compositions, %			Structure	Physical Properties	
	C	Ni	Cr		Vickers Hardness	Specific Gravity
Stainless Steel (316L)	0.03	13.5	17.0	Austenite	198	8.0
Hastelloy C	0.08	53.5	16.5	Austenite	210	8.7
Material A	0.05	5.5	25.5	Austenite and ferrite	280	7.7
Material B	0.03	6.0	28.0	Austenite and ferrite	500	7.7

corrosion at the same time. This is indispensable for obtaining reliable test results.

The chemical compositions and physical properties of the materials are listed in Table 2. They are stainless steel of Type 316L and Hastelloy C as reference materials and Materials A and B, which have been used for the pump components.

Slurries were prepared from the particles and the corrosive liquids in Table 3. The liquids were of nearly the same chemical composition as those in an actual stack gas scrubber. Silica sand particles were used for the reference slurry. The gypsum particles were the same as those contained in the slurry of the scrubber.

Corrosion tests were conducted in the jet-in-slit apparatus by flowing the corrosive liquids without particles. The slurries of the solid particles and deionized water were used for the erosion tests, and those of the solid particles and the corrosive liquids for the erosion-corrosion tests.

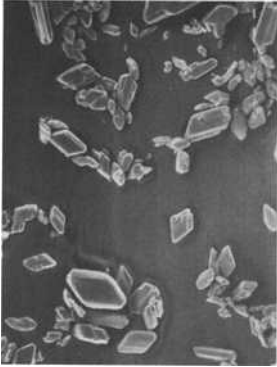
Test Results

No weight loss for the specimen was found after the corrosion test of 50 h on any material in any corrosive liquid. Thus, they had good corrosion resistances against the liquids.

Some results of the erosion test as well as the erosion-corrosion tests are shown in Figs. 3 and 4. Fairly good linear relations existed between the volume loss of the specimen and test duration, and constant damage rates independent of the test duration were obtained from the slopes of the lines.

The erosion-corrosion tests in the slurries of silica sand and corrosive liquids were carried out in the test apparatuses. The results are shown in Fig. 5 (vibratory apparatus) and Fig. 6 (jet-in-slit apparatus). The damage rate in mm^3/h was divided by the surface area, and the flow rate of particles, to obtain damage rates in mm/kg . The damage rates of the material were of nearly the same magnitude independent of slurry liquids. Each apparatus has established the same order in damage rate, namely, stainless steel > Hastelloy C > Material A > Material B.

TABLE 3—Slurries.

Liquid of Slurry	Particles	Particle Properties		SEM Photograph
		Mean Diameter, μm	Vickers Hardness	
Deionized Water	Silica Sand	77	1200	
H_2SO_4 sol., pH 4				
H_2SO_4 sol., pH 4 Cl^- (CaCl_2), 200 ppm	Gypsum	40	20-50	
H_2SO_4 sol., pH 2				

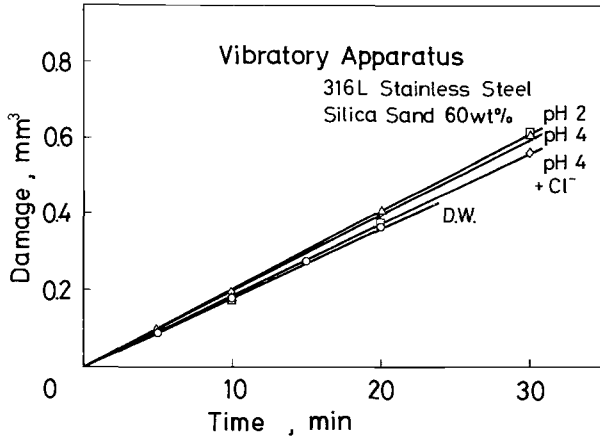


FIG. 3—Erosion-corrosion damage versus testing time for 316L stainless steel: frequency, 19.9 kHz; amplitude, 20 μ m; slurry, silica sand (60 weight %) and respective liquids, 60°C.

Figure 7 shows the specimens of Materials A and B that were damaged in the apparatuses. They show a matted surface, which is the typical appearance of metallic materials eroded by the repeated impacts of solid particles. The appearance did not depend on the slurry impinged.

Erosion-corrosion tests in the gypsum slurry were conducted only in the jet-in-slit apparatus (the particle size was so small that cavitation occurred in the vibratory apparatus). The damage rates shown in Fig. 8 are extremely small as

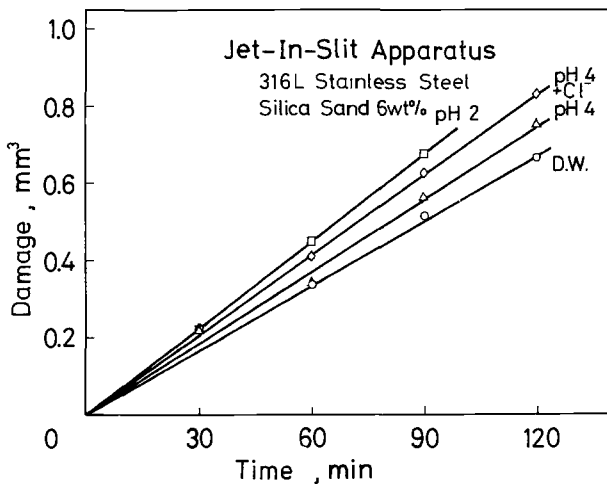


FIG. 4—Erosion-corrosion damage versus testing time for 316L stainless steel: jet velocity, 1.7 m/s; slurry, silica sand (6 weight %) and respective liquids, 60°C.

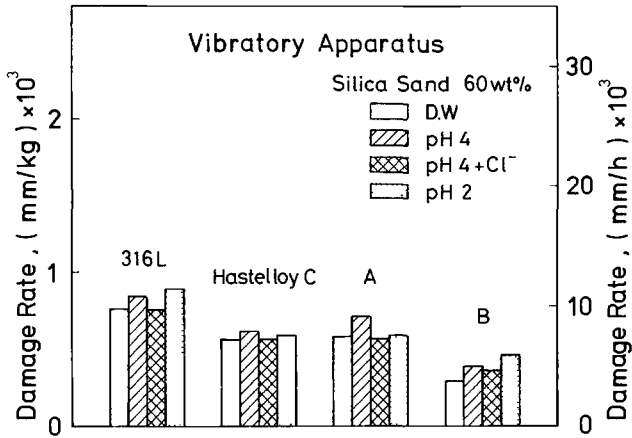


FIG. 5—Damage rates of materials in vibratory apparatus: frequency, 19.9 kHz; amplitude, 20 μ m; slurry, silica sand (60 weight %) and respective liquids.

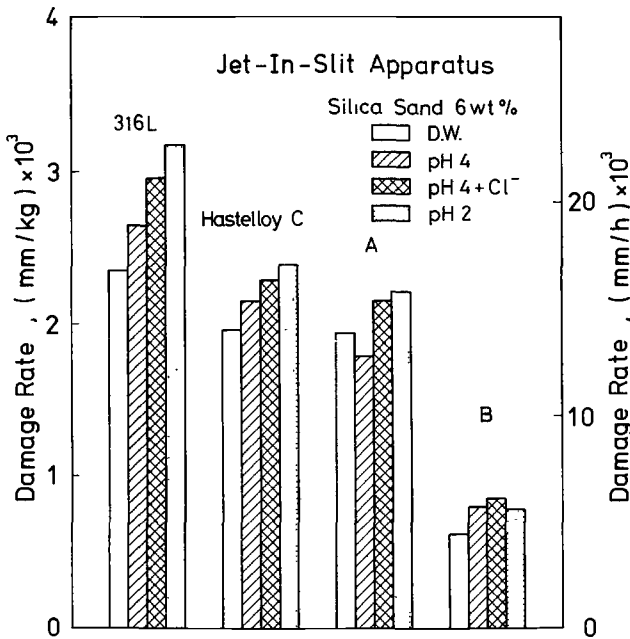


FIG. 6—Damage rates of materials in jet-in-slit apparatus: jet velocity, 1.7 m/s; slurry, silica sand (6 weight %) and respective liquids.

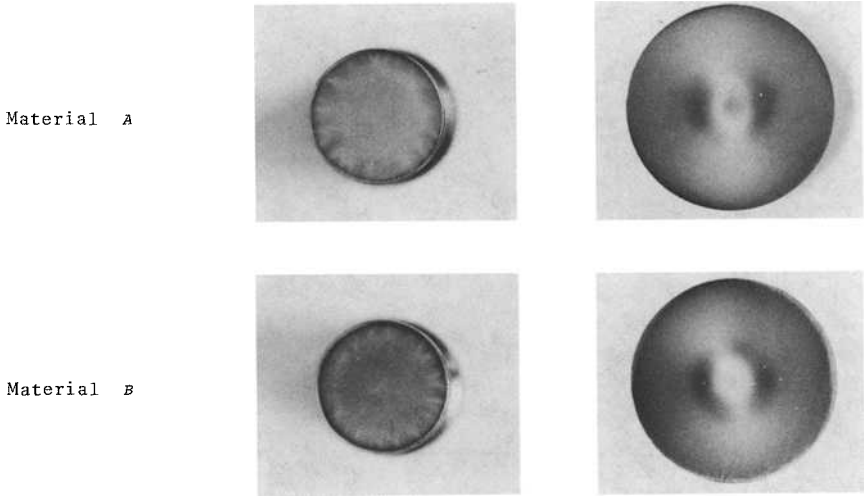


FIG. 7—Appearances of test surface of Materials A and B damaged in vibratory apparatus (left) and in jet-in-slit apparatus (right).

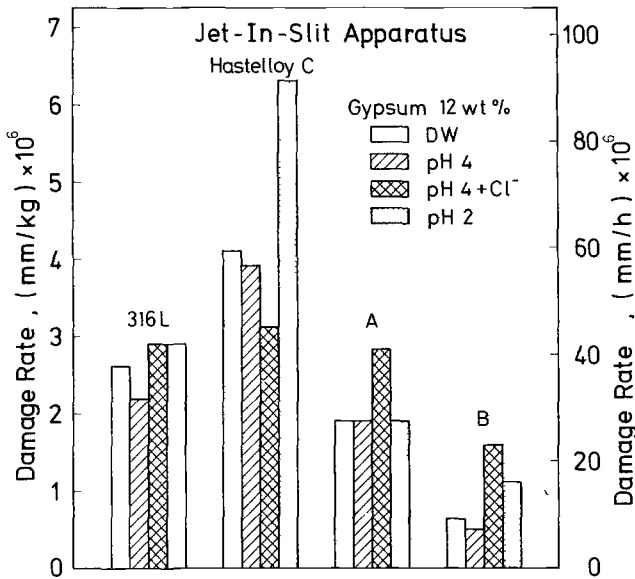


FIG. 8—Damage rates of materials in jet-in-slit apparatus: jet velocity, 1.7 m/s; slurry, gypsum (12 weight %) and respective liquids.

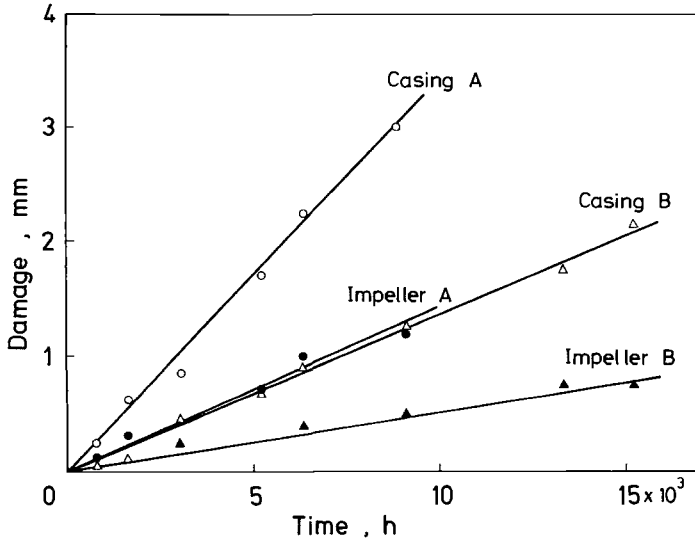


FIG. 9—Erosion-corrosion damage versus operation time for pump components in actual service.

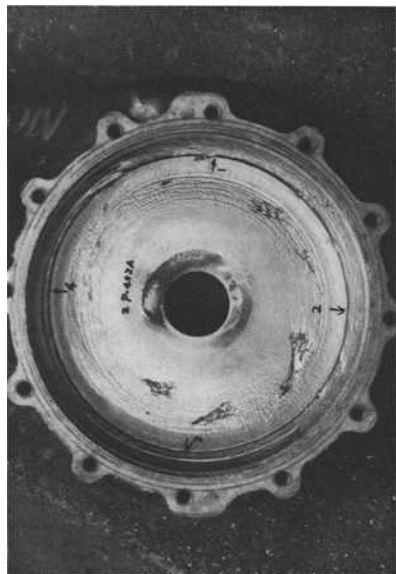
compared to those in the silica sand slurry (Fig. 6). This may be attributed to the size as well as to the hardness of the particle. As to the order in damage rate, stainless steel and Hastelloy have exchanged their positions, though Materials A and B stayed in the same position. The specimen surfaces showed a matted appearance as well.

Damage on Pump Components

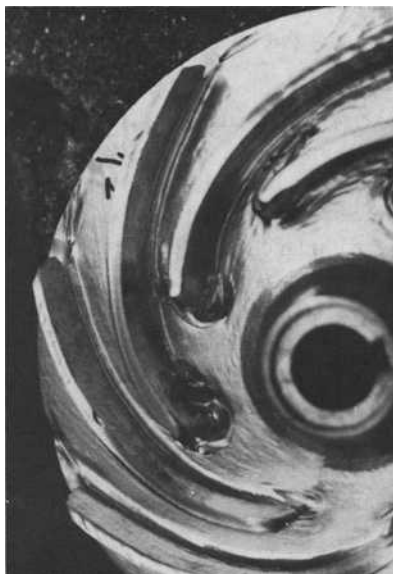
Materials A and B were used for the components of Pumps A and B, respectively, which had a common size: bore diameter, 125 mm; impeller diameter, 265 mm; revolution, 1750 rpm; discharge quantity, 85 m³/h. They pumped gypsum slurry of sulfuric acidity at the same time under nearly the same condition: the solid particle concentration ranged between 20 and 40 weight %, and pH value between 2 and 4.

The average depth of the damage on the blade top of the impellers and the surface of the casings was measured at regular intervals. Figure 9 shows the results. It should be recognized that the damage depth increased linearly with the duration of the operation just as in the case of the test apparatuses. In each pump, the casing was damaged more deeply than the impeller, and the damages of Pump B were one half or one third smaller than Pump A, which is in good agreement with the test results shown in Figs. 6 and 8.

Figure 10 shows the damaged surfaces of the pump components. Both surfaces showed a matted as well as wavy appearance, and the damage on Material B is shallower than on Material A.



Casing A



Impeller A



Casing B



Impeller B

FIG. 10—Appearances of pump component surfaces in actual service.

Discussion

Test results obtained by the jet-in-slit apparatus agreed well with the actual performance in the pumps not only on the order but also on the relative magnitude of the damage rate. In other words, a quantitative relationship has been established between the test results and the actual damage of the pump. By using the relationship, it is possible for the apparatus to assess quantitatively the damage rate of any material which is to be used as pump components under the same operating condition.

It is, however, indispensable to know the effects of the test parameters on the test results for estimating the damage rate to any material which is to be used under other conditions. With this object in mind, a quantitative comparison of the damage rate between the test results and the field performance of Material B is given in Table 4, in which the damage rate in mm/h of the pump components was divided by the bulk particle flow rate to obtain the damage rate per unit mass of the particle, that is, mm/kg. It arouses interest that the damage rate in mm/h of the specimen in the gypsum slurry is of nearly the same magnitude as those of the pump components, though the rate in mm/kg is 10^3 larger than those of the components. On the contrary, the damage rates of specimens in the silica sand slurry are much larger than any damage rates of the actual pump.

Slurry Particles

An advantage in using the silica sand slurry is the shortening of the test duration. For example, it takes a minimum of 20 h to determine the damage rate of Hastelloy C in the gypsum slurry, but only 2 h is enough for precise measurements in the silica sand slurry. As to the test results, however, stainless steel and Hastelloy C changed positions in the order of damage rate when the silica sand slurry was used for the gypsum slurry (compare Fig. 6 with Fig. 8). This suggests that the actual slurry in question should be used even though the purpose of the test might be a rough selection of materials. In the tests for estimating the damage rate of a material in the actual plant, it is absolutely necessary to use the actual slurry.

TABLE 4—Comparison between test results and actual performance of Material B.

	Damage Rate, mm/h	Damage Rate, mm/kg
JET-IN-SLIT TEST		
Silica sand slurry	6.2×10^{-3}	8.6×10^{-4}
Gypsum slurry	2.3×10^{-5}	1.6×10^{-6}
ACTUAL PERFORMANCE IN PUMP		
Impeller	5.5×10^{-5}	3.2×10^{-9}
Casing	1.4×10^{-4}	8.2×10^{-9}

Slurry Liquid

Tests on a material in the vibratory apparatus by silica sand slurries have resulted in nearly the same magnitude of damage rates independent of the slurry liquid (Fig. 5). A similar tendency was recognized in the test results of the jet-in-slit apparatus where silica sand particles were used (Fig. 6). In contrast to these results, the damage rates of the material varied, largely depending on the slurry liquid, when gypsum particles were used (Fig. 8). This is apparently because the erosiveness of gypsum particles is less intense than that of silica sand, and, correspondingly, the effect of corrosion has appeared more distinctly on the test results. Thus, in this aspect as well, it is necessary to use the actual slurry in laboratory tests.

Particle Impact Parameters

The average velocity of slurry flow over the impeller surface is on the order of 1 m/s, which is the volumetric flow rate divided by the area of the flow cross section. Over the casing surface, it is on the order of 10 m/s given the assumption that the slurry is circulating at the same velocity as the impeller. It is generally recognized that the erosion rate by particles impingement is proportional to the 2.3 (ductile material) \sim 6 (brittle material) power of the impact velocity [6]. The difference in the damage depth between the impeller and the casing is less than expected from the slurry flow velocities. This discrepancy may be attributed to the differences in the particle flow rate and their impact angle. These parameters are characteristic of each component and depend decisively on the operating conditions.

The particles' impact velocity in the jet-in-slit apparatus is 1.7 m/s as shown in Table 1, which is naturally not coincident with those in the pump. It is impossible and not necessary for them to coincide, because the quantification of the impact velocity effect is possible; hence, the damage rate under any impact velocity may be easily estimated based on test results under known conditions.

As to impact angle, we have recently confirmed that it affects the synergistic action of erosion with corrosion [7]. In the case of materials susceptible to corrosion, therefore, the laboratory tests have to be conducted under the same impact angle as the actual machines.

Conclusion

Slurry erosion-corrosion tests were conducted on metallic materials of practical use by two kinds of testing apparatus, that is, the vibratory apparatus and the jet-in-slit apparatus. The test results obtained in the jet-in-slit apparatus have agreed well with the actual service performance of the materials as slurry pump components in the exhaust gas desulfurization process of a steam power plant.

The reasons why the test results of the jet-in-slit apparatus have agreed with the actual performance of the material might be the low damage rate (mm/h) in the apparatus, which was inevitable in using the actual slurry in the field. The successful measurement of such a low damage rate has been attributed to the specimen with a large testing surface and yet of small weight. It can also be attributed to the stability of the apparatus, which could bear the operation of such a long duration.

It is expected that the results of the vibratory apparatus might coincide with the actual performance of materials if the silica sand slurry was used in the actual pump. The gap between the test results and the actual performances may, however, be partly attributed to the vibration of the specimen. A large acceleration (20 000 g at a frequency of 20 kHz and amplitude of 25 μm) is induced in the specimens. It has been confirmed that this did have an effect on the damage mechanism of cavitation erosion when the vibratory unit was used in the accelerated cavitation test [8]. The same effects on the slurry erosion are possible.

References

- [1] Stauffer, W. A., *Metal Progress*, Vol. 67, No. 1, Jan. 1956, pp. 102–107.
- [2] Matsumura, M., Oka, Y., Hatanaka, H., and Yamawaki, M., *Boshoku Gijutsu (Corrosion Engineering, Journal of the Corrosion Engineering Society of Japan)*, Vol. 29, No. 2, Feb. 1980, pp. 65–69.
- [3] Matsumura, M., Oka, Y., Hatanaka, H., and Yamawaki, M. in *Proceedings, 5th International Conference on Erosion by Liquid and Solid Impact*, Cambridge, England, Sept. 1979, Royal Aircraft Establishment, Farnborough, England.
- [4] Oka, Y. and Matsumura, M., "Wear of Materials 1983," American Society of Mechanical Engineers, New York, Apr. 1983, pp. 360–366.
- [5] Oka, Y., Matsumura, M., Ohsako, Y. and Yamawaki, M., *Boshoku Gijutsu (Corrosion Engineering, Journal of the Corrosion Engineering Society of Japan)*, Vol. 33, No. 5, May 1984, pp. 278–283.
- [6] Tilly, G. P., *Wear*, Vol. 14, No. 4, Oct. 1969, pp. 241–248.
- [7] Oka, Y., Matsumura, M., Ohsako, Y. and Yamawaki, M., *Proceedings, Japan Society of Corrosion Engineering*, May 1984, pp. 25–28.
- [8] Matsumura, M., Okumoto, S., and Saga, Y., *Bulletin of the JSME*, Vol. 25, No. 204, June 1982, pp. 898–905.

John E. Miller¹

The SAR Number for Slurry Abrasion Resistance

REFERENCE: Miller, J. E., “The SAR Number for Slurry Abrasion Resistance,” *Slurry Erosion: Uses, Applications, and Test Methods, ASTM STP 946*, J. E. Miller and F. E. Schmidt, Jr., Eds., American Society for Testing and Materials, Philadelphia, 1987, pp. 155–166.

ABSTRACT: With the use of the Miller Number for slurry abrasivity and its usefulness in the slurry pumping industry in predicting pump wear, it became obvious that the same test could be run in “reverse” to determine the effect of a “standard” slurry on a candidate material, thereby giving a relative measure of how a particular material would perform. In fact, about half of the 20 Miller machines in existence throughout the world are used specifically for wear or abrasion-resistance tests.

In this presentation the machine will be briefly described along with the basic procedure for determining SAR (slurry abrasion resistance) as derived from the Miller Number procedure.

KEY WORDS: abrasivity, slurry, abrasion resistance, corrosion, wear, wear resistance

The Miller Number, per se, is an index of the abrasivity of slurry [ASTM Method for Slurry Abrasivity by Miller Number (G 75-82)]. In the test, the mass-loss rate of a “standard” metal wear block is determined when worn by various slurries consisting of 50% by mass concentration of abrasive in distilled water at room temperature.

For many years, an approximate Miller Number system had been used to run a “wear test” of various solids. An unknown specimen (metal or any other coated or solid material) is run in a “standard” sand slurry, and the mass-loss is measured to determine the resistance to slurry abrasion. The latter test is known as the SAR (Slurry Abrasion Resistance). The two tests differ.

It has become evident that the information obtained by the SAR test should be compared with the results of the Miller Number test to aid in the selection of materials for pumps and parts. Accordingly, the new SAR test is now run with the same strict standards as the Miller Number test and is calculated in the

¹ Consultant, White Rock Engineering, Inc., P.O. Box 740095 Dallas, TX 75374.

same manner. Both numbers are related to the rate of mass-loss early in the test.

There is a crossover point in the comparison where the Miller Number and the SAR Number are the same, namely Number 111. In this case, the wear block and specimen are the same (27% chrome iron); the slurry is the same—the “any” slurry of the Miller Number becomes “standard” slurry of 50% by mass of AFS 50-70 sand in distilled water.

As long as SAR tests are run on a series of materials, there should be no problem in comparing the relative quality of the specimens run in this series. As more data are accumulated, a broader comparison to other materials will be accrued.

Test Equipment

The device used to measure the relative abrasion resistance of various materials (Figs. 1–2) consists in general of a standard 215.4 by 12.7 mm (0.5 by 1.0 in.) specimen (see Fig. 3) driven at a rate of 48 strokes/min with a 200-mm (8-in.) stroke, riding in the bottom of a tray containing a 50% by mass slurry of standard AFS 50-70 sand mixed in distilled water. A dead mass of 1.866 kg (5 lb) is applied. For each test, the bottom of the tray is equipped with a new

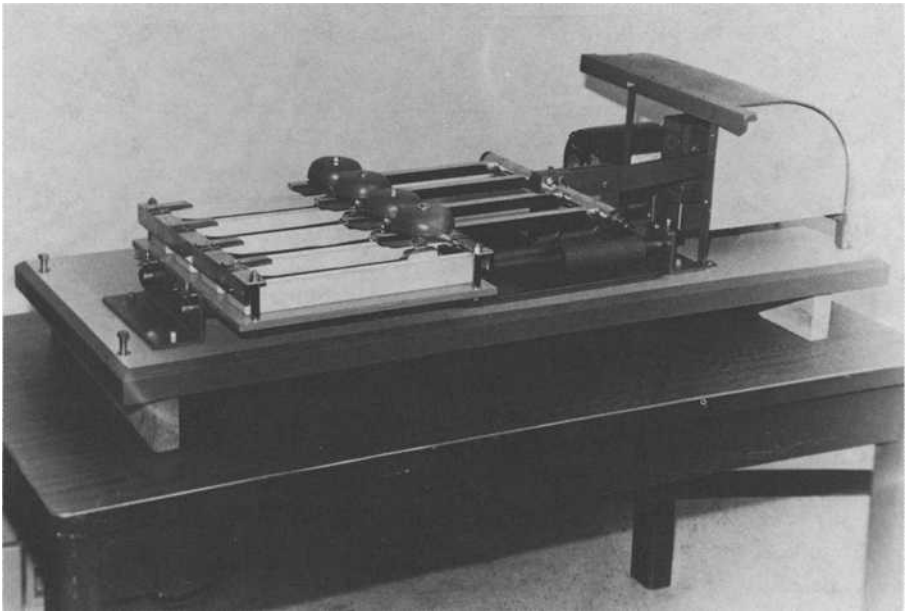


FIG. 1—Miller machine complete.

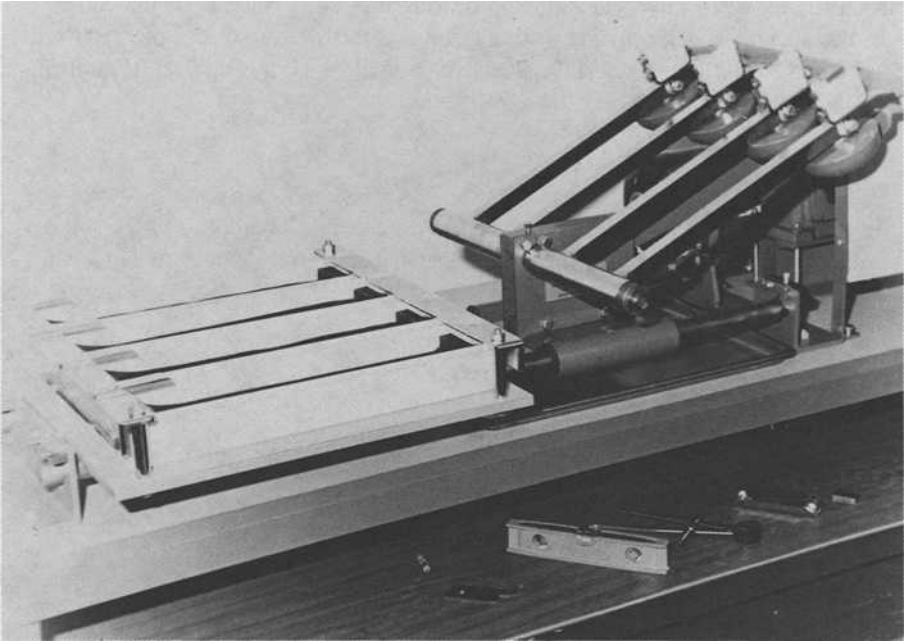


FIG. 2—Arms in racked position.

piece of neoprene sheet to act as a lap. The interior of the tray is of a flat-bottomed “V” shape to confine the slurry particles to the path taken by the specimen. At the end of each stroke, the specimen is lifted 1.5 mm ($\frac{1}{16}$ in.) off the lap by a cam action to allow fresh material to flow under. The block holder is made of plastic, as are the trays, so that electrolysis in certain slurries is eliminated.

Procedure

The specimen is weighed to 0.10 mg after being scrubbed in detergent and dried for 15 min. under a heat lamp. The specimen is aligned in the holder,

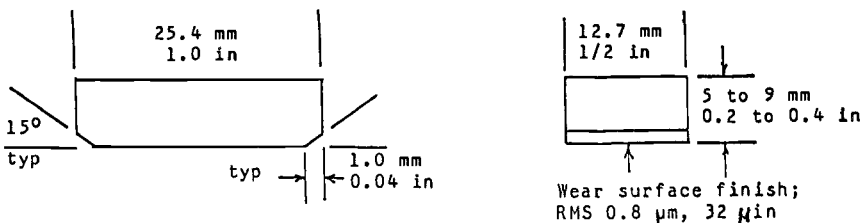


FIG. 3—Specimen dimensions.

placed in the slurry tray, and the reciprocating motion is started. At the end of 4 h, the specimen is removed, washed, and weighed, and the loss of material is recorded. This is repeated four times for a total of 16 h. Duplicate samples are run simultaneously to provide a verification.

Lap Wear

In most cases there is perceptible wear only on the rubber lap, but for some reason certain slurries exhibit more than usual wear. Four degrees of lap wear are reported:

1. *Trace*: Perceptible—block track dulled.
2. *Light*: Mostly scratches or striations.
3. *Heavy*: Less than a 0.8-mm ($1/32$ -in.) groove.
4. *Severe*: Wear block “plows” groove 0.8 mm (1.32 in.).

Calculation of Results

SAR Number

The specimen mass-loss, the average of two runs in a standard slurry, is recorded (Fig. 4).

An actual curve can be plotted (Fig. 5). The basic mathematical equation for the curve in Fig. 5 is

$$\text{mass-loss, mg} = A \times \text{hours}^{**}B \quad (1)$$

Using the least squares method, the values of A and B are calculated for a curve closely matching the test data curve. In this case, the following values are determined

$$A = 8.65$$

$$B = 0.81$$

The equation for the example becomes

$$\text{mass-loss, mg} = 8.65 \times \text{hours}^{**}0.81$$

	WEIGHTS, GMS		LOSS, MG		LOSS, MG CUM. AVE.
	BLOCK 1	BLOCK 2	BLOCK 1	BLOCK 2	
INITIAL	16.4746	16.4069	0.0	0.0	0.0
AFTER 4 HRS	16.4478	16.3809	26.8	26.0	26.4
AFTER 8 HRS	16.4274	16.3613	20.4	19.6	46.4
AFTER 12 HRS	16.4085	16.3427	18.9	18.6	65.2
AFTER 16 HRS	16.3924	16.3266	16.1	16.1	81.3

FIG. 4—Typical test data.

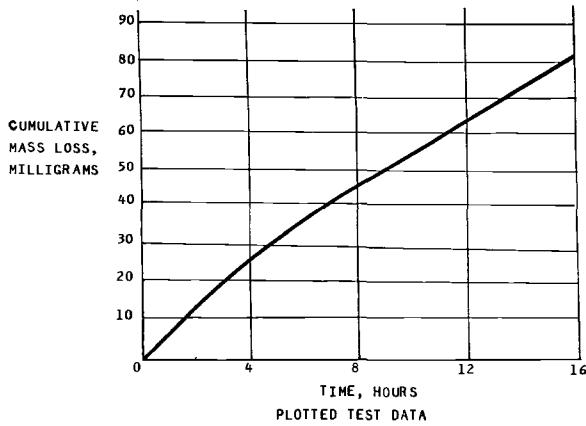


FIG. 5—Plotted test data.

The SAR Number is described as an index related to the rate at which the specimen loses mass at 2 h into the test, which can be calculated by using the first derivative of Eq 1 at 2 h. (This becomes the slope of the line tangent to the curve at 2 h.)

For example

$$\text{mass-loss rate, mg/h} = A \times B \times 2^{B-1} \tag{2}$$

The plotted loss rate at 2 h is shown in Fig. 6. The mass-loss rate at 2 h into the test is a straight line tangent at 2 h on the mass-loss curve (Fig. 5).

It is desirable to have a meaningful whole number for the expression of the

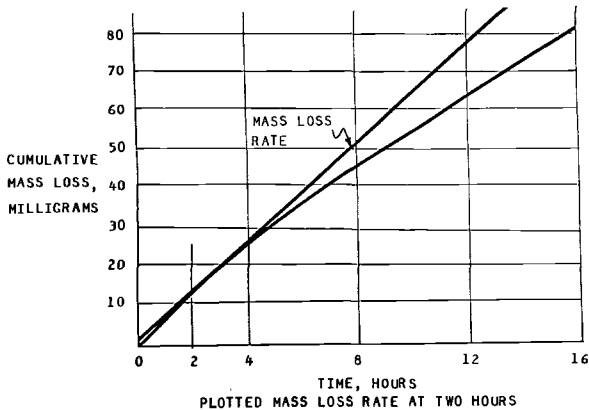


FIG. 6—Plotted rate loss at 2 h.

SAR NUMBER - SLURRY ABRASION RESISTIVITY BY MILLER NUMBER SYSTEM
STANDARD SLURRY

TEST NUMBER : B
 TEST DATE : 21-MAY-84
 PROJECT DESC : ABRASION RESISTANCE OF 27% CHROME IRON
 SLURRY DESC : AFS TESTING SAND 50-70
 SLURRY CONC : 50% BY MASS
 WEAR SPECIMEN : 27%CHROME IRON
 LAP MATERIAL : MIL-R-6855 CLASS 2 GRADE 80 NEOPRENE

WEAR SPECIMEN	TEST DATA				CUM AVE LOSS	
	3		4		ACTUAL	*BEST FIT
	MASS GRAM	4HR LOSS MG	MASS GRAM	4HR LOSS MG	MG	MG
INITIAL	16.4746	0.0	16.4069	0.0	0.0	0.0
AFTER 4 HOURS	16.4478	26.8	16.3809	26.0	26.4	26.6
AFTER 8 HOURS	16.4274	20.4	16.3613	19.6	46.4	46.5
AFTER 12 HOURS	16.4085	18.9	16.3427	18.6	65.2	64.6
AFTER 16 HOURS	16.3924	16.1	16.3266	16.1	81.3	81.6

BEST FIT MASS LOSS = (8.64651)(HOURS)**(.809375)

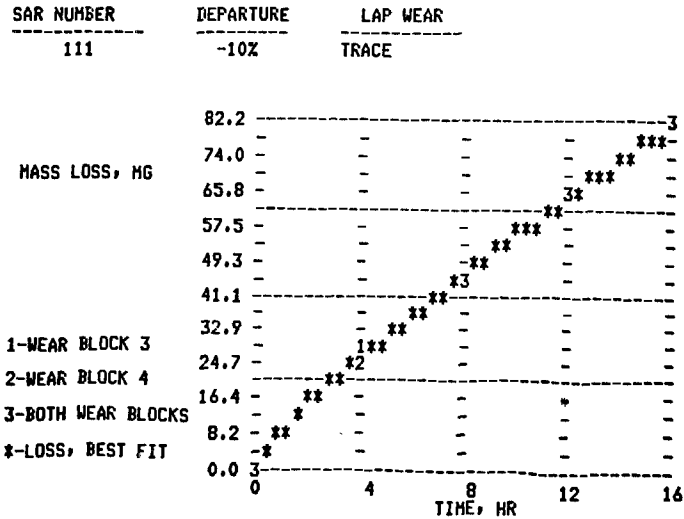


FIG. 7—Sample computer printout of typical SAR Number.

abrasion effects. It was decided that the range of the whole number would be from 1, for minor mass loss, to 1000, for extreme mass-loss; this is accomplished by the use of a scaling factor, C, determined to be 18.18. The equation for the SAR Number can thus be written as

$$\text{SAR Number} = C \times A \times B \times 2^{*(B - 1)} \tag{3}$$

In the example

$$\text{SAR Number} = 18.18 \times 8.65 \times 0.81 \times 2^{*(0.81 - 1)} = 111$$

An optional computer program is available for calculating results (see sample printout, Fig. 7).

ASTM-675 SLURRY ABRASIVITY DETERMINATION BY MILLER NUMBER
STANDARD SLURRY

TEST NUMBER : A
 TEST DATE : 21-MAY-1984
 PROJECT DESC : ABRASIVITY OF AFS 50-70 SAND
 SLURRY DESC : AFS 50-70 SAND
 SLURRY CONC : 50% BY MASS
 WEAR SPECIMEN : 27% CHROME IRON
 LAP MATERIAL : MIL-R-6855 CLASS 2 GRADE 80 NEOPRENE

WEAR SPECIMEN	TEST DATA				CUM AVE LOSS	
	1		2		ACTUAL	BEST FIT
	MASS GRAM	4HR LOSS MG	MASS GRAM	4HR LOSS MG	MG	MG
INITIAL	16.4746	0.0	16.4069	0.0	0.0	0.0
AFTER 4 HOURS	16.4478	26.8	16.3809	26.0	26.4	26.6
AFTER 8 HOURS	16.4274	20.4	16.3613	19.6	46.4	46.5
AFTER 12 HOURS	16.4085	18.9	16.3427	18.6	65.2	64.6
AFTER 16 HOURS	16.3924	16.1	16.3266	16.1	81.3	81.6

BEST FIT MASS LOSS = (8.64651)*(HOURS)**(.809375)

MILLER NUMBER	DEPARTURE	LAP WEAR
111	-10%	TRACE

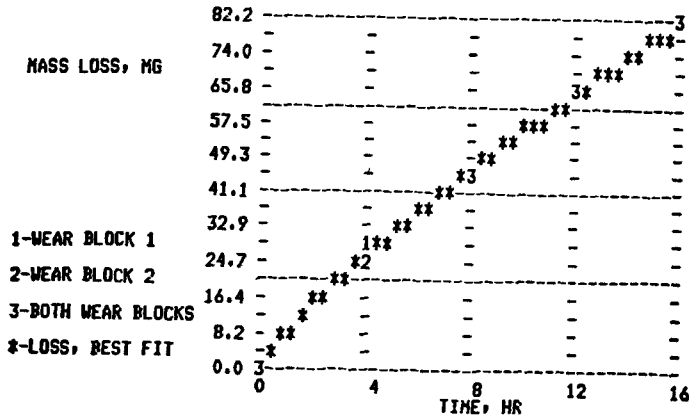


FIG. 8—Sample computer printout of typical Miller Number.

Figure 8 shows the computer printout run as a Miller Number, that point where the Numbers are equal.

Use of SAR Number

Because the SAR Number is a function of the mass-loss, it is evident that a high number represents a “poor” selection of material, yet the 27% chrome iron block used in the example is an accepted metal for most slurry services. Therefore, if one intends to pump the highly abrasive sand as used in the test, a more wear-resistant material would be looked for. Because the SAR Number

is relatively new, the accumulation of more data will add to its significance in the use for material selection.

Typical SAR Numbers

Because of the proprietary nature of such test data, actual SAR Numbers cannot be published at this time, but as a general guide, the following are given

Material	SAR Number
Chrome plate	50
27% chrome iron	111
Solid ceramic	227
Polyvinylchloride (PVC)	667

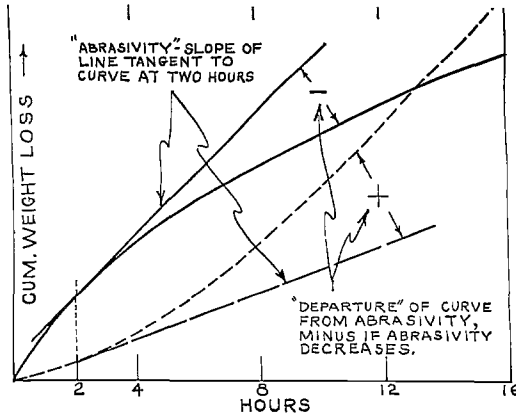


FIG. 9—Departure.

APPENDIX

Departure

The SAR Number is sometimes reported with an additional value called *departure* that represents the effect of slurry particle breakdown as indicated by a change of abrasivity as the test progresses. This value is a minus (−) if there is a loss of abrasivity and a plus (+) if there is a gain in abrasivity (Fig. 9). This effect may be encountered if the mechanical action of different specimen materials tends to “breakdown” the sand particles at a different rate. Or it could represent a “work hardening” of the metal.

Formulas for Departure

$$\text{departure} = \frac{A \times B \times (B - 1) \times 2^{B-2} \times 100}{A \times B \times 2^{B-1}} \quad (4)$$

In the example

$$\text{departure} = \frac{8.65 \times 0.81 \times (0.81 - 1) \times 2^{(0.81 - 2)} \times 100}{8.65 \times 0.81 \times 2^{(0.81 - 1)}} = -10\%$$

DISCUSSION

K. Metz (written discussion)—If possible, it would be desirable to use a more easily calculated value for the SAR Number.

J. E. Miller (author's closure)—The method of calculating the SAR Number goes a long way back, to the beginning of the Miller Number in 1967. It was during a full-scale loop test on the Savage River iron concentrate pump where it was realized that the solids in the slurry would “wear out” after a short time of being recirculated through a choke used to create a representative pressure. The principle of the Miller Number was conceived after searching the literature on the subject. The original test simply measured the weight loss of a “standard” metal wear block, positioned on a weighted arm, reciprocating against a rubber lap in the bottom of a tray containing a 50% by mass of solid particles. For the Savage River test, the simple weight loss was satisfactory and enabled one to keep the slurry abrasivity constant by the regular addition of “fresh” solids to replace the “worn out” material. Because the test performed so well in that case, it was decided to pursue it as a useful tool in the slurry pumping industry. Testing with other slurries revealed the fact that some slurries “wear out” as represented by each successive 4-h run, each showing a certain reduction in metal loss. But, surprisingly, certain other slurries exhibited an opposite effect—the metal loss actually increased with additional running time. Therefore, it can be seen that if two slurries reached a common end-value of mass loss, the slurry with a “minus” loss would possess a greater abrasivity in the “fresh” state (early in the test) than one with a “plus” loss. So it was concluded that this “early” abrasivity would be more representative of the effect on the wear of pump parts. Accordingly, it was decided that a more practiced approach would be to use the *rate* of mass loss early in the test. Accordingly, the four 4-h runs provided the points required to construct a curve from which the rate of mass loss at 2 h into the test could be obtained by the first derivative of the curve at the 2-h point. In the SAR Number, we felt that some method of testing a wear specimen of material in a “standard” slurry would provide a relative comparison to the “standard” 27% chrome iron wear block in the Miller Number test, remembering the later discovery that slurries of less than about a Miller Number 50 are “easy” to pump in typical pumps, while over 50 required special attention to pump type, displacement elements, speed, etc., even to the extent of flushing the stuffing box backing with clear liquid.

K. Metz (written discussion)—Does the sand “degrade” or change in some way for different materials?

¹ Dresser Industries—Security Division, P.O. Box 24647, Dallas, TX 75224.

J. E. Miller (author's closure)—The Departure from a straight line on the metal loss versus time curve (as just described for the Miller Number) was adopted for the SAR Number simply for academic interest in case some materials generate a different curve in the “standard” slurry. This could happen if materials respond to work hardening or fatigue. The Departure for 27% chrome iron in “standard” ASTM sand is –9%, showing that the abrasivity index is decreasing, either due to sand “wearing out” or work hardening of the wearing surface, or both. The Departure in SAR Number tests for other materials vary up to –18%. In those cases the effect evidently comes from the material. We include Departure in an “annex” in the proposed standard procedure, again purely for academic interest.

K. Metz (written discussion)—Have you run Cr-iron standards with the test materials to see if the Miller Number for the slurry changes?

J. E. Miller (author's closure)—If we interpret this question correctly, the following short tabulation will show the relationship:

Wear Block	Slurry	Miller Number	SAR Number
27% chrome	AFS sand	104	104
304L	AFS sand	...	748
27% chrome	Acidized frit	189	...
304L	Acidized frit	...	299 ^a

^a Nonstandard SAR number.

It can be seen that 304L material run in acidized frit slurry would experience 13 times that of 27% chrome in AFS sand slurry (an extremely bad situation!). We propose to call the Value 13 the DI (Destructive Index).

K. Metz (written discussion)—How accurately are the test blocks made?

J. E. Miller (author's closure)—We call for the area in contact with the slurry to be exactly 0.42 in.², but tests on blocks with great departure from that area has little effect on the final metal loss. The unit pressure resulting from differences in area compensates for the wear rate.

K. Metz (written discussion)—Since percent weight loss is the same as percent volume loss, a comparison might be made this way, if the blocks are the same size at the beginning.

J. E. Miller (author's closure)—We do not attempt to make the wear blocks of a definite thickness, so we do not rely on any dimensional changes as a result of the test. The ability to refinish the same wear block so that additional tests can be run is of great economic value.

K. Metz (written discussion)—Have you seen any significant changes in the Miller or SAR Numbers based on differences in the hardness of the rubber lap?

J. E. Miller (author's closure)—We worried about that in the early tests. While we did not try materials of the same type but of different durometer hardness, we did use other materials such as polyurethane and Buna-N with

greatly different hardness, but no measurable difference could be detected. A series of high-temperature SAR tests (40°C, 66°C) using the ‘standard’ neoprene lap again furnished no evidence that the rubber hardness loss due to temperature affected the results.

Test Methods

A New Flow-Through Slurry Erosion Wear Test

REFERENCE: Madsen, B. W. and Blickensderfer, R., "A New Flow-Through Slurry Erosion Wear Test," *Slurry Erosion: Uses, Applications, and Test Methods, ASTM STP 946*, J. E. Miller and F. E. Schmidt, Jr., Eds., American Society for Testing and Materials, Philadelphia, 1987, pp. 169–184.

ABSTRACT: A new flow-through slurry test developed by the Bureau of Mines significantly reduces abrasive particle degradation and contamination of wear debris in the slurry during the test. Fresh slurry is continuously fed into the test container as used slurry is discharged. Sixteen stationary specimens form the walls of the container in which the slurry is circulated by an impeller. Slurries of silica sand in water can range from 1.3 to 34 weight % solids as the sand flow ranges from 90 to 1600 g/min. An American Foundrymen's Society (AFS) 50/70 mesh test sand was used. Results of tests conducted on a variety of materials showed that the wear rate was constant with time for each material. In contrast, when no fresh slurry was added, as in a conventional slurry pot test, the wear rate decreased significantly as the test proceeded. This decrease is attributed to micropolishing of the surfaces of the abrasive particles. The relative effects of cutting wear and deformation wear during slurry erosion are described.

KEY WORDS: abrasion, accelerated tests, alloy, beneficiation, corrosion, electrochemistry, erosion, mine haulage, slurries, solids flow, steels, wear, wear tests

The Bureau of Mines has been conducting research for reducing the wear of mining and mineral processing equipment. Moving minerals as a slurry is an efficient means of transportation and is done during many mineral processing operations. However, the movement of these slurries can cause significant wear, especially in places where the slurry flow changes direction. Pumps, elbows, tee junctions, valves, flotation cells, and hydrocyclones are component parts of mineral beneficiation systems that are subject to wear. In a slurry, abrasive erosion is produced by the solid particles, and corrosion also may occur from the liquid. Reliable wear data will help engineers to design slurry transport and mineral beneficiation equipment that will last longer.

¹ Metallurgist and supervisory metallurgist, respectively, Albany Research Center, Bureau of Mines, U.S. Department of the Interior, Albany, OR 97321.

Various types of slurry wear tests are reported in the literature and include slurry pot, pipeline, and jet impingement. All of these tests involve the wear condition shown as low-stress, two-body abrasive wear. Many variations of slurry pot tests have been devised. Jackson [1] used a rotating wire, Tsai et al. [2] used two rotating metal tubes, and Bess [3] used a rotating disk as specimens in baffled pots containing abrasive slurries. These slurry pot tests allowed the testing of only one or two specimens at the same time. Postlethwaite et al. [4], Hocke and Wilkinson [5], and Elkholy [6] used closed-loop slurry pipeline test systems. Postlethwaite used rectangular specimens that were flush with the inside wall of the pipeline, and Hocke used rectangular specimens with a slurry jet impingement. These slurry wear tests have the shortcomings of abrasive particle degradation and slurry contamination by wear debris when in a mode that uses recycled slurries. In field slurry systems, a slurry may degrade slightly as it travels, but at any given point in the system the slurry will vary only slightly. A slurry test therefore is needed that provides a consistent slurry feed to simulate field conditions. In such a test, the suspended particles may provide a cutting action when they have irregular surfaces, or they may cause surface deformation when they have a smooth surface, but they must always be consistent. In addition, the galvanic activity or abrasivity caused by wear debris can be minimized by using a short retention time of the particles in the test.

This report presents a new method of flow-through slurry wear testing. The test uses a fresh slurry that is continuously fed to a slurry pot rather than being recycled. Laboratory data are presented that show advantages of the new flow-through test system.

Equipment and Specimens

The slurry test apparatus consists of a slurry pot and equipment to feed the slurry to the pot at a controlled rate. Figure 1 is a photograph of the test apparatus, and Fig. 2 is a schematic. The schematic shows two alternate circuits for the test slurries. One circuit is for flow-through slurry tests, and the other is for recycled-slurry tests.

Flow-Through Slurry Test Equipment

Dry abrasive is fed from a hopper located above a slurry mixer where liquid is added to form the slurry. Silica sand (AFS 50/70 mesh test sand) and city tap water were used in all of these tests. The weight percent solids was adjusted by varying the size of a nozzle at the bottom of the dry abrasive hopper while maintaining a constant liquid flow rate. The slurry was gravity fed from the slurry hopper to a pump and then pumped to the bottom of the slurry pot.

The slurry pot included an impeller that rotated the slurry past specimens located around the inside of the pot. The impingement angle was probably about the same as the 11.5° angle between adjacent specimens. The central region of

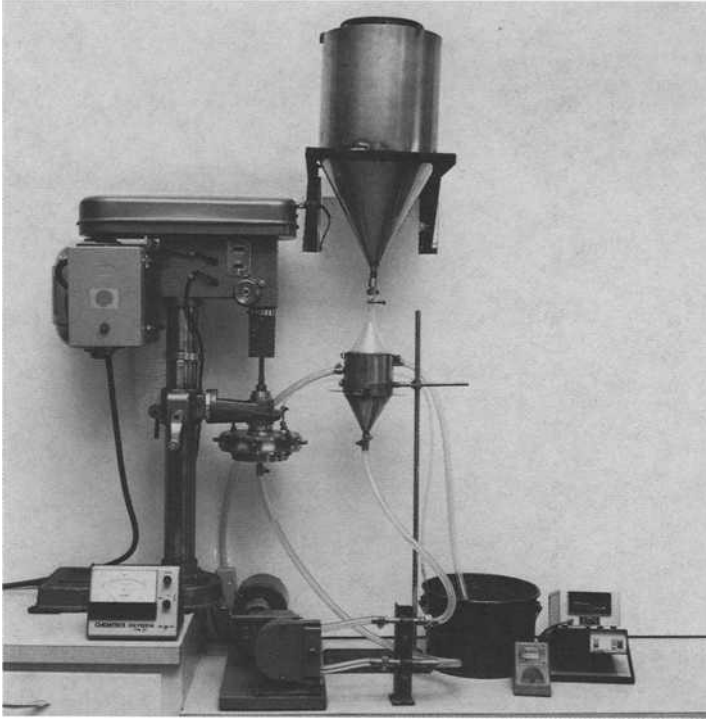


FIG. 1—Slurry wear test apparatus.

the slurry pot was a plastic ring with 16 adjacent flat segments that formed a hexadecagon to hold specimens, as shown in Fig. 3. The distance between opposite sides of the plastic ring was 160 mm. This center section was bolted to stainless steel top and bottom sections that were sealed with O-rings. Ultra-high molecular weight (UHMW) polyethylene inserts were used to protect the stainless steel top and bottom sections from wear. These inserts were periodically replaced if they became too worn.

The impeller was a commercial helical gear made of UHMW polyethylene. The gear was 132 mm outside diameter and 19 mm thick. Its 30 teeth were approximately 5.5 mm deep. The large number of gear teeth moved the slurry past the specimens at a velocity close to that of the tip of the gear teeth. The disassembled slurry pot is shown in Fig. 4. The gear occupied most of the space in the test pot. Consequently, the volume of slurry in the pot was very small, only 150 mL. The 45° helical angle of the gear helped lift particles from the bottom of the pot to the top. Early tests also showed the advantage of UHMW polyethylene for fabrication of the gear to minimize impeller wear during the testing. Geometry changes of the gear due to wear can result in inconsistent data.

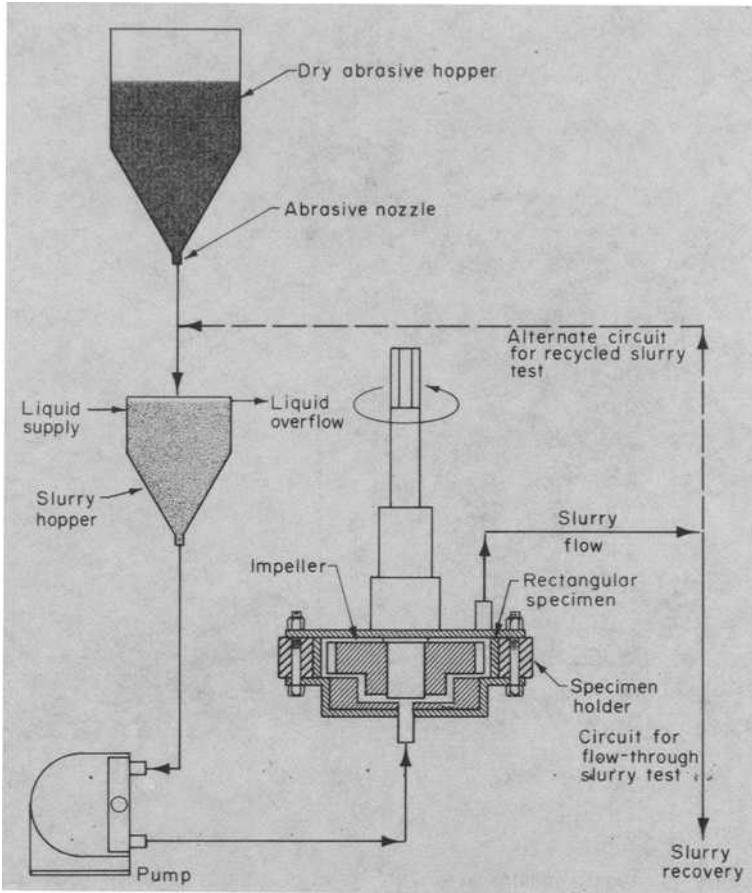


FIG. 2—Schematic of slurry wear test apparatus.

As shown in the overall view of the apparatus (Fig. 1), a modified drill press supported the slurry pot and drove the impeller. A magnetic sensor mounted near the top of the drill press sent pulse signals to an electronic counter that was calibrated to display impeller tip velocity in m/s. The velocity was varied from 1.3 to 21 m/s by changing the belt system of the drill press. The waste slurry was settled so that clear liquid could flow to a drain.

Use of this flow-through system made it possible to maintain a steady-state temperature. A thermocouple was used to monitor the temperature of the slurry before entering and after leaving the slurry pot. Short residence time of the slurry in the pot resulted in a temperature rise of less than 1°C. Also, the pH and oxygen content of the slurry were measured.

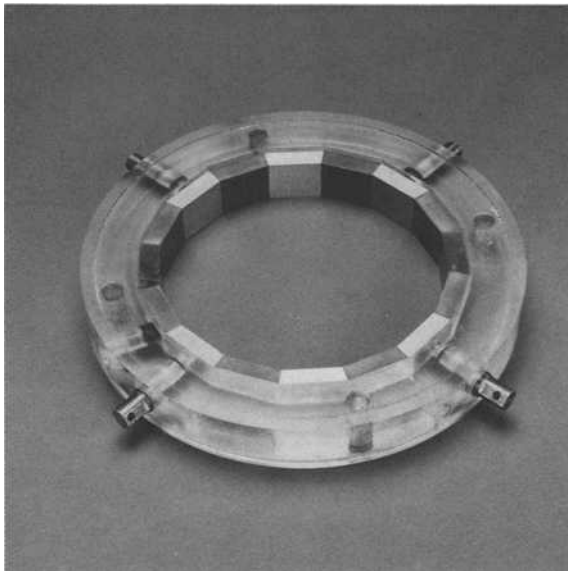


FIG. 3—Center section of slurry pot showing plastic ring and alternating metallic and plastic specimens.

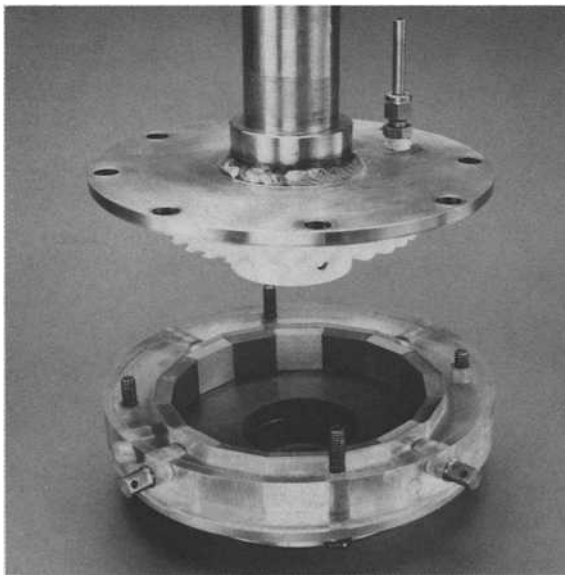


FIG. 4—Slurry pot and impeller.

Test Specimens

Specimens were 24 by 32 by 10 mm thick with the test surface ground and polished through 400 mesh. The ends of the specimens were beveled to fit adjacently inside the plastic ring. To avoid galvanic effects between unlike specimens, eight metal specimens were alternated with eight UHMW polyethylene specimens around the inside of the plastic center section of the slurry pot, shown in Fig. 3. Test results showed that the small geometric changes of the specimens did not affect their wear rates or the rates of the adjacent specimens.

The specimens were reused after regrinding their wear surface. A nonmetallic spacer was placed behind each specimen to maintain a clearance of approximately 1.6 mm between the wear surface and the impeller. To fit inside the plastic ring after regrinding and shimming, an appropriate amount of material was ground from one end of each specimen. The wear-resistant polyethylene specimens were reused several times without remachining. Wear was measured as weight loss, which was converted to volume loss by dividing by the specimen's density. Wear rates are not reported as thickness per unit time because the wear was not uniform over the wear surface, but are reported as total volume loss per unit time.

Recycled-Slurry Test Equipment

The slurry can be recycled to allow basic studies showing the effects of particle degradation, wear debris, and the interaction between cutting and deformation wear mechanisms. No additional equipment was needed to carry out recycled-slurry tests. The discharge from the slurry pot was simply routed back to the slurry hopper, as shown by the dashed line in Fig. 2.

Electrochemical Measurements

The design of the slurry pot, with its fixed specimens, allowed electrochemical measurements to be made simultaneously with slurry abrasion. Specimens served as electrodes. One working electrode and at least two counter electrodes were used to achieve current symmetry. The electrical contacts, visible in Figs. 3 and 4, made contact with the back of the four electrodes. The reference electrode Luggin probe tip, not shown, protruded through one of the polyethylene specimens. The specimens, except for the wear surface and the point of electrical contact, were coated with an electrical insulator. A thin coating of nylon was baked onto the surfaces of the specimens for this purpose. The point of electrical contact between the contact probes and the electrode specimens were insulated from the solution by means of an O-ring seal. Preliminary measurements of the electromotive force of working electrode specimens during slurry wear were conducted. The equipment was thought to be useful for measuring corrosion potential and corrosion current and establishing interactions between erosion and corrosion.

Experimental Procedure

Specimens were prepared for testing by cleaning ultrasonically in water with detergent, rinsing with water and alcohol, air drying, and weighing to the nearest 0.1 mg. The hardness of each specimen was measured with a Rockwell A or Rockwell C hardness tester. All hardness values were converted to the Vickers hardness scale in order to compare all specimens on a common scale. Eight metal specimens were alternated with eight polyethylene specimens inside the plastic center ring, and the pot was assembled. One or more A514 steel specimens were included in each test to serve as standards. Wear was measured as weight loss, which was converted to volume loss by dividing by the specimen's density.

Flow-Through Slurry Test Procedure

The impeller, slurry pump, liquid feed, and abrasive feed were started simultaneously, and the time was noted. The impeller velocity was continuously monitored, and the pH and oxygen content of the slurry input and discharge were measured every 10 to 20 min. After 30 min, the slurry pump and impeller were stopped, and the specimens were removed and reweighed. The specimens were put back into the slurry pot, and this procedure was repeated for a total test time of 2 h.

The apparatus allowed the use of slurries ranging from 1.3 to 34 weight % solids. The tests reported here used 2 weight % solids, which required a flow of 89 g/min of dry sand and a liquid flow rate of 4.34 L/min. With this flow, the average retention time of slurry in the pot was only 2 s.

Recycled-Slurry Test Procedure

With few exceptions, the test procedure for the recycled-slurry system was the same as for the flow-through slurry. The system was filled with water and abrasive prior to the test. No abrasive feed was used, but the slurry temperature was maintained during the test by feeding additional water through the slurry hopper, where it was mixed with recycled slurry. Excess water overflowed to the drain from the outlet near the top of the slurry hopper. A plastic screen ensured that no abrasive particles were carried out the overflow.

Test Results

Over 50 different materials have been evaluated in the slurry pot. The tests reported represent a range of wear rates and demonstrate the difference between the flow-through and recycled-slurry tests.

Flow-Through Slurry Test Results

Using the flow-through slurry test, the wear losses were found to be proportional to the test time for all of the alloys tested. Figure 5 displays results obtained for specimens in a slurry of 2 weight % solids of silica sand and water, an impeller velocity of 15.7 m/s, and a temperature of 16°C. The oxygen content was about 9 ppm (near saturation for this temperature), and the pH was always near 7. The wear losses for each of the specimens closely fit a straight line, as seen in the figure. Thus, wear rates were essentially constant.

Wear rate data were normalized to the wear rate of a standard, Type A514 steel with a Vickers hardness (HV) of 284 [Brinell hardness (HB) 269]. The mean value of the standard wear rate was obtained from several tests conducted with the same nominal operating conditions. Four tests with the standard A514 steel conducted at the operating conditions listed in Fig. 5 resulted in a mean wear rate of 21.1 mm³/h and a standard deviation of 0.96 mm³/h. The wear rate data were normalized according to the equation

$$R = \frac{R_i S_{\text{mean}}}{S_i} \quad (1)$$

where

R = normalized wear rate,

R_i = measured wear rate for test i ,

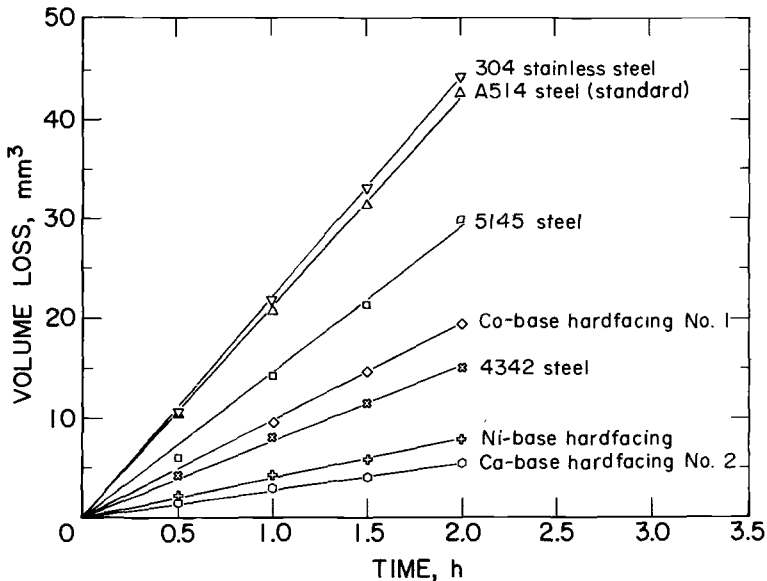


FIG. 5—Slurry wear of seven alloys using the flow-through slurry system. Silica sand in tap water, 16°C, 2 weight % solids, 15.7-m/s impeller speed.

S_{mean} = mean wear rate of standard specimen in all tests under the same conditions, and

S_i = wear rate of standard specimen in test i .

Table 1 presents the normalized wear rates for 17 materials. The materials represented include steel alloys, hard facings, and UHMW polyethylene. The test conditions, hardness, and carbon content are included in the table. The data show a wide range of wear rates among the various materials, differing by a factor of 43. Among the materials, Type 1020 steel had the highest wear rate; the UHMW polyethylene had the lowest wear rate, only 2.5% of that of the standard type, A514 steel. For the metallic specimens these results illustrate the importance of hardness and carbon content for high wear resistance.

Recycled-Slurry Test Results

The wear rates of specimens during recycled slurry testing decreased during the test and therefore differed from those found for the flow-through tests. Figure 6 shows wear data for several specimens when using recycled 2 weight % silica sand in water, an impeller speed of 15.7 m/s, and a temperature of 16°C. Because the wear changed at different rates for different specimens, the relative wear of the specimens changed with time. For example, cobalt-base hard facing No. 1 lost twice as much volume as did 5145 steel after 0.2 h, but

TABLE 1—Flow-through slurry wear rates for several materials. Test conditions: 2 weight % silica sand (50/70 mesh) in tap water, impeller velocity 15.7 m/s, temperature range 6 to 17°C.

Material	Wear Rate, ^a mm ³ /h	Hardness, ^b HV	Carbon, Weight Percent
1020 steel	23.0	130	0.18
304 stainless steel	22.3	157	0.06
A514 steel	21.1	284	0.19
316 stainless steel	18.5	151	0.04
5145 steel	15.6	298	0.61
1080 steel	15.2	172	0.78
8740 steel (heat treated)	14.3	585	0.42
4142 steel (heat treated)	10.2	580	0.30
Cobalt-base facing No. 1	8.91	438	1.33
4342 steel (heat treated)	7.08	690	0.42
1060 steel (heat treated)	6.11	695	0.59
1080 steel (heat treated)	5.27	789	0.78
Nickel-base hard facing	3.61	585	0.56
Cobalt-base hard facing No. 2	2.43	518	1.15
White cast iron (17Cr)	2.17	655	3.00
Cobalt-base hard facing No. 3	1.37	513	1.18
UHMW plastic	0.537 ^c	NA	NA

NOTE: NA = not available.

^a Normalized wear rates.

^b Some specimen hardness values were converted from Rockwell and Brinell scales.

^c Average wear rate of eight specimens.

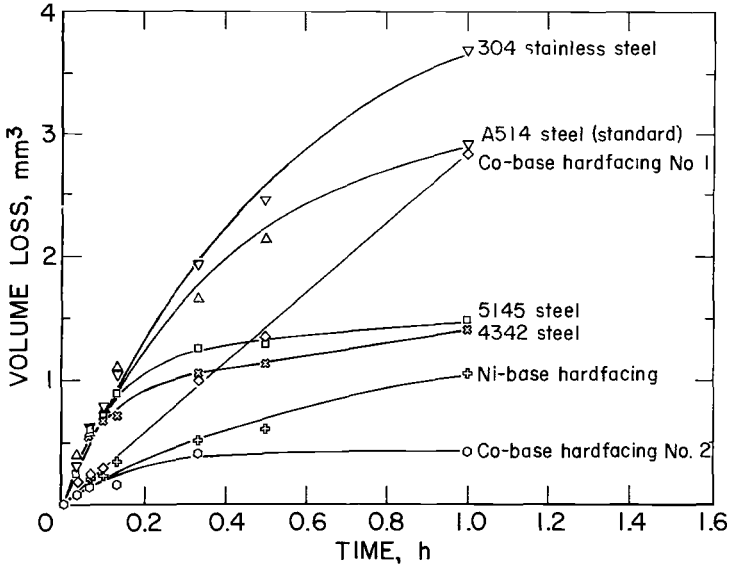


FIG. 6—Slurry wear of seven alloys using the recycled-slurry system. Silica sand in tap water, 16°C, 2 weight % solids, 15.7-m/s impeller speed.

the reverse was true after 1 h. The decrease in wear rate with time is attributed to progressive wear of the abrasive particles.

To obtain data that simulate field conditions, the initial wear rates are needed. The initial wear rates can be approximated roughly by extrapolating the recycled slurry wear curves to zero time and measuring the initial slope of the curve. This extrapolation is inaccurate because the wear rate changes rapidly at the beginning of a test. Tsai et al. [2] recognized this fact and used the first-time point on their volume loss versus time curves. This method gives a ranking very different from that observed in the flow-through test, as can be seen by comparing Figs. 5 and 6. In addition, when absolute wear rates are sought (in order to compare variables such as impeller speed and percent solids), even greater errors can result because the wear rate of the abrasive particles is affected by the test conditions.

To aid in understanding the wear process, a mathematical model was devised to describe the wear kinetics of specimens exposed to recycled slurries. The model consists of two terms: one term describes the cutting wear rate, and the other describes the deformation wear rate. The total wear rate is the sum of the cutting wear rate and the deformation wear rate. Cutting wear involves removal of metal by plowing or chipping by sharp points on the abrasive particles. Deformation wear results from metal fatigue near the surface caused by repeated impacts on the smooth surfaces by abrasive particles, as evidenced by scanning electron microscope (SEM) photographs. The basis for the model is an exponential

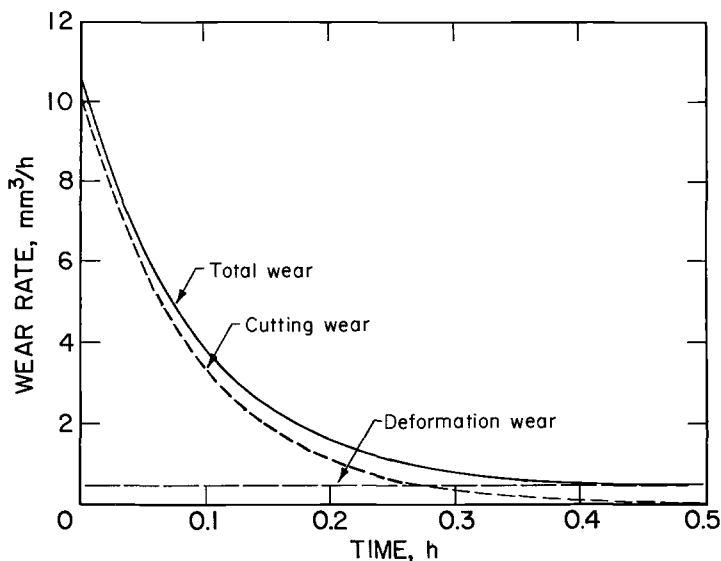


FIG. 7—Relative amount of cutting and deformation wear for 4342 steel as a function of time in recycled slurry test.

decrease in the number of sharp cutting points on the particles with respect to time as the particles are micropolished.

The model was used to calculate constants that describe the wear rates of materials. After the kinetic parameters were obtained, the contributions of cutting and deformation wear were calculated as functions of time. Figure 7 presents calculated curves that show how the cutting and deformation wear rate changed during the test period for the 4342 steel alloy. The amount of cutting wear decreased dramatically as the abrasive particles wore. The size of these particles did not change significantly during testing, but their surfaces became smoother. The deformation wear rate is believed to be proportional to the kinetic energy of the abrasive particles. Because the size and therefore the kinetic energy of the individual particles remained nearly constant, the deformation wear also remained constant, as shown in Fig. 7.

Comparison of Recycled and Flow-Through Tests

The flow-through test gave significantly greater wear than the recycled test. This is clearly shown in Fig. 8 for the standard steel, type A514. The flow-through test resulted in a constant wear rate of 21.1 mm³/h; the recycled test resulted in a decreasing wear rate that approached zero after 1 h even though the specimen hardness was unchanged during the test.

Initially, the wear rates for both tests should be the same. Using the

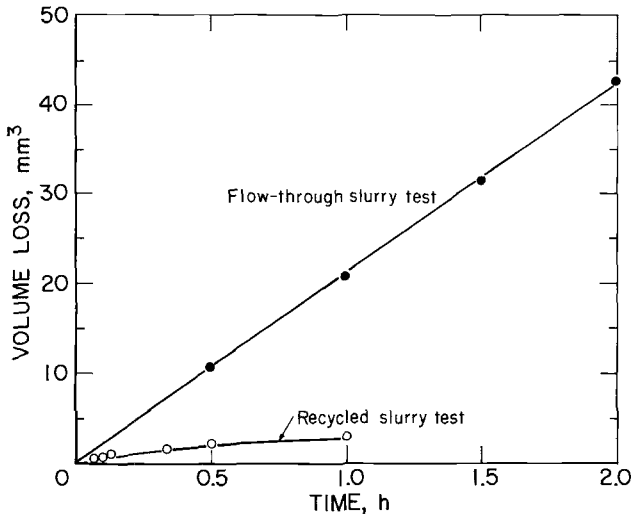
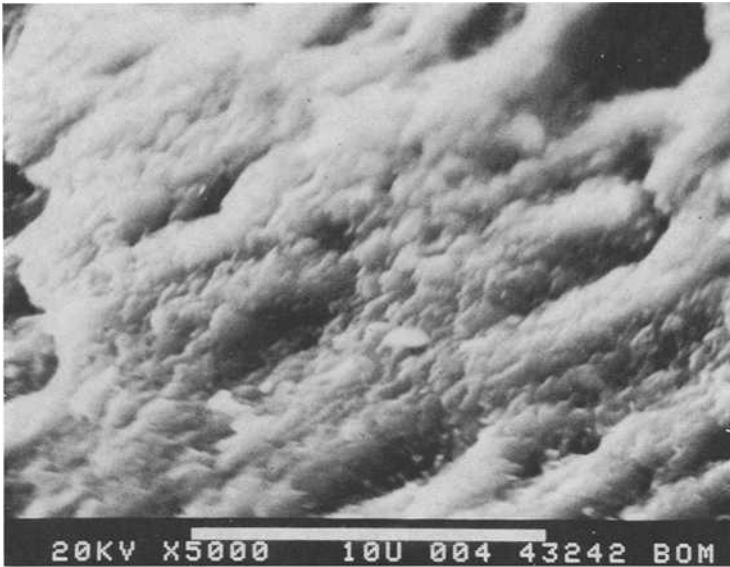


FIG. 8—Comparison of slurry wear for the flow-through and recycled slurry systems. A514 steel, test conditions same as listed in Fig. 5.

mathematical model for the recycled test and setting the time to zero gave an initial wear rate of 8 mm³/h. Because this is only 37.5% of the wear rate measured in the flow-through test, it appears that the extrapolation to zero did not give an accurate wear rate. Obtaining experimental data close to time zero is not practical because of errors in timing and weighing.

An explanation for the difference in the wear rates is shown in Fig. 9 by comparing the surfaces of particles from the flow-through (top) and recycled (bottom) tests. The recycled test lasted 1.67 h. Although no differences in particle size and shape were observed at $\times 100$, the photographs at $\times 5000$ show a great difference between particle surfaces. The particle from the flow-through test had many sharp points that were less than 1 μm , but the recycled particle had been micropolished and was quite smooth. The smooth silica sand particles caused a much lower wear rate than when the fresh abrasives wore the specimen surface. In addition, the smooth specimen surface is responsible for some of the reduction of the wear rates during recycled tests. The size of the sharp points on the flow-through slurry particle was consistent with the size of grooves found on the surfaces of worn specimens.

Figure 10 shows the wear surfaces of A514 steel specimens that resulted from the two types of tests. A specimen exposed for 1 h in the flow-through test, as seen in the photograph on the top, had many fine grooves over the entire surface. This is typical of cutting wear. The photograph at the bottom shows a specimen exposed for 1.67 h in a recycled slurry test. The relatively smooth surface, the development of a wave pattern, and the development of flakes indicated a deformation wear mechanism.

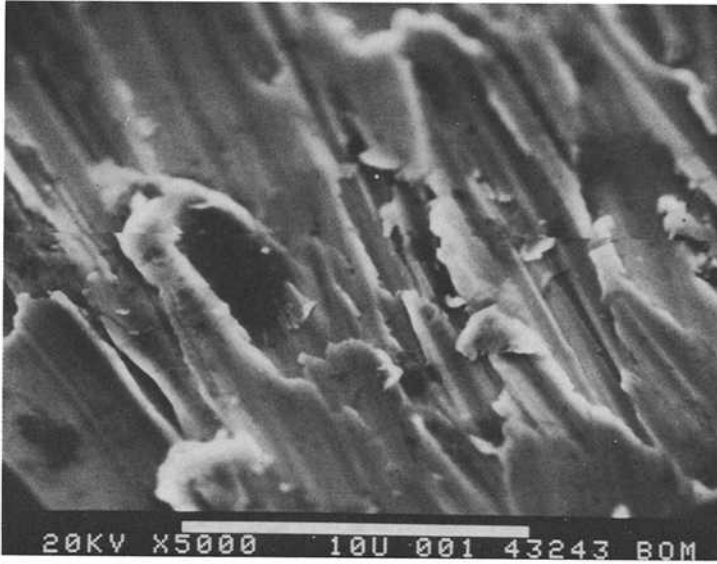


SAND-FLOW THROUGH

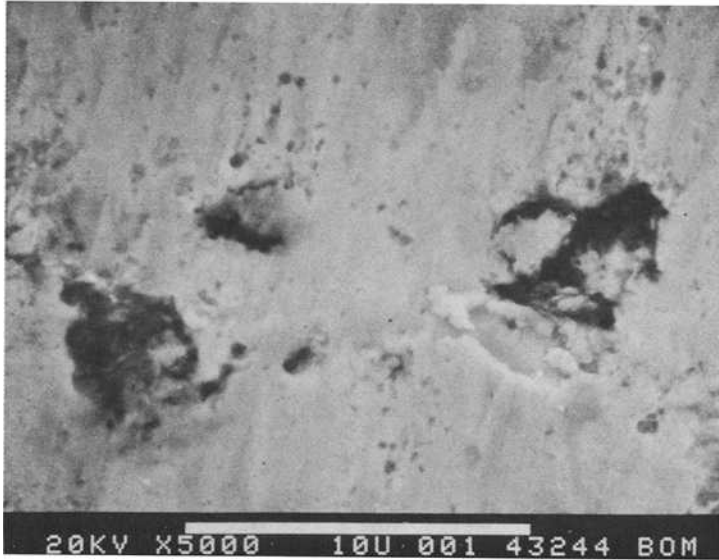


SAND-RECYCLED 100 MIN

FIG. 9—Comparison of abrasive particles used in the flow-through (top) and recycled (bottom) slurry tests. Magnification $\times 5000$ (reduced 15% for reproduction). Duration of the recycled test was 1.67 h. Test conditions were the same as listed in Fig. 5.



A514 STEEL-FLOW THROUGH



A514 STEEL-100 MIN RECYCLE

FIG. 10—Comparison of wear surfaces for A514 steel specimens worn in flow-through (top) and recycled (bottom) slurry tests for 1 h and 1.67 h, respectively. Magnification $\times 5000$ (reduced 15% for reproduction). Test conditions same as listed in Fig. 5.

Conclusions

A slurry wear test apparatus was devised and evaluated. The equipment described can be used to test 16 specimens at once using either a flow-through or recycled slurry. The flow-through slurry test produced a constant wear rate over a period of time as a result of the continuous cutting wear produced by a fresh supply of abrasive particles. In the recycled-slurry test mode, the wear rate decreased markedly with time because of micropolishing of the irregular surfaces on the abrasive particles. After the particle surfaces became smooth, only deformation wear occurred. Most wear tests are present use recycled slurries. The constant wear rate provided by the new flow-through slurry test simulates field conditions wherein a given component is exposed to a relatively consistent slurry.

References

- [1] Jackson, L. D. A., "Controlling Abrasion in Slo Slurry Pipeline Systems," *Canadian Mining Journal*, Vol. 95, 1974, p. 42.
- [2] Tsai, W., Humphrey, J. A. C., Cornet, I., and Levy, A. V., "Experimental Measurement of Accelerated Erosion in a Slurry Pot Tester," *Wear*, Vol. 68, 1981, pp. 289-303.
- [3] Bess, M. L., "Erosion-Corrosion of Cast Pump Alloys," presented at Pacific NW Met. and Miner. Conference, Seattle, WA, 6 May 1977; available from BuMines, Albany Research Center, P.O. Box 70, Albany, OR 97321.
- [4] Postlethwaite, J., Brady, B. J., Hawrylak, M. W., and Tinker, E. B., "Effects of Corrosion on the Wear Patterns in Horizontal Slurry Pipelines," *Corrosion-NACE*, Vol. 34, No. 7, National Association of Corrosion Engineers, Houston, TX, 1978, pp. 245-250.
- [5] Hocke, H. and Wilkinson, H. N., "Testing Abrasion Resistance of Slurry Pipeline Materials," *Tribology International*, Oct. 1978, pp. 289-294.
- [6] Elkholy, A., "Prediction of Abrasion Wear for Slurry Pump Materials," *Wear*, Vol. 84, 1983, pp. 39-49.

DISCUSSION

B. S. Phull (written discussion)—You mentioned the use of an oxygen meter in your test. Could you describe what type of oxygen meter this was? If it is a dissolved oxygen type, using a teflon membrane on the sensor, did you not have any wearing out problems of the membrane?

B. W. Madsen and R. Blickensderfer (authors' closure)—I used a Horizon Ecology dissolved oxygen meter, No. 5946-10. The membrane on the sensor is very delicate and would be ruined in seconds if exposed to a fast-moving slurry. However, in my tests, I placed it in the slurry hopper where dry sand is mixed with incoming water. The slurry is not moving in this hopper except for the slow feed rate out of its bottom. The probe is to one side of this hopper and does not come in contact with the abrasive particles. Therefore the membrane does not wear out, but is changed periodically as in ordinary use.

¹ Laque Center for Corrosion Technology, Inc., Wrightsville Beach, NC.

Test Approach for Dense Slurry Erosion

REFERENCE: Roco, M. C., Nair, P., and Addie, G. R., "Test Approach for Dense Slurry Erosion," *Slurry Erosion: Uses, Applications, and Test Methods, ASTM STP 940*, J. E. Miller and F. E. Schmidt, Jr., Eds., American Society for Testing and Materials, Philadelphia, 1987, pp. 185–210.

ABSTRACT: The paper presents two test devices to simulate erosion wear by friction and by impact in dense slurry flow. The empirical coefficients determined experimentally are introduced in a predictive model, which numerically simulates the wear by directional impact of solid particles, random impact, and coulombic friction. The last two components are specific for high concentrated slurries ($C \geq 5$ to 10% by volume).

The device for erosion by friction has a moving frame with a fast oscillating motion in a horizontal plane. The layer of abrasive particles slides on the bottom side, where the exposed specimens are located. Tests performed with alumina and sand particles are discussed.

The directional and random impacts are both simulated on an inclined wall, which divides into two parts a confined jet of suspension. The experimental results are illustrated for four worn materials under the impingement of a sand-water slurry stream.

The equivalence between the energy dissipated by particles-wall interactions and erosion intensity gives a unified way to determine all erosion components. The suggested test devices provide the coefficients of proportionality. The approach can be used for the dense slurry flows usually encountered in industrial applications, for various flow regimes and wall geometries.

KEY WORDS: erosion wear, slurry flow, wear by friction, particle impingement, equipment handling slurries, erosion test apparatus, energy approach

Nomenclature

- a* Acceleration
- C* Solid concentration by volume
- $d_{50\%}$ Solid particle size (50% by weight)
- D* Pipe diameter

¹ Professor and research assistant, respectively, Department of Mechanical Engineering, University of Kentucky, Lexington, KY 40506-0046.

² Professional engineer, Georgia Iron Works Industries, Inc., 5000 Wrightsboro Road, Grovetown, GA 30813.

I_{tg}, I_n, I_{fr}	Interaction work of solid particles on the wearing wall, caused by tangent and normal components of solid velocity and friction, respectively
\vec{F}	Force vector
F_{DS+SL}	Force vector due to particle interactions by collisions (dispersive stress) and coulombic contacts (supported load)
h	Height of particle sliding bed
m	Parameter in the mixture velocity equation
N	Rotational speed
Q	Flowrate
R_1, r_w	Interior radius and peripheral wall radius of the pump casing, respectively
Δs	Loss in thickness by erosion wear
$\Delta \dot{s}$	Time rate of erosion
$\Delta \dot{s}_{av}$	Erosion rate averaged on the peripheral part of the casing radial cross section
$\Delta \dot{s}_{fr}$	Erosion rate caused by friction
$\Delta \dot{s}_v$	Erosion rate caused by directional impact
$\Delta \dot{s}_r$	Erosion rate caused by random impingement
t	Time
$\tan \theta, \tan \beta$	Coefficients of dynamic friction by particle collisions and coulombic contact, respectively
V	Mixture velocity
$V_S, V_{S\alpha}$	Solid velocity at the wall
V_{tg}	Tangential velocity at the wall
$\phi_{fr}, \phi_v, \phi_r$	Specific erosion rate per unit of energy dissipated by friction, directional and random impact, respectively
$\phi_k(\alpha), \phi_{k0}, \phi_{k90}$	Specific erosion rate per unit of kinetic energy dissipated when the impingement angle is α , $\alpha = 0$, and $\alpha = 90^\circ$, respectively
σ_{SL}, τ_{SL}	Normal and shear stress due to "supported load" (stress transmitted through coulombic contact), respectively
σ_{DS}, τ_{DS}	Normal and shear stress due to "dispersive stress" (stress transmitted through particle collisions and lubrication), respectively
$\sigma_k(\alpha)$	Normal stress caused by solid particle impingement in the α direction
ψ_1, ψ_2	Stream function for the through flow and unit vortex in the pump casing, respectively
α	Impact angle (degree)
κ	Coefficient showing the ratio of particles which cannot be maintained in suspension by turbulence

The directional impact erosion in dilute slurry flows is caused by the mean convective velocity of solid particles relative to the boundary walls. The particle/particle interaction stresses in dense slurry flows determine two supplementary

wear components. They are caused by the random impingement of particles from the sheared suspension layers close to the wall and the friction of sliding particles in coulombic contact pressing onto the wall. All three erosion components can be correlated respectively to the following stresses in the two-phase flow: (1) the directional dynamic pressure due to solids; (2) the dispersive stress in sheared suspensions; and (3) the supported load stress. The equivalence between the energy dissipated by particles/wall mechanical interaction and wear intensity gives a unitary way to determine all erosion components. Two new test devices are suggested to determine the coefficients of proportionality. The wear mechanism caused by the solid particles strangled between two neighboring walls in relative motion is neglected in the present analysis.

The erosion wear produced in the equipment handling slurries has been the object of numerous studies, especially for aspects of practical interest [1-4]. The wear process is a complex phenomenon depending on many variables, several of which are interdependent. The two-phase flow pattern plays a determinant role in this process. Experimental correlations are frequently used to estimate erosion wear. For instance, the amount of material removed by a jet impinging on a plate is related to the solid particle velocity, concentration, particle size, density, abrasiveness, and angle of impingement [1,5,6]. A more general analysis can be made relating the wear intensity to the energy of interaction between the solid particles and exposed walls [2,7].

The erosive wear in industrial equipment is usually a combination of various wear mechanisms, which depend on the local solid velocity and impact angle, concentration, dimension, and shape of particles. It appears appropriate to experimentally analyze the effects of various mechanisms one by one, then to estimate their contributions at each location from the flow predictions, and to find the global wear rate by summing the effects of all the components. The superposition of various effects is a simplifying computational approximation, which works better when a wear mechanism is predominant.

The first test apparatus discussed in this paper simulates only the wear by friction caused by a sliding layer of particles.

The directional and random impacts are both simulated on an inclined wall probe (with variable angle of inclination) introduced in a confined jet of suspension of constant cross section.

The wear predictions were compared to experiments on centrifugal pump components. The wear measurements using a "superficial layer thickness" approach are presented in this paper.

For applications, (1) one determines the distributions of the directional solid velocity, dispersive stress, and supported load from the flow computation in the vicinity of the worn wall; then, (2) the energy approach is employed with the experimental coefficients of proportionality to predict the total wear distribution.

This work is a continuation of our previous studies to determine the flow structure and wear in equipment handling slurries [8-10].

Erosion Wear Patterns in Dense Slurry Flow

The solid particles in two-phase flows may be in turbulent suspension or supported by coulombic contacts on other particles or on the boundary wall. The particles will interact with the wall when either their mean flow convective velocity is directed toward the wall, fluctuating solid velocities are generated by the flow mechanisms in the wall vicinity, or deposited particles move—pressing along the wall. The solid particle convective velocity plays an important role, especially in dilute flow with large particles (when the hindered solid/liquid relative velocity is larger than the turbulent friction velocity). The particle fluctuating velocities in the vicinity of the boundary solid walls are generated by the turbulence within the carrier liquid and by the interparticle collisions particularly at high concentrations ($C > 5$ to 10% by volume) and large shear stresses.

The erosion wear occurs when the local stresses exceed the yield stresses, via ductile or brittle failure or their combination. The mechanisms of material removal depend on the pair of materials involved (particles/wall), as well as on the two-phase flow pattern. We consider that the erosion wear process in dense slurry flow has three components (Fig. 1), caused by: (a) the directional impingement of solid particles; (b) the random impingement of particles in turbulent motion, and (c) the friction of a sliding bed pressing onto the wall [10]. These components are respectively related to the specific stresses acting in dense slurry flows: (a) dynamic pressure of solid phase (σ_k), (b) dispersive stress (σ_{DS}), and (c) supported load (σ_{SL}). The specific normal stresses in dense slurry flow (σ_{DS} and σ_{SL}) were discussed in Ref 9. The first objective is to find correlations between the wear intensity and the energy dissipated in these three cases.

Besides the erosion wear, the equipment handling slurries may also be subject to corrosion, cavitation, and scaling. Corrosion and cavitation accelerate the erosive wear. Scaling such as calcium carbonates generally protects the worn surfaces, but may also accelerate local wear due to the flow recirculations. In our experiments used for model development, the effect of corrosion was practically eliminated by using two plastic wearing materials, polyamide resin

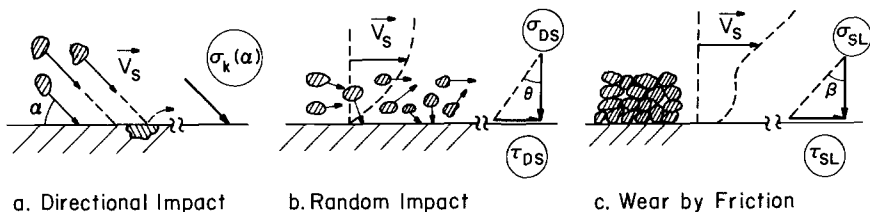


FIG. 1—Wear patterns caused by slurry flow.

and epoxy resin. The small-scale experiments and the full-scale centrifugal pumps were operated at flow rates and pressures at which cavitation did not occur. No scaling was observed in the experiments.

The proposed predictive approach combines computational and experimental steps to incorporate the effects of the two-phase flow pattern, particle/wall interaction mechanisms, and material characteristics. The general succession of these steps is suggested by Fig. 2. First, the small-scale experiments provide the empirical coefficients for the three types of wear for any pair of materials (solid particles and exposed wall). Then, the flow indices, interaction energy between particles and wall, and wear rate distribution are numerically estimated. A preliminary test of the model is performed for a quasi-two-dimensional channel, when necessary. The approach can be applied to various flow situations encountered in applications, such as pumps, valves, and pipes.

The analysis at particle scale (combining the stochastic investigation of particle impingements onto the wall with the local fatigue/plastic deformation prediction of the worn wall for individual impact events) may replace the small-scale experiments when the particle dynamics will be better understood and mathematically formulated.

Wear by Sliding Bed (By Friction)

The solid particles which cannot be maintained in suspension by the hydrodynamical forces slide or rest on the solid boundary wall, transmitting a normal stress (σ_{SL}). The sliding bed of particles can be observed, for instance, at the bottom region of circular pipes, on the exterior wall of the pipe elbows, in centrifuges, or in the pump casings [10-12].

To simulate the erosion by friction we have proposed an oscillatory device in which the particles slide and rotate on the exposed surfaces similar to the

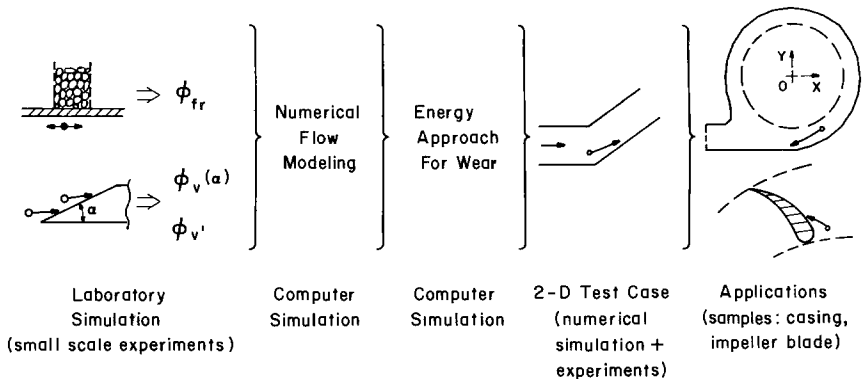


FIG. 2—Steps of the predictive approach.

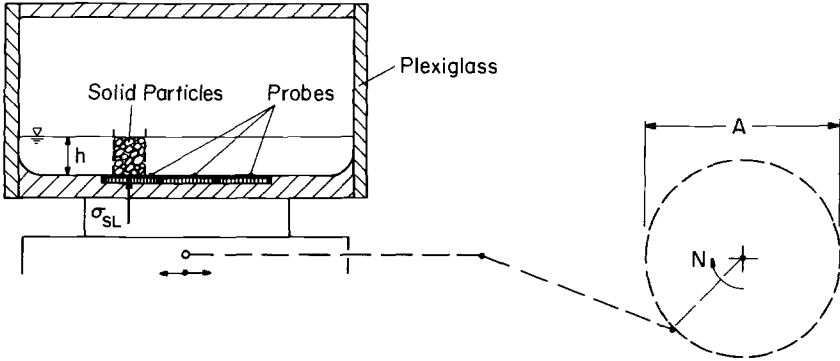


FIG. 3—Testing device for wear by sliding solid particles.

motion encountered in application situations. The moving frame has a flat oscillatory motion in such a way that the “bed of particles” slides on the bottom side, where the specimens or probes (exposed surfaces) are located (Fig. 3). The motion is in the horizontal plane. The relative weight of particles in fluid is transmitted toward the bottom by a normal stress (supported load stress, $\sigma_{SL} = (\rho_S/\rho_F - 1) C h$, where C is the solid concentration in the particulate bed, $\rho_S =$ solid density, $\rho_F =$ fluid density, and h is the bed height). The fluid may be any carrier liquid (usually water) or gas (usually air). The particulate material may be replaced periodically with a batch system, or continuously with a flow-through system. The amplitude (A) and frequency (N) of the oscillations may be varied within a large range. Various specimens of wearing materials may be tested in parallel for the same particulate system.

Results obtained with the frequency $N = 505$ rpm and amplitude $A = 50.8$ mm are illustrated in Figs. 4 and 5. The first test (Fig. 4) was run with a mixture of water and sand particles $d_{50\%} = 0.27$ mm. The three plate samples were covered with a thin layer of polyamide resin ($s \approx 30$ μm). The supported load is $\sigma_{SL} = 135$ N/m². The reduction in thickness of the resin coating was measured in this case with a micrometer. For more complex geometries, another method described later in this paper had to be used. The curve given in Fig. 4 averages the measurements made on three specimens. It illustrates the decrease of the erosion rate in time due to the particle attrition ($\Delta\dot{s}_{SL} = \tan \theta$ diminishes in time). The erosion rate ($\Delta\dot{s}_{SL}$) for further calculations with new sand is equal to $\tan \theta_o$ (θ_o measures the inclination of the tangent to the curve at origin, Fig. 4).

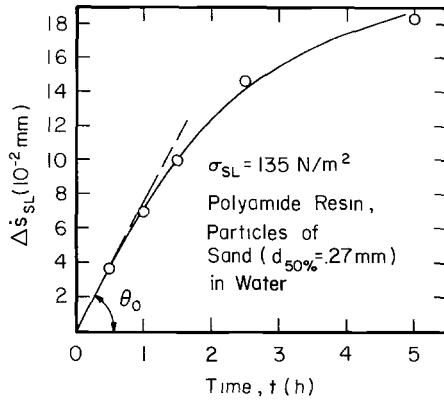


FIG. 4—Experimental results for wear by friction: sand particles on polyamide resin.

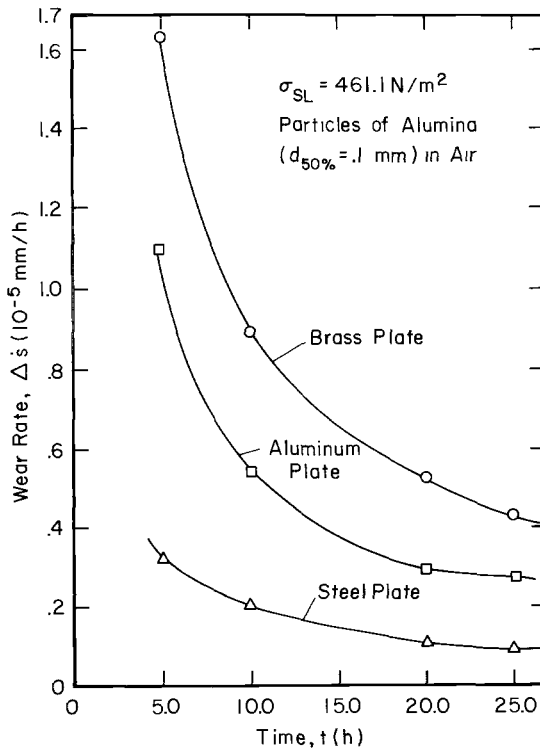


FIG. 5—Experimental results for wear by friction: alumina particles on plates of various materials.

We define a specific erosion per unit of energy dissipated ϕ_{fr}

$$\phi_{fr} = \frac{\Delta \dot{s}_{SL}}{(\tau_{SL} - \tau_{SL_o}) \cdot V_{tg}} \quad (1)$$

where

$\Delta \dot{s}_{SL}$ = loss in thickness per unit time,

τ_{SL} = shear stress at the specimen surface due to the supported load,

τ_{SL_o} = threshold value for incipient wear, and

V_{tg} = tangential displacement of solid particles in unit time.

The shear stress τ_{SL} is determined from the normal stress σ_{SL} and a coefficient of dynamic friction $\tan \beta \approx 0.3$, $\tau_{SL} = \sigma_{SL} \cdot \tan \beta$. The supported load stress σ_{SL} is generally estimated from the flow conditions [9,10].

In Fig. 5 are shown some results obtained with alumina particles ($d_{50\%} = 0.1$ mm) in air. The exposed surfaces were made of three different materials (brass, aluminum, steel). The decrease of the wear rate ($\Delta \dot{s}_{SL}$) in time (t) is due to the particle attrition ($\Delta \dot{s}_{SL}$ is proportional to $t^{-0.33}$).

Erosion on an Inclined Wall

Since the directional and random impact (see Fig. 1, *a* and *b*) are difficult to separate, we simulate both components on the same apparatus. Figure 6 shows the scheme of the impact specimen, with an inclined surface at angle α compared to the mean flow of the slurry stream (V). The specimen is introduced into a confined stream of constant cross section. A two-dimensional computational model can be used in this case. The two-dimensional assumption was verified from the erosion wear distributions. When the angle α is zero, only the random impact of particles in turbulent motion occurs. This effect is important at high concentrations and high shear stresses. The collisions between solid particles cause the so-called "dispersive stress" α_{DS} [9]. A scheme of the measuring positions on the specimen is given in Fig. 6. There are 25 measuring points, five on each row at the same distance from the specimen's leading edge. The rows and columns are equally spaced at 6.35 mm. The mixture velocity was maintained constant in the tests reported here ($V = 9$ m/s), at a value close to that encountered in the pump components. The concentration of water/sand ($d = 0.27$ mm) mixture was about 6% by volume. Each test lasts about 8 min.

The setup (2-D inclined wall in confined stream of suspension) provides reliable data for wear measurements, suitable for comparisons to the numerical predictions. For our objectives, it has some advantages compared to the commonly used, particle-laden free jet test. For any free jet angle, there is a spectrum of effective impact angles of individual particles, which is difficult to determine and to relate to the local wear distribution, particularly in inclined jets ($\alpha \neq$

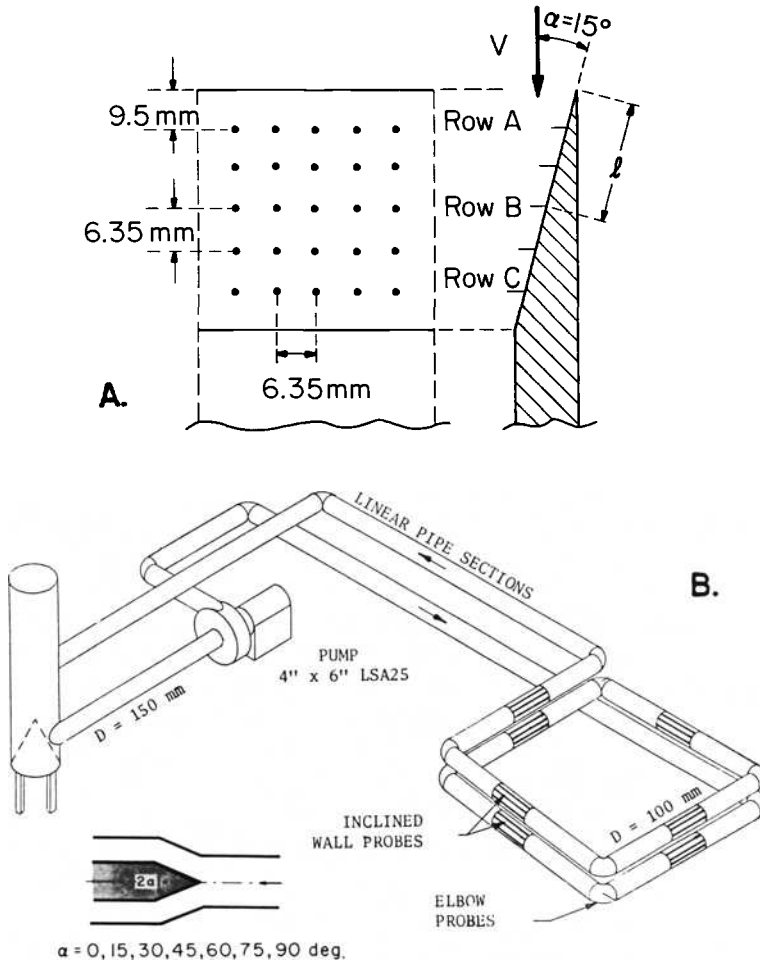


FIG. 6—Inclined wall specimen: (A) Measuring positions; (B) The hydraulic loop for inclined wall probe.

90°). Furthermore, the jet is not confined, and the mixing with the surrounding fluid causes supplementary computational problems.

The location of the measuring positions on the inclined wall probe is correlated to the flow computational mesh, where the velocity, impact angle, concentration, and wear are calculated (Fig. 11a).

The directional impact varies with the distance from the leading edge of the specimen (with l shown in Fig. 6). The absolute value and the orientation of the velocity vector change with l . This variation is reflected in the shape of the

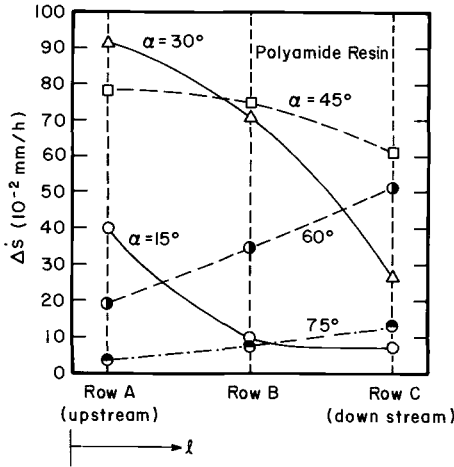


FIG. 7—Experimental wear rate on the inclined wall probe: $\Delta \dot{s}(\ell)$ for various α .

curves erosion rate ($\Delta \dot{s}$) versus attach angle (α) for various rows of the measuring positions (Fig. 7). Numerical simulation of the flow (see the paragraph on applications) can explain the curve alteration. In further calculations of local erosion, we will employ the curve for the row located upstream (that is, Row A, in Fig. 7).

The wear rate distribution $\Delta \dot{s}$ on the inclined wall at rows A, B, and C for plate inclination α is illustrated in Fig. 8.

Figure 9 shows the average erosion rate on plates covered by polyamide

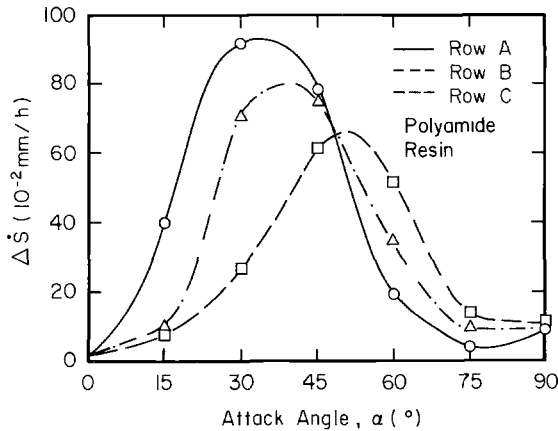


FIG. 8—Experimental wear rate $\Delta \dot{s}(\alpha)$ for various ℓ .

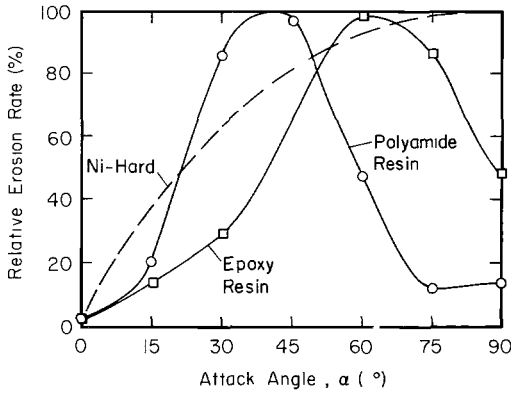


FIG. 9—Experimental wear rate averaged on the inclined probe.

resin, epoxy resin, and of Ni-hard. Relative units are used for erosion rate ($\Delta\dot{s}(\alpha)/\Delta\dot{s}_{max}$).

An energy approach is considered in order to interpret and extrapolate the results. The specific erosion rates per unit dissipated energy by particle/wall mechanical interaction for the directional impact (corresponding to the mean flow, ϕ_v) and random impact (corresponding to the turbulent kinetic energy $\phi_{v'}$) are

$$\phi_v(\alpha) = \Delta\dot{s}_v/[2 \cdot \sigma_k(\alpha) \cdot V_{s,\alpha}^n - k_o] \tag{2}$$

$$\phi_{v'} = \Delta\dot{s}_{v'}/[V_{s,tg}(\tau_{DS} - \tau_{DS_o})] \tag{3}$$

where

- k_o, τ_{DS_o} = threshold indices,
- $V_{s,\alpha}, V_{s,tg}$ = solid velocity with angle α and tangential to the wall, respectively,
- τ_{DS} = dispersive stress [9],
- $\sigma_k(\alpha) = C \frac{\rho_s V_{s,\alpha}^2}{2}$,
- C = solid concentration by volume, and
- $n \approx 1$, experimental coefficient.

The total erosion rate on the impact specimen is

$$\Delta\dot{s}_k = \Delta\dot{s}_v + \Delta\dot{s}_{v'} \tag{4}$$

where $\Delta\dot{s}_k$ defines the time rate of the erosion wear caused by the total kinetic energy of solid particles (k) hitting the exposed wall. A global coefficient $\phi_k(\alpha)$ may also be defined for a given impact angle α

$$\phi_k(\alpha) \approx (\Delta\dot{s}_v + \Delta\dot{s}_{v'})/[\rho_s C V_{s,\alpha}^{2+n} - k_o(\alpha)] \tag{5}$$

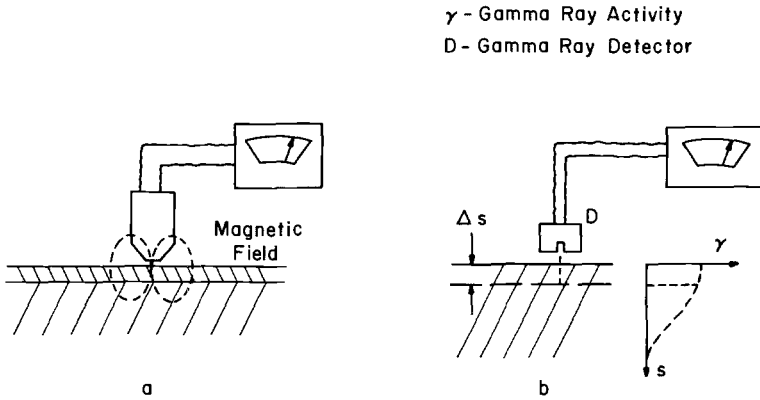


FIG. 10—Measuring techniques for wear distributions: (a) coating thickness approach; (b) with radionuclides.

where

$\phi_k(\alpha)$ = specific loss in thickness by erosion per unit kinetic energy of particles, dissipated by directional and random impingement, and
 $k_o(\alpha)$ = threshold kinetic energy for incipient wear.

Measuring Wear Distribution

The techniques usually applied to measure erosion wear (loss in weight, micrometer measurements, etc.) have some limitations when accurate wear distributions on complex geometries (for instance, on pump components) are required. In our experiments we focused on some new measuring techniques which have in common the following principle: on the wearing surface a thin layer of tested material is applied (for instance, a plastic resin, rubber, etc.) or a thin layer of the original material is marked (for instance, radioactivated), and by measuring the reduction in thickness of this layer one can determine the wear distribution. Two “superficial layer thickness” techniques were adopted for laboratory and in situ measurements (scheme in Fig. 10).

For the dielectric coatings employed in our tests (polyamide resin and epoxy resin), the thickness is determined from the intensification of the localized magnetic field of a magnet as it closely approaches the surface of the lined metallic materials. The coating thickness gage has a precision of about $\pm 2 \mu\text{m}$ in these tests.

The surface layer activation technique is employed for measuring the wear of the original metallic material. A small amount of radionuclides is induced on the surface of the wearing material (Fig. 10b, [13]). The decrease in radioactive (for example, gamma ray) intensity after the correction for natural

decay half-time is a measure of the wear. The precision is about 1% decrease in radioactive activity.

The suggested measuring techniques can be used for complex geometries (as the pumps and valve surface exhibit); the wear distribution on a chosen surface can be obtained in a short period of time (about 1 h) before the surface alters its shape (as it usually happens in the "loss of weight" approach); and the accuracy of measurement is good (2 μm in our tests). The "superficial layer thickness" techniques just discussed are more reliable and versatile as compared to the "whole thickness" and other measurements commonly applied when the wearing wall has two parallel surfaces (for instance, the radiometric and ultrasonic measurements of a pipe wall).

Numerical Analysis and Applications

Flow Modeling

Numerical flow simulation provides the distributions of the solid velocity, concentration, and impact angle at the wearing walls. With these parameters one can obtain the interaction energy between particles and walls (that is, the solid-phase stresses $\sigma_k(\alpha)$, τ_{DS} , τ_{SL} and solid velocity V_S , Fig. 1) and then the wear intensity.

The successive steps in the general algorithm are:

1. Calculate the mixture velocity, V , from the momentum equations.
2. Obtain the solid particle velocity, V_S , from the dynamic equilibrium of a cloud of particles in the flow field by using Eulerian or Lagrangian descriptions.
3. Determine the concentration distribution, C , by solving the corresponding governing equation, including the effects of convection, diffusion, and phase interactions.
4. Calculate the supported load and other solid phase stresses at the wearing walls.
5. Apply the energy approach to correlate the flow indices to erosion wear, assuming the superposition of the erosion by directional impact, random impingement, and friction ($\Delta\dot{s} = \Delta\dot{s}_v + \Delta\dot{s}_v' + \Delta\dot{s}_f$).

The model assumptions and numerical techniques are chosen as a function of the flow complexity and available test data. For multispecies particulate flow in pipelines, the volume-averaging techniques and one-equation turbulence modeling (eddy-diffusivity or kinetic energy model) [14,15] give a complete solution of the required solid stresses. For more complex geometries, physical simplifications and numerical approximations of the governing equations acceptable for each flow situation are adopted. For instance, the mixture velocity computation in the centrifugal pump components is often performed using the inviscid flow assumption (that is, the inertial forces are assumed predominant)

or considering constant turbulence indices in some pump areas (that is, the turbulence length scale is of the same order of magnitude within the corresponding flow area). Specific numerical approximations are the quasi-three-dimensional models in impellers [16] or casings [17].

A sample of the basic equations used for centrifugal pump casing computation are given in the Appendix. The finite-element method (FEM) was used with linear or quadratic up-wind interpolations for 2-D numerical solutions (see Fig. 11). Finite-volume techniques proved to be more economical and versatile for three-dimensional geometries [18]. The Eulerian description of solid particle motion is recommended versus Lagrangian description for dense slurry flows in which the relaxation time of solids is relatively small. The tracking approach may be considered in computation for dilute particulate systems [19].

Experimental

The development of the suggested approach for dense slurry erosion involved three kinds of experiments: (1) small-scale laboratory tests for empirical coefficients (Fig. 12 shows the test ring for inclined wall specimen); (2) flow and wear measurements on pumps and other equipment at full scale in laboratory (Figs. 13–15); and (3) operation performance measurements and pilot tests in industrial conditions (Fig. 16). Only the small-scale experiments will be required for the predictive approach in further wear calculations. The full-scale measurements in the laboratory provide reliable data for model testing and scale-up capabilities.

Partial views of the laboratory facility for centrifugal slurry pumps and slurry pipelines are given in Figs. 12–15.

Some Results for Pumps

We illustrate in Figs. 17 and 18 the application of the approach for two materials on the same pump (LSA 32/25, annular casing) in comparison to the experimental results.

The effect of the pump flow rate on erosion wear distribution on a larger pump casing is presented in Fig. 19. The wear profile is also very sensitive to the particle size and pump rotational speed.

The application of the model for industrial conditions gives a way to select the most suitable pumps for given applications, as well as to modify some casing dimensions (tongue dimension, casing width, etc.) to reduce the areas and the intensity of maximum wear. Comparisons between measurements performed in industrial units and model predictions were presented by Roco et al. [20].

The flow pattern explains the location of maximum wear for various flowrates, solid particulate materials, and concentrations in the tested equipment (pumps, pipes, joints). The difference between the wear distributions in a circular slurry

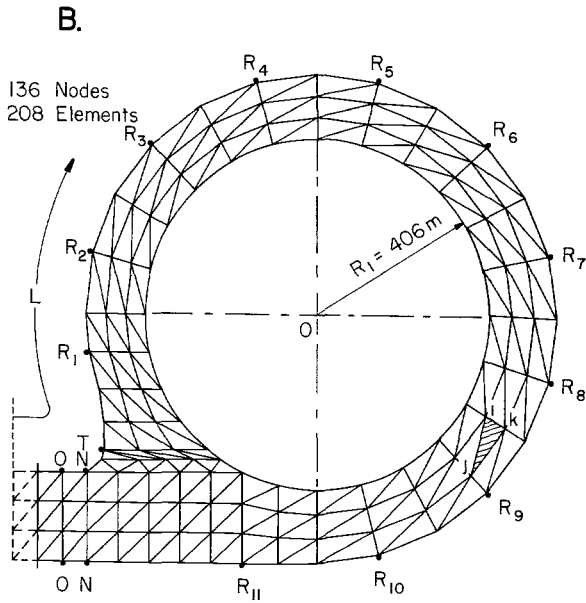
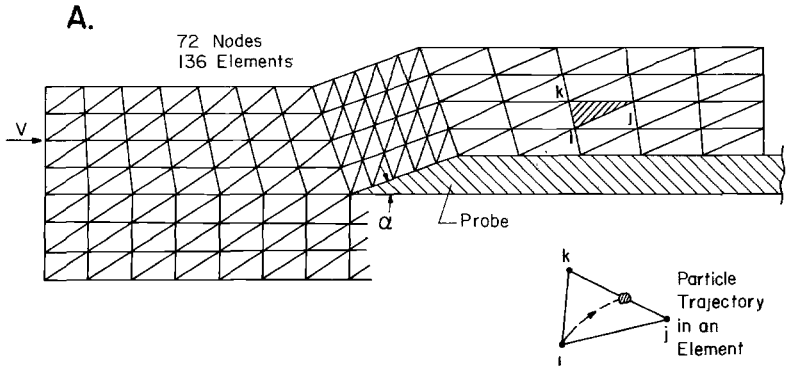


FIG. 11—Finite-element method domain discretization: (A) for inclined wall probe; (B) for casing 1233D.

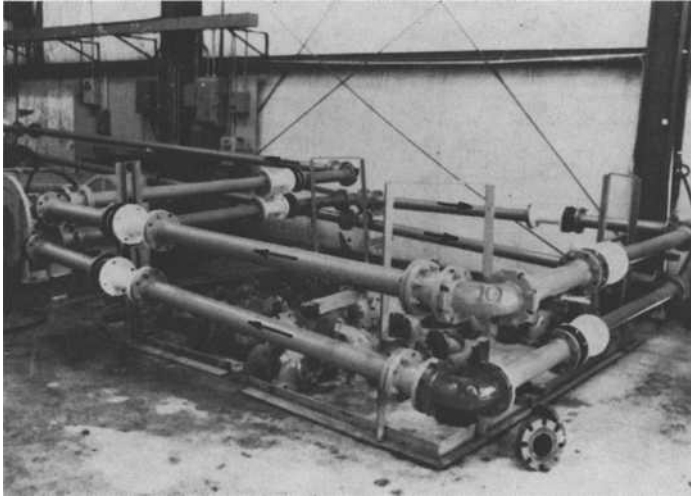


FIG. 12—Partial view of the “inclined wall specimen” pipe loop.

pipe for three typical flow patterns is illustrated in Fig. 20 [21]. The peak of maximum wear can move from the pipe bottom when the velocity decreases about and under the critical sediment value, as sketched in Fig. 20a. Comparisons to experimental results in pipes were discussed in Refs 21 and 22.

From the analysis of the wear rate along the casing perimeter for a large range of variation of different flow parameters (Q , C , d , ρ_s/ρ_L , or N), one can optimize the pump design [20]. For instance, in Fig. 21, the wear profiles are plotted for various solid particle concentrations (C). At $C = 10\%$ by volume, the wear rate reaches a maximum $\Delta\dot{s}_{\max} = 3.5 \cdot 10^{-5}$ m/h, having a nonuniform profile along L . At $C \approx 30\%$ by volume, the wear rate is quasiuniform-distributed, and the curve does not reach even $\Delta\dot{s}_{\max}/2$.

Conclusions

1. The suggested energy approach for dense slurry erosion is based on the proportionality between the particle/wall interaction work and the material removed. The coefficients of proportionality depend on the wear mechanism. The two-phase particulate flow pattern in the vicinity of the exposed surface has a determinant influence on the wear process.

2. The erosion wear caused by random particle impingement and the frictional sliding bed of particles on the wall (b and c in Fig. 1) are characteristic for high concentrated slurry flows.

3. Two new test devices are proposed to simulate and evaluate separately the wear by friction and by impact in dense slurry flows: (a) oscillatory test

COMPUTER CONTROL (FOR OPERATION AND DATA ACQUISITION)

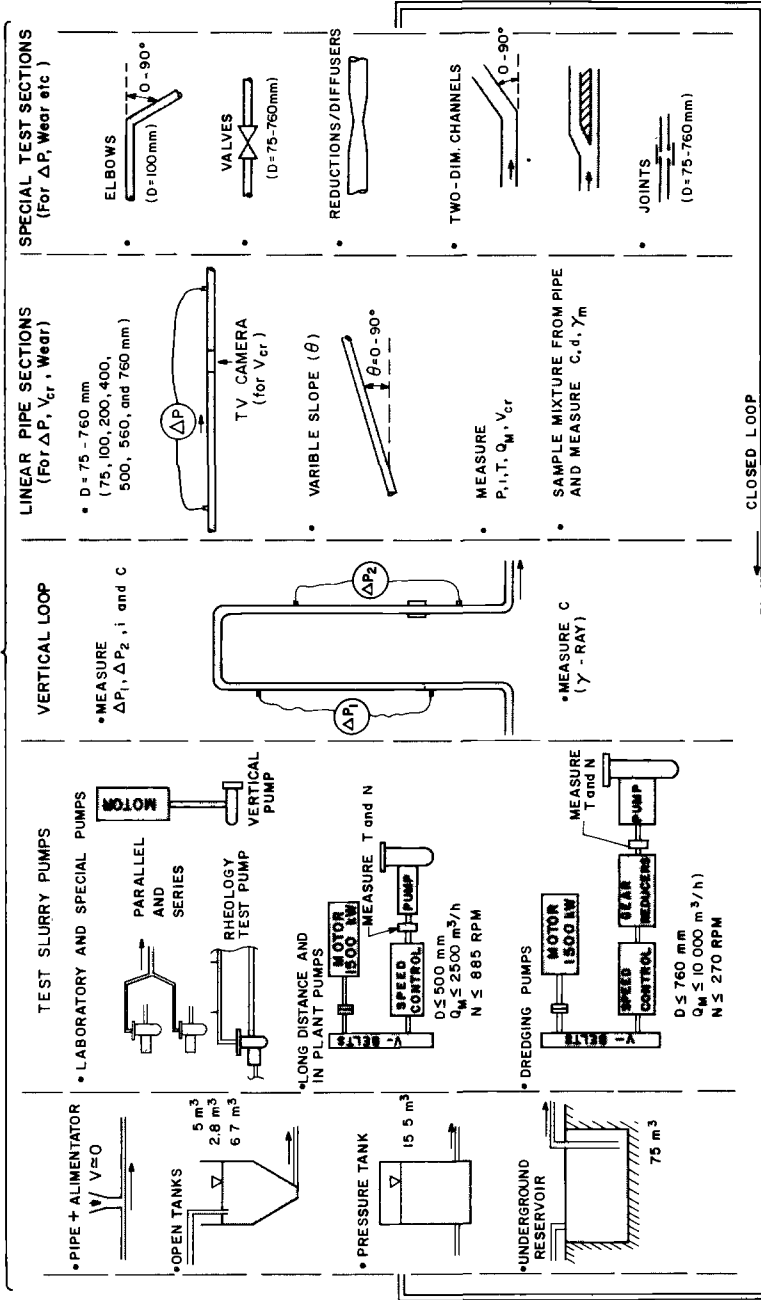
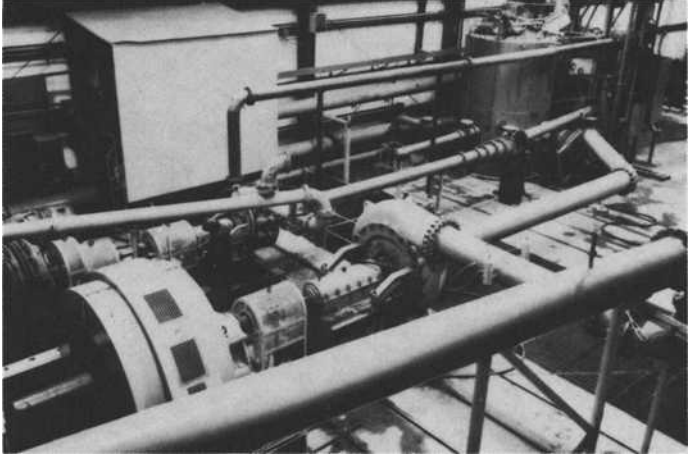


FIG. 13—Scheme of the laboratory for full-scale slurry pipes and pumps experiments.

A.



B.

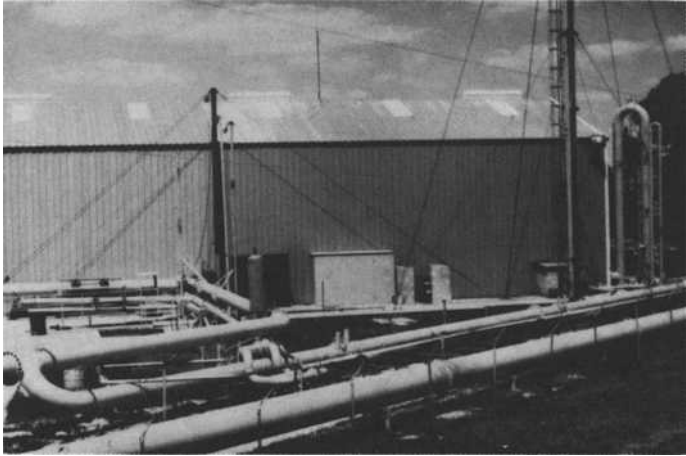


FIG. 14—Partial views of the laboratory: (A) interior pump station; (B) exterior view.

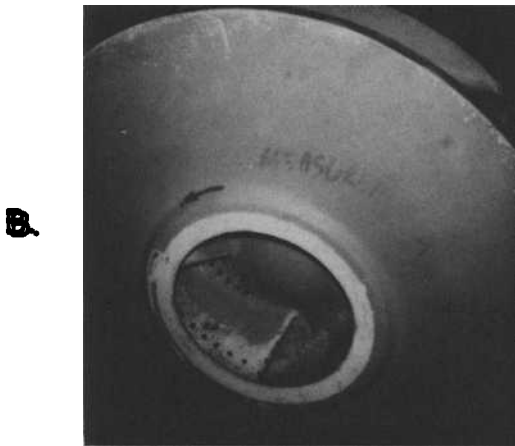
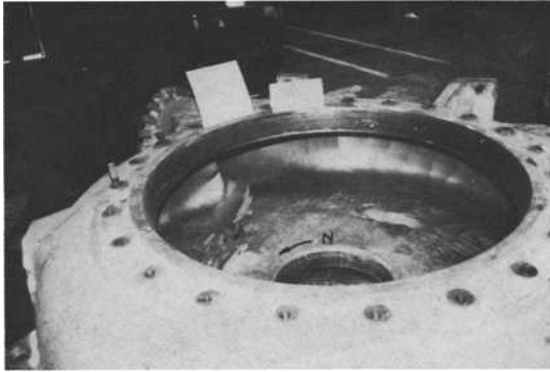


FIG. 15—Pump wear components tested in laboratory (coating thickness approach): (A) centrifugal pump casing lined with epoxy resin of about $40\ \mu\text{m}$ thickness; (B) centrifugal pump impeller lined with four layers of polyamide resin of $50\ \mu\text{m}$ thickness.

A.



B.



C.



FIG. 16—*Pump components after operation: (A, B) pump casing; (C) pump impeller.*

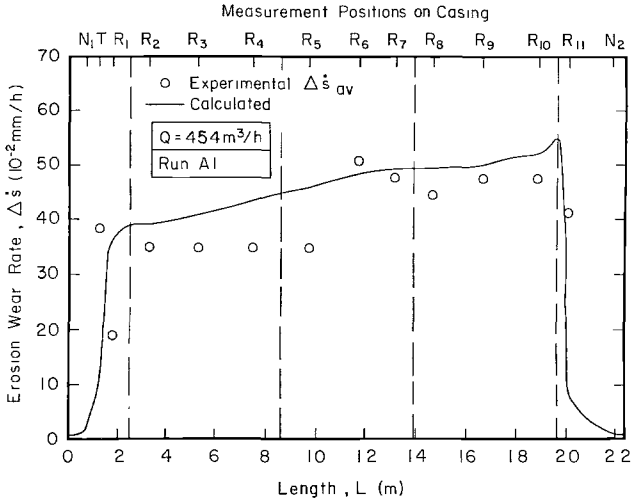


FIG. 17—Erosion wear distribution on the 1233D pump casing polyacrilamide resin coating, $Q = 454 \text{ m}^3/\text{h}$, $C = 6\%$ by volume, sand 0.27 mm.

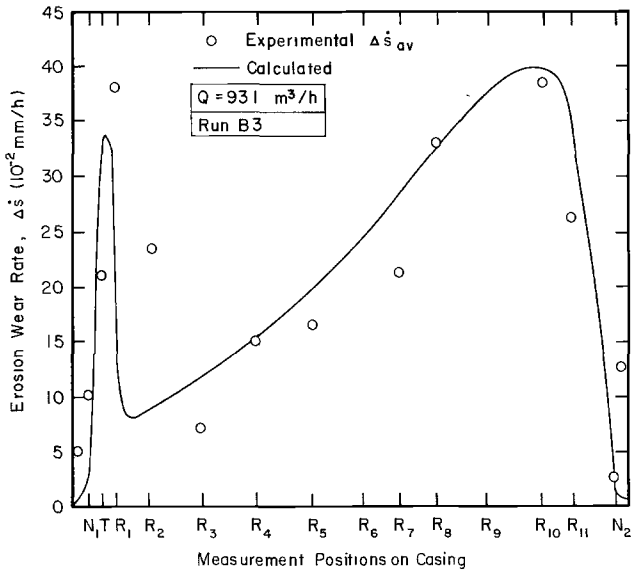


FIG. 18—Erosion wear distribution on the 1233D casing: epoxy resin coating, $Q = 931 \text{ m}^3/\text{h}$, $C = 6\%$ by volume, sand 0.27 mm.

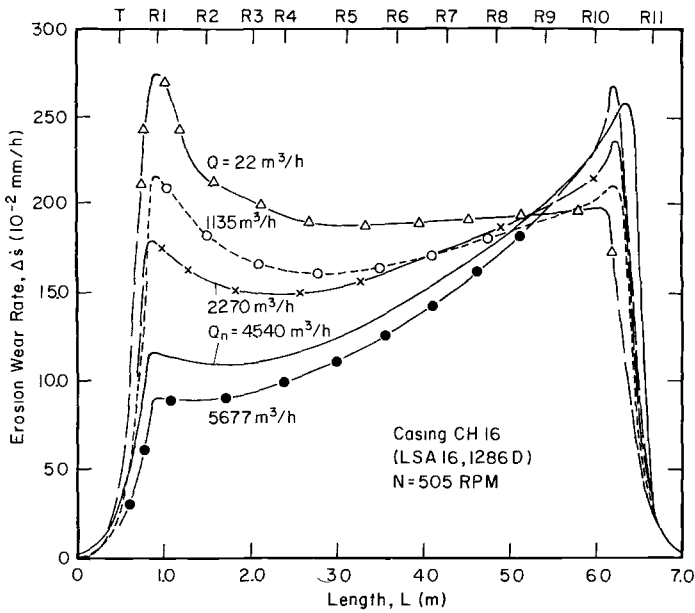


FIG. 19—Effect of the flow rate on erosion wear distribution in casing.

device, and (b) inclined wall specimen device. The resultant experimental coefficients are successfully used in the computational model for different flow conditions.

4. The approach can be applied to equipment handling dilute or dense slurries for a large range of operational parameters, for design purposes and equipment selection.

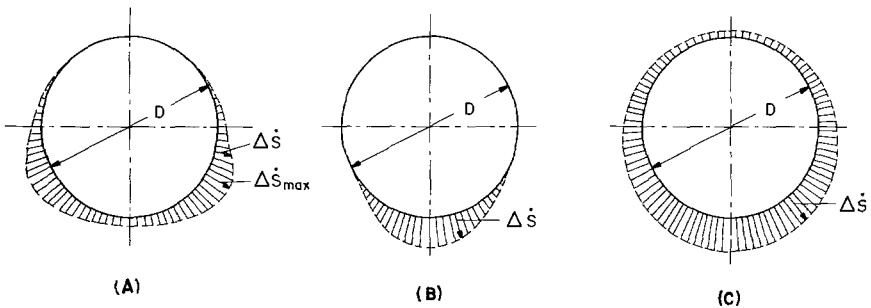


FIG. 20—Typical wear patterns in slurry pipes: (A) flow with sliding or fixed bottom layer of particles; (B) about and over critical sediment velocity; (C) suspension flow.

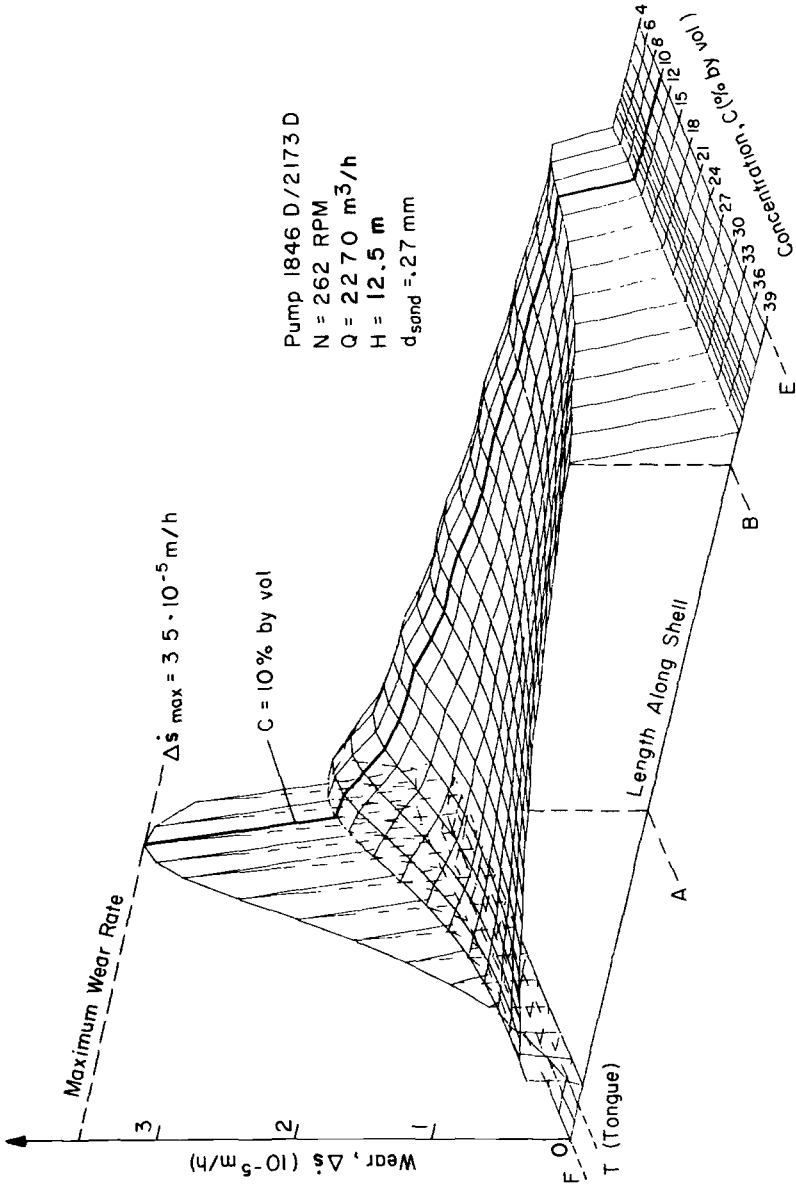


FIG. 21—Erosion wear distribution on the casing 1846D for various concentrations (C = 4 – 39%).

Acknowledgments

The partial support received at the University of Kentucky from National Science Foundation Grant CBT-8511958 for the development of the general approach for flow and wear prediction in equipment handling slurries is acknowledged. The Institute of Mining and Minerals Resources/Department of Energy (IMMR/DOE) supported the initial experimental investigation on small-scale wear apparatuses in the University of Kentucky. The pump manufacturer, the Georgia Iron Works (GIW), cosponsored the large-scale laboratory experiments and application of the proposed approach to improve the design of GIW slurry pumps.

APPENDIX**Basic Equations Used for Numerical Flow Simulation in Pump Casing**

The successive steps in algorithm (simplifying assumptions: inertial and pressure forces predominate, casing width averaged equations) [10]:

1. Mixture velocity (finite-element method, inviscid, parametric)

$$\nabla^2 (\psi_1 + m \cdot \psi_2) = 0 \quad (a)$$

2. Solid particle velocity (dynamic equilibrium of a cloud of particles)

$$\vec{F}_{\text{inertial}} + \vec{F}_{\text{drag}} + \vec{F}_{\text{centrifugal}} + \vec{F}_{\text{pressure}} + \vec{F}_{DS+SL} = 0 \quad (b)$$

3. Solid particle concentration (C)

$$\vec{V}_s \cdot \nabla C - \nabla(\epsilon_s \cdot \nabla C) = 0 \quad (c)$$

4. Supported load on casing wall in the radial direction ($(\sigma_{SL})_r$)

$$(\sigma_{SL})_r = \int_{R_1}^{r_w} \kappa \cdot (\rho_s - \rho) \cdot a \cdot C \cdot dr \quad (d)$$

5. Total erosion rate ($\Delta \dot{s}$)

$$\Delta \dot{s} = \phi_{ko} \cdot I_{tg} + \phi_{kn} \cdot I_n + \phi_{fr} \cdot I_{fr} \quad (e)$$

$\phi_{ko} = 0.38 \cdot 10^{-10}$, $\phi_{kn} = 0.48 \cdot 10^{-3}$, $\phi_{fr} = 10^5$ for polyamide resin

$\phi_{ko} = 0.3 \cdot 10^{-10}$, $\phi_{kn} = 0.24 \cdot 10^{-3}$, $\phi_{fr} = 0.8 \cdot 10^{-5}$ for epoxy resin

References

- [1] Finnie, J., "Erosion of Surfaces by Solid Particles," *Wear*, Vol 3, No. 3-4, 1960.
- [2] Soo, S. L., "Dynamic Interactions of Granular Materials," in *Granular Materials*, M. Shahinpoor, Ed., Trans Tech Publications, Rockport, MA, 1983, p. 687.
- [3] Elmore, C., Funk, E., and Rabinowicz, E., "Abrasiveness of Fine Grain Particles in Slurry Machinery," in Vol. 7, *Proceedings*, Slurry Technology Association, Washington, DC, 1982, p. 327.
- [4] Bree, S. E. M. et al., "On the Erosion Resistance in Water-Sand Mixtures of Steels for Application in Slurry Pipelines," Vol. *Hydrotransport 8*, British Hydromechanical Research Association, Cranfield, England, 1982, p. 161.
- [5] Murthy, J. and Crowe, C. T., "Aerodynamic Effects on the Erosion of Finite Size Targets," in *Particulate Laden Flows in Turbomachinery*, American Society of Mechanical Engineers, New York, W. Tabakoff, Ed., 1983, p. 43.
- [6] Benchaita, M. T., Griffith, P., and Rabinowicz, E., "Erosion of Metallic Plate by Solid Particles Entrained in a Liquid Jet," *Journal of Engineering for Industry*, Vol. 105, 1983, p. 215.
- [7] Neilson, J. H. and Gilchrist, A. G., "Erosion Mechanisms," *Wear*, Vol. II, 1968, p. 111.
- [8] Roco, M. C. and Reinhart, E., "Calculation of Solid Particle Concentration in Centrifugal Pump Impellers using Finite Element Technique," Vol. *Hydrotransport 7*, British Hydromechanical Research Assoc., Fluid Engineering Dept., Cranfield, England, 1980, p. 359.
- [9] Roco, M. C. and Shook, C. A., "Modeling Slurry Flow: Effect of Particle Size," *Canadian Journal of Chemical Engineering*, Vol. 61, No. 4, 1983, p. 494.
- [10] Roco, M. C., Nair, P., Addie, G. R. and Dennis, J., "Erosion of Concentrated Slurries in Turbulent Flow," *Journal of Pipelines*, Vol. 4, No. 3, 1984, p. 213.
- [11] Mills, D. and Mason, J. S., "The Interaction of Particle Concentration and Conveying Velocity on the Erosion Wear of Pipe Bends in Pneumatic Conveying Lines," *Proceedings, International Powder and Bulk Solid Handling Conference*, Rosemont, IL, May 1976, Powder and Bulk Solid Handling Society, London, England.
- [12] Tuzson, J. J., "Laboratory Slurry Erosion Tests and Pump Wear Rate Calculations," *Particulate Laden Flows in Turbomachinery*, Ed. W. Tabakoff, American Society of Mechanical Engineers, New York, 1982, p. 49.
- [13] Sioshansi, P. and Blatchley, C., "Surface Layer Activation Technique for Monitoring and In-Situ Wear Measurement in Turbine Components," AIAA-84-1410, American Institute of Aeronautics and Astronautics, New York, 1984.
- [14] Roco, M. C. and Shook, C. A., "Turbulent Flow of Incompressible Mixtures," *Proceedings 4th International Symposium on Turbulent Shear Flows*, NSF/ONR/USAF/ASME, Karlsruhe, 1983, p. 12.1 (also, *Journal of Fluids Engineering*, Vol. 107, June 1985, p. 224).
- [15] Roco, M. C. and Mahadevan, S., "Scale-up Technique of Slurry Pipelines," *Synfuels and Coal Energy*, J. B. Dicks, Ed., American Society of Mechanical Engineers, New York, 1985, p. 93. (Also, *Journal of Resources Energy Technology*, Vol. 108, Dec. 1986.)
- [16] Keck, H., and Haas, W., "Finite Element Analysis in Quasi-three-dimensional Flow in Turbomachinery," in *Finite Elements in Fluids*, Vol. 4, Gallager et al. Ed., John Wiley & Sons, New York, 1982, p. 531.
- [17] Roco, M. C., Nair, P., and Addie, G. R., "Casing Headloss in Centrifugal Slurry Pumps," Vol. 26, *Design Methods for Two-Phase Flow in Turbomachinery*, Fluids Engineering Division, American Society of Mechanical Engineers, New York. (Also *Journal of Fluids Engineering*, Vol. 108, Dec. 1986.)
- [18] Roco, M. C. and Balakrishnan, N., "A Finite Volume Approach for Transport Flow Phenomena," *Finite Elements and Fluid Flows*, G. F. Carey and J. T. Oden, Eds., Austin, TX, 1984, p. 357. (Also, *Journal of Rheology*, Vol. 29, No. 4, 1985, p. 431.)
- [19] Beacher, B., Tabakoff, W., and Hamed, A., "Improved Particle Trajectory Calculations Through Turbomachinery Affected by Coal Ash Particles," *Journal of Engineering for Power*, Vol. 104, 1982, p. 64.
- [20] Roco, M. C., Addie, G. R., Visintainer, R. J., and Ray, E. L., "Optimum Wearing High Efficiency Design of Centrifugal Slurry Pumps," in *Proceedings*, Vol. 11, Slurry Technology Association, Washington, DC, pp. 277-285, 1986.

- [21] Roco, M. C. and Cader, T., "Distribution of Wear in Slurry Pipelines," 6th Conference on Internal and External Pipe Protection, Vol., *BHRA—Fluid Engineering*, British Hydromechanical Research Assn., Cranfield, England, 1985, pp. 55–68.

Gilbert A. Saltzman,¹ Tristan O. Merediz,² Dilip K. Subramanyam,³ and Howard S. Avery³

Experience with the Wet Sand/Rubber Wheel Abrasion Test

REFERENCE: Saltzman, G. A., Merediz, T. O., Subramanyam, D. K., and Avery, H. S., "Experience with the Wet Sand/Rubber Wheel Abrasion Test," *Slurry Erosion: Uses, Applications, and Test Methods*, ASTM STP 946, J. E. Miller and F. E. Schmidt, Jr., Eds., American Society for Testing and Materials, Philadelphia, 1987, pp. 211–242.

ABSTRACT: Slurry abrasion tests utilizing a rotating wheel to slide the abrasive medium across the surface of a wear specimen have been in use for many years. One form of this test used by a wide variety of laboratories consists of a rubber-rimmed steel wheel rotating in a silica sand, slurry-filled chamber. The historical development of this Wet Sand/Rubber Wheel Abrasion Test, including the results of round-robin testing conducted by Division 18 of the Society of Automotive Engineers' (SAE's) Iron and Steel Technical Committee, is discussed. Test variables that must be controlled and their effects on test results are given in terms of guidelines for future work aimed at standardization.

KEY WORDS: abrasion, abrasive wear, slurry abrasion, wear, wear testing

Rubber wheel abrasion testing has been performed and reported for over 40 years using both dry sand and turbulent slurry. The effects of wheel materials, abrasive characteristics, dry versus wet abrasives, applied forces, etc. have been addressed in many other publications.

This paper covers the experiences of various laboratories with the Wet Sand/Rubber Wheel Abrasion Test, both in the development of the test and the refinement of the apparatus. The wear characteristics of the materials tested are discussed to show the applicability of this abrasion test. The variables encountered in performing the tests are also discussed so as to put into proper order the

¹ Technical director, Metallurgical Industries, 1 Coldstream Way, Tinton Falls, NJ 07724.

² Senior engineer, Industry Development Group, Dorr-Oliver, Inc., P.O. Box 9312, Stamford, CT 06904-9990.

³ Metallurgist and consultant (retired), respectively, Abex Corp., 65 Valley Road, Mahwah, NJ 07430-0610.

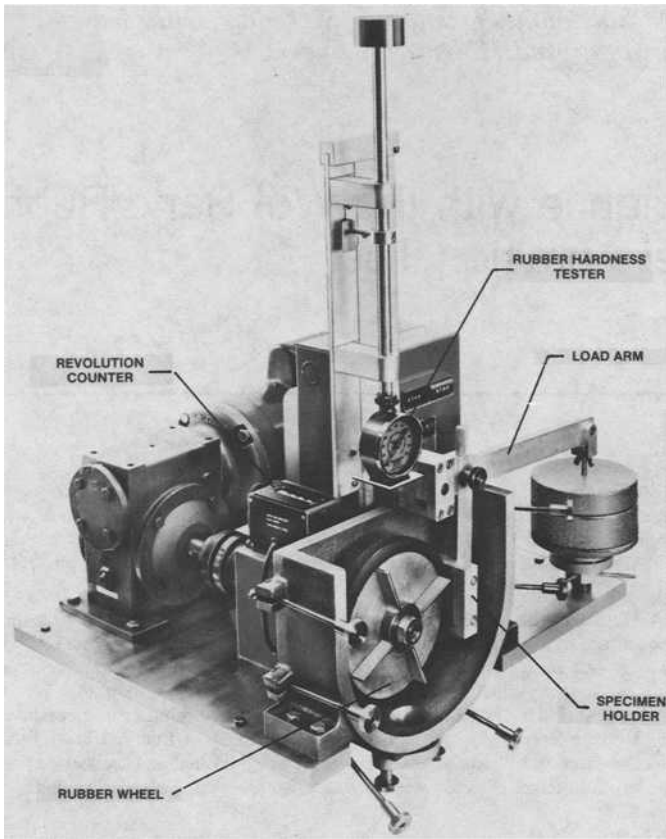


FIG. 1—Wet sand/rubber wheel abrasion tester (front cover removed).

issues that remain to be resolved before the procedure can be finalized into an ASTM standard through future work.

The apparatus for this abrasion test has been refined to its present configuration as shown in Fig. 1 and is commercially available. The number of users of this test has grown through the years, and their needs, interest, and applications have expanded. It is hoped that this paper will help to bring the present and the future users together to perform the final test work and resolve the issues that remain before this test method can be adopted as a standard.

Background

R. D. Haworth pioneered the rubber wheel abrasion test in the late 1940s [1]. His aim was to simulate the wear in oil well slush pump liners, and, after

considering five types of abrasive wear [2–8], he substituted a rubber wheel for the steel wheel used by Brinell [8] because slush pump pistons are made of rubber. Also, he assumed that the contact area and unit pressure remained approximately constant, while the resilience of the rubber permitted the abrasive particles to embed in the wheel, thereby preventing their breakdown.

Haworth studied many variables and materials, finding useful correlations with the wear of slush pump liners and centrifugal abrading machine blades. His device used a notched wheel that rubbed against the vertical face of a 76.2 by 25.4 by 12.7-mm (3 by 1 by ½-in.)-thick specimen and carried either wet or dry abrasive picked up from a trough around the lower part of the wheel. Based on these studies, he standardized on the following test conditions:

1. Wheel speed—250 rpm.
2. External applied load between specimen and wheel—40 lb.
3. Wheel surface travel—1219.2 m (4000 ft).
4. Abrasive size—28 to 35 mesh.

Table 1 presents test data obtained by Haworth using the standardized conditions just listed and shows the effects of different abrasives under both wet and dry conditions. He found that abrasive wear resistance was directly proportional to carbon content and that dry abrasion was more severe than wet. Results of wet test conditions are more pertinent to the current test.

The Society of Automotive Engineers (SAE) established in 1962 a division (No. 18) of the Iron and Steel Technical Committee (ISTC) to deal with unlubricated wear of ferrous materials. The objectives were to provide a forum for discussions of mutual interests, for the presentation of technical papers, and for the initiation of joint experimental activity. The committee adopted a commercial unit available from the Fargo Machine and Tool Co.

The primary interest of the committee members was to establish correlations between laboratory tests and service experience with farm, earth moving, and materials handling and processing equipment. Because of Haworth's extensive research and the commercial availability of the Fargo machine, standardization by round-robin methods was recommended, with a rubber wheel instead of steel to eliminate the higher stresses imposed by the steel.

Test work by Borik [9] in 1967 and 1968 for the committee led to changes in machine configuration. Besides the change from a steel to a rubber rim, the curved stirring paddles were replaced by straight ones and the speed of the rubber wheel was changed from 100 rpm (used earlier by Borik) to 240 rpm. The dimensions of the specimen were changed to 57.2 by 25.4 by 6.4 mm (2¼ by 1 by ¼ in.). A number of variables that affected the test were also recognized during this period. They were:

1. Wheel diameter which changed as the wheel wore—an opportunity factor that had to be compensated for.

TABLE 1—Average weight loss of cast iron-chromium alloys. The values were obtained on relatively small cast samples. (Reprinted from Ref. 1, p. 833.)

Symbol	Treatment	Chemical Analysis—Cr				Hardness Rockwell C ^a	Abrasive—Wheel Speed (rpm) and Load					
		C	Si	Mn	Cr		Dry Quartz 250/40 #	Wet Quartz 250/40 #	Dry Quartz 1035-20 #	Dry Ottawa Sand 250-40 #	Dry Feldspar 250-40 #	Dry Alumina 250-40 #
SAE 1020	Hot-rolled	0.20	BHN 131	67.4	60.4	52.3	16.9	48.0	90.0
AA1	As-cast	0.89	1.93	35/42	77.7	42.1	80.0	9.1	34.5	...
AA1	1500° OQ—300° D†	1.67	0.66	0.98	1.95	56/60	110	40.0	106	...	32.8	96.0
AA2	As-cast	43/47	81.8	40.1	83.5	11.8	16.3	86.0
AA2	1500° OQ—300° D	...	0.52	...	1.18	57/62	90.1	23.2	83.5	11.8	16.3	89.2
AA3	As-cast	2.82	47/51	15.4	6.1	14.9	3.6	6.4	62.0
AA3	1500° OQ—300° D	53/58	14.7	6.8	15.6	3.2	6.4	87.3
AA4	As-cast	3.87	0.73	...	1.05	53/57	9.0	4.0	9.4	2.4	3.4	87.3
AA4	1500° OQ—300° D	57/61	9.0	4.9	8.8	2.1	5.0	53.4
BB1	As-cast	0.78	...	0.82	6.59	53/58	180	84.3	112	26.6	39.4	134
BB1	1800° OQ—300° D	58/63	180	67.9	...	21.3
BB2	As-cast	1.80	0.30	0.72	6.29	47/52	107	54.2	81.5	12.0	18.2	103
BB2	1800° OQ—300° D	59/64	103	23.7	...	11.5
BB3	As-cast	3.03	0.64	...	7.19	53/58	15.0	7.4	14.4	3.0	2.3	81.0
BB3	1800° OQ—300° D	65/69	11.8	4.1	...	3.1
BB4	As-cast	4.13	0.78	...	6.59	54/59	9.0	6.6	11.1	3.2	3.4	81.0
BB4	1800° OQ—300° D	61/67	9.4	5.3	...	3.1
CC1	As-cast	1.21	...	0.55	14.10	28/34	106	65.5	78.5	13.8	28.2	85.3
CC1	1800° OQ—300° D	...	0.43	0.66	14.20	57/62	145	47.6	91.2	12.6	27.4	...
CC2	As-cast	1.91	43/47	69.4	30.9	44.4	7.3	10.2	89.7
CC2	1800° OQ—300° D	...	0.90	...	14.50	63/67	66.9	16.5	37.5	6.8	10.5	97.8
CC3	As-cast	3.19	53/57	18.7	15.0	10.6	3.8	3.7	57.7
CC3	1800° OQ—300° D	...	0.88	...	13.40	60/70	0.7	2.4	5.6	2.0	1.9	86.8
CC4	As-cast	3.85	54/58	0.4	11.2	3.8	1.5	1.5	47.4
CC4	1800° OQ—300° D	65/69	3.3	1.8	3.8	1.3	1.5	74.5
DD1	As-cast	1.25	0.46	0.58	30.10	18/23	66.0	44.9	75.6	7.3	19.1	74.5
DD1	1800° OQ—300° D	...	0.94	0.68	25.25	26/29	78.1	48.5	97.3
DD2	As-cast	1.96	44/48	66.7	20.3	25.6	5.5	6.9	97.3
DD2	1800° OQ—300° D	...	0.93	...	31.60	56/60	74.6	12.8	73.4
DD3	As-cast	2.85	56/60	23.9	9.8	16.5	3.9	4.9	73.4
DD3	1800° OQ—300° D	...	1.13	...	31.20	61/63	19.4	6.0	3.7	1.2	0.9	38.1
DD4	As-cast	3.76	56/60	1.9	3.3	3.7
DD4	1800° OQ—300° D	63/65	1.6	2.1

*—OQ = oil quenched; †—D = draw.

2. Force applied—a severity factor (wear rate increased with increasing applied force).
3. Rubber wheel hardness—a severity factor (harder wheels produced more wear).
4. Rubber finish—marked differences in wear from a freshly ground rubber surface to that of a used surface were noted.
5. Rubber quality (for example, porosity).
6. Slurry density—at high slurry densities the sand would segregate and pack in the chamber.
7. Slurry deterioration—reusing the slurry for a series of tests resulted in a loss of abrasiveness.

Borik also performed experiments to demonstrate reproducibility between tests and the consistent ranking of the wear resistance of several materials. Subsequent work led to his paper in 1970 titled, “Rubber Wheel Abrasion Test” [9]. This paper provided a historical review and included a modified experimental procedure which featured a three-wheel technique. A major difference between Borik’s technique and that specified by the attached draft of SAE’s Wet-Sand Rubber-Wheel Abrasion Test Method (Appendix) was the use of each of the three wheels for a run-in followed by a second test run within the original wear scar, with the specimens being resurfaced in between each wheel usage. The number of wheel revolutions was also different. Borik selected a three-wheel procedure because he found that differences in wear rates could amount to as much as 30% of the total weight loss as a result of rubber wheel hardness variations. He plotted the logarithm of weight loss obtained with each wheel as a function of the rubber hardness and applied a linear regression fit to the data. The test results were then reported as the weight loss, corresponding to 55 durometer⁴ (obtained by interpolation).

The first round-robin test series was conducted in 1972 by the members of the SAE committee using the procedure given in Borik’s paper as a guide. Pearlitic 1080 steel at about HRC 40, SAE 4140 steel, and air-hardened 25% chromium iron were selected as test materials. A surface finish of 20 $\mu\text{in.}$ or better was specified on the samples.

Based upon further investigations by Borik, the committee decided to adopt the following changes in procedure:

1. Use of styrene butadiene rubber (SBR) wheels.
2. Elimination of the 600-grit silicon carbide polishing operation formerly required on neoprene wheels.
3. Use of wheel hardnesses of 50, 60, and 70 durometer.
4. Data to be normalized to 60 durometer from the three-wheel (hardness versus log weight loss) plot.

⁴ All rubber hardnesses subsequently reported are the Shore A scale.

5. Use of 1000 revolutions for materials softer than HRC 20, with the weight losses multiplied by five and reported as 5000-revolution equivalents.

The suitability of the lever and pivot location was first questioned at this time.

The results from the initial round-robin proved the ability to rank the different test materials consistently at all participating laboratories (Table 2). However, each of the labs reported that the three data points on the logarithm of weight loss versus rubber hardness plot did not fall on a straight line, but curved downward. This trend was not consistent with Borik's straight line results obtained earlier with neoprene wheels and resulted in the elimination of SBR wheels. Neoprene wheels were adopted as the standard.

Borik, meanwhile, had developed a simplified testing procedure that eliminated sample resurfacing between rubber wheel changes and reduced the frequency of wheel dressing (once every eight runs of 1000 revolutions).

A second round-robin test series was performed in 1974 by the same laboratories and on the same materials. This round-robin used Borik's latest procedural changes and neoprene wheels. The results showed that:

1. Neoprene rubber wheels permitted more reproducible results than SBR.
2. The "simplified" testing procedure appeared to be satisfactory.
3. Excellent correlation was observed within data sets obtained by any given laboratory, thereby making it possible for all laboratories to rank the materials. It was suggested that a reference material was essential to more closely relate data between laboratories.

A SAE draft was drawn up in 1975 encompassing the procedure used in the second round-robin series. The standard reference material recommended was 1090 steel since it is commonly used by manufacturers of agricultural equipment, many of whom were involved in the SAE round-robins.

TABLE 2—*Wet Sand SBR Wheel Abrasion Test:
first round-robin test series, weight loss values, grams.^a*

Material Tested	Climax Molybdenum	Ford Motor Co.	International Harvester
Pearlitic 1080 steel, Rc 28	0.724	0.562	0.332
	0.726	0.512	0.346
	0.730		
Hardened and tempered SAE 4140 steel, Rc 53	0.542	0.386	0.252
	0.519	0.392	0.240
	0.472		
HC 250 type iron as cast, Rc 60	0.113	0.0917	0.0773
	0.119	0.0891	0.068
	0.112		

NOTE: Rc = Rockwell hardness.

^a Normalized to durometer 60 wheel hardness basis.

Inconsistencies in machine configuration resulting in different applied loads remained a problem. Applied force measurements were attempted at various labs using load cells and moment calculations, but without conclusive results. Problems with the neoprene wheels also affected test results. Both the Fargo Machine & Tool Co. and various users found significant differences in wheel hardness both as-received and after "aging" in storage.

A third round-robin was conducted in 1976 to investigate the suitability of the recommended 1090 steel reference material. Five laboratories participated. The results varied widely between labs (Fig. 2). Subsequent work by R. W. Klan at the John Deere Laboratory revealed that the primary cause for this variability in the test results was a variation in hardness of 1090 steel. The result of this investigation was, therefore, the introduction of a formula into the recommended practice that permitted the 1090 steel weight loss values to be adjusted to a standard hardness level of HRC 30.

A fourth round-robin test series was initiated in 1977 following collaboration between Fargo Machine Tool Co. and DuPont to establish rubber formulations.

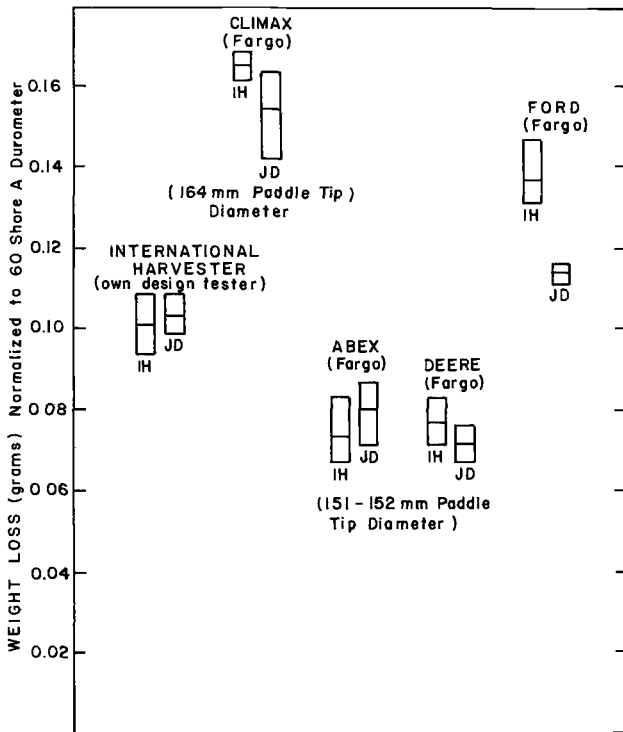


FIG. 2—Wet sand/rubber wheel abrasion test results of third round-robin test series. Upper notation indicates laboratory and tester used in parentheses. Lower notation identifies specimen supplier (JD = John Deere, IH = International Harvester).

This series, however, was never completed because it only showed that the problems with the neoprene wheels had not been resolved. Differences in absolute weight losses could be traced to wheels from different neoprene batches from one supplier or to wheels from different suppliers, even though the wheels had been made to the same formulation.

Changes in committee membership and company representation through the years led to a fifth round-robin series following a 1980 meeting. The neoprene wheels for this series were supplied to all participants from a single source to avoid some of the previous problems. Tests were performed by seven laboratories on four different materials. Details of this round-robin are given in the next section on present status.

Table 3 is a summary of the round-robin activity to date. As a result of changing interests and priorities, SAE member involvement in this test ebbed, and ASTM Committee G-2 on Wear and Erosion became actively involved. The Fargo test machine is currently available from George Fischer Foundry Systems, Inc. A reportedly equivalent unit is available from Falex Corp. Other commercial or noncommercial testers that conform to available drawings and specifications can be used.

TABLE 3—Summary of SAE round-robin series, Wet Sand/Rubber Wheel Abrasion Test.

Series No.	Date	Wheel Type	Materials Tested	Participating Laboratories
1	1972	SBR	1080 4140	Climax Molybdenum Ford Motor Co.
2	1974	Neoprene	25% Cr-Fe 1080 4140	International Harvester Climax Molybdenum Ford Motor Co.
3	1976	Neoprene	25% Cr-Fe 1090	International Harvester Abex Corp. Climax Molybdenum John Deere Ford Motor Co.
4 ^a	1977	Neoprene	1090 17-4-PH 316 Stainless D-2	International Harvester Abex Corp. Climax Molybdenum John Deere ESCO
5	1980 to 1981	Neoprene	1090 304 Stainless D-2 T-1	International Harvester Abex Corp. Cabot Corp. Climax Molybdenum H. W. Dietert Co. Dorr-Oliver Inc. ESCO International Harvester

^a This test series was never completed.

Present Status of Test

A task group was formed in 1983 within ASTM Committee G-2 to continue the work done by SAE ISTC Division 18 on the Wet Sand/Rubber Wheel Abrasion Test, the ultimate objective being the development of an ASTM standard practice. The first assignment of the group was to collect, summarize, and evaluate the data obtained in the last interlaboratory test (ILT) conducted by the SAE (Round-Robin Series No. 5—Table 3). Each of the seven participating laboratories tested four steels: D-2 tool steel, 1090 steel, T-1 steel, and Type 304 stainless steel. ILT results are summarized in Tables 4 through 7.

It was observed that the Dorr-Oliver (D-O) weight losses for all four steels were the lowest reported by any lab. D-O also reported the highest hardness values for all steels. Conversely, the Dietert weight losses were the highest and hardnesses lowest for three of the four steels (excepting 304 stainless). This seemed more than a coincidence, so the return of ILT specimens was solicited from participants in order to check hardness values at one laboratory. Specimens from four labs, Climax, D-O, Abex, and George Fischer Foundry Systems (for Dietert), were retested at the Abex Research Center. These values are those listed in the tables. D-O hardnesses are now in good agreement with the other labs. Dietert's hardnesses for 1090 and T-1 now agree well with the others; only the D-2 steel hardness remains low. Close examination of the Dietert specimen surfaces showed evidence of heat checks and grinding burns, indicating that surface finish may have been an added variable in their case. Specimens from D-O and Dietert were resurfaced according to Abex standard practice, and were retested by the two labs. Retest weight losses from D-O are shown in the tables. All are greater than originally, and therefore in better agreement with values obtained by the others. The results of retest by Dietert are not included.

Statistics for the four materials are provided in Tables 4–7. The high variation coefficients for weight loss, even if compensated for wheel hardness, indicate inadequate standardization for general use, though the test has proved useful for individual laboratories. Confirming previous experience, if abrasion factor reporting is used with a standard reference material, interlaboratory agreement is much better, the coefficients approaching the desirable 5% value. The 1090 steel that has served as reference here can be more closely specified, and should be, since its variability in the round-robin was minimized by having all specimens come from the same stock. An abrasion factor is defined as the weight (volume) loss of the specimen divided by that of the standard material (1090) tested under identical conditions.

Abrasion factors versus annealed 1020 steel have been reported for many years. Using a 60-durometer normalized weight loss of 146.8 mg as the mean of 19 runs (coefficient of variation = 3.66%) on the Abex Fargo tester, these abrasion factors are 0.3379 for 1090, 1.059 for T-1, 0.0664 for D-2, and 2.452 for 304 stainless.

TABLE 4—Summary of fifth SAE round-robin test results, 1090 Steel.^a

	CHEMICAL ANALYSIS											
	%C	%Mn	%P	%S	%Si	%Ni	%Cr	%Mo	%Al	%V	%Ti	%Cu
	0.91	0.69	0.024	0.041	0.23	0.04	0.15	0.01	0.037	0.003	0.016	0.13
Laboratory	TEST RESULTS											
	Dietert	I-H	Climax	Abex	Cabot	ESCO	D-O					
Hardness—HRC	27.3 (29.2)	30.2 (28.2)	28.1 (29.6)	28.5 (29.2)	31.3	29.9	32.4 (28.6)					
W60 wt loss, mg	73.8	61.8	57.5	49.6	47.3	43.5	30.6 (38.9)					
No. of tests	4	4	4	2	4	2	3					
STATISTICAL ANALYSIS (Avg HRC = 29.5)												
	Mean	Range	Standard Deviation	Coefficient of Variation	No. of Labs							
Weight loss	53.2	34.9	12.91	24.26	7							

^a Data in parentheses represents retest values used in statistical analysis.

TABLE 5—Summary of fifth SAE round-robin test results, T-1 low-alloy steel^a

	CHEMICAL ANALYSIS											
	%C	%Mn	%P	%S	%Si	%Ni	%Cr	%Mo	%Al	%V	%Ti	%Cu
	0.17	0.85	0.007	0.008	0.22	0.02	0.47	0.11	0.027	0.028	0.017	0.023
Laboratory	TEST RESULTS											
	Dietert	I-H	Climax	Abex	Cabot	ESCO	D-O					
Hardness—HRC	21.6 (24.2)	24.2 (22.1)	24.1 (24.0)	23.2 (23.4)	24.0	24.0	27.7 (24.0)					
W60 wt loss, mg	236.0	187.0	162.3	155.4	123.7	134.7	92.6 (123.0)					
No. of tests	4	4	4	2	4	2	3					
Abrasion factor versus 1090 steel	3.198	3.026	2.823	3.133	2.615	3.097	3.162					
STATISTICAL ANALYSIS (Avg HRC = 24.1)												
	Mean	Range	Standard Deviation	Coefficient of Variation	No. of Labs							
Weight loss	160.3	113.0	41.79	26.07	7							
Abrasion factor	3.008	0.583	0.2156	7.168	7							

^a Data in parentheses represents retest values used in statistical analysis.

TABLE 6—Summary of fifth SAE round-robin test results, D-2 Tool Steel.^a

		CHEMICAL ANALYSIS									
%C	%Mn	%P	%S	%Si	%Ni	%Cr	%Mo	%Al	%V	%Ti	%Cu
1.68	1.31	0.33	0.16	10.96	0.77	...	0.82	...	0.019
Laboratory		TEST RESULTS									
		Dietert	I-H	Climax			Abex	Cabot	ESCO	D-O	
Hardness—HRC		57.4 (57.6)	60.0 (60.8)	60.3 (60.7)	60.8 (61.0)	61.0	60.2	62.1 (60.6)			
W60 wt loss, mg		15.75	10.75	9.25	9.75	9.45	8.5	5.73 (7.6)			
No. of tests		4	4	4	2	2	2	3			
Abrasion factor versus 1090 steel		0.2134	0.1739	0.1609	0.1966	0.1998	0.1954	0.1954			
STATISTICAL ANALYSIS (Avg HRC = 60.2)											
		Mean	Range	Standard Deviation	Coefficient of Variation	No. of Labs					
Weight loss		9.217	3.15	1.243	13.48%	6					
Abrasion factor		0.187	0.0389	0.01535	8.209%	6					

^a Data in parentheses represents retest values used in statistical analysis.

TABLE 7—Summary of fifth SAE round-robin test results, 304 stainless steel.

CHEMICAL ANALYSIS											
%C	%Mn	%P	%S	%Si	%Ni	%Cr	%Mo	%Al	%V	%Ti	%Cu
0.07	1.65	0.015	0.007	0.64	8.57	19.22	...	0.015
TEST RESULTS											
Laboratory	Dietert	I-H	Climax	Abex	Cabot	ESCO	D-O				
Hardness, HRB	80.6 (79.3)	78.2 (78.9)	76.8 (75.3)	75.8 (74.4)	81.5	80.2	91 (74.3)				
W60 wt loss, mg	492.8	498.8	432.8	360.0	375.6	558.3	305.2 (334.1)				
No. of tests	4	4	4	2	4	2	3				
Abrasion factor versus 1090 steel	6.678	8.071	7.527	7.258	7.941	12.83	8.589				
STATISTICAL ANALYSIS (Avg HRB = 77.6)											
	Mean	Range	Standard Deviation	Coefficient of Variation	No. of Labs						
Weight loss	436.1	224.2	82.91	19.01%	7						
Abrasion factor	7.677	1.911	0.7541	9.822%	6						

^a Data in parentheses represents retest values used in statistical analysis.

A good wear test should have reproducibility, ranking ability, and validity for predicting service performance [10–11]. This rubber wheel slurry abrasion test has repeatedly shown ranking ability [1,9,12], some correlation with service performance [13], and good reproducibility when carefully conducted in an individual laboratory. The critical focus of the round-robin work, therefore, should be on statistical analysis of how well various laboratories agree and the potential for improvement of this agreement. This fifth round-robin includes laboratories for which the test is new as well as some with years of pertinent experience.

Most of the labs provided four replicate tests. This is appropriate if the coefficient of variation and the allowable sampling error have the same numerical value [14–15], and 95% confidence is desired. Selection of the allowable sampling error is usually a matter of judgment and was not addressed with these tests.

Standard deviations or the standard error of a test are usually calculated by the root mean square of the deviation from the mean if enough items are available. However, for small numbers of observations (as in these tests), estimates from the range by means of the factors in *Manual on Quality Control of Materials*, ASTM STP 15-C [14], as has been done here, is more efficient. Coefficients of variation (standard deviation/mean \times 100) are useful here as they facilitate comparing variation of populations that have different averages. However, because of the small number of observations it should be recognized that a small (good) coefficient should be interpreted as indicating that the variation can be at least that bad. Suspiciously “wild” values may be rejected with 90% confidence from the range calculations by another statistical procedure [16] as was done here for the 15.75 mg D-2 value in Table 6, and the 12.83 factor in Table 7.

Materials Tested

Appreciation of the usefulness of the SAE draft of the Wet-Sand Rubber-Wheel Abrasion Test (Appendix) in ranking a variety of materials in terms of relative abrasion resistance can be gained by a scrutiny of test results obtained at different laboratories. These are listed in Table 8 and grouped according to alloy families. Weight and volume losses are both reported since volume loss is the more significant factor in comparing materials with different densities. The data clearly indicate that the “low stress” abrasion resistance in each family of alloys correlates directly with either carbon content (where applicable) or hardness.

Variables Affecting Test Results

The results of tests performed to date with the Wet Sand/Rubber Wheel abrasion equipment are affected by variables in the test equipment, the test

TABLE 8—Wet-Sand Rubber-Wheel Abrasion Test results for various material groups.
Data on different groups obtained at different laboratories.

Material	Hardness, HRC (HRB)	Adjusted Loss at 60 Durometer	
		Weight, mg	Volume, mm ³
ALLOYS			
1005	(65.4)	351.8	44.7
1020	(68.8)	274.2	34.9
1030	(78.9)	229.5	29.2
1040	(87.1)	197.5	25.2
1050	(85.7)	182.7	23.3
1090	30	86.0	11.0
COATINGS			
Fe-Cr-Ni-B-Si-C	53	18.4	2.67
Fe-Cr-C-Mn	56	16.9	2.35
WC/Ni-Cr-Si-B (composite)	54	17.3	1.80
Ni-Cr-Si-B-C	61	6.07	0.85
WC/Ni-Cr-Si-B (composite)	65	7.73	0.70
IRON BASE ALLOYS			
316L stainless	(76)	361.2	45.2
1020 Steel	(78)	173.4	22.1
Fe-Cr-C	52	29.6	3.1
Fe-Cr-C-Mo	55	17.6	2.35
D2 tool steel	61	9.98	1.30
NICKEL-BASE ALLOYS			
Ni-Si-B (N-20)	27.5	164.3	20.1
Ni-Si-B (N-4779)	39	128.4	15.7
Ni-Si-B (N-4778)	54	77.5	9.57
Ni-Cr-Si-B (N-4777)	50.5	37.9	4.69
Ni-Cr-Si-B-C (N-4775)	56	6.41	0.82
COBALT-BASE ALLOYS			
Co-Cr-Mo (S-21)	28	236.6	26.9
Co-Cr-W-C (S-6)	41	135.7	16.2
Co-Cr-W-C (S-12)	45	87.0	10.0
Co-Cr-W-B (S-157)	48	38.7	4.71
Co-Cr-W-C (S-1)	53.5	34.8	3.95
MISCELLANEOUS MATERIAL			
1090		0.040 5	5.21
304 SS		0.316	39.3
Ferralium ^a SS alloy		0.162	20.9
17-4-PH		0.265	33.4
D-2		0.062 1	8.39
T-1		0.094 1	12.2
Illium PD ^b SS alloy		0.177	22.2
Sintered WCO No. 2		0.000 6	0.045
Silicon carbide		0.000 75	0.247
Sintered WC-Co No. 1		0.004 81	0.358
Sintered WC-Co No. 3		0.006 05	0.425
UHMWPE		0.001 53	1.62
Filled Kynar		0.524	279.0
Meehanite		0.103	14.2
Almanite		0.063 5	8.9
Spherulite		0.057 9	8.2

^a Trade Mark of Laughley Alloys, Ltd., Slough, England.

^b Trade Mark of Stainless Foundry and Engineering, Milwaukee, Wisconsin.

material, and the abrasive used. This section is devoted to a discussion of these variables.

Rubber Wheels

The first round-robin tests used SBR. As mentioned previously, SBR was discarded due to nonlinearity in semilogarithmic plots of weight loss versus rubber hardness. Neoprene was adopted as a substitute based upon Borik's work.

Problems with the neoprene wheels, however, were encountered very early in the test work. Formulations for the neoprene rubber were developed at participating laboratories and at DuPont in collaboration with the Fargo Machine and Tool Co.

The present Recommended Practice defines the specification, class, and grade for the three rubber wheels according to the designation set forth by ASTM Classification System for Rubber Products in Automotive Applications (D 2000-80) (SAE-J200). The designation defines the ingredients for the rubber, but does not specify the processing or handling techniques to be used during manufacturing. Variations in some of these aspects may be responsible for differences in wheel properties.

The resiliency of the neoprene rubber probably influences wear characteristics, although at this point a method has not been developed to measure this factor. Differences in resiliency, or response to deformation, have been observed for wheels of equivalent hardness as well as between old and new wheels, yet their effect on the test results has not been measured.

It is recommended that the rubber wheels be stored flat to minimize flat spots on the rim, and away from heat and ultraviolet rays to minimize changes in rubber quality.

Abrasives

The Wet-Sand Rubber-Wheel Abrasion Test uses rounded quartz sand tightly sized, between 50 and 70 mesh (Fig. 3). Contact stresses are affected by the diameter of the abrasive particles; hence, the size of the sand particles must be controlled to within a relatively tight range to ensure reproducibility of results. Large variations in grain size would also produce segregation during storage and handling. The Ottawa-Silica Sand Co. (Ottawa, IL) is the current source for testing sand. While batch-to-batch variations in abrasive size have been found to be minimal, the angularity of the sand needs to be quantified to ensure long-term test reproducibility, and the suitability of other suppliers, if required.

A fresh batch of slurry is used with each test run to ensure consistency in slurry quality. This is necessary since some deterioration in the abrasive can occur, especially when the harder rubber wheels are employed during testing.

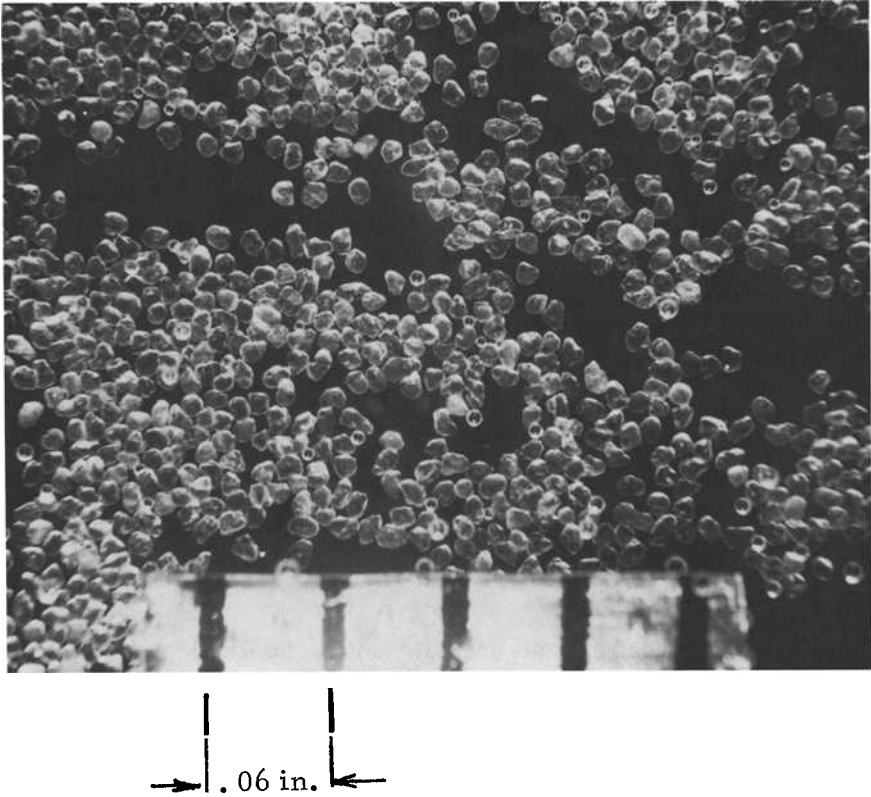


FIG. 3—Rounded quartz sand used for wet sand/rubber wheel abrasion test.

Test Material

Segregation—The cooling conditions experienced by cast materials determine the degree of chemical segregation that is inevitably present in them. Heavier section sizes (encountered in many applications) typically experience slower solidification rates; hence, the degree of segregation is usually greater. These localized variations in chemical composition can affect the response of the alloy to heat treatment, resulting (for example, in the case of many steels) in cross-sectional variations in both microstructure and hardness. If the cast material cannot be homogenized by subsequent deformation and thermal treatments, nonhomogeneity can cause variations in abrasion resistance, a factor that should be recognized and compensated for in component design.

Surface Finish—In many materials, mechanical deformation and heat from machining and grinding operations can cause surface damage such as heat checks as well as changes in microstructure, which in turn can affect their

response to abrasion tests. Great care should be taken in specimen preparation to minimize these effects.

Soundness—Industrial material processing techniques such as casting, welding, and powder consolidation can give rise to unsoundness in the test material. Such porosity usually decreases the abrasion resistance of the material.

Test Equipment

A commercial test apparatus was built and marketed by Fargo Machine & Tool Co. (Fig. 1 of Appendix). Due to subsequent changes in ownership of this company, a number of modifications made to the apparatus in accordance with committee recommendations have not been conveyed to many users to enable retrofits to the older machines.

The sample holder was changed very early in the development stages to accept the larger rectangular sample of the current practice. The holder is designed for a specimen that is 9.5 mm thick. Since the SAE Recommended Practice calls for a standard sample thickness of 6.4 mm, shims have to be employed to raise the specimen so that the test surface is always flush with the top of the holder.

The location of the pivot point on the lever arm has been a point of contention through the years because the resultant load on the specimen may vary. A survey of the equipment (the results of which are not yet complete) used by the laboratories that participated in the latest round-robin test series may indicate the need for stricter standardization.

Other changes in the apparatus included the length and shape of the stirring paddles attached to each side of the rubber wheel. The original paddles were curved, but were later made straight. The straight paddles were subsequently shortened.

Laboratory Techniques

It is important to recognize that in spite of strict controls on apparatus, specimen preparation, and procedure, test precision is always subject to the vagaries of the individual performing the test.

Since the test is begun under zero-load conditions and the load is applied by lowering a screw jack, the time taken to perform this task could have a bearing on the results, especially if the load is not applied uniformly.

The specimens are normally weighed to the nearest tenth of a milligram (10^{-4} g) as specified in the test procedure. This accuracy is achievable on most analytical balances. Many of the newer balances, however, have overall limitations on capacity, and this can present a problem with heavier (denser) materials such as tungsten carbides. Materials that experience very small weight

losses are particularly sensitive to carelessness in the weighing technique and cleaning procedure.

The measurement of rubber wheel hardness can be prejudiced by the test operator. Hence, the measurement must be carried out in accordance with ASTM Method for Rubber Property—Durometer Hardness (D 2240-84). The currently available test apparatus incorporates a standard durometer tester mounted on the unit to facilitate wheel hardness measurements.

The rubber wheel must be dressed periodically to ensure concentricity and squareness of the rim with the axis of the wheel, and that the rubber rim is free of embedded sand particles and surface imperfections. Since a variety of dressing techniques are prevalent, a standardized finishing treatment may be necessary using commercial abrasive paper of a specified grit size. This would ensure constancy in wheel surface condition before each test.

The use of shims is sometimes necessary to maintain a uniform specimen thickness and to ensure that the sample is always returned to the same position in the holder since the wear scars produced subsequent to the “run-in” have to be within one another. If subsequent wear scars do not coincide with earlier ones, test results are questionable.

Data reporting techniques have never been incorporated as part of any recommended practice. Since the test is still in the developmental stage, as much care as possible should be taken to record pertinent information during testing. Certain formats would facilitate internal laboratory data exchange and verification. One such addition that has been recommended is photocopying of the wear scar after each run in order to enable a retrospective examination of the wear scar shape.

Finally, it should be worth noting that effective machine maintenance is a virtual prerequisite to long-term reproducibility of test results.

Future Work

Having demonstrated both the usefulness of the test as well as its current limitations and problems, it would be worthwhile to list some of the considerations that will be given attention in the next series of interlaboratory tests expected to be conducted in the near future. It is hoped that these considerations will help in minimizing variability in test results and speed standardization of the test.

Test Material Selection

Previous experience with the test has shown that certain materials such as 304 stainless, high-chromium iron, and 1090 steel can give rise to considerable variation in interlaboratory results. In the case of 304 stainless, the problem

may be attributed to a combination of factors, such as sensitivity to machining and high weight loss (that is, poor abrasion resistance). In the case of both the high-chromium iron as well as the 1090 steel, the problem is section-sensitivity that produces variations in microstructure and hardness due to chemical segregation.

The chosen alloy will therefore be drawn from a single source in each case and in the form of either bar stock or small cast-to-size test blocks. Final surfacing will be carried out at one location. If these precautionary measures prove to be fruitful, they will need to be quantified and incorporated into the standard practice. While individual laboratories could (for their own use) determine the effects of varying section sizes as well as chemical composition on abrasion resistance, it may ultimately prove necessary to establish reliable sources of standard reference material, such as the National Bureau of Standards [supplier of H-13 tool steel standards for the ASTM Practice for Conducting Dry Sand/Rubber Wheel Abrasion Test (G 65-84)]. Weight or volume loss figures obtained on these standards would provide each laboratory with an indication of the reliability of its test results.

Rubber Wheels

While there is no incentive to change the type of rubber (neoprene) used for wheels, consideration will be given to possible alterations in formula that would enhance wheel quality and shelf life. More attention will be paid to processing methods, and these methods are expected to be defined in future drafts of test procedures, if possible. It would also be worthwhile to determine the effects on test results of exchanging both wheels and samples between laboratories.

Test Apparatus

A survey was conducted recently among laboratories that participated in the latest round-robin to determine differences in test equipment that might have resulted in applied load variations. Participants were asked to calculate, using moments, the magnitude of the applied force at the point of contact between the rubber wheel and specimen. The use of a proving ring to measure the static force on the specimen has been suggested. While this is also not an accurate indication of the actual force between the wheel and specimen (due to wheel rotation during testing), it should prove to be useful in standardizing test equipment.

Procedure

Two procedural modifications have been suggested to increase versatility of use and to overcome some existing limitations of the Wet Sand/Rubber Wheel Abrasion Test. These are:

1. Increasing the number of wheel revolutions from the existing 1000 to 5000 for harder-wearing materials.

2. A one-wheel procedure involving a run-in followed by a second test within the original scar. The appropriate wheel hardness would be close to 60 durometer since all current weight loss values are adjusted to this value. Since it is likely that the one-wheel method would also require extrapolation to 60 durometer, the linear relationship between the logarithm of weight loss and rubber wheel hardness would have to be established first using the three-wheel technique. Despite interlaboratory differences in the slope of these semi-log plots and occasional departures from linearity exhibited by some materials, it has been suggested that extrapolation is justified since the degree of correction involved is small.

The single-wheel method of testing also has the potential of test cost reduction.

Summary

The rubber wheel slurry abrasion test pioneered by Haworth over 40 years ago was brought to near its current form by Borik in the late 1960s. Meanwhile, a division of the SAE's Iron and Steel Technical Committee, established in 1962, undertook to correlate laboratory slurry abrasion tests and service experience with farm, earth moving, and materials handling equipment. Round-robin testing was started by the SAE Committee in 1972. In 1975, an SAE draft was drawn up encompassing the procedure used in a second round-robin series. Subsequent round-robin tests led to several changes in the test. These changes and a summary of round-robin activity to date are described.

The present status of the Wet Sand/Rubber Wheel Abrasion Test, and a detailed evaluation of the last (fifth) SAE round-robin test, is given. The usefulness of the test in terms of materials tested, and the effects of test variables on results, are discussed in detail. Finally, future work needed to accomplish the standardization of this test is considered.

APPENDIX

SAE DRAFT XJ1185*
WET-SAND RUBBER-WHEEL ABRASION TEST METHOD
(November, 1978)

1. *Scope*—This recommended practice describes a method for using a water-sand slurry in a rubber-wheel abrasion test machine to quantitatively determine the relative resistance of ferrous materials to low-stress abrasive wear, such as encountered in soil tillage** in the absence of appreciable impact.

2. *Apparatus Required*

2.1 *Abrasion Machine*—The test apparatus*** is illustrated in Figure 1. Important components of the apparatus are numbered and identified in the legend. Several essential dimensions of these components are also given in the figure.

The test apparatus consists of a steel hub (1) with a neoprene rubber rim (2) (this assembly henceforth is called the “rubber wheel”) which rotates through a quartz sand slurry (not shown in the figure) at a speed of 245 ± 5 rev/min. A test specimen (3) is positioned in a specimen holder (4) which is attached to a lever arm (5) carrying a weight (6). Through leverage, the weight (6) presses the test specimen (3) against the rubber wheel with a force of 222 N (50 lbf). The weight (6) has a mass of approximately 9.5 kg (21 lb) and must be adjusted so that the force exerted by the rubber wheel on the specimen with the rubber wheel at rest has a value of 222.4 ± 3.6 N (50.0 ± 0.8 lbf), as determined by calculation of the moments acting around the pivot point for the lever arm.

The rubber wheel (1), powered by a 746 watt (1 hp) electric motor and gear box, is flanked by stirring paddles (7) that agitate the slurry during the test. The slurry is contained in a slurry chamber (8) that has a removable side wall (9) and a removable top cover (10).

2.2 *Neoprene Rubber Rim on the Rubber Wheel*—The following specification,

* This is a draft prepared by the SAE Iron and Steel Technical Committee Division 18. It is not an approved SAE Technical Report. It is printed through permission of SAE.

** D.A. Stolk, Field and Laboratory Abrasion Tests on Plowshares, SAE Paper 700690, 1970.

*** Can be obtained from Fargo Machine and Tool Company, Detroit, Michigan or possible alternate supplier.

class and grades of neoprene rubber must be used for the rims of the three rubber wheels used in the test:

General Specification ASTM D2000 – SAE J200

a) 2BC515K11Z1Z2Z3Z4

Z1 Elastomer – Neoprene GN-A

Z2 Type A durometer hardness $50 \pm 2^*$

Z3 Not less than 50% rubber hydrocarbon content

Z4 Medium thermal black reinforcement

b) 2BC615K11Z1Z2Z3Z4

Z1 Elastomer – Neoprene GN-A

Z2 Type A durometer hardness $60 \pm 2^*$

Z3 Not less than 50% rubber hydrocarbon content

Z4 Medium thermal black reinforcement

c) 2BC715K11Z1Z2Z3Z4

Z1 Elastomer – Neoprene GN-A

Z2 Type A durometer hardness $70 \pm 2^*$

Z3 Not less than 50% rubber hydrocarbon content

Z4 Medium thermal black reinforcement

The neoprene rubber stock is bonded to the steel hub and cured in a suitable steel mold such as that used by Detroit Rubber Company, Detroit, Michigan (Mold No. 7378). Typical curing temperature and time are 150 C (300 F) and 20 minutes. The rubber rim should be free of defects and be uniform in hardness.

Before determining the rubber hardness, it is recommended that the rubber rim be dressed. This can be done by placing the rubber wheel in a lathe on an expandable arbor and grinding it square with a freshly dressed grinding wheel such as Norton 38A60J5VBE, having dimensions of approximately $130 \times 13 \times 13$ mm ($5 \times \frac{1}{2} \times \frac{1}{2}$ inches) rotating at a speed of 3500 rpm, while the rubber wheel rotates at 86 rpm. The rubber wheel should be crossed at 0.43 mm (0.017 inch) per revolution. After the dressing, each rubber wheel should be carefully measured to determine the diameter and width of the rubber rim; the initial diameter of the rubber wheel is usually about 180 mm (7 inches) and the width of the rubber rim about 13 mm ($\frac{1}{2}$ inch). The dressing of the rubber wheel reduces the diameter of the wheel by about 0.13 to 0.25 mm (0.005 to 0.010 inches). It is recommended that the rubber wheel be dressed again after it has accumulated approximately 6000 revolutions during testing. Experience has shown that more than 6000 revolutions

* All durometer hardness values in the text refer to shore Type A durometer hardness. The range of ± 2 hardness units in the above specification corresponds to measuring the hardness at a temperature of $23 \pm 2^\circ\text{C}$ ($73 \pm 4^\circ\text{F}$) for the freshly molded wheels; for subsequent use of the wheels, the range is increased to ± 3 to allow for minor aging effects and for departure of the ambient temperature from the specified range.

LEGEND

- | | |
|---------------------------|--------------------|
| 1. Steel Hub | 12. O-Ring |
| 2. Neoprene Rubber Rim | 13. Bearing Pin |
| 3. Test Specimen | 14. Shaft |
| 4. Specimen Holder | 15. Bearing Box |
| 5. Lever Arm | 16. Bearing Cover |
| 6. Weight | 17. Nut |
| 7. Stirring Paddles | 18. Drain Opening |
| 8. Slurry Chamber | 19. Bearing |
| 9. Removable Side Wall | 20. Retaining Knob |
| 10. Cover (Schematically) | 21. Bracket |
| 11. Key | |

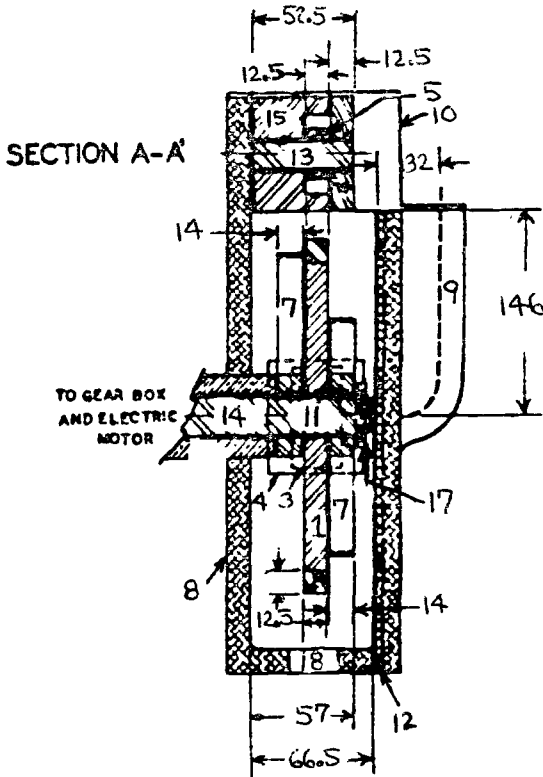


FIG. 1 (Appendix)—Continued.

has an adverse effect on the reproducibility of the test results. The shelf life of the rubber rim may not exceed two years. Wheels should be stored so that there is no force on the rubber surfaces.

The Type A durometer hardness of the rim should be determined on the outside curved surface at eight equally spaced locations, averaged and reported in the form: A/48.6/5, where A is the type of durometer, 48.6 is the average of eight readings, and 5 is the time in seconds that the pressure foot of the shore-A hardness tester is in firm contact with the rubber rim surface. The determination of the durometer hardness should follow the ASTM Specification D2240-75. The five-second dwell time for the pressure foot in contact with the rubber rim should be rigorously adhered to.

- 2.3 *Abrasive Slurry*—The abrasive slurry used in the test consists of a mixture of 0.940 kg of deionized water and 1.500 kg of quartz sand of intermediate sharpness such as the AFS* testing sand [screen size minus 50, plus 70 mesh (200 to 300 μm)] produced by Ottawa Silica Company, Ottawa, Illinois. This sand has the advantage of uniform morphology. Abrasion test results should include a reference to the sand used.
3. *Test Specimen*—The test specimens are prepared by machining and/or by grinding ferrous stock to the following final dimensions:

$$\begin{aligned} \text{Thickness: } & 6.4 \begin{matrix} +0 \\ -0.2 \end{matrix} \text{ mm } \left(0.25 \begin{matrix} +0 \\ -0.01 \end{matrix} \text{ Inches} \right) \\ \text{Width: } & 25.4 \begin{matrix} +0 \\ -0.8 \end{matrix} \text{ mm } \left(1.00 \begin{matrix} +0 \\ -0.03 \end{matrix} \text{ Inches} \right) \\ \text{Length: } & 57.2 \begin{matrix} +0 \\ -0.8 \end{matrix} \text{ mm } \left(2.25 \begin{matrix} +0 \\ -0.03 \end{matrix} \text{ Inches} \right) \end{aligned}$$

The last 0.3 mm (0.01 inches) of stock on the two major (test) surfaces should be carefully wet ground to a surface finish of about 0.5 to 0.75 μm (20 to 30 microinches) AA as measured across the direction of grinding. The direction of grinding should be parallel to the longest axis of the specimen. The finished surface should be free of a decarburized layer, heat checks and other defects.

4. *Test Procedure*—Before the start of a test, the slurry cage should be thoroughly rinsed to eliminate any remnants of the slurry from the previous test. The rubber wheel of nominal 50 durometer hardness (the lowest level of the three hardness levels used) is installed, and its actual hardness determined. Prior to testing, each specimen is demagnetized, freed of static charge, degreased in acetone, weighed to the nearest 0.1 mg, and installed in the specimen holder.

* American Foundrymen's Society.

The slurry chamber is then filled with the 1.500 kg of the quartz sand and the 0.940 kg of deionized water at room temperature, and a cover is fitted over the open top of the slurry chamber to prevent the slurry from splashing out. The machine is started and the specimen is gently engaged with the rotating rubber wheel to produce a "run-in" wear scar. The wear scar removes the surface layer and exposes fresh material which is not affected by the surface preparation. The run-in is continued for 1000 revolutions of the rubber wheel. The counter, preset to 1000 revolutions, is used to terminate the test automatically. Following the run-in, the slurry is drained from the slurry case and discarded. The specimen is removed, cleaned, dried and reweighed.

The next step represents the actual abrasion test which is conducted on the same wear scar using the same wheel of nominal 50 durometer hardness. Care must be taken to install the specimen in the specimen holder with the same orientation as before. This test follows the same procedure as that for the run-in, starting with a fresh slurry and ending with weighing of a clean dry specimen. The difference in the weights before and after the test gives the weight loss of the specimen.

The procedure in the preceding paragraph is repeated with each of two rubber wheels of higher hardness levels, nominally 60 and 70 durometer. These runs are also abraded in the same wear scar and with the same specimen orientation but without a run-in.

The test results, in terms of the specimen weight loss in grams, are then normalized to correspond to the travel of a wheel having a diameter of 177.8 mm (7.000 inches) and width of 12.7 mm (0.500 inches) using the following formula:

Adjusted Weight Loss in Grams

$$= \frac{177.8 \text{ mm} \times 12.7 \text{ mm} \times \text{Actual Weight Loss in Grams}}{[\text{Actual Dia. (mm)}] \times [\text{Actual Width (mm)}]}$$

or

$$= \frac{7.000 \text{ in.} \times 0.500 \text{ in.} \times \text{Actual Weight Loss in Grams}}{[\text{Actual Dia. (in.)}] \times [\text{Actual Width (in.)}]}$$

The values of the adjusted weight loss (i.e. three values for each sample material) are then plotted on a logarithmic scale against the rubber wheel hardness plotted on a linear scale. The final result is obtained by fitting a least square line to the three data points and solving the equation of the line for the weight loss corresponding to a rubber hardness of exactly 60 durometer. The fitting may also be done using a computer. The 60 durometer adjusted weight loss facilitates comparisons between materials. The volume loss, which is a more correct measure of material loss due to abrasion, should be computed after the densities of the sample materials are determined, preferably by water immersion (by a method such as ASTM Procedure C693-74). In some cases, the differences in the densities of selected ferrous materials

being compared may be small enough to eliminate the need for conversion of the weight loss values to volume losses.

5.1 *Standard Test Material*—In order to ensure that the apparatus gives reproducible results, it is recommended that samples of a standard material be tested, as described in section 5.2, to monitor the effectiveness of the test procedure and the apparatus. Fine-Grained SAE 1090 steel, which is used in commercial plowshares, is recommended as a suitable standard material.* The composition limits for SAE 1090 steel are 0.85–0.98% C, 0.60–0.90% Mn, 0.15–0.30% Si, 0.04% P max. and 0.05% S max. The steel should be hot-rolled to approximately 13-mm (½ inch) thick flat bar stock and be subsequently normalized. The normalizing treatment should consist of austenitizing at a temperature of 900 ± 10 C (1650 ± 20 F) for 45 minutes followed by cooling in still air to room temperature. The resulting Rockwell-C hardness should be within the range of 22 to 32.

5.2 *Recommended Use of the Standard to Monitor Test Performance*—Compensate the 60-durometer weight loss obtained for the 1090 standard material for specimen hardness as follows:

Determine the Rockwell-C hardness of the specimen on the wear scar side by taking three measurements between the edge and the scar along each side of the scar and two between the scar and each end. The specimen hardness is the average of these.

Compute the *Hardness-Compensated Weight Loss* as follows:

$$\begin{aligned} HCWL = & (60\text{-Durometer Weight Loss}) \\ & + 0.00266 (\text{specimen HRC}-30.0 \text{ HRC}) \end{aligned}$$

This value represents the adjusted weight loss the specimen would have exhibited had its hardness been 30 HRC.

Upon commencing test operations, users of the recommended practice should test four samples of the standard normalized 1090 steel described in Section 5.1. The average of the four HCWL values would be calculated. A ratio, *R*, would then be calculated by dividing 0.0714 gm (the adjusted weight loss of the standard test material at a hardness of 30.0 HRC) by the just-mentioned average HCWL value. When testing a sample of unknown wear resistance, the number of revolutions of the rubber wheel would be kept at 1,000, and a value for the “ratio proportioned weight loss” (RPWL) would be calculated by multiplying the adjusted weight loss for the sample by *R*. The resultant RPWL value would be divided by the density of the sample to obtain the corresponding volume loss, which would be reported.

Once after every five test samples a single standard normalized 1090 specimen

* Samples of normalized SAE 1090 steel may be obtained from Fargo Machine and Tool Company, Detroit, Michigan or other suitable source.

should be tested. If the product of the resultant HCWL value and the previously obtained R value lies within the range of 0.0602 and 0.0826, testing of sample specimens would be continued. However, if the product lay outside of this range, the operator would run two additional standard specimens and calculate the average HCWL for all three standard specimens. He would then obtain a new value for R by dividing 0.0714 gm by the average HCWL for the three standard specimens. The new R value would then be used in proportioning the adjusted weight losses calculated for samples run subsequently.

If any one of the following events takes place, the procedure described in 5.2 for testing the standard 1090 steel specimens should be repeated:

- A) One, or more, of the wheels is retreaded,
- B) A new operator is employed.
- C) Use of the test machine is suspended for a period of six months or more,
or
- D) Use of sand from a new shipment is commenced.

References

- [1] Haworth, Jr., R. D., "The Abrasion Resistance of Metals," *Transactions*, Vol. 41, American Society for Metals, Metals Park, OH, 1949, pp. 819-854.
- [2] Rosenberg, S. J., "Resistance of Steels to Abrasion by Sand," *Transactions*, Vol. 18, American Society for Steel Treating, Metals Park, OH, 1930, pp. 1093-1124.
- [3] Ellis, O. W., "Wear Tests on Ferrous Alloys," *Transactions*, Vol. 30, American Society for Metals, Metals Park, OH, 1942, pp. 249-286.
- [4] Norman, T. E. and Loeb, Jr., C. M., "Wear Tests on Grinding Balls," *Metals Technology*, T. P. 2319, American Institute of Mining and Metallurgical Engineers, New York, 1948.
- [5] Blake, J. M., "Wear Testing of Various Types of Steels," *Proceedings*, Vol. 28, Part II, American Society for Testing and Materials, Philadelphia, 1928, pp. 341-355.
- [6] Avery, H. S., "Hard Surfacing by Fusion Welding," a monograph published by the American Brake Shoe Co., 1947.
- [7] Weiss, C. R., "Relative Wear of Metals due to Abrasion," *Iron Age*, Vol. 129, Part II, 1932, p. 1166.
- [8] Brinell, J. A., "Researches on the Resistance of Iron, Steel and Some Other Materials to Wear," *Jernkontorets Annaler*, Vol. 76, 1921, p. 347-398.
- [9] Borik, F. "Rubber Wheel Abrasion Test," SAE Paper 700687, Society of Automotive Engineers, Warrendale, OH, 1970.
- [10] Avery, H. S., "The Measurement of Wear Resistance," *Wear*, Vol. 4, No. 6, 1961, pp. 427-449.
- [11] Avery, H. S., "Classification and Precision of Abrasion Tests," in *Wear of Materials-1977*, American Society of Mechanical Engineers, New York, pp. 148-157.
- [12] Diesburg, D. E. and Borik, F., "Optimizing Abrasion Resistance and Toughness in Steels and Irons for the Mining Industry," *Vail Symposium-1974*, Climax Molybdenum Co., Greenwich, CT, pp. 15-41.
- [13] Stolk, D. A., "Field and Laboratory Abrasion Tests on Plowshares," SAE Paper 700690, Society of Automotive Engineers, Warrendale, OH, 1970.
- [14] *Manual on Quality Control of Materials*, ASTM STP 15-C, American Society for Testing and Materials, Philadelphia, 1951.
- [15] ASTM Designation E122-72, "Standard Recommended Practice for Choice of Sample Size

to Estimate the Average Quality of a Lot or Process," American Society for Testing and Materials, (1972).

- [16] Dean, R. B. and Dixon, W. J., "Simplified Statistics for Small Numbers of Observations," *Analytical Chemistry*, Vol. 23, 1951, pp. 636-638.

DISCUSSION

K. Metz¹ (written discussion)—(1) How do materials rank in this test as compared to the dry sand test [ASTM Practice for Conducting Dry Sand/Rubber Wheel Abrasion Test (G 65-84)]? Have you tried any tests with varying pH values for the slurry? The old B 611-76 test (ASTM Method for Abrasive Wear Resistance of Cemented Carbides) used 30-mesh alumina (Al_2O_3) grit, which is significantly harder than silica (SiO_2). Have you run any slurries using this material? (2) Do you have a procedure for testing coatings, such as chrome plate “D-gun,” or electroless nickel? It would seem that the slurry method could possibly avoid the problem of heat buildup that can occur in the dry sand test.

G. Saltzman, T. Merediz, D. Subramanyam, and H. Avery (authors' closure)

Material Ranking

Limited published data are available for comparing material rankings in the wet sand and dry sand (rubber wheel) tests. In some of the earlier test series, reversals in the ranking order of 1080 and 4140 steels were observed. The table that follows compares dry sand data from ASTM G 65-84 (Table X1.3) with average data from the last SAE interlaboratory test. It is assumed that values for 304 stainless steel are a good approximation of those that would be obtained for 316 stainless.

Material	Dry Sand			Wet Sand		
	Rockwell Hardness	Vol. Loss, mm ³	Ratio	Rockwell Hardness	Vol. Loss, mm ³	Ratio
316 stainless	B80	260	3.25
304 stainless	B78	54.5	8.3
1090 steel	C24-26	80	1.0	C29.5	6.8	1.0
D2 tool steel	C59-60	36	0.45	C60	1.19	0.2

From this very limited example it appears that the order of ranking is generally the same in both tests. However, the greater differentiation between materials in the wet sand test (as indicated by the greater range in wear ratios based on 1090) would seem to indicate a potential for ranking order reversals of materials not greatly disparate in abrasive wear resistance.

¹ Dresser Industries—Security Division, Dallas, TX 75137.

Slurry-pH Variation

The duration of the test is assumed to be too short for pH changes to have any effect on weight loss. This situation, however, may not apply to highly acidic slurries, for example. If the effect of such slurries is to be investigated, it would be necessary to modify the test apparatus with regard to the corrosion resistance of the interior of the slurry chamber, as well as the moving parts inside.

Alundum Slurries

The only reported recent study the authors are aware of was presented at the Denver symposium by Dr. Alberto Sagues (Kentucky Center for Energy Research Laboratory, Lexington, KY). His results indicated that for the materials tested, the linear relationship between weight loss and rubber wheel hardness was still valid for alumina slurries. Weight losses were higher in this case.

Test Procedure for Coatings

Unlike procedure "D" in G 65-84, no formal procedure currently exists. One of the authors has successfully run tests on plasma-sprayed coatings by lowering the number of wheel revolutions (that is, decreasing test duration) and also decreasing test severity by using softer rubber rims. Another of the authors has used an incremental method (200-wheel-revolution increments with a single 60-durometer wheel) for a wide variety of thin coatings and surface treatments.

Hydraulic and Metallurgical Criteria in Slurry Pumping System Design

REFERENCE: Sinha, S. K., “Hydraulic and Metallurgical Criteria in Slurry Pumping System Design,” *Slurry Erosion: Uses, Applications, and Test Methods, ASTM STP 946*, J. E. Miller and F. E. Schmidt, Jr., Eds., American Society for Testing and Materials, Philadelphia, 1987, pp. 243–260.

ABSTRACT: Hydraulic transportation of slurries is being adopted for short-distance, loop-in-process industries as well as for long-distance pipeline transportation of mining ores. The presence of slurry causes excessive wear on pump components as well as on the system. Wear depends on the type of slurry to be transported by the pumping system. It is, therefore, essential to select proper metallurgy so that the life of the system is increased and so that minimum possible repair and maintenance are required. There is a need for more technological innovation to adopt a proper sealing system and to use special elastomers and other materials to increase the life of the pump components. Centrifugal pumps are used normally for the short loop system, where medium and low pressure is required. Positive displacement pumps are used for long-distance transportation with a high-pressure and low discharge requirement. Special care is required to design the hydraulic passage, depending on the size of the solid being pumped in the design of components for centrifugal pumps. Glandless pumps are also developed to avoid the complex sealing system.

KEY WORDS: slurry pumps, pumping system design

Solids pumping applications have proliferated, ranging from the relatively simple in plant loops to the spectacular long-distance transport of mine ores and concentrates. Several installations around the world testify to the practicality and, in most cases, the economic advantage of this mode of transportation. Among the first slurry pumps were mud pumps, which have been used in oil fields for more than half a century. Commercial decisions on the selection of pumps are related primarily to two factors. The first factor is abrasivity of slurry as judged by Miller number, and the second factor is the discharge pressure.

While long-distance slurry systems have come of age, pump wear and its cost in terms of maintenance and replacement is still a highly important factor

¹ Head, Engineering, Bharat Pumps & Compressors, Ltd., Naini, Allahabad, India.

in the total economics of slurry handling. Wear caused by solid particles is a complex phenomenon that depends on many factors. Pump type, pump design, and the composition of slurry all play a part.

Factors Affecting Wear

Wear is influenced by four main factors:

1. Solid particles in slurry.
2. Properties of slurry as a fluid.
3. The properties of the pump material in contact with slurry.
4. Hydraulic design.

Solid Particles

All types of wear increase as the hardness of the eroding particle exceeds that of the surface. In deformation wear, the elastic limit increases with the degree of deformation, and a highly deformed surface layer is formed. After a maximum stress is reached, a crack will begin within the deformed surface layer parallel to the contact area, and a part of the surface will flake off. This process continues, damaging pump parts.

Grain size and sharpness of particle—At high velocities a particle sets up stress concentrations in the pump contact surface, resulting in cracking at a depth that is proportional to the size of the particle. Thus large particles are expected to do more damage than small ones. Sharp-edged particles do more damage than rounded ones.

Impingement Angles—The effect of impingement angle on wear depends on the type of material being eroded. Wear is greatest at the lower impingement angle with relatively soft, ductile materials like rubber and aluminum. Cutting wear causes the most damage in this case. If pump materials are hard and brittle, impingement perpendicular to the surface causes maximum damage.

Properties of Slurry

It is generally accepted that wear increases at a linear rate with increasing concentration of solids in the slurries being pumped within a certain range beyond which wear rate does not change.

The Miller abrasivity tester developed by John E. Miller is used to measure the relative abrasivity of slurries. The Miller number consists of two parameters. The first parameter is called abrasivity and represents the rate of weight loss from the metallic wear block.

The second parameter is called attrition and represents the effect of slurry

particle breakdown as measured by a loss of abrasivity. Miller numbers for some slurries, for example, are as follows:

Coal A	11
Coal B	28
Limestone	30
Magnetite	64

Miller numbers are used for relative abrasivity, and the pump material can be selected accordingly.

Properties of Pump Material

Materials used in slurry pumping fall into four general categories:

1. Metals.
2. Rubbers.
3. Plastics.
4. Ceramics.

Metals—Ferrous metals are usually more resistant to deformation wear than nonferrous metals because of higher toughness. Austenite manganese steels are often used because of their good weldable property. Martensitic white iron and nickel-hard are also used. Special 28% chrome steel and FCR 700 BHN hardness are preferred for slurry applications. Ferrous metals:

(a) Wear-resistant alloyed gray cast iron. The addition of special additives to gray cast irons provide hardness qualities, making them machinable to a greater or lesser extent.

(b) Spheroidal graphite cast iron. This metal is also found to be very good for hard slurries.

(c) White martensitic cast iron. These are very hard white cast irons containing nickel and chromium with high resistance to wear through abrasion.

(d) Cast iron with high concentration of carbon, 3.4 to 3.7%, chromium 18 to 20%, and molybdenum have remarkably high resistance to abrasion.

(e) Ni-Resist cast irons. Ni-Resist is a trade mark covering a group of cast irons with an alloying element to give a perfect austenitic structure with excellent properties.

(f) Cast irons containing 28 to 25% chromium. These cast irons have the special feature of being constituted exclusively of ferrite and small quantities of eutectic ferrite carbides.

Some manufacturers have developed special cast iron with less than 1% carbon and some molybdenum. This gives excellent corrosion and abrasion resistance property with 700 HB (Table 1).

TABLE 1—*Hardness of various metals used for slurry application.*

Overall Hardness at Centre	Matrix	Brinell Hardness
MACHINABLE METALS		
Ni-Resist cast iron	Austenite	130 to 195 (286 after work hardening)
Alloyed pearlitic cast iron	Fine pearlite	250 to 300
Mn or Ni-Cr sorbitic cast iron	Lite sorbite	270 to 300
Tempered martensitic cast iron	Martensite	280 to 340
Acicular cast iron	Bainite	260 to 340 (well-polished)
NONMACHINABLE METALS		
Quenched and tempered sorbitic iron	Martensite	360 to 420
Unprocessed cast martensitic iron	Martensite	400 to 450
Quenched and annealed martensitic cast iron	Martensite	400 to 460
15 to 18% Cr cast iron	Carbide	400 to 460
Alloyed white cast iron	Carbide + pearlite	400 to 475
Ni-hard cast iron	Carbide + martensite	
High carbon and 1½% Cr cast iron	Carbide + martensite	

The addition of chrome and molybdenum increases the resistance to abrasion of steel, whereas nickel and manganese reduce the resistance to abrasion but increase the strength of steel.

Martensitic steels are more resistant to wear than fine pearlitic steels, but they are less strong and have less resistance to impact. Annealing increases the strength of steels without reducing their resistance to abrasion. 13% chrome steels have both excellent resistance to abrasion and remarkable strength.

Rubbers—Rubbers have excellent resistance to deformation wear but do not generally possess resistance to high shear stress. Therefore, rubber-lined pumps are good where deformation wear is expected but are not used for pumping slurries with sharp particles. Large particles are not permitted with rubber-lined pumps.

Plastics—Plastics such as Teflon and epoxy resin are used for coating parts and also for seals. For expendables, polyurethane has proved to give better life, but complete plastic pumps have so far not undergone rigorous tests with difficult slurries.

Ceramics—Ceramics are also good materials for sealing and have high resistance to grinding wear and erosive wear.

Hydraulic Consideration

The following factors cause abrasion:

1. Rotational speed.
2. Inappropriate hydraulic design profiles.
3. Surface irregularities due to casting faults.
4. Use of the pump outside specified limits.

A slow speed of rotation is selected to reduce abrasion, which would mean larger rotor diameter and uneconomic design. On the other hand, wider passages of impeller would be required for handling solids, which would mean higher speeds, thus a compromise is made in selecting the medium speed to obtain optimum design.

One of the abrasion parameters is the particle speed, which is substantially the same as that of the circulating liquid. The particle trajectory will be the same as or different from the fluid depending on effects due to its mass, geometric profile, and specific gravity. Because kinetic energy of the impinging particle varies as the square of the absolute velocity, wear in pump increases rapidly with increasing flow velocity. Wear is also affected by the pattern of flow inside the pump. Since rapid changes in flow direction create wear, accumulating eddies, and vortices, recirculation of fluid inside the pump should be avoided.

The tests carried out at British Hydromechanics Research Association (BHRA) on impeller wear with coal fines from washery containing 20% ash content showed that most of the wear on the impeller is taking place on the pressure side of the blade. If the surface finish is smoother, the wear is less. The irregularity in hydraulic profiles may cause rapid damage to the pump parts.

The cavitation phenomenon originates when the absolute pressure at a specific point on the vane at the inlet to the rotor reaches a critical value; net positive suction head (NPSH) cavitation is encountered relatively frequently in solids-handling pumps used by the chemical industry. As the materials used are generally of excellent ductility, the characteristic traces of damage by cavitation do not always appear on working parts of the pump. Instead there are signs of secondary effects like damage to keys, loosening of the rotor, breakage of shaft, etc.

The efficiency of centrifugal slurry pumps is low because of the robust nature of impeller design and the relatively wide throat impeller clearance. The head and capacity of the pump can be decreased or increased by simply changing the speed of the pump. Belt-driven units are generally common to obtain variable speed.

The head flow characteristic of a centrifugal slurry pump is relatively flat. This means that if in a centrifugal pumping system the flow rate drops to a point too near to the deposition velocity where the system head loss curve hooks, the pump characteristics could cause the flow rate to drop below critical velocity. Continuous operation below critical velocity will result in a fixed bed of solids deposited in the pipeline. In most multipump systems this is overcome by installing a few variable speed pumps.

Types of Slurry Pumps

Slurries in the form of drilling muds have long been pumped in oil fields throughout the world by the use of piston and plunger pumps. A summary of major slurry pump installations is given in the Appendix.

Pumps used in slurry pipeline generally fall into two categories:

1. Positive displacement pumps.
2. Centrifugal pumps.

Special Pumps: Lock Hopper Pump

The lock hopper system utilizes two pressure vessels to alternately inject slurry into the pipeline. Injection is provided by the water pressure acting on a diaphragm which separates the slurry in the vessel from the water supplying hydraulic pressure. The diaphragm (Fig. 1) is a free-moving rubber spherical piston which alternately drives the slurry from the vessel and drives the water back to the mixing tank.

The piston of the piston pump, driven by a crankshaft, remains in constant contact with the cylinder wall during each stroke. This action would result in high wear if the pump were used for pumping abrasive materials such as iron ore.

A modified plunger pump was therefore introduced for such service. It has a plunger which is continuously flushed with clean water during the suction stroke, thus greatly reducing internal wear. It is preferred for use with abrasive slurries (Figs. 2 and 3)

Liquid seal is created by the injection of water or other appropriate liquid ahead of plunger packing in such a way that packing does not come in contact with abrasive liquid. This design would require considerable space between the valve chest and plunger face. Thus large clearance volume would be needed, which will mean low volumetric efficiency. The problem of vapor locking is to be avoided in the design.

The diaphragm pump utilizes a membrane to separate a clean liquid on the piston (or plunger side) from an abrasive slurry (Fig. 4).

Positive displacement pumps consist of two principle elements: power end and fluid end (Fig. 5).

For slurry pipeline service, pumps must operate continuously for long periods and should be designed to last as long as the life of the project. The power ends of the pumps originally designed for oil well drilling are therefore modified to increase the conventional bearing life from 30 000/35 000 to 100 000 h. Similarly, parts for chain drive and gears are also designed for longer life.

Fluid End

The fluid end of a plunger pump may consist of two or more single-acting plungers. Whereas in the case of a piston pump, single- or double-acting pistons would take the place of the plungers.

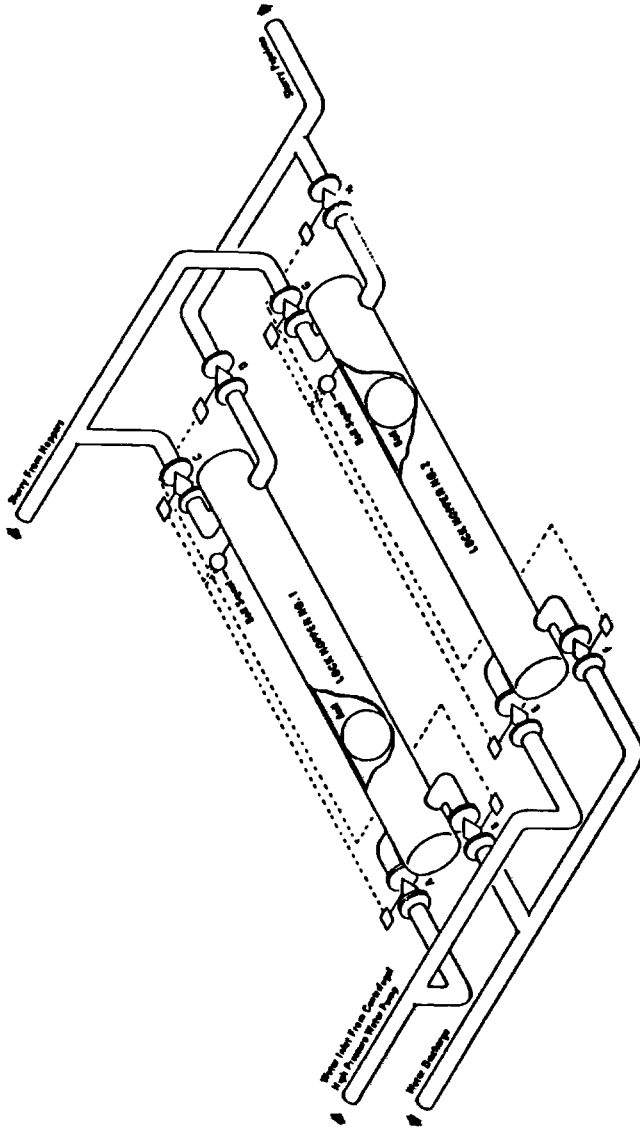


FIG. 1—The lock hopper system.

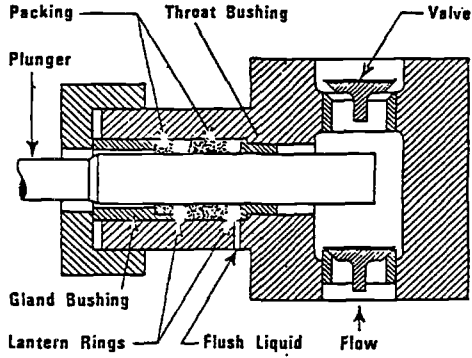


FIG. 2—Plunger pump—fluid end.

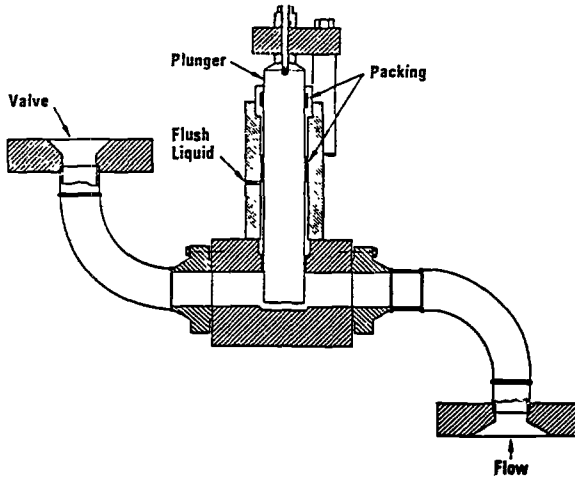


FIG. 3—Vertical plunger pump—fluid end.

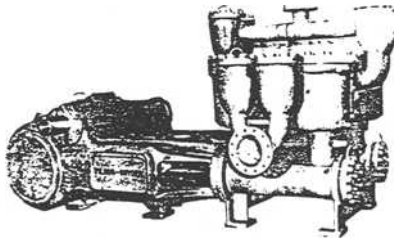


FIG. 4—Diaphragm pump with an 18-in. stroke.

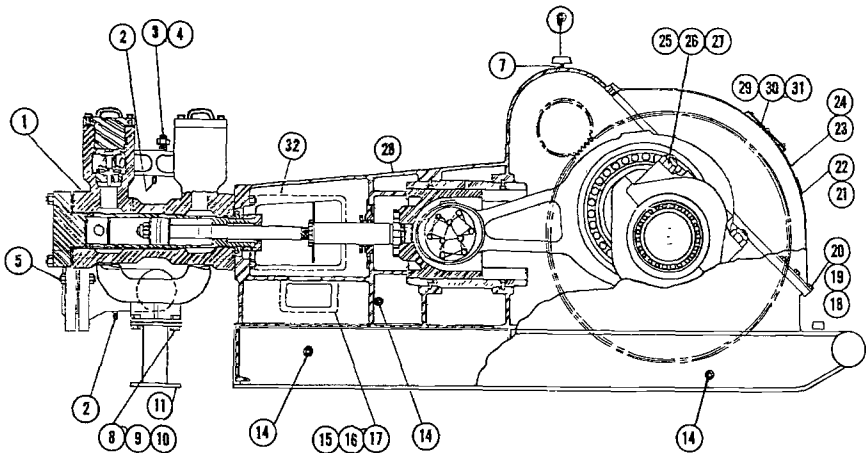


FIG. 5—Positive displacement pump. See Tables 2 and 3 (overleaf) for key to numbers.

The parts experiencing wear are valves, valve seats, plunger or piston packing, plunger sleeves or cylinder liners, and brass bushing. Consequently, these parts should have quick replacement features.

Fluid End Valve

A slurry valve must have two fundamental characteristics.

1. It must have sufficient strength to resist loads imposed by fluid pressure above it.
2. It must be able to seal against this pressure in the presence of solid particles of various sizes.

In general, fluid velocity must be limited through the valve because of erosion at high velocities. When this is properly taken into account in the valve design, this will result in limiting the bearing area between the valve and the valve seat.

To provide adequate supporting means for the pressure loads, there must be sufficient metal to metal bearing area. Hence a compromise in the design will have to be made, and ribs are generally used with elastomeric seal.

Packings

A nonadjustable-type lip packing gives superior service. Full section packings are not satisfactory and are avoided. There is a tendency for abrasives to enter the sealing surface. If the abrasive is imbedded in the packing, a grinding lap occurs which greatly accelerates the wear of the metal surfaces on the rod or plunger.

TABLE 2—Legend for Fig. 5.

Item	Required	Description	Comm. No.
1	1	Fluid end studded	17-402-301
2	6	1-in. X-hvy bull plug	42-753-008
3	12	1 $\frac{3}{8}$ to 8 by 7-in. stud	49-006-443
4	36	1 $\frac{3}{8}$ by 8-in. hvy hex. nut	75-511-754
5	16	1 $\frac{3}{8}$ to 6 by 9 $\frac{1}{4}$ -in. stud w/2 hvy hex. nuts	40-890-047
6	2	Breather	06-025-469
7	2	Nipple-breather	06-025-472
8	8	1 $\frac{1}{4}$ -in. lockwasher	75-770-310
9	8	1 $\frac{1}{4}$ to 7 by 3 $\frac{1}{2}$ -in. hex. hd. machine bolt	75-074-855
10	8	1 $\frac{1}{4}$ to 7-in. hvy hex. nut	75-510-320
11	1	Fluid end support	17-402-045
12	8	1 $\frac{1}{2}$ to 6 by 3 $\frac{3}{4}$ -in. hex. hd. capscrew	75-635-188
13	8	1 $\frac{1}{2}$ -in. lockwasher	75-770-312
14	5	2 std. cored pipe plug	86-485-116
15	20	$\frac{3}{8}$ to 11 by 1-in. hex. hd. H.T. capscrew	75-634-358
16	2	Access cover gasket	17-400-059
17	2	Access cover	17-400-054
18	1	Crankcase cover	17-400-048
19	1	Crankcase cover gasket	17-400-049
20	32	$\frac{3}{4}$ to 10 by 1 $\frac{1}{2}$ -in. hex. hd. H.T. capscrew	75-634-373
21	1	Lubrication instruction plate	17-127-119
22	4	No. 10 by $\frac{3}{8}$ -in. drive screw	75-632-012
23	1	Name plate	08-596-184
24	4	No. 2 by $\frac{1}{4}$ -in. drive screw	75-631-938
25	4	2 $\frac{1}{2}$ by 8-in. Type "U" elastic stopnut	75-509-036
26	4	Stud-main brg.	49-006-330
27	2	Main bearing caps	17-402-050
28	1	Frame end studded	17-402-054
29	2	Inspection cover	17-400-149
30	24	$\frac{1}{2}$ to 12 \times 1-in. lg. hex. hd. H.T. capscrew	75-634-349
31	1	Gasket	17-400-150
32	2	Cradle cover	17-400-151

Polyester elastomers are being widely used in sealing because of their high strength and wear characteristics coupled with excellent chemical- and oil-resistant properties.

Piston and Plungers

There is distinctly different behavior between packing in a piston pump and plunger packing in a single-acting pump.

The shape of lip-type packing in a single acting piston pump is made in such a way that the lip points towards the piston as it moves away during the suction stroke. The lips are relaxed due to lack of sealing pressure to hold the lips tightly against the metal surface. During the discharge stroke, the lip will seal the slurry between the piston and cylinder. The slurry piston is so constructed as to have three basic elements: the sealing elastomer, the fabric section, and a backup metal plate. Under hydraulic loading the rubber is pushed back against

TABLE 3—*Legend for Fig. 5.*

For 9 $\frac{1}{2}$ -in. by 18-in.	
Suction flange gasket	49-006-491
Suction dampener gasket	49-006-492
Discharge flange gasket	49-006-503
Discharge dampener gasket	49-006-504
For 12-in. by 18-in.	
14-in.–150 lb suction conn. gasket C/N 49-006-489	1 each at Station No. 1 Job No. 09-200-337
14-in.–300 lb suction flange gasket C/N 49-006-488	2 each at Station No. 3 & 4 Job No. 09-200-348
	1 each at Station No. 1 Job No. 09-200-337
4-in.–300-lb dampener gasket C/N 49-006-502	1 each at Station No. 3 & 4 Job No. 09-200-348
4-in.–150-lb dampener gasket C/N 49-006-490	1 each at Station No. 1 Job No. 09-200-337
10-in.–600 lb discharge flange gasket C/N 49-006-491	2 each at Station No. 1, 3 & 4
4-in.–600-lb discharge dampener gasket C/N 44-006-492	1 each at Station No. 1, 3 & 4
10-in.–600-lb suction	} Station No. 2
8-in.–900-lb discharge	
4-in.–600-lb suction Dampener	
4-in.–900-lb discharge dampener	

the fabric section and out against the liner to form a seal. The fabric section provides extension clearance control, and the metal backup plate provides structural capacity to hold the piston load. The interrelationship of these elements is a carefully balanced scheme of design.

In a plunger pump, the plunger moves towards the lip during the suction stroke and away during the pressure stroke. Thus, abrasives can enter under the packing lips; when lips are tight under pressure, they serve to scrap as well as to seal off abrasive material at the same time. For these reasons it is necessary that a clean liquid interface is created between the packing and the abrasive liquid for satisfactory plunger pump service.

Maintenance

The life of expendables has been considerably improved by use of special materials and designs evolved due to experimental analysis and the site experience on several pipeline installations. Initially only a life of 90 h was experienced for rubber valve inserts as against 1100 h for polyurethane inserts (Table 4).

Station Piping Design

Two types of pressure variations occur in a positive displacement pump station piping. The first type is the normal pressure pulse fluctuations associated

TABLE 4—*Life of expendables in slurry service.*

	Piston Pump	Plunger Pumps
Valves	1100 h	500 h
Piston rod	3000 h	. . .
Piston liner	4000 h	. . .
Packing	6000 h	425 h

with the sinusoidal variation in flow rate as the pump valve opens and closes with the stroke of the pump. The volume of dampener required to even out the variations in flow rate is readily determined using universal gas laws.

The second type of pressure fluctuation is more complex and potentially more serious. It is associated by pressure transients induced by sudden valve opening, thereby causing water hammer.

The suction conditions of the first positive displacement pump station in a slurry system are particularly important because the station is normally fed by centrifugal pumps. When a piston starts on a suction stroke, the suction valve opens and the suction pressure drops. The suction pressure then builds up before the next suction valve opens. In this period the flow is accelerating in the suction piping. The energy in the suction system is supplied by a centrifugal pump.

It should be noted that the sudden suction valve opening induces a pressure transient (spike) in the suction piping. Suction stabilizers are used to avoid pulsation and vibrations.

In order to minimize pressure pulsations, pump station piping should be as simple as practical, preferably in a single plane, with adequate supports. In addition, the allowable pipe wall hoop stresses should be reduced to take into account cyclic fatigue stresses of moderate to high frequency.

Centrifugal Pumps

Centrifugal pumps are the workhorse of in-plant commercial slurry systems. Their application is generally restricted to short distances because of their limited head capability, lower allowable casing pressures, and lower efficiencies. On long distance slurry pipeline systems, they serve as booster pumps providing suction pressure required for mainline reciprocating pumps.

Rubber-lined pumps are generally limited to fine slurries in which the maximum particle size is less than 8 mesh. Impeller tip speed is generally limited to 1341 m (4400 ft)/min in these pumps.

Wear-resistant, metal-lined pumps or pumps with special metallurgy having hardness up to 700 HB are used for pumping corrosive particles. Higher impeller tip speed is permissible in case of metal pumps.

As wear causes an accumulated loss of material, clearance between the rubbing surfaces increases, reducing the efficiency and the working life of

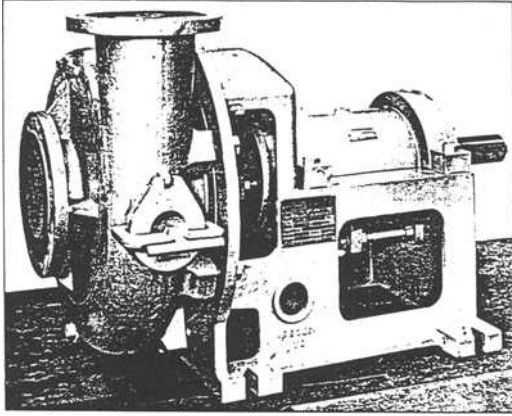


FIG. 6—*Jeumont-Schneider pump LC.*

pump. Centrifugal slurry pumps are therefore designed with special wear plates between rotating and stationary parts, and liberal clearances are provided in the design.

For pumping, aluminum slurry centrifugal pumps were earlier used with stuffing box packings, where it was required to inject water to stop leakage. The pressure of water was injurious to the process, and the maintenance of such a system was a costly process.

New mechanical seals are now developed to deal with suspensions that are abrasive, crystalline, and susceptible to precipitation or separation or to centrifugal forces (Figs. 6 and 7).

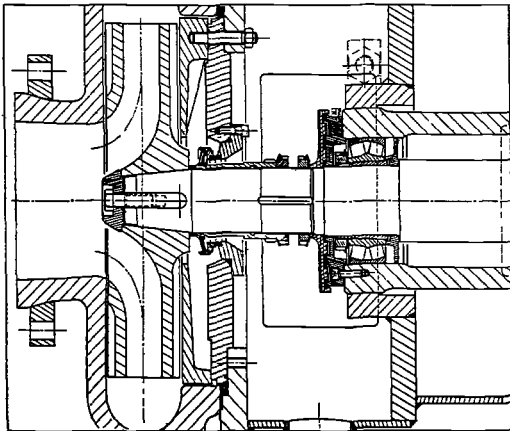


FIG. 7—*Section Querschnitttriss.*

Conversion of Water Performance to That of Slurry

Centrifugal pumps are normally tested with water, and then performance is evaluated for slurry pumping at the site.

Whenever a pump is handling solids in water, the power input to the pump is directly proportional to the specific gravity of the mixture Sm . Specific gravity of mixture

$$Sm = \frac{1 - C}{1 - c_w} \quad (1)$$

where

C = volume fraction of solids,
 c_w = weight fraction of solids, and

$$C = \frac{Sm - S_w}{S_s - S_w}$$

where suffixes m , w , and s stand for mixture, water, and solids, respectively, and S stands for specific gravity. For cold water $S_w = 1.0$.

Similarly weight fraction

$$C_w = \frac{\text{weight of solids}}{\text{weight of mixture}} = \frac{S_s (Sm - 1)}{S_m (S_s - 1)} = C \frac{S_s}{Sm} \quad (2)$$

Hence always $C_w > C$

$$Sm = \frac{1 - C}{1 - c_w} \quad (3)$$

For homogeneous mixture, pipe friction loss is the same as for clear water if expressed in meters of mixture. At best efficiency point (bep) for a given capacity: head(mixture) = $H(\text{water})$ – additional losses caused by the presence of solids in pump passages.

The consistency conversion chart is given in Figs. 8 and 9 when pumping liquids of higher density than water (solids in suspension).

NPSH required = NPSH required for water. But NPSH available in meters of mixture is reduced by the fact that the atmospheric pressure expressed in metres of mixture may be considerably low.

The net effect of solids in suspension in water handled by centrifugal pumps is in increase of the average of apparent specific gravity. For a given capacity such as at bep, head mixture produced by the impeller is same as H water—additional hydraulic losses are caused by the presence of solids in pump passage.

For homogeneous mixtures, pipe friction losses expressed in meters of mixture are the same as for clear water.

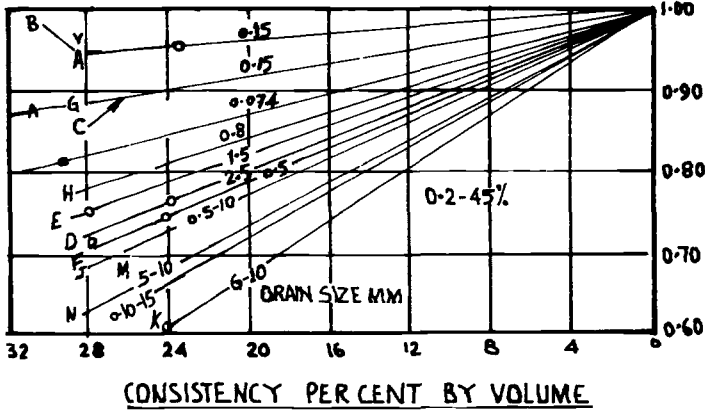


FIG. 8—Ratio of efficiency mixture/efficiency water versus consistency.

The efficiency of a pump handling solid liquid mixture is reduced in the same ratio as the head of mixture to head of clear water

$$\frac{H_m}{H} = \frac{e_m}{e}$$

The ratio of break horse power (bhp) at bep to that obtained when handling water is appreciably lower than the S_m , indicating that there is a reduction in disk friction loss as compared to that of newtonian fluids of the same density.

TABLE 5—Legend for Figs. 8 and 9.

SYMBOL	SOLIDS	SIZE GRAIN	SOURCE	REMARKS
A	CLAY-SPL	< 0.15	HERBICH ET AL	$H_m/H = e_m/e$
B	PHOSPHATE MATRIX		ANTUNES	$H_m/H = e_m/e$
C	FLY ASH	< 0.074	HASEGAWA	$H_m/H = e_m/e$
D	STAND	2.5	TERADA	$H_m/H = e_m/e$
E	STAND	1.3	TERADA	$H_m/H = e_m/e$
F	STAND	0.5	TERADA	$H_m/H = e_m/e$
G	GYPSUM		ANTUNES	$H_m/H = e_m/e$
H	STAND	0.8	FAIRBANKS	$H_m/H = e_m/e$
J	STAND	0.5-1.0	HASEGAWA	$H_m/H = e_m/e$
K	GRAVEL	6-10	HASEGAWA	$H_m/H = e_m/e$
L	STAND	< 0.5	O'BRIEN	$H_m/H = e_m/e$
M	COAL	0-0.5	SASAKI	$H_m/H > e_m/e$
N	COAL	5-10	SASAKI	$H_m/H > e_m/e$
O	COAL	10-15	SASAKI	$H_m/H > e_m/e$
P	DIFFERENT	MIXTURE	HOTTA	$H_m/H = e_m/e$

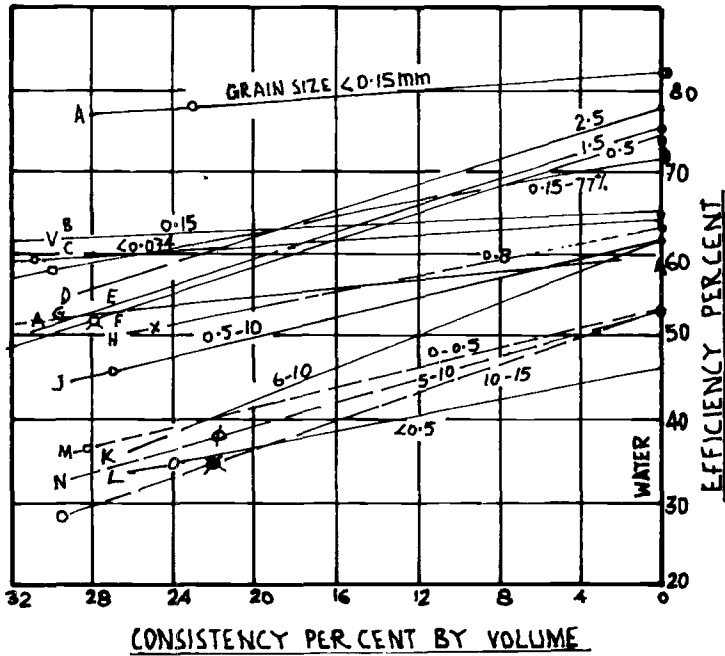


FIG. 9—Efficiency versus consistency.

Conclusion

With a promising future ahead for slurry pipeline, a great deal of emphasis has been placed on the pumps to move these granulated solids/liquid mixtures. Generally speaking, the pumps to be installed on a new generation slurry pipeline will be adaptations of existing pumps.

Reciprocating pumps have the desirable characteristic of maintaining high volumetric efficiency at any desired flow rate. This allows a greater flexibility in system design. Piston pumps are used for less abrasive slurries up to 13 790 kPa (2000 psi) pressure, and for plunger pumps for higher pressure to pump high abrasive slurries.

Abrasive-laden fluids such as slurries have a deteriorating effect on impellers and casings due to erosion caused by fluid and suspended particles. Centrifugal pumps therefore are used where the internal velocity of flow is relatively low. The development of special material is necessary to make centrifugal pumps viable for use in high-pressure applications.

The crucial point is to achieve long life of expendables to make the system economically viable. In the future, many schemes for the transportation of coal, iron, and other slurries are envisaged in India and in other parts of the world.

APPENDIX

Slurry Material	System	Length, Miles	Diameter, Inches	Annual Throughput	Initial Operation	Type of Pump	Manufacturer	Pump Drive HP	Flow per Pump, gallons per min (m ³ /h)	Max Discharge Pressure, psi (kg/cm ²)	Concentration, % by Wt.	Max Particle Size, mesh
Coal	Consolidation	108	10	1.3	1957	Double acting duplex piston	Wilson-Snyder	450	550 (124.85)	1200 (86.5)	50	14
Limestone	Black Mesa	273	18	4.8	1970	Double acting duplex piston	Wilson-Snyder	1500 1750 1750	2100 (476.7) 1400 (317.8) 2100 (476.7)	1080 (76.05) 1785 (125.70) 1165 (82.09)	45 to 50	14
	Calaveras	17	7	1.5	1971	Double acting duplex piston	Continental Eimco	700	820 (186.14)	1275 (89.79)	70	28
	Rugby Trinidad	57 6	10 8	1.7 0.6	1964 1959	Vertical triplex plunger -do- -do-	Armco Steel Wilson-Snyder	750 180	286 (64.92) 310 (70.37)	2100 (147.88) 960 (67.60)	50 to 60 80	35 48
Copper concentrate	Columbia Bougainvillea	17 17	7 6	0.4 1.0	1944 1972	Vertical triplex plunger -do-	Ingersoll-Rand Aldrich	700	482 (109.41)	2000 (190.84)	55 to 70	65
	West Iraman	69	4	0.3	Under construction	Triplex plunger -do-	Wilson-Snyder	300	138 (31.33)	2300 (161.97)	60 to 65	100
Magnetite concentrate	KBI Turkey	38	5	1.0	-do-	Triplex plunger -do-	Wilson-Snyder	350	250 (56.75)	2100 (197.8)	45	100
	Tasmania	53	9	2.3	1961	Centrifugal	-do-	600	387 (87.85)	2000 (190.84)	55 to 60	160
	Waipipi (land) Waipipi (off-shore)	04 1.3	8 12	1.0 1.0	1911 1911	Centrifugal -do-	Allen Sherman Hoff Harleton/Barratt Haenertens	250 800	2300 (522.1) 6450 (1464.15)	400 (28.17) 685 (48.23)	45 45	28 28
Gilsonite	American Gilsonite	72	6	0.4	1957	Double acting duplex piston	Wilson-Snyder	300	165 (37.5)	2150 (151.4)	48	4
Deeds Nickel refinery tailings	Japan Western running	44 4.3	12 4	0.6 0.1	1968 1970	Triplex plunger	Mars Ingersoll-Rand Aldrich	500 30	821 (186.4) 98 (22.2)	710 (50) 415 (29.2)	18 49.60	Slimes 48

Acknowledgments

The author is thankful to the management of Bharat Pumps & Compressors Ltd., Naini/Allahabad for giving permission to submit this paper.

Bibliography

- Lin, S. H., "Pressure Drop for Slurry Transport," General Electric Co.
Rizzone, M. L., Miller, J. E., and Schmineanan, T. E., "Slurry Pumps—Some Design Considerations."
"Solid Handling Pumps," Hydraulic Pumps Department, Jeumont-Schneider.
"System for Slurry Transportation," *Engineering and Mining Journal*, June 1979.
Thompson, T. L., Frey, R. J., Cowper, N. T., and Wasp, E. S., "Slurry Pumps—A Survey."

Subject Index

A

- Abrasion**
 metal-ceramic coatings
 performance, 37–38
 tests in Alundum and silica sand slurries, 23–25, 27–28
 wear morphology, 31–35
- Abrasion resistance**
 CM 500L-coated steel mud pump liners
 field simulation, 107, 111–114
 laboratory tests, 105–107, 109–111
 Miller Slurry Abrasivity Test adaptation, 105–107
 optimum hardness value, 114
 wear life predictions, table, 113
- Abrasive wear, alloy and stainless steels under dry and wet corrosive conditions, fig., 10**
- Alloy and carbon steels**
 1018
 abrasion tests in Alundum and silica sand slurries, 23–25, 27–28, 31–35
 CM 500L-coated mud pump liners, 105–114
 erosion tests in Alundum and silica sand slurries, 25, 29–31, 35–37
 erosivity of coal particles in coal-solvent slurries, 68–76
 1020, 1060, 1080, 4142, and 8740, flow-through slurry wear rates, table, 177
 1065
 ball mill test, 6, 9, 11–16
 hub test, 6–11
 1090, fifth SAE round-robin test results, table, 220
 4340
 ball mill test, 6, 9, 11–16
 hub test, 6–11
 4342
 cutting and deformation wear in recycled slurry test, fig., 179
 slurry wear in flow-through slurry system, fig., 176
 slurry wear in recycled-slurry system, fig., 178
 5145
 flow-through slurry wear rate, table, 177
 slurry wear in flow-through slurry system, fig., 176
 slurry wear in recycled-slurry system, fig., 178
 A36
 corrosion loss in limestone slurry scrubbers, 121–130
 linear polarization and weight

- loss measurements, fig., 128
 - pitting, spray slurry effect, 132
 - scrubber location effect, fig., 126
 - A514
 - flow-through slurry wear rate, table, 177
 - slurry wear comparison in flow-through and recycled systems, fig., 180
 - slurry wear in flow-through slurry system, fig., 176
 - slurry wear in recycled-slurry system, fig., 178
 - wear surfaces comparison in flow-through and recycled slurry tests, fig., 182
 - Astralloy V
 - ball mill test, 6, 9, 11–16
 - hub test, 6–11
 - Hadfield manganese
 - ball mill test, 6, 9, 11–16
 - hub test, 6–11
 - Ni- and Co-based hardfacings,
 - slurry wear in recycled slurry system, 177–182
 - T-1 low-alloy, fifth SAE round-robin test results, table, 221
 - various, Wet Sand/Rubber Wheel Test results, table, 225
 - Alumina particles
 - oscillatory device for simulating wear by friction, 189–192
 - wear patterns in dense slurry flow, 188–189
 - Aluminum alloys
 - Al 6061
 - ball mill test, 6, 9, 11–16
 - hub test, 6–11
 - Aluminum, recycled coal-water slurry erosivity, 81–84
 - Alundum slurries
 - abrasion of metal coatings
 - material loss, 27–28
 - test procedure, 23–25
 - erosion of metal coatings
 - material loss, 29–31
 - test procedure, 25
 - particulate hardness and abrasion/erosion, 37–40
 - Ash content, coal, effect on erosivity, 67–68, 76
 - ASTM Standards
 - A 36/A36M-84a:121
 - D 1141-75:12
 - D 2000-80:226
 - D 2240-84:229
 - E 10-84:94
 - E 140-84:96
 - E 384-84:94
 - G 1-81:121
 - G 65-84:23
 - G 75-82:93
 - G 75-82:155
- B**
- Ball mill test for corrosive wear
 - alloy and stainless steels, 6, 13–16
 - methods, 9
 - Nitronic 30, 6, 13–15
 - Brinell hardness, 94
 - pipe materials, table, 97
 - slurry materials, table, 98
- C**
- Carbon steels (*See* Alloy and carbon steels)
 - Ceilcote systems, characteristics, application rates, and costs, table, 136
 - Centrifugal pumps, 254–255
 - conversion of water performance to slurry performance, 256–257
 - Ceramics, in pumps, 246
 - Chemical vapor deposition, 104
 - reactor, fig., 105

- CM 500L
 coated steel mud pump liners,
 wear life prediction, table,
 113
 controlled nucleation thermochem-
 ical deposition, 104, 107–
 109
 long-time simulation tests for
 slurry resistance, fig., 112
 optimum hardness value, 114
 properties, table, 108
 slurry abrasion behavior
 in alkaline slurry, fig., 111
 of chromium plating and, fig.,
 112
 in neutral slurry, fig., 110
 on steel, long-time simulation,
 fig., 102
- Coal-kerosene slurries
 erosion of 1018 steel, 68–73
 ash content effect, 67–68, 71–73
 ash oxide effects, 67–68
 particle shape and distribution
 effects, 63, 68
 particle size effects, 66–68, 69–
 72
 pot tester, 67–68
- Coal-oil slurries
 erosivity for mild and stainless
 steels
 erosion-corrosion interaction, 57
 mass loss data, 52–56
 pot tester, 50–51, 60–61
 solids loading effects, 52–53, 55
 specimen rotation speed effects,
 57–58
 stabilizing additives, 56–57
- Coal particles
 shape, effect on erosivity, 63, 68,
 76
 size, effect on erosivity, 68–73,
 75–76
- Coal vacuum bottoms-tetrahydrofuran
 slurries
 erosion of 1018 steel, 73–76
 cumulative erosion rates, fig.,
 75
 incremental erosion rates, fig.,
 74
- Coal-water slurries
 erosivity of mild and stainless
 steels
 erosion-corrosion interaction, 57
 mass loss, 52, 54, 56
 solids loading effects, 54
 stabilizing additives, 56
 recycling during erosivity testing
 mineralogy, 85–87
 peaking behavior, 81–84
 procedure, 80–81
 viscosity, pH, and particle size
 changes, 84–85
- Coatings
 CM 500L (*See* CM 500L)
 thickness, wear distribution meas-
 urement, 196–197
 Wet Sand/Rubber Wheel Test,
 table, 225
- Cobalt-based hardfacings, slurry wear
 in recycled slurry system,
 177–182
- Coke-oil slurries
 erosivity of mild and stainless
 steels
 erosion-corrosion interaction, 57
 factors affecting, 53–56
 pot tester, 50–51
 solids loading effects, 51–53
 specimen rotation speed effects,
 57–58
 stabilizing additives and, 56–57
- Concentration effects, erosivity of
 coal-oil, coal-water, and
 coke-oil slurries, 52–56
- Controlled nucleation thermochemical
 deposition
 chemical vapor deposition reactor,
 104, fig., 105

- CM 500L coating on steel mud pump liners
 - development, 104, 107–109
 - properties, table, 108
 - Corrosion-erosion protection
 - limestone slurry scrubbers, 134–138
 - coating failures, 136–138
 - materials selection, 134–136
 - surface preparation, 137–138
 - Corrosion rates
 - in limestone spray slurry, 121–130
 - 316 and T304L stainless steel, table, 127
 - A36 carbon steel, table, 126–128
 - two-electrode linear polarization system, 119–130
 - Corrosive wear
 - alloy and stainless steels, 9–16
 - hub test, fig., 11
 - ball mill test, fig., 13
 - ball mill test with synthetic seawater, fig., 15
 - Corrosivity, in limestone slurry scrubbers, 121–122
- D**
- Departure value, formulas, 163
 - Diaphragm pump, 248, fig., 250
 - Dry sand rubber wheel abrasion test, 38
- E**
- Electrical capacitance, pipeline erosion measurement, 93
 - Energy approach, erosion wear distribution, 195–197
 - Epoxy resin, 188, 194–195
 - Erosion
 - in dense slurry flow
 - energy approach, 195–196
 - numerical flow simulation, 197–198
 - predictive approach, 189
 - procedure, 198
 - flow-through and recycled-slurry tests
 - comparison, 179–182
 - equipment and specimens, 170–174
 - procedures, 175
 - wear losses and wear rates, 175–179
 - metal-ceramic coatings
 - performance, 39–40
 - tests in Alundum and silica sand slurries, 25–26, 29–31
 - wear morphology, 35–37
 - Erosion-corrosion interaction, effect of stabilizing additives, 57
 - Erosion-corrosion tests
 - vibratory and jet-in-slit apparatuses, 143–145
 - damage on pump components, 150–151
 - materials and damage rates, 145, 148–149
 - particle impact parameters, 153
 - slurries, table, 146, 152–153
 - Erosion testing
 - peaking behavior, 88–89
 - peaking behavior of recycled coal-water slurries, 81–84
 - in pipeline systems
 - absolute measurements, 92–93
 - comparative hardness values for pipeline materials, table, 97
 - Miller numbers and hardness values for slurry materials, table, 98
 - relative values, 93–96
 - Erosivity
 - coal particles in coal-solvent slurries, 67–73
 - ash content effects, 67–68
 - incremental and cumulative erosion, 68–73

- oxide shape and distribution
 - effects, 68
 - particle size distribution effects, 68
- coal vacuum bottoms in coal-solvent slurries, 73–76
- relative, coal-oil, coal-water, and coke-oil slurries, 47–61
- Erosivity testing
 - coal-water slurry recycling, 80–88
 - mineralogy, 85–87
 - peaking behavior, 81–84
 - viscosity, pH, and particle size changes, 84–85
- F**
- Flow, dense (*See* Slurry flow, dense)
- Flow rate, effect on erosion wear distribution in casing, fig., 206
- Flow-through slurry test
 - electromechanical measurements, 174
 - equipment and specimens, 170–174
 - particles, comparison with recycled slurry test particles, fig., 181
 - procedure, 175
 - and recycled-slurry tests, 179–182
 - wear losses and wear rates, 176–177
- Friction erosion, oscillatory device for simulation, 189–192
- Fuel recycling during erosivity testing
 - mineralogy, 85–87
 - peaking behavior, 83–84, 87–89
 - slurry erosivity, 81–84
 - viscosity, pH, and particle size changes, 84–85
- G**
- Gypsum slurries, erosion–corrosion tests, 145–146, 152–153
- H**
- Hardfacings, Ni- and Co-based, slurry wear in flow-through and recycled-slurry tests, 175–179
- Hardness
 - Alundum and silica particulates, 37–40
 - CM 500L, optimum value, 114
 - indices for pipeline erosion, 94–95
 - metal-ceramic coatings
 - abrasion performance, 37–38
 - Alundum abrasion tests, fig., 31
 - erosion performance, 39–40
 - silica abrasion tests, fig., 29
 - silica and Alundum erosion tests, fig., 33
 - table, 22
- Hastelloy C, slurry erosion–corrosion, 145–150
- Hub test for corrosive wear
 - alloy and stainless steels, 6, 9–11
 - methods, 6–9
- I**
- Impact
 - erosion wear patterns by particle, 188–189
 - particles-wall interaction, 195–197
- Impingement
 - angle, effect on pump wear, 244
 - particles in dense slurry flow, 188–189
- Inclined wall
 - erosion wear by impact, 192–196
 - total wear distribution, energy approach, 197–198
- J**
- Jet impingement slurry erosion tester, 25–26
 - suitability for coatings, 40–42
- Jet-in-slit method for erosion–corrosion tests

- apparatus and procedure, 144–145
 - damage rates, fig., 148–149
 - materials, 145
- K**
- Kerosene-coal slurries (*See* Coal-kerosene slurries)
 - Kinetics, corrosion, in limestone slurry scrubbers, 131, 135
 - Knoop Hardness Number, 94, 96
 - pipe materials, table, 97
 - slurry materials, 98
- L**
- Lap wear, degrees, 158
 - LCO-17
 - abrasion tests
 - materials loss, 27–28
 - procedure, 23–25
 - wear morphology, 31–35
 - erosion tests
 - materials loss, 27–28
 - procedure, 25
 - wear morphology, 35–37
 - LCO-22
 - abrasion tests
 - materials loss, 27–28
 - procedure, 23–25
 - wear morphology, 31–35
 - erosion tests
 - materials loss, 27–28
 - procedure, 25
 - wear morphology, 35–37
 - Limestone slurry scrubbers
 - corrosion protection
 - coating failures, 136–138
 - materials selection, 134–136
 - surface preparation, 137–138
 - corrosion rate
 - distribution and chemical composition of deposits, table, 130–131
 - effect of dissimilar metals and scaling deposits, 131–134
 - linear polarization method, 119–121
 - probe multiplier, 123–125
 - weight-loss and linear polarization results, tables, 127–128
 - weight-loss method, 121
 - Linear polarization, two-electrode
 - corrosion rates in limestone slurry scrubbers, 119–123
 - comparison with weight-loss methods, table, 126–128
 - method, 119–121
 - pitting factor, 130–134
 - probe multiplier, 123–125
 - Lock Hopper pumps, 248, fig. 249
 - LW-5
 - abrasion tests
 - materials loss, 27–28
 - procedure, 23–25
 - wear morphology, 31–35
 - erosion tests
 - materials loss, 27–28
 - procedure, 25
 - wear morphology, 35–37
 - LW-26
 - abrasion tests
 - material loss, 27–28
 - procedure, 23–25
 - wear morphology, 31–35
 - erosion tests
 - materials loss, 27–28
 - procedure, 25
 - wear morphology, 35–37
- M**
- Metal-ceramic coatings
 - abrasion performance, 37–38
 - abrasion tests in Alundum and silica sand slurries
 - materials loss, 27–28
 - procedure, 23–25
 - wear morphology, 31–35

- erosion performance, 39–40
 - erosion tests in Alundum and silica sand slurries
 - materials loss, 29–31
 - procedure, 25
 - wear morphology, 35–37
 - hardness, 29, 31, 33, 37, 40, 42
 - Metals, deformation wear in pumps, 245–246
 - Metrology, pipeline erosion measurement, 93
 - Mild steel
 - erosion damage pattern in coke-oil slurry, 58, fig., 60
 - erosivity in coal-oil and coke-oil slurries, 52–55
 - surface damage in coke-oil slurry, 57, fig. 59
 - Miller number, 93–94
 - pump material selection, 244–245
 - SAR test and, 155–156
 - slurry materials, table, 98
 - Miller Slurry Abrasivity Test
 - adaptation for abrasion resistance, 105–107
 - apparatus modifications, table, 108
 - procedure modifications, table, 107
 - for CM 500L-coated steel mud
 - pump liners, 105–107
 - field simulations, 107, 111–114
 - laboratory test methods, 105–107, 109–111
 - Miller Slurry Abrasivity Tester, fig., 106
- N**
- Neutron activation, pipeline erosion measurement, 93
 - Nickel-based hardfacings, slurry wear in recycled slurry system, 177–182
 - Nitronic 30
 - abrasive wear under wet and dry corrosive conditions, fig., 10
 - corrosive wear, figs., 11, 13, 15
 - ball mill test, 6, 9, 11–16
 - hub test, 6–11
 - Nucleonic gaging, pipeline erosion measurement, 93
 - Numerical flow simulation
 - dense slurries, 197–198
 - pump casing, basic equations, 208
- O**
- Oscillatory device for simulating erosion by friction, 189–190
 - Oxides, coal, effects on erosivity, 68, 76
- P**
- Packings
 - piston and plunger pumps, 252–253
 - in slurry pumps, 251–252
 - Particle(s)
 - impingement angle, effect on pump wear, 244
 - shape, effect on erosivity, 63, 68, 76
 - size
 - changes during coal-water slurry recycling, 84–85
 - and sharpness, effect on pump wear, 244
 - velocity, vibratory and jet-in-slit erosion-corrosion tests, 143, 153
 - Particles-wall interaction, 195–197
 - Peaking behavior
 - cause, 87–88
 - characterization, 83–84
 - erosion testing and, 88–89
 - Permanent magnet gaging, pipeline erosion measurement, 93

- Petroleum coke-oil slurries (*See* Coke-oil slurries)
- pH, changes during coal-water slurry recycling, 84–85
- Pipeline erosion by slurries
 absolute measurement methods, 92–93
 hardness values for pipe materials, table, 97
 Miller numbers and hardness values for slurry materials, table, 98
 relative erosion values, 93–96
 research, 98–99
- Pipes, typical wear patterns, fig., 206
- Piping, positive displacement pumps, 253–254
- Piston pumps, 248
 life of expendables, table, 254
- Pitting factor, in limestone slurry scrubbers, 130–134
- Plastics, in pumps, 246
- Plunger pumps, 248, fig., 250
 life of expendables, table, 254
- Polyamide resin, 188, 194–195
- Positive displacement pumps, 248, fig. 251
 station piping design, 253–254
- Pot tester
 coal-oil, coal-water, and coke-oil slurries, 50–51
 coal-solvent slurries, 65–67, 76
 problems, 60–61
 for relative corrosivity of coal-oil, coal-water, and petroleum coke-oil slurries, 50–51
- Predictive model for numerical simulation of wear by impact and friction, 197–198
- Pumps
 casing, basic equations for numerical flow simulation, 208
 centrifugal, 254–257
 erosion component, energy approach, 197–200
 positive displacement
 fluid end, 248–251
 fluid end valve, 251
 lock hopper, 248
 maintenance, 253
 packings, 251–252
 pistons and plungers, 252–253
 station piping design, 253–254
 vibratory and jet-in-slit erosion-corrosion testing apparatuses and procedures, 143–145
 component damage, 150–151
 materials, 145
 wear, factors affecting
 hydraulic design, 246–247
 pump material properties, 245–246
 slurry properties, 244–245
 solid particles, 244
- Pyrite, in sink fraction during coal-water slurry recycling, 86–87

Q

- Quartz sand, in Wet Sand/Rubber Wheel Abrasion Test, 226

R

- Radionuclides, wear distribution measurement, 196–197
- Recycled slurry test
 electromechanical measurements, 174
 equipment and specimens, 174
 flow-through tests and, 179–182
 particles, comparison with flow-through test particles, fig., 181
 procedure, 175
 slurry wear, 177–179

- wear kinetics, 178–179
- Rubber, deformation wear in pumps, 246
- “Rubber Wheel Abrasion Test” (Borik), 215
- Rubber Wheels, in Wet Sand/Rubber Wheel Abrasion Test, 226, 229, 230

S

- Sand particles
 - oscillatory device for wear by friction, 189–192
 - wear patterns in dense slurry flow, 188–189
- Sand-water slurries, impact erosion on an inclined wall, 192–196
- SAR number
 - calculation, 159–161
 - departure value, 163
 - typical, 162
 - uses, 161–162
- SAR test (*See* Slurry Abrasion Resistance Test)
- Scrubbers, limestone slurry (*See* Limestone slurry scrubbers)
- Silica sand slurries
 - abrasion of metal-ceramic coatings materials loss, 27
 - test procedure, 23–25
 - abrasive particles, comparison in flow-through and, recycled slurry tests, fig., 181
 - erosion-corrosion tests, 145–146, 152–153
 - erosion of metal coatings material loss, 29–31
 - test procedure, 25–26
 - flow-through and recycled-slurry tests, 176–179
 - particulate hardness and abrasion/erosion, 37–40
- Sink fraction, during coal-water slurry recycling, 85–87
- Sliding-bed erosion, oscillatory device for simulation, 189–192
- Slurry Abrasion Resistance Test
 - equipment, 156–157
 - lap wear, 158
 - procedure, 157–158
 - SAR number
 - calculation, 158–161
 - departure value, 163
 - typical, 162
 - uses, 161–162
- Slurry flow, dense
 - erosion on an inclined wall, 192–196
 - numerical analysis and applications flow modeling, 197–198
 - procedures, 198
 - results for pumps, 198–200
 - wear by friction, 189–192
 - wear distribution measurement, 196–197
 - wear patterns, 188–189
- The Society of Automotive Engineers Iron and Steel Technical Committee, 213
- SAE Draft XJ1185 (Wet-Sand Rubber-Wheel Abrasion, Test Method), 232–239
- Stainless steels
 - 17-4 PH
 - ball mill test, 6, 9, 11–16
 - hub test, 6–9
 - 304
 - ball mill test, 6, 9, 11–16
 - erosivity of coal-oil, coal-water, and coke-oil slurries, 52–61
 - fifth SAE round-robin test, 223
 - flow-through slurry wear, fig., 176
 - flow-through slurry wear rate, table, 177
 - recycled-slurry wear, fig., 178

- hub test, 6–9
- 316
 - ball mill test, 6, 9, 11–16
 - corrosion loss in limestone slurry scrubbers, 121–130
 - flow-through slurry wear rate, table, 177
 - hub test, 6–9
 - recycled slurry wear, fig., 178
- 316L
 - corrosion loss in limestone slurry scrubbers, 121–130
 - vibratory and jet-in-slit tests for erosion-corrosion, 145–150
- 409
 - ball mill test, 9, 11–16
 - hub test, 6–9
- 410
 - ball mill test, 6, 9, 11–16
 - hub test, 6–9
- 416, recycled coal-water slurry erosivity, 81–84
- Nitronic 30 (*See* Nitronic 30)
- Standardization, in pipeline erosion studies, 98
- Stauffer's Gridding Pot Device, 142
- Steel mud pump liners, 111–114
 - CM 500L coating
 - controlled nucleation thermochemical deposition, 104
 - properties, table, 108
 - field simulation procedures, 107, 111–114
 - laboratory testing procedures, 105–107, 109–111
 - Miller Abrasivity Test
 - modifications, 105–107
 - apparatus, table, 108
 - procedure, table, 107
- Surface activation, pipeline erosion measurement by, 93

T

- Tetrahydrofuran-coal slurries (*See* Coal-tetrahydrofuran slurries)
- Thermosetting resins, for limestone slurry scrubbers, 134–137
- Tool steel D-2, fifth SAE round-robin test, table, 222
- Tungsten carbide, recycled coal-water slurry erosivity, 81–84

U

- UHMW polyethylene, flow-through slurry wear rate, table, 177
- Ultrasonic gaging, pipeline erosion measurement, 93

V

- Vacuum bottoms, coal (*See* Coal vacuum bottoms)
- Valves, slurry, 251
- Velocity effects, surface damage, 57–58
- Vibratory method for erosion-corrosion tests
 - apparatus and procedure, 143–144
 - damage rates, fig., 148
 - materials, 145
- Vickers Hardness Number, 94–96
 - for pipe materials, table, 97
- Viscosity, changes during coal-water slurry recycling, 84–85

W

- Wear
 - CM 500L-coated steel mud pump liners
 - field simulation experiments, 107, 111–114
 - laboratory test methods, 105–107, 109–111
 - prediction, table, 113

- deformation
 - metals in pumps, 245–246
 - rubbers in pumps, 246
- distribution in casing, flow rate effect, fig., 206
- by friction
 - alumina particles on various plate materials, fig., 191
 - sand particles on polyamide resin, fig., 191
- by impact
 - in dense slurry flow, 192–196
 - energy approach to, 195–197
- morphology of metal-ceramic coatings
 - abrasion tests, 31–35
 - erosion tests, 35–37
- patterns
 - in dense slurry flow, 188–189
 - in slurry pipes, fig., 206
- Wear resistance, SAR number calculation, 158–161
- Wear tests
 - flow-through (*See* Flow-through slurry test)
 - recycled (*See* Recycled-slurry test)
- Weighing, pipeline erosion measurement, 93
- Weight-loss method for corrosion rates in limestone slurry
 - scrubbers
 - comparison with linear polarization methods, table, 126–128
 - procédure, 121
- Wet Sand/Rubber Wheel Abrasion Test
 - 304 stainless steel, table, 223
 - 1090 steel, table, 220
 - D-2 tool steel, table, 222
 - round-robin tests
 - first, 215–216
 - second, 216–217
 - third, 217
 - fourth, 217–218
 - fifth, 218–224
 - summary, table, 218
 - status, 219–224
 - T-1 low-alloy steel, table, 221
 - variables
 - abrasives, 226
 - laboratory techniques, 228–229, 230–231
 - rubber wheels, 226, 230
 - test equipment, 228
 - test material, 227–228
 - various material groups, table, 225
- Wet sand/rubber wheel abrasion testing machine, 24–25
- suitability for coatings, 38–39

Author Index

A
 Addie, G. R., 185
 Avery, H. S., 211

B
 Bhat, D. G., 103
 Blickensderfer, R., 169
 Burda, P. A., 118

C
 Clark, H. M., 47

D
 DeKay, Y. R., 103

G
 Gilders, R. D., 78

H
 Hoey, G. R., 78

J
 Jee, N., 62

L
 Lee, Y.-H., 47
 Levy, A. V., 62

M
 Madsen, B. W., 169
 Matsumura, M., 141

Merediz, T. O., 211
 Miller, J. E., 1, 155

N
 Nair, P., 185

O
 Oka, Y., 141

R
 Roco, M. C., 185

S
 Sagüés, A. A., 19
 Sakai, M., 141
 Saltzman, G. A., 211
 Sargent, G. A., 19
 Schumacher, W. J., 5
 Sedman, K. G., 78
 Sethi, V. K., 19
 Sinha, S. K., 243
 Sorell, G., 62
 Spencer, D. K., 19
 Subramanyam, D. K., 211
 Summer, R. M., 91

T
 Thornley, J. C., 78

Y
 Yamawaki, M., 141

ISBN 0-8031-0941-5